

A New Visco-Plastic Device for Seismic Protection of Structures

Yasser El-Husseini Ibrahim

Dissertation submitted to the faculty of the Virginia Polytechnic Institute and State University in partial fulfillment of the requirements for the degree of

Doctor of Philosophy

In

Civil and Environmental Engineering

Dr. Finley A. Charney

Dr. Thomas M. Murray

Dr. Raymond H. Plaut

Dr. Carin L. Roberts-Wollmann

Dr. Mahendra P. Singh

02-07-2005
Blacksburg, VA

Keywords: Visco-plastic, Viscoelastic, Dampers, Passive control, Seismic, Earthquakes.

Copyright 2005, Yasser Ibrahim

A New Visco-Plastic Device for Seismic Protection of Structures

Yasser E. Ibrahim

Abstract

A new visco-plastic damper for seismic protection is introduced. This device combines and enhances many of the proven characteristics of both displacement-dependent and velocity-dependent devices.

The device consists of a block of a high-damping viscoelastic material sandwiched between two steel shapes (plates or channels) bent in a certain configuration to amplify the deformations in the device in order to obtain large tensile and compressive strains in the viscoelastic material. Under low levels of vibrations, the device dissipates energy through amplified strains in the viscoelastic material only; however, under moderate to strong levels of vibrations, a new source of energy dissipation is added through the yielding of the steel elements. The inelastic behavior of the steel elements is controlled by the rigidity of the viscoelastic material. In addition to the energy dissipation, the device provides stiffness through the steel elements as well as the viscoelastic material. Moreover, one of the main advantages of the device is that its behavior is fully controlled through different parameters.

First, a nonlinear time history analysis was conducted on structures with a preliminary model of the device using SAP2000 program to check the effectiveness of the device on the response of different structures under ground excitations. The device resulted in better improvement in the structural response compared to the existing viscoelastic dampers.

A three-dimensional finite element model was developed for the device using the finite element package, ABAQUS. The hyperelastic and viscoelastic behavior of the block of the viscoelastic material were considered. The inelastic behavior of the steel elements was considered as well using the Von Mises yielding criterion. The device was analyzed under different dynamic loadings with different frequencies.

Three simplified models were developed using SAP2000 program in order to facilitate the modeling of the device for structural engineers. These models were compared to the detailed finite element model to check their accuracy. The best model was used in the analysis of a multi-story steel frame with the visco-plastic devices under different ground excitations. Two different arrangements of the device were considered. The devices caused significant reduction in the story displacements, base shear and bending moment at column bases.

Dedication

TO:

My parents

My wife

My kids: Mariam and Ahmed

Acknowledgement

I would like to take the opportunity to express my deepest appreciation and gratitude for all the people who helped me during my work in this research.

First I would like to thank my advisor and committee chair, Dr. Finley Charney, for all of his support, guidance, and patience. I have learned a lot from his knowledge and practical experience in the area of Earthquake Engineering and structural Dynamics. It was really a privilege to work with him. I would also like to thank my committee members, Dr. Thomas Murray, Dr. Raymond Plaut, Dr. Carin Roberts-Wollmann and Dr. Mahendra Singh for taking the time to provide valuable insight for my thesis and for all the help they have offered me during the time I have spent at Virginia Tech.

I would like to thank my wife for her love, encouragement and support during my work towards the PhD degree. Special thanks for my parents for all what they did for me throughout my life. I owe to them every success I have in my life.

Finally, I would like to thank the Egyptian Government which supported me financially to pursue my research here in the United States.

TABLE OF CONTENTS

Chapter 1: Introduction	1
1.0 Introduction.....	1
1.1 Objective of the Research	2
1.2 Scope of the Research.....	3
1.3 Outline of the Research.....	4
Chapter 2: Literature Review	6
2.0 Introduction.....	6
2.1 Damping in Structures	6
2.1.1 Classification of Damping	7
2.1.1.1 Material Damping	7
2.1.1.1.1 Composite Materials	8
2.1.1.1.2 Viscoelastic Materials	9
2.1.1.1.3 Metallic Yielding	9
2.1.1.2 Nonmaterial Damping.....	10
2.1.1.2.1 Acoustic Radiation Damping	10
2.1.1.2.2 Coulomb Friction Damping	10
2.1.1.2.3 Viscous Damping.....	11
2.1.2 Mathematical Models for Viscoelastic Materials	12
2.1.2.1 Maxwell Model.....	12
2.1.2.2 Kelvin Model	13
2.2 Passive Energy Systems.....	14
2.2.1 Displacement-dependent Devices.....	16
2.2.1.1 Metallic Dampers.....	16
2.2.1.1.1 X-shaped Plate Dampers.....	16
2.2.1.1.2 Triangular Plate Dampers	20
2.2.1.1.3 Applications of Metallic Dampers in Structures.....	20
2.2.1.2 Unbonded Steel Braces.....	21
2.2.2 Velocity-dependent Devices	24
2.2.2.1 Viscoelastic Dampers.....	24
2.2.2.1.1 Configuration of Viscoelastic Damper	24
2.2.2.1.2 Design of Viscoelastic Dampers.....	25
2.2.2.2 Viscous Fluid Dampers.....	27
2.2.2.2.1 Types of Viscous Dampers	27
2.2.2.2.2 Effect of Nonlinearity in Viscous Dampers.....	27
2.2.2.3 Effectiveness of Viscoelastic and Viscous Fluid Dampers.....	31
2.2.2.4 Optimization of Viscoelastic and Viscous Fluid Dampers	34
2.2.2.5 Some Applications of Viscoelastic and Viscous Fluid dampers	38
2.2.3 Dampers Installation in Structures.....	40
2.2.3.1 Different Locations of Dampers	40
2.2.3.2 Comparison between the Effectiveness of Dampers for Different Placements	41
.....	41
2.3 Summary	43

Chapter 3: Rubber Compounds	45
3.0 Introduction.....	45
3.1 Compounding.....	45
3.2 Vulcanization	45
3.3 Properties and Application of Basic Crude Rubber Types	46
3.3.1 Natural Rubber (NR).....	46
3.3.2 Styrene Butadiene Rubber (SBR)	46
3.3.3 Neoprene (CR).....	47
3.4. Rubber Reinforcement.....	48
3.4.1 Carbon Black Properties	48
3.4.1.1 Particle Size	48
3.4.1.2 Surface Area.....	49
3.4.1.3 Hydrogen Content.....	50
3.4.1.4 Oxygen Content	50
3.5 Effect of Carbon Black on Rubber Properties	50
3.5.1 Modulus	50
3.5.2 Tensile Strength.....	52
3.5.3 Energy Dissipation through Dynamic Strains.....	53
3.6 High-damping rubber.....	56
3.7 Energy Dissipation through Axial and Shear Strains	57
3.8 Summary	60
Chapter 4: Detailed Description of the Device	61
4.0 Introduction.....	61
4.1 Device Description.....	62
Chapter 5: Preliminary Analysis of the Device	65
5.0 Introduction.....	65
5.1 Device Modeling.....	65
5.2 Single-Story Structure.....	67
5.2.1 Effect of the Damping Constant of the Dashpots	69
5.2.2 Effect of the Stiffness of the Linear Springs.....	71
5.2.3 Effect of the Cross Sections of the Steel Elements.....	71
5.2.4 Effect of the Device Aspect Ratio	74
5.2.5 Effect of the Device on the Response of the Single-Story Structure.....	76
5.3 Multi-Bay Multi-Story Steel Frame.....	79
5.3.1 Effect of Device Parameters on the Structural Response	82
5.3.2 Effect of the Device on the Response of the Multi-story Structure.....	86
5.3.3 Comparison between Visco-plastic Device and Conventional Viscoelastic Dampers	94
5.3.4 Different Arrangement of the Devices in the Multi-Story Structure	102
5.4 Comments on the device modeling using SAP2000.....	111
5.4.1 Material Modeling	111
5.4.2 Analysis Type	111
5.5 Conclusions.....	113

Chapter 6: Detailed Finite Element Analysis	115
6.0 Introduction.....	115
6.1 Material Modeling	115
6.1.1 Modeling Rubber Block.....	115
6.1.1.1 Hyperelasticity	115
6.1.1.1.1 Hyperelastic models.....	116
6.1.1.1.1.1 Polynomial Model.....	117
6.1.1.1.1.2 Ogden Model	118
6.1.1.1.2 Modeling the Hyperelasticity in ABAQUS	119
6.1.1.1.3 Modeling the Hyperelasticity of Rubber Block.....	121
6.1.1.2 Viscoelasticity.....	122
6.1.1.2.1 Viscoelastic Model.....	123
6.1.1.2.2 Modeling the Viscoelasticity in ABAQUS.....	125
6.1.1.2.3 Modeling the Viscoelasticity of Rubber Block.....	125
6.1.2 Steel Elements.....	126
6.1.2.1 Stress-Strain Curve for Steel Elements.....	126
6.1.2.2 The Von Mises Yield Criterion.....	127
6.1.2.3 Modeling the inelastic behavior of the steel	127
6.2 Geometric modeling of the device.....	130
6.3 Parametric study.....	133
6.3.1 Effect of Steel Type	133
6.3.2 Effect of the Aspect Ratio.....	142
6.3.3 Effect of Rubber Breadth.....	151
6.3.4 Effect of the Cross Section of Steel Elements	160
6.4 Performance of the Visco-Plastic Device under Different Loadings.....	169
6.5 Summary.....	174
Chapter 7: Simplified Device Models	176
7.0 Introduction.....	176
7.1 Simplified Models.....	176
7.1.1 Simple Model, M1	176
7.1.1.1 Model Mass.....	177
7.1.1.2 Modeling the Hyperelasticity of the Rubber Block	179
7.1.1.3 Modeling the Viscoelasticity of the Rubber Block.....	180
7.1.1.4 Modeling the Steel Elements	186
7.1.1.5 Comparison between ABAQUS Model and the Simplified Model, M1	186
7.1.2 Simple Model, M2	189
7.1.3 Simple Model, M3	191
7.2 Summary.....	192
Chapter 8: Analysis of Multi-Story Structures with Devices using the Simplified Model	195
8.0 Introduction.....	195
8.1 Multi-Story Structure with One Device per Floor	195
8.2 Multi-Story Structure with Two Devices per Floor.....	207
8.3 Summary.....	209

Chapter 9: Summary and Conclusions	216
9.0 Summary	216
9.1 Conclusions	219
9.2 Future work	220
References	221
Vita	228

List of Figures

Figure 1.1: Details of proposed visco-plastic device	3
Figure 2.1: Typical hysteretic loop for a viscoelastic material under cyclic load	9
Figure 2.2: Hysteretic loop for bilinear material	10
Figure 2.3: Mathematical models for viscoelastic material	13
Figure 2.4: Geometry of X-shaped device (Dimensions in in.)	17
Figure 2.5: ADAS devices; a) configuration, b) deformation.	18
Figure 2.6: Configuration of unbonded steel brace	22
Figure 2.7: Typical viscoelastic damper	24
Figure 2.8: Different types of fluid viscous dampers. [Constantinou et al. (1998)]	28
Figure 2.9: Force against velocity for different values of the damping exponent, N (C is constant)	29
Figure 2.10: Hysteretic loops for linear and nonlinear dampers (C is constant).	29
Figure 2.11: Distribution of viscoelastic dampers: a) fully damped; and b) 22 optimally placed	35
Figure 2.12: Different damper placements and their effectiveness [Sigaher and Constantinou (2003)]	42
Figure 3.1: Effect of carbon black loading on Young's modulus for natural rubber.....	52
Figure 3.2: Effect of carbon black loading on tensile strength for natural rubber.....	54
Figure 3.3: Effect of carbon black loading on elongation at break for natural rubber	54
Figure 3.4: Deformations in the visco-plastic device (under compression)	59
Figure 4.1: Details of visco-plastic device.....	62
Figure 5.1: Models; a: Device, b: single-story steel frame with the device.....	68
Figure 5.2: Effect of damping constant on the response of the single-story frame under harmonic excitation. (K1-S2-H3-LP-H)	70
Figure 5.3: Effect of spring constant on the response of the single-story frame under harmonic excitation. (C2-S2-H3-LP-H)	72
Figure 5.4: Effect of the device cross-section on the response of the single-story frame under harmonic excitation. (C2-K1-H3-LP-H).....	73
Figure 5.5: Effect of the aspect ratio of the device on the response of the single-story frame under harmonic excitation. (C2-K1-S2-LP-H).....	75
Figure 5.6: El Centro earthquake	77
Figure 5.7: Northridge earthquake	77
Figure 5.8: Effect of the analysis type on the response of the single-story Frame. (C2-K2-H3-S3-LP).....	78
Figure 5.9: Details of the Nine-story five-bay used in the analysis.....	80
Figure 5.10: Model of the analyzed nine-story steel frame with the devices (See Figure 5.1 for details of the device model).	81
Figure 5.11: Effect of the aspect ratio of the steel elements on their stiffness (VE material not included).	81
Figure 5.12: Effect of damping constant on the response of the nine-story frame under harmonic excitation (K1-S1-H3-LP-H).	83
Figure 5.13: Effect of spring constant on the response of the nine-story frame under harmonic excitation. (C3-S1-H3-LP-H)	84

Figure 5.14: Effect of device cross-section on the response of the nine-story frame under harmonic excitation. (C3-K1-H3-S1-LP-H)	85
Figure 5.15: Effect of the device on the response of the nine-story frame under harmonic excitation. (C4-K1-H3-S1-LP-H)	88
Figure 5.16: Effect of the device on the floor displacements and bending moments at column bases of the nine-story frame under harmonic excitation. (C3-K1-H3-S1-LP-H)	89
Figure 5.17: Effect of the device on the response of the nine-story frame under El Centro earthquake. (C4-K1-H3-S1-LP-E)	90
Figure 5.18: Effect of the device on the floor displacements and bending moments at column bases of nine-story frame under El Centro earthquake (C3-K1-H3-S1-LP-E)	91
Figure 5.19: Effect of the device on the response of the nine-story frame under Northridge earthquake. (C4-K1-H3-S1-LP-NR)	92
Figure 5.20: Effect of the device on the floor displacements and bending moments at column bases of the nine-story frame under Northridge Earthquake. (C3-K1-H3-S1-LP-NR).....	93
Figure 5.21: Effect of using the new device instead of the conventional damper on the response of the nine-story frame under harmonic excitation. (C4-K1-H3-S1-LP-H)	96
Figure 5.22: Effect of using the new device instead of the conventional damper on the floor displacements and bending moments at column bases of the nine-story frame under harmonic excitation. (C4-K1-H3-S1-LP-H)	97
Figure 5.23: Effect of using the new device instead of the conventional damper on the response of the nine-story frame under El Centro earthquake. (C4-K1-H3-S1-LP-E)	98
Figure 5.24: Effect of using the new device instead of the conventional damper on the floor displacements and bending moments at column bases of the nine-story frame under El Centro earthquake. (C4-K1-H3-S1-LP-E)	99
Figure 5.25: Effect of using the new device instead of the conventional damper on the response of the nine-story frame under Northridge earthquake. (C4-K1-H3-S1-LP-NR).....	100
Figure 5.26: Effect of using the new device instead of the conventional damper on the floor displacements and bending moments at column bases of the nine-story frame under Northridge earthquake. (C4-K1-H3-S1-LP-NR)	101
Figure 5.27: The nine-story five-bay steel frame with two devices per floor.....	104
Figure 5.28: Effect of using two devices per floor on the response of the nine-story frame under harmonic excitation. (C4-K1-H3-S1-LP-H)	105
Figure 5.29: Effect of using two devices per floor on the floor displacements and bending moments at column bases of the nine-story frame under harmonic excitation. (C4-K1-H3-S1-LP-H)	106
Figure 5.30: Effect of using two devices per floor on the response of the nine-story frame under El Centro earthquake. (C4-K1-H3-S1-LP-E)	107
Figure 5.31: Effect of using two devices per floor on the floor displacements and bending moments at column bases of the nine-story frame under El Centro earthquake. (C4-K1-H3-S1-LP-E).....	108

Figure 5.32: Effect of using two devices per floor on the response of the nine-story frame under Northridge earthquake. (C4-K1-H3-S1-LP-NR)	109
Figure 5.33: Effect of using two devices per floor on the floor displacements and bending moments at column bases of the nine-story frame under Northridge earthquake. (C4-K1-H3-S1-LP-NR).....	110
Figure 5.34: Effect of analysis type on the response of the single-story frame. (C2-K2-H3-S3).....	112
Figure 6.1: Typical stress-strain curve for hyperelastic material.....	116
Figure 6.2: Schematic of deformations in different tests used to model hyperelasticity.....	119
Figure 6.3: Uniaxial tension-compression tests on high-damping rubber	122
Figure 6.4: Biaxial tension test on high-damping rubber	123
Figure 6.5: Creep and recovery for a viscoelastic material	123
Figure 6.6: Relaxation shear test on high-damping rubber.....	126
Figure 6.7: Typical stress-strain curve for steel.....	128
Figure 6.8: Stress-strain curve used by ABAQUS for high-strength steel.	129
Figure 6.9: Linear reduced-integration element subjected to bending moment, M	130
Figure 6.10: Modeling the device in ABAQUS.....	132
Figure 6.11: Deformation shape of the device under tension	132
Figure 6.12: Deformation shape of the device under compression	132
Figure 6.13: Effect of steel type on the deformations of the device under tensile loading.	136
Figure 6.14: Effect of steel type on the energy dissipation of the device under tensile loading.....	137
Figure 6.15: Effect of steel type on the deformations of the device under compressive loading.....	138
Figure 6.16: Effect of steel type on the energy dissipation of the device under compressive loading.....	139
Figure 6.17: Effect of steel type on the deformations of the device under harmonic loading.....	140
Figure 6.18: Effect of steel type on the energy dissipation of the device under harmonic loading.....	141
Figure 6.19: Effect of the device aspect ratio on the deformations of the device under tensile loading.	145
Figure 6.20: Effect of the device aspect ratio on the energy dissipation under tensile loading.....	146
Figure 6.21: Effect of the device aspect ratio on the deformations of the device under compressive loading.....	147
Figure 6.22: Effect of the device aspect ratio on the energy dissipation under compressive loading.....	148
Figure 6.23: Effect of the device aspect ratio on the deformations of the device under harmonic loading.	149
Figure 6.24: Effect of the device aspect ratio on the energy dissipation under harmonic loading.....	150
Figure 6.25: Effect of the rubber breadth on the deformations of the device under tensile loading.....	154

Figure 6.26: Effect of the rubber breadth on the energy dissipation under tensile loading.	155
Figure 6.27: Effect of the rubber breadth on the deformations of the device under compressive loading.	156
Figure 6.28: Effect of the rubber breadth on the energy dissipation under compressive loading.	157
Figure 6.29: Effect of the rubber breadth on the deformations of the device under harmonic loading.	158
Figure 6.30: Effect of the rubber breadth on the energy dissipation under harmonic loading.	159
Figure 6.31: Effect of steel cross section on the deformations of the device under tensile loading.	163
Figure 6.32: Effect of steel cross section on the energy dissipation under tensile loading.	164
Figure 6.33: Effect of steel cross section on the deformations of the device under compressive loading.	165
Figure 6.34: Effect of steel cross section on the energy dissipation under compressive loading.	166
Figure 6.35: Effect of steel cross section on the deformations of the device under harmonic loading.	167
Figure 6.36: Effect of steel cross section on the energy dissipation under harmonic loading.	168
Figure 6.37: Effect of the loading frequency on the deformations of the device	170
Figure 6.38: Effect of the loading frequency on the energy dissipation by the device.	171
Figure 6.39: Response of device under different displacement amplitudes	172
Figure 6.40: Energy dissipation of the device under different displacement amplitudes.	173
Figure 7.1: Simplified model, <i>M1</i>	177
Figure 7.2: Stress-strain curve obtained from the uniaxial tension and compression tests on high-damping rubber specimen.	179
Figure 7.3: Force-displacement relationship of the multilinear spring representing the rubber hyperelasticity.	180
Figure 7.4: Modeling of a high-damping rubber block in ABAQUS	182
Figure 7.5: Typical stress-strain curve of rubber specimen under dynamic tests.	182
Figure 7-6: Stress-strain curve of high-damping rubber block under different axial harmonic stresses.	184
Figure 7.7: Comparison between the results of finite element model and simplified model, <i>M1</i>	188
Figure 7.8: Simplified model, <i>M2</i>	189
Figure 7.9: Comparison between the results of finite element model and simplified model, <i>M2</i>	190
Figure 7.10: Simplified model, <i>M3</i>	191
Figure 7.11: Comparison between the results of finite element model and simplified model, <i>M3</i>	194
Figure 8.1: Configuration of the simplified model used in the analysis.	196

Figure 8.2: The analyzed nine-story frame with simplified model of devices. (One device per floor)	199
Figure 8.3: Effect of the device on the response of the nine-story frame under harmonic excitation.	201
Figure 8.4: Effect of the device on the floor displacements and bending moments at column bases of the nine-story frame under harmonic excitation.	202
Figure 8.5: Effect of the device on the response of the nine-story frame under El Centro earthquake.	203
Figure 8.6 Effect of the device on the floor displacements and bending moments at column bases of the nine-story frame under El Centro earthquake.	204
Figure 8.7: Effect of the device on the response of the nine-story frame under Northridge earthquake.	205
Figure 8.8: Effect of the device on the floor displacements and bending moments at column bases of the nine-story frame under Northridge earthquake.	206
Figure 8.9: The analyzed nine-story frame with simplified model of devices. (Two devices per floor).	207
Figure 8.10: Effect of using two devices per floor on the response of the nine-story frame under harmonic excitation.	210
Figure 8.11: Effect of using two devices per floor on the floor displacements and bending moments at column bases of the nine-story frame under harmonic excitation.	211
Figure 8.12: Effect of using two devices per floor on the response of the nine-story frame under El Centro earthquake.	212
Figure 8.13: Effect of using two devices per floor on the floor displacements and bending moments at column bases of the nine-story frame under El Centro earthquake. ...	213
Figure 8.14: Effect of using two devices per floor on the response of the nine-story frame under Northridge earthquake.	214
Figure 8.15: Effect of using two devices per floor on the floor displacements and bending moments at column bases of the nine-story frame under Northridge earthquake. .	215

List of Tables

Table 2.1: Recommended values for damping ratios for different structures.....	8
Table 3.1: Comparison between rubber compounds.....	47
Table 5.1: General symbols for the analysis.....	69
Table 6.1: Stress and strain for steel.....	129
Table 6.2: Loading types used in the parametric study.....	133
Table 7.1: Calculation of the phase angle of the high-damping rubber.....	183
Table 7.2: Damping constant Estimation.....	186

Chapter 1: Introduction

1.0 Introduction

Most structures are subjected to vibrations. These vibrations may arise from wind forces, earthquake excitation, machine vibrations, or many other sources. In some cases, especially under strong earthquake excitations, these vibrations can cause structural damage or even structural collapse. The higher the inherent or natural damping in structures, the lower the likelihood the damage will be excessive. However, for structures subjected to strong vibrations, the inherent damping in the structure is not sufficient to mitigate the structural response. In many situations, supplemental damping may be used to control the response of these structures. In this regard, many researchers have studied, developed and tested different supplemental damping techniques. The basic supplemental damping techniques applied to structures are:

- a) Passive control devices.
- b) Active and semi-active control devices.

The common principle of these devices is that they all need power to generate motion control forces to reduce the structural response under vibrations. However, the power source is different in each device. For passive control devices, the device generates control forces at the points of attachments and the power needed to develop such forces are originated from the motion of the points of attachments. The amplitude and direction of these forces are determined by the relative motion of these points. On the other hand, for active control devices, a controller is attached to the structure to develop motion control forces. The magnitude and direction of these forces are determined according to the controller input data, which is obtained through a variety of sensors. The main drawback of the active control devices is that they need an external power source, and in some applications, the required power is large. Semi-active devices are similar in many aspects to passive systems, but use battery power controllers to adjust their mechanical properties. As with purely passive devices, the forces in the device are developed from the motion of the attachments points.

Concerning the passive devices, they are usually categorized into two main categories; displacement-dependent and velocity-dependent devices. The displacement-dependent devices, like steel plate dampers and friction dampers, dissipate energy through yielding of the damper elements or through sliding friction. Velocity-dependent devices, like viscous fluid dampers and viscoelastic dampers, rely on viscoelasticity in dissipating energy. Velocity-dependent devices provide damping and (optionally) stiffness to the structures and are used to dissipate energy for all levels of excitations. On the other hand, displacement-dependent devices provide added stiffness to structures and they dissipate energy under moderate and strong excitations only.

In this research, a new passive device called a “Visco-Plastic Damper” is presented. The device consists of a block of a viscoelastic material sandwiched between two steel shapes (plates or channels) bent in a certain configuration. The device is shown in Figure 1.1 and is described in depth in *Chapter 4*.

Under low levels of excitation, this device dissipates energy through the viscoelastic material only. Under strong excitations, the energy is dissipated through the viscoelastic material in addition to the yielding of the steel elements of the device. The yielding of these elements is controlled by the viscoelastic material. The main advantage of this new device is that its behavior is fully controlled by a large number of parameters.

1.1 Objective of the Research

In this research, a new visco-plastic passive energy device for seismic protection is introduced. The device is very controllable and it is fabricated from readily available materials. It shares the advantages of a variety of existing dampers. The device dissipates energy under all levels of vibrations. The purpose of this research is to study the different parameters that affect the behavior of the new visco-plastic device and how the device can affect the response of multi-story structures under different ground excitations.

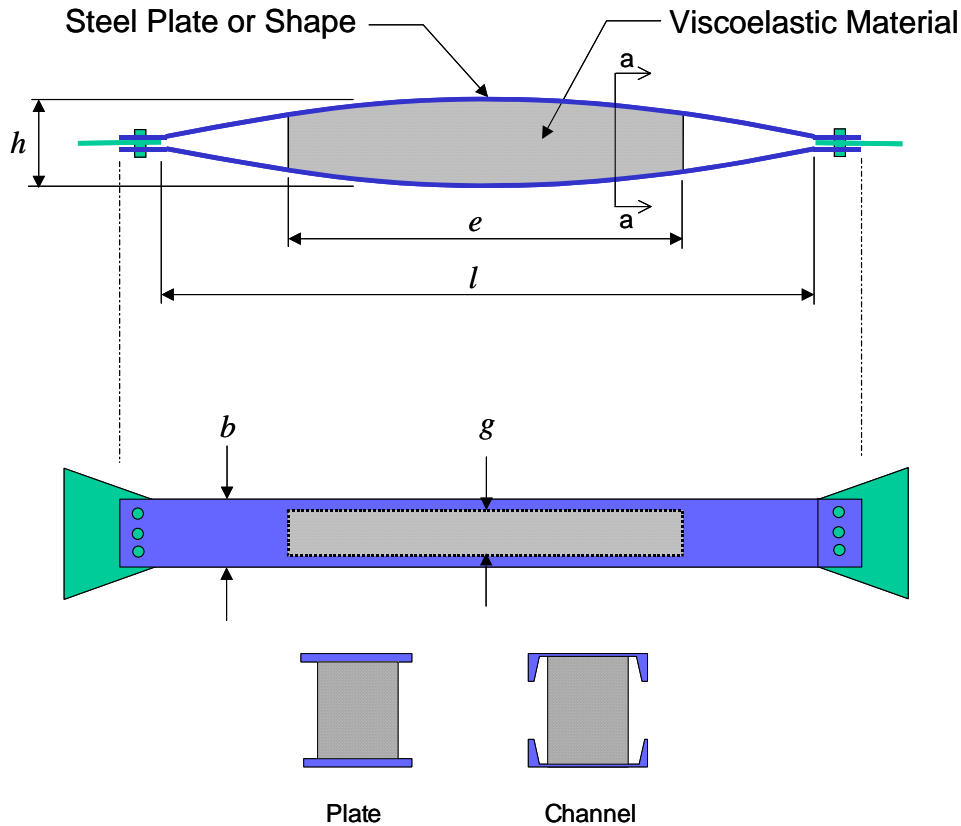


Figure 1.1: Details of proposed visco-plastic device

1.2 Scope of the Research

Under low levels of vibrations, the visco-plastic device dissipates energy through tensile and compressive strains in the viscoelastic material rather than shear strains, as in existing viscoelastic dampers. For moderate and strong vibrations, another source of energy dissipation is introduced through the inelastic deformations in steel elements. The first step in this research is to carry out a preliminary analysis using SAP2000 in order to investigate the effectiveness of the device on the response of structures and to compare this device to existing viscoelastic dampers. In this step, the viscoelastic material is modeled using discrete springs and dashpots while the steel elements are modeled using elastic frame elements. The second step is to investigate the different parameters that affect the performance of the device through a detailed finite element analysis using ABAQUS. The hyperelasticity and viscoelasticity of the viscoelastic material are considered. The inelastic behavior of steel elements is modeled using the Von Mises yield criterion. In order to facilitate the modeling of the device for structural engineers,

simplified models are presented and compared to the results obtained from the detailed finite element analysis. The best simplified model is then used to model the device to investigate its effectiveness on a multi-story steel frame structure under harmonic excitation, as well as real records of the El Centro and Northridge earthquakes. Finally, after demonstrating the effectiveness of the device, some useful conclusions and recommendations for future work are presented.

1.3 Outline of the Research

In Chapter 2, a literature review is presented to provide a technical background on issues related to the device. The topics covered are damping in general and an overview of several passive energy systems, including displacement-dependent and velocity-dependent dampers.

In Chapter 3, some rubber processes (compounding and vulcanization) are defined briefly. Also, different rubber compounds are presented showing their advantages and disadvantages as well as the suitable application for each compound. The properties of fillers, mainly carbon black, and how they can enhance the rubber properties to achieve the desired performance are discussed.

A detailed description of the geometry of the device and how it works is presented in Chapter 4. Also, different device parameters that can control the device are introduced.

In Chapter 5, a preliminary analysis of the device using the SAP2000 program is described. The device is modeled using discrete dashpots and springs. The effect of different device parameters on the device effectiveness is studied. The effectiveness of the device is investigated through the response of a single-story and a multi-story multi-bay steel frame. The devices are attached to these frames with different arrangements. The response of the multi-story frame with these devices is compared to the response of the same frame with “conventional viscoelastic” dampers.

In Chapter 6, a detailed finite element analysis of the device is presented. The analysis was conducted using the finite element package, ABAQUS. The finite element analysis

considers the real behavior of steel and rubber materials. A parametric study is carried out to investigate the effect of different parameters on the device behavior.

To facilitate the analysis of multi-story structures with visco-plastic devices, a simplified model of the device using SAP2000 is introduced in Chapter 7. Different simplified models are presented and compared to the detailed finite element analysis. A very good approximation is obtained.

In Chapter 8, the best simplified model obtained in Chapter 7 is used in the analysis of a nine-story five-bay steel frame under harmonic excitation as well as real records of El Centro and Northridge earthquake excitations. The effect of the device on the story displacements, bending moment at column bases and total base shear are discussed in detail.

Finally, the results are summarized in Chapter 9 and final conclusions are presented. Recommendations for future work are also provided.

Chapter 2: Literature Review

2.0 Introduction

To understand the behavior of the proposed device and its advantages compared to other existing dampers, it is important first to present different topics related to damping and to this device in particular. The following topics are presented in this chapter:

1. Different types of damping and how it is developed in the structural elements.
2. Passive energy systems including velocity-dependent devices, such as viscous fluid and viscoelastic dampers and displacement-dependent devices, such as metallic dampers and unbonded steel braces.

2.1 Damping in Structures

The capacity of a structure or a structural component to dissipate vibration energy is known as damping. The principal mechanism involved in damping is the conversion of instantaneous strain and kinetic energy into heat, which is dissipated into the surrounding environment.

In simple systems, such as laboratory models, most of the energy dissipation arises from the thermal effect of repeated elastic straining of the material and from the internal friction when a solid is deformed. However, in actual structures, many other mechanisms contribute to the energy dissipation. In a vibrating building, these mechanisms include friction at steel connections, opening and closing of the microcracks in concrete and the friction between the structural and nonstructural components such as the partition walls.

In general, in traditional structures, the mass and stiffness properties of various members can be modeled with reasonable degree of accuracy. However, it is difficult to characterize the damping properties. Most experimental results suggest that the damping forces are nearly independent of frequency, which is contrary to the inherent frequency-dependence of viscous damping forces. In general, true viscous idealization is sufficient only for low levels of damping.

The different types of the damping and how damping is developed in the structural elements and the surrounding medium are briefly presented.

2.1.1 Classification of Damping

Damping can be classified in many different ways. The basic classification is based on material properties. The damping forces depend on the molecular friction of the material. This kind of damping is known as material or structural damping. Another type of damping encountered in a vibrating system is introduced through the surrounding medium, in which the vibration takes place. This kind of damping is called nonmaterial damping.

Typical structures have 1% to 5% critical damping as an inherent damping, which may be attributed to non-structural elements, such as partition walls and external claddings in addition to the cracks in reinforced concrete structures or connections in steel and wood structures. Newmark and Hall (1982) recommended some damping ratios to be used in the analysis of different structures. These values are shown in Table 2.1.

2.1.1.1 Material Damping

In general, all engineering materials dissipate energy during cyclic deformations. Some materials, such as rubber and plastics, dissipate much more energy per cycle of deformation than others, such as steel and aluminum. For the common structural materials, under low levels of elastic vibration, the energy dissipation per unit volume per cycle is very small compared to others, like viscoelastic materials.

Under cyclic loads, the relation between the stress and strain forms hysteretic loops. These hysteretic loops are very useful in understanding the damping. The area enclosed by the hysteretic loop represents the energy dissipation capacity for any material. Unless the material is stressed into the plastic range, the common structural materials have a very thin hysteretic loop. For viscoelastic materials, the hysteretic loops are very large [Nashif

et al. (1985)]. Figure 2.1 shows a typical hysteretic loop for a viscoelastic material under cyclic load.

Table 2.1: Recommended values for damping ratios for different structures

Stress Level	Type and Condition of Structures	Damping Ratio (%)
Working stress, less than $\frac{1}{2}$ yield point	• Welded steel, prestressed concrete, well reinforced concrete (slight cracking).	2-3
	• Reinforced concrete with considerable cracking.	3-5
	• Bolted and/or riveted steel, wood structures with nailed or bolted joints.	5-7
At or just below yield point	• Welded steel, prestressed concrete without complete loss in prestress.	5-7
	• prestressed concrete with no prestress left	7-10
	• Reinforced concrete	7-10
	• Bolted and/or riveted steel, wood structures with nailed or bolted joints.	10-15
	• Wood structures with nailed joints.	15-20

2.1.1.1.1 Composite Materials

Fiber-reinforced composite materials are used extensively in the aerospace, automotive and sport industries.

The damping of a composite material is usually higher than that of the common structural materials, such as steel and aluminum. Damping properties, like stiffness, are highly directional. This means that the damping properties along the fiber direction are different from those along the direction normal to the fiber. The damping property of composite

materials depends slightly on the temperature, strain energy and vibration amplitude [Nashif et al. (1985)].

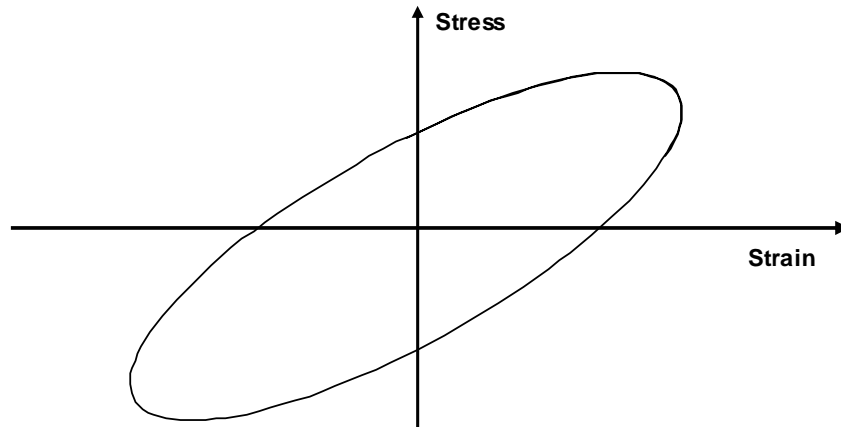


Figure 2.1: Typical hysteresis loop for a viscoelastic material under cyclic load

2.1.1.1.2 Viscoelastic Materials

Viscoelastic damping exists in many polymeric and glassy materials. The damping arises from relaxation and recovery after the deformation. The dynamic behavior of the polymeric materials, resulting from their chemistry, is of great importance for noise and vibration control.

Polymeric materials can be manufactured to have the desirable properties like strength, durability, creep resistance, thermal stability and a wide variety of damping characteristics.

2.1.1.1.3 Metallic Yielding

All engineering materials respond elastically under low levels of stresses. However, if the stress amplitude is high enough, the material undergoes some plastic strains, which leads to a hysteresis loop as shown in Figure 2.2. The area enclosed by the hysteresis loop represents the energy dissipation per volume during one loading cycle. Under moderate

to high levels of seismic excitation, structures usually experience plastic deformations in different elements. This behavior is desired to mitigate the seismic risk, however severe yielding may lead to excessive damage and loss of use or collapse of the structure. Other forms of metallic yielding can be introduced into structures through metallic dampers, which are specific metallic devices added to the structures in order to absorb the energy during the seismic excitations through their inelastic behavior.

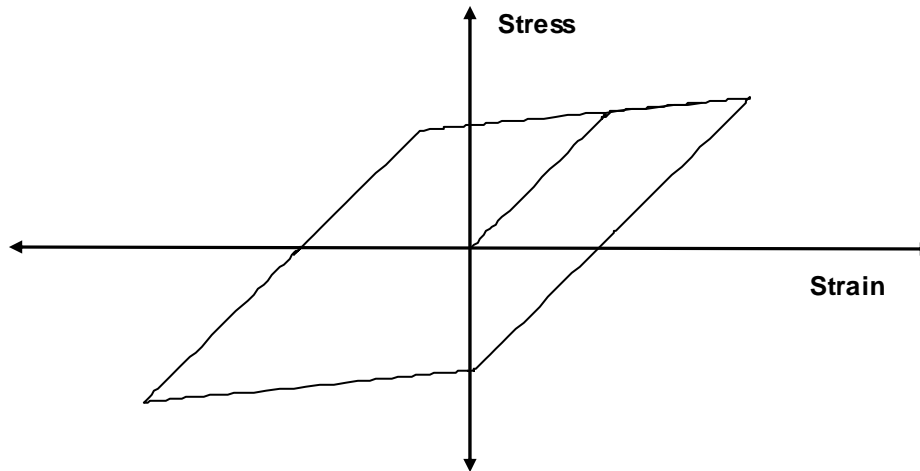


Figure 2.2: Hysteretic loop for bilinear material

2.1.1.2 Nonmaterial Damping

2.1.1.2.1 Acoustic Radiation Damping

The vibrational response of a structure depends on the surrounding fluid medium like air, water, oil or any other gas or liquid. This surrounding medium may lead to significant changes of the natural frequencies and mode shapes. The damping effect depends on the fluid density, the velocity of sound waves within the fluid and the structure's mass and stiffness.

2.1.1.2.2 Coulomb Friction Damping

Coulomb damping, also known as dry damping, is produced from the sliding of two dry surfaces. These frictional forces are proportional to the normal load between the two surfaces with the constant of proportionality being the constant of friction for the

material. The direction of these forces is usually against the velocity vector of the moving surface [Nashif et al. (1985)].

The Coulomb damping force is assumed to be independent of the relative velocity of motion between the two surfaces. The concept of Coulomb damping is usually applied in structural joints. Damping force is introduced from the slipping at the joint and this gives rise to energy dissipation at the joint.

2.1.1.2.3 Viscous Damping

For any system, if the resisting force is proportional to the velocity of the motion, the system can be considered viscously damped. This mechanism can be observed in a moving body in a viscous fluid or in the air. The viscous damping force, F_D , is the fluid resistance during oscillation and is a function of the vibration velocity and the damping constant, C .

$$F_D = C \dot{u} \quad (2-1)$$

where C is a proportional constant called the coefficient of viscosity and \dot{u} is the relative velocity between the particle and the fluid.

Although it is not the case in structures, but due to the simplicity of the mathematical model, structures are usually considered viscously damped. The mathematical model is often represented by a simple dashpot, which is very easy to use in analyzing engineering vibration models.

The main advantage of this model is the physical and mathematical simplicity. This model usually provides satisfactory accuracy for low levels of inherent damping (e.g. 1 to 10 %). However, it rarely represents the exact behavior of structural elements for higher damping ratios (case of supplemental damping). One can improve this model by introducing various combinations of springs and dashpots, but it will increase the complexity of the model.

2.1.2 Mathematical Models for Viscoelastic Materials

The behavior of any viscoelastic material can be represented by a combination of elastic and viscous behaviors. For linear elastic material, the normal stress is given by:

$$\sigma = E\varepsilon \quad (2-2)$$

where E is the modulus of elasticity or Young's modulus, and ε is the axial strain.

For such a material, the stress and strain are time-independent. This behavior can be modeled by a linear spring.

For linear viscous material, the resisting force is proportional to the motion velocity. The stress-strain relationship for a bar with a cross sectional area, A , and length, l , can be described by:

$$\sigma A = C \dot{u} = Cl \frac{d\varepsilon}{dt} \quad (2-3)$$

where C is the proportionality constant, or the damping constant. In this case, the stress and strain are time-dependent. This relation can be modeled by a dashpot.

There are two well-known models usually used in modeling viscoelastic materials; Maxwell model and Kelvin model.

2.1.2.1 Maxwell Model

In this model, the material is modeled by a spring and a dashpot in series. The model is shown in Figure 2.3 a. The stress and strain are given by:

$$\sigma = \sigma_1 = \sigma_2 \quad (2-4)$$

$$\varepsilon = \varepsilon_1 + \varepsilon_2 \quad (2-5)$$

where σ_1 and ε_1 are the stress and strain in the linear spring while σ_2 and ε_2 are the stress and strain in the dashpot.

2.1.2.2 Kelvin Model

In this model, the material is modeled by a spring and a dashpot in parallel. The model is shown in Figure 2.3 b. The stress and strain are given by:

$$\sigma = \sigma_1 + \sigma_2 \quad (2-6)$$

$$\varepsilon = \varepsilon_1 = \varepsilon_2 \quad (2-7)$$

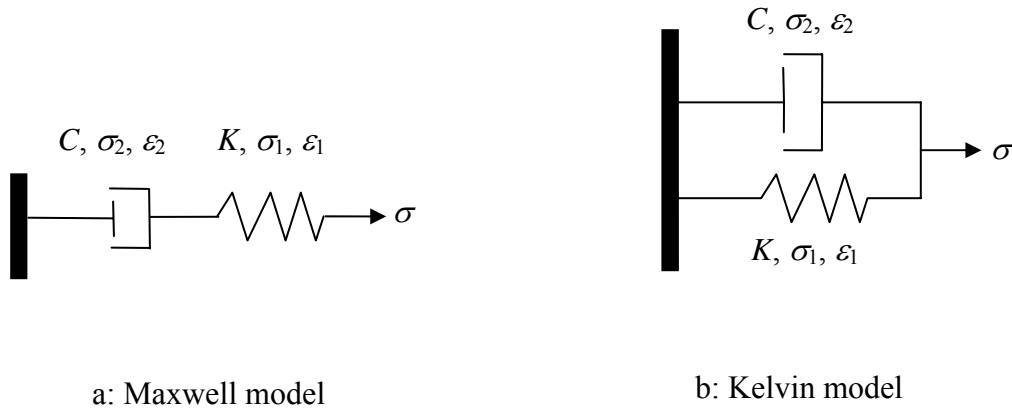


Figure 2.3: Mathematical models for viscoelastic material

2.2 Passive Energy Systems

Under moderate and strong seismic excitations, structures without supplemental damping can experience severe damage in structural and non-structural elements. These structures can often resist such excitations without a complete collapse, and accordingly, life safety is maintained. On the economical side, the cost of repairing these structures is often excessive. Moreover, loss of use is also an economic issue.

There are many ways to improve the structural performance under such seismic excitations. The basic concept is to minimize the deformation demand of these structures. This can be achieved by the following approaches:

- a) Base isolation system
- b) Seismically-controlled system

Base-isolated structures are basically supported on laterally soft springs which increase the period of vibration of the structure well beyond the strong components of ground motion, thereby reflecting the seismic input energy away from the structure. The main disadvantage of this system is that under seismic excitations with periods of vibrations close to the new larger structural period, it may result in higher deformations due to the resonance. Also, the electrical, mechanical and plumbing systems at the base must be designed to accommodate large displacements. However, dampers may be used in association with the base-isolation systems to overcome this problem.

The seismically-controlled systems include active, semi-active and passive systems. These systems need power to develop control forces that reduce the structural response under different types of vibrations. For passive control devices, the device generates control forces at the points of attachments. These devices use no external power, because the power needed to develop such forces are originated from the motion of the points of attachments. The amplitude and direction of these forces are determined by the relative motion of these points. In active control devices, a controller is attached to the structure to develop motion control forces. A control algorithm determines the forces based on real-time data provided by a variety of sensors. The main drawback of the active control

devices is that they need an external power source and in some applications, the needed power is large. Semi-active devices are originated from passive systems with battery-supplied power to adjust their mechanical properties by a controller. The forces are developed from the motion of the attachments points.

Focusing on the passive control systems, there are two basic types of these devices

- a) Displacement-dependent devices
- b) Velocity-dependent devices

Displacement-dependent devices dissipate energy through sliding friction, like friction dampers, or through the inelastic behavior of the damper elements, like metallic dampers. These devices provide lateral stiffness to the structure and consequently reduce its deformation demand. However, increasing the stiffness may damage the building contents due to the excessive accelerations. Higher stiffness often increases base shear, and bending moment at column bases as well.

Velocity-dependent devices, like viscous fluid dampers and viscoelastic dampers, dissipate energy through forces proportional to the velocity of the motion. Velocity-dependent devices provide damping (and stiffness in some cases) to the structures and are used to dissipate energy for all levels of excitations while displacement-dependent devices usually provide stiffness and the energy dissipation takes place under moderate and strong excitations only.

In the following section, attention will be paid to the metallic damper and unbonded steel brace as displacement-dependent devices as well as the viscoelastic and viscous fluid dampers as velocity-dependent devices since the proposed visco-plastic device shares the characteristics of these devices.

2.2.1 Displacement-dependent Devices

2.2.1.1 Metallic Dampers

To achieve a good structural design to resist seismic excitations, it is usually necessary to rely on inelastic behavior of structural elements. This behavior results in dissipation of the seismic energy transferred to the structures, which improves the structural response. However, the structural elements may experience severe yielding that affects the post-event usability of the structure. The basic concept of the metallic dampers is to introduce specific metallic elements in order to absorb the energy during the seismic excitations through their inelastic behavior.

Kelly et al. (1972) and Skinner et al. (1975) were the first researchers to consider the idea of using separate metallic dampers for energy dissipation. They considered different types of these dampers such as torsional beam, flexural beam and U-strip dampers.

Many researchers considered the metallic dampers and their implementation in structures. The most well-known and used types of these dampers are the X-shaped and triangular plate dampers. These types of metallic dampers are presented.

2.2.1.1.1 X-shaped Plate Dampers

The flexural plate steel dampers are the most used types of the metallic dampers. This type includes the X-shaped and V-shaped plate dampers. Bergman and Goel (1987) performed cyclic tests on X-shaped and V-shaped plate dampers. The geometry of these types is shown in Figure 2.4. The dampers were attached to a full-scale single-story building. Three dampers were tested under constant displacement amplitude. Different displacement amplitudes up to 1.5 in. were applied with a forcing frequency of 0.33 Hz for 10 cycles. The X-shaped dampers performed better than the V-shaped dampers regarding the energy dissipation as well as their durability.

Another type of the X-shaped dampers, known as the Added Damping and Stiffness, ADAS, was introduced [Xia et al. (1990)]. The ADAS device is an assemblage of steel

plates. When installed in a building frame, the devices are connected to the beams so that the story drifts cause relative horizontal displacements, which lead to energy dissipation through the yielding of large volume of steel. A typical configuration of ADAS devices and how they deform when subjected to shear forces due to story drifts are shown in Figure 2.5.

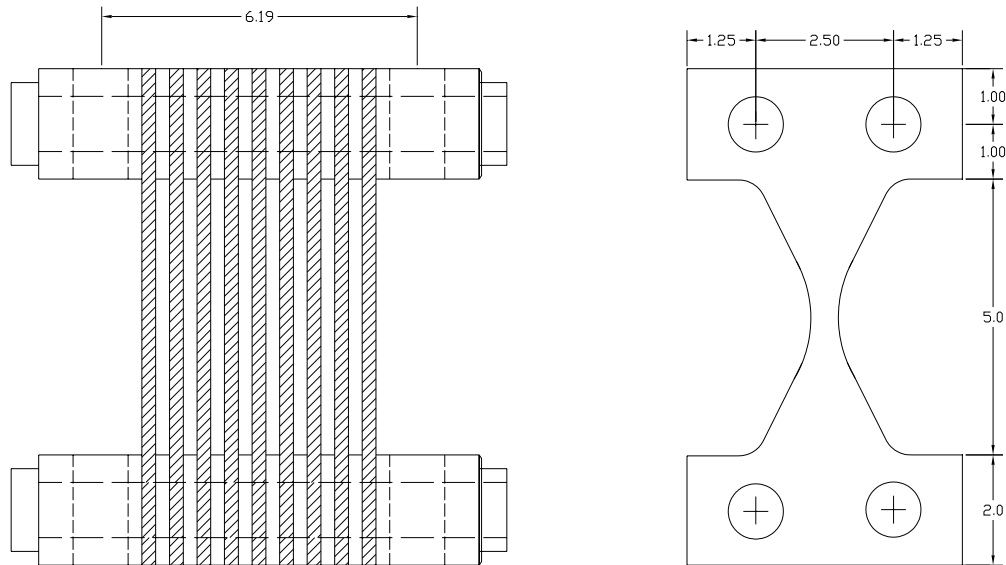
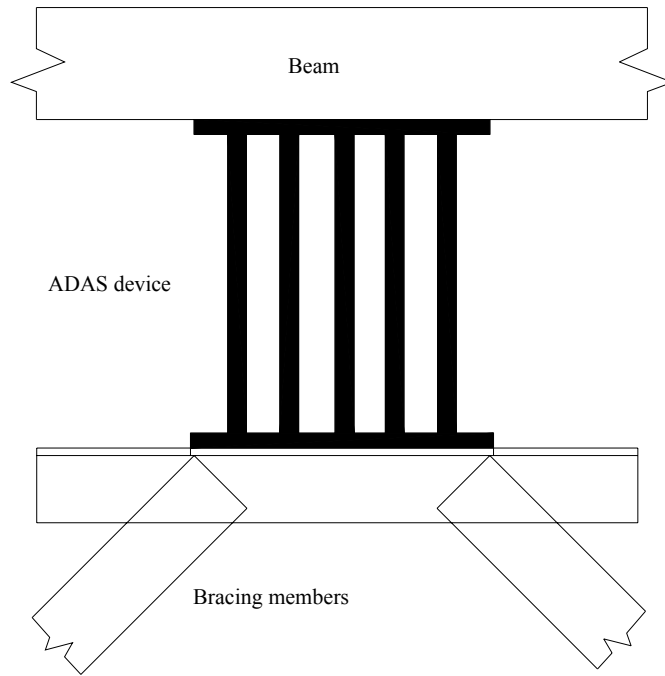


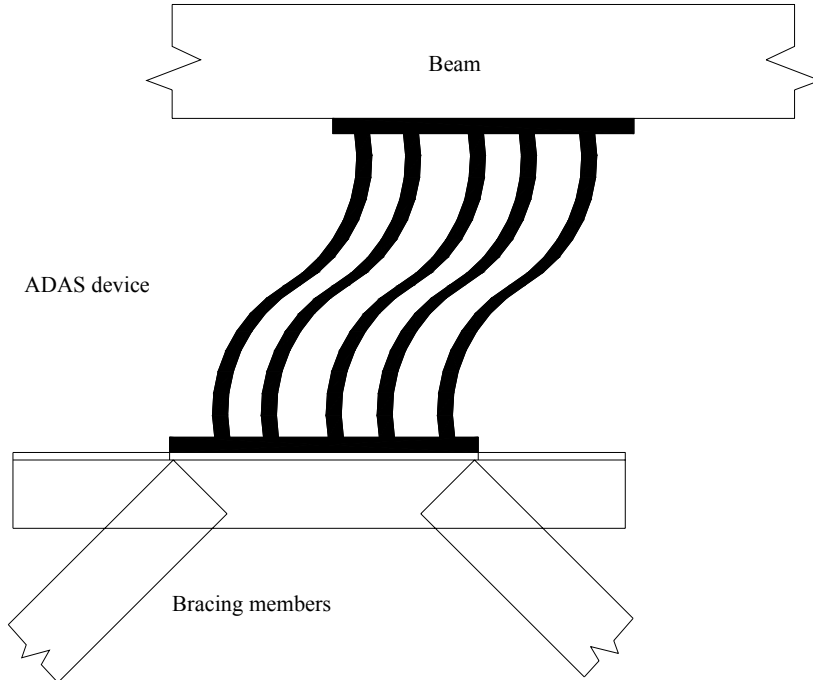
Figure 2.4: Geometry of X-shaped device (Dimensions in in.)

The main advantages of these devices are:

- Large inelastic deformations are constrained in ADAS elements, which are designed for this purpose. After moderate to strong earthquake excitations, these devices can be easily replaced.
- The devices considerably increase the equivalent viscous damping in structures, which results in a reduction in structural response under vibrations. Also, the energy dissipation demands for other structural elements are reduced.
- ADAS devices can be used in new structures as well as in existing structures for retrofitting.



a) Configuration of ADAS devices



b) ADAS devices deformations under story shears.

Figure 2.5: ADAS devices; a) configuration, b) deformation.

Xia et al. (1990) studied the different parameters that can affect the device behavior such as the device yield force, the device yield displacement and the distribution of the devices. Three ten-story moment frames with different ADAS elements were considered in the study. The response of these structures with the ADAS devices was determined by using the DRAIN-2D program [Powell (1973)].

The following important conclusions were obtained:

- The device yield force should be large enough to provide sufficient energy dissipation within the design ductility ratios.
- The device yield displacement should range between 0.0014 to 0.002 H, where H is the story height.
- The ADAS devices yield forces can be distributed in proportion to the design shear forces while the stiffness of the ADAS elements can be distributed according to the story stiffnesses of the frame without devices.

Whittaker et al. (1991) tested the X-shaped plate dampers under cyclic tests as well as earthquake simulator tests. The hystereses obtained from these dampers are similar to that obtained by Bergman and Goel (1987) for small displacement amplitudes while they are different under large displacement amplitudes. This difference may arise due to the axial effects associated with the finite deformations at large displacement amplitudes [Soong and Dargush (1997)]. The axial deformation are resisted by the supporting frame in Bergman and Goel case however there is no vertical constraints in Whittaker et al. case.

Whittaker et al. (1991) examined the performance of the ADAS dampers under simulated earthquake excitations as well. Six ADAS dampers were attached to three-story single-bay ductile moment-resistant space frames. The first two natural periods of the frame without the dampers are 0.74 and 0.22 seconds, respectively while the first two natural periods of the structure with the chevron braces and ADAS elements are 0.47 and 0.17 seconds, respectively. Three different simulated records were used including a soft soil synthetic (THSSR), 1985 Chile N10E and 1940 El Centro S00E. The results showed a considerable improvement in structural response under different simulated earthquake records.

2.2.1.1.2 Triangular Plate Dampers

The second type of the metallic plate dampers that are widely used is the triangular plate damper. Tsai et al. (1993) conducted some experiments on the triangular plate dampers. First, they performed cyclic testing of the damper, which they referred to it as TADAS. They considered different plate dimensions and patterns of cyclic loads. After that, they performed pseudodynamic testing of a two-story steel frame. They studied the performance of the structure with and without the damper under simulated 1940 El Centro S00E. The results showed significant reduction of the floor displacement upon the use of the TADAS elements.

2.2.1.1.3 Applications of Metallic Dampers in Structures

Steel plate dampers have been used in many structures. In 1990, ADAS dampers were used in retrofitting a building after damaged in Mexico City [Martinez-Romero (1993)]. The building is a 13-story reinforced concrete frame with brick-infilled end walls. The building was exposed to moderate damage during Mexico City earthquake in 1985. The building was upgraded; however more damage occurred during 1986 and 1989 seismic excitations. Two hundreds and fifty ADAS dampers were installed in the outer frame bays for retrofitting. The fundamental periods of vibrations were reduced from 3.82 and 2.33 seconds to 2.24 and 2.01 seconds, respectively. Structural analysis for the redesign showed that a 40 % reduction in interstory drifts was obtained while the base shear was unchanged.

ADAS elements were used in retrofitting Cardiology Hospital Building in Mexico City in 1990 [Martinez-Romero (1993)]. The building consists of 6-story reinforced concrete frame structure. Nonlinear time history analysis using Drain-2D was used for the redesign. The results showed reduction in interstory drifts and base shear as well.

2.2.1.2 Unbonded Steel Braces

The basic idea behind these braces is to dissipate energy through inelastic behavior in steel braces without buckling of the braces. Typically these braces consist of a ductile metal core (commonly steel) in a continuous steel tube filled with concrete or mortar. A typical configuration of this brace type is shown in Figure 2.6. The axial loads are carried by the steel core while the outer tube and the filler provide the lateral resistance to prevent the buckling of the brace. The steel core has a large inelastic capacity since the lateral and local buckling are restricted. A slip unbonding layer between steel core and concrete is provided to ensure that the loads are carried by the steel core only. The unbonded braces are considered dampers in the way that they dissipate energy through the slippage between the core and the casing. The first attempt to develop these braces was done by Kimura et al. (1976). The brace consisted of a conventional brace encased in a square steel pipe filled with mortar. The problem with that brace was the transverse deformations of the mortar under compression after many loading cycles, which lead to permanent void space large enough to allow buckling.

Experimental tests were conducted on the same brace, but confined with reinforced concrete instead of mortar. It was also observed that concrete cracked after many loading cycles which allowed brace buckling [Wada et al. (1989)]. Different studies were conducted to enhance the performance of this brace until the current configuration was obtained [Watanabe et al. (1988), Wada et al. (1989), and Watanabe and Nakamura (1992)].

Shiba et al. (1998) compared the effect of conventional braces and the unbonded braces on the response of a 15-story structure under two input motions representing moderate and severe earthquakes. The peak ground acceleration was 0.25 g and 0.5 g , for both ground motions, respectively. The unbonded steel braces were designed to yield before the main frame. Accordingly, the yield strength of the unbonded braces was three times smaller than that of the conventional braces. The results showed that under moderate ground motion, the reduction of the story drifts and shear forces were reduced by about 25 % due to the use of the unbonded steel braces instead of conventional braces.

However, under severe earthquake, the difference in response was not clear as the first case. The response at lower stories was reduced more than the upper stories. The base shear was reduced by 20 % due to the use of unbonded braces instead of the conventional braces.

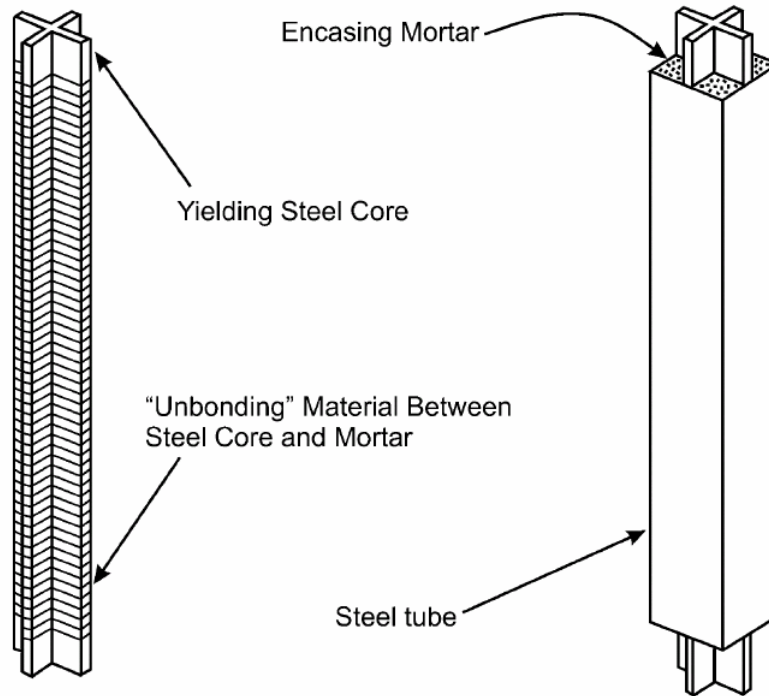


Figure 2.6: Configuration of unbonded steel brace

Black et al. (2004) conducted many experimental tests on the unbonded steel braces to verify the results of the theoretical prediction on the stability of the braces and to examine the inelastic capacity of the braces under severe earthquakes. Different cross sections and steel grades were used. They found that the most critical stability mode was the plastic torsional buckling of the inner core. They concluded that the flange of the yielding portion should have a width-to-thickness ratio of 5, if the yielding portion extends outside the confining core. They concluded that the unbonded brace is a reliable alternative to conventional braces in the way they provide rigidity to the structure to control story drifts and dissipate energy to enhance structural response under earthquakes.

The unbonded steel braces have been used in many structures in the United States [Black et al. (2004)]. One hundred and thirty two unbonded steel braces were used for the Plant and Environmental Sciences Building in the University of California in Davis. The building is a three-story steel structure with a basement with an area of 125,000 ft². For retrofitting the Marin County Civic Center Hall of Justice in County of Marin in California, 44 unbonded steel braces were used. The building is 6-story reinforced concrete structure with an area of 600,000 ft². Three hundreds and forty four unbonded steel braces were installed for the Wallace F. Bennett Federal Building in Salt Lake City in Utah. The building is 8-story reinforced concrete with an area of 300,000 ft².

2.2.2 Velocity-dependent Devices

2.2.2.1 Viscoelastic Dampers

The viscoelastic dampers were first applied to structures in 1969 in the twin towers of the World Trade Center in New York City, New York to reduce motion under wind loads. Another use of the viscoelastic dampers was in the Columbia Seafirst Building. This Columbia Tower is a 76-storey building rising to a height of 938 ft. above ground level. To reduce the wind-induced motions, the designers used 260 viscoelastic dampers to be installed alongside the main diagonal bracing members in the core of the building. Viscoelastic dampers typically consist of a solid viscoelastic material sandwiched between steel plates. Energy is dissipated through large shear strains in the viscoelastic material. Implementation of viscoelastic dampers causes a small increase in structural stiffness due to the inherent storage stiffness of the viscoelastic material. One of the primary advantages of the viscoelastic dampers is that they dissipate energy under all levels of ground motion.

2.2.2.1.1 Configuration of Viscoelastic Damper

The typical configuration of the viscoelastic damper is as shown in Figure 2.7, which is constructed from two viscoelastic layers bonded by three rigid surfaces. The damper is placed in the structure where vibration is expected to cause shear deformations in the viscoelastic material.

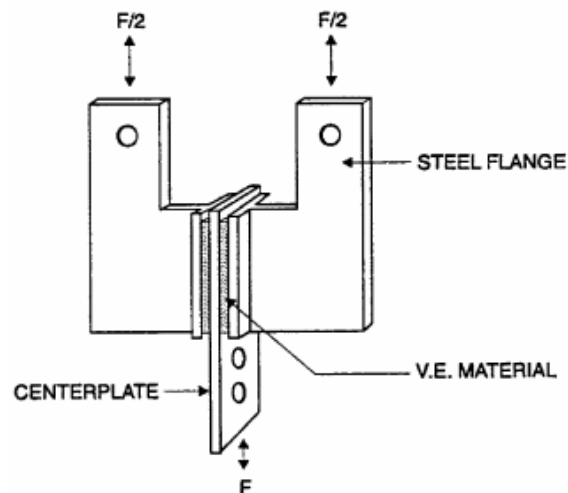


Figure 2.7: Typical viscoelastic damper

2.2.2.1.2 Design of Viscoelastic Dampers

The behavior of the viscoelastic damper is greatly influenced by different factors. These factors are the environmental temperature, the number of load cycles, the amount of strain and the excitation frequency. The temperature should be considered in two ways; the environmental temperature and the rise in temperature within the material due to the cyclic loads. Mahmoodi (1969) performed a series of tests to investigate the effect of temperature on the behavior of viscoelastic materials. He found that the energy dissipation by the viscoelastic material per one cycle varies inversely with the temperature. Also, he observed that the relationship between the temperature and the number of load cycles is linear in the first 100 cycles and after about 400 cycles, the relationship can be considered constant. The results of the experiments indicated that only 2-4 % of the energy dissipated by the viscoelastic dampers is stored in the material, which means that the generated heat in the viscoelastic material is dissipated quickly so that the temperature of the viscoelastic material does not rise to high values.

The main goal of using the viscoelastic dampers is to dissipate energy from the vibrating structure. It is recommended in the design of viscoelastic dampers that the dampers dissipate energy as much as possible to reduce the damage of the surrounding elements. Samali and Kwok (1995) summarized the research work relevant to viscoelastic dampers and identified the factors that can improve their performance.

For a viscoelastic material subjected to a sinusoidal shear loading, the total energy dissipated in one cycle can be calculated from [Samali and Kwok (1995)]

$$E_T = \pi \gamma_0^2 G'' V \quad (2-8)$$

where γ_0 is the shear strain, V is the volume of viscoelastic material, and G'' is the shear loss modulus, which can be obtained from:

$$G'' = G' \tan \delta \quad (2-9)$$

where G' is the storage shear modulus, and δ is the phase angle between the shear stress and strain.

According to equation (2-8), Samali and Kwok (1995) indicated that the parameters that can improve the effectiveness of a viscoelastic material in viscoelastic dampers are the shear strains and volume of viscoelastic material. The following comments were presented:

- viscoelastic dampers should be placed in locations that are subjected to large deformations in order to increase the shear strains developed in the viscoelastic material. In practical applications, there are only few locations, which are suitable for placing dampers. Hence, increasing the effectiveness of viscoelastic dampers through increasing shear strains is limited.
- Any increase in the viscoelastic volume should be considered along with the stiffness requirement and the thermal properties of the system. Any change in the volume of the viscoelastic material, whether through the shear area, thickness or width, will affect the stiffness of the damper. The energy dissipation through the viscoelastic material to the surrounding environment depends on the viscoelastic material thickness, the available heat conduction area, and the overall thermal conductivity of the system.

2.2.2.2 Viscous Fluid Dampers

Recently, viscous fluid dampers were widely used in structures as passive control devices. The energy is dissipated through the viscous fluid dampers by moving a piston that forces a viscous fluid through orifices in the piston head. The force developed in the damper is proportional to the velocity of the moving piston.

2.2.2.2.1 Types of Viscous Dampers

Viscous dampers dissipate energy through the moving of a body in a viscous fluid. Different ideas have been developed having the same concept in order to improve the response of buildings under seismic and wind loads. One design approach of viscous dampers is to dissipate energy through the conversion of mechanical energy to a heat. This can be applied through deforming highly viscous substance by a moving piston (Schwahn and Delinic, 1988). An example of this type is shown in Figure 2.8 a. Another design approach depends on moving a viscous damping wall in its plane through a viscous fluid contained in a narrow rectangular steel container [Miyazaki and Mitsusaka (1992)]. The wall is attached to the upper floor while the container is fixed to the lower floor. Figure 2.8 b shows an example of this type. The most common type of viscous dampers is shown in Figure 2.8 c. In this type, the energy dissipation is developed through a moving piston that forces a fluid to pass through small orifices around and through the piston head [Constantinou et al. (1993), Constantinou and Symans (1993)]. Fluid velocity is very high in the other side of the piston head, thus the upstream pressure energy converts almost entirely into kinetic energy. Accordingly, the fluid expands into the full volume on the other side of the piston head and slows down and then loses its kinetic energy into turbulence. The difference in pressure between the upstream and downstream produces a large damper force.

2.2.2.2.2 Effect of Nonlinearity in Viscous Dampers

In general the force developed in a viscous damper can be determined by the following relation:

$$F = C \text{ sign}(V) |V|^N \quad (2-10)$$

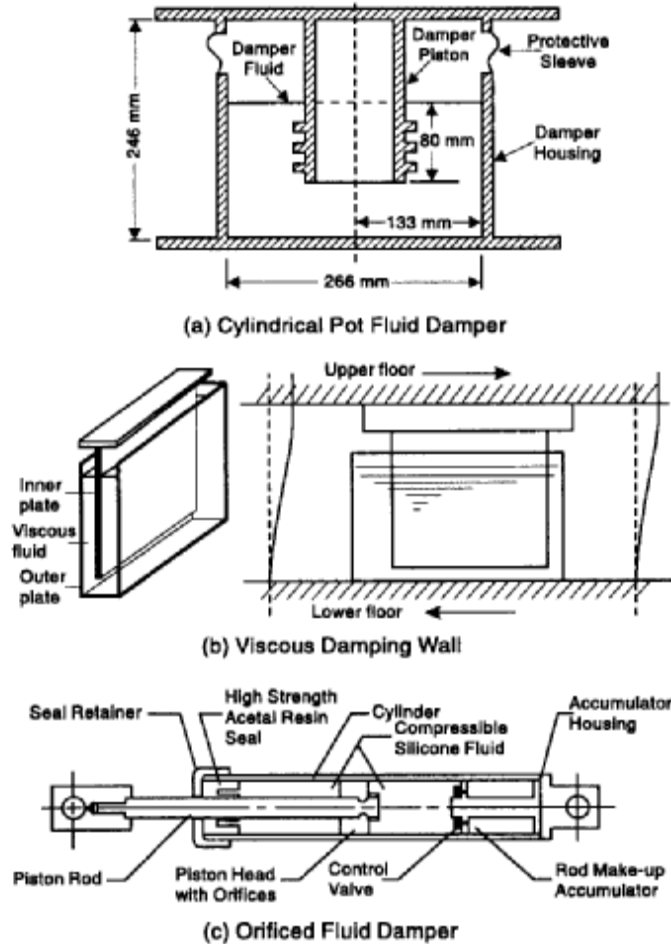


Figure 2.8: Different types of fluid viscous dampers. [Constantinou et al. (1998)]

where F is the damper force, C is an arbitrary constant, V is the relative velocity of the piston, and N is an exponent that can range from 0.3-1.95 and remains constant over the full range of velocities.

Figure 2.9 shows the relation between the force and the velocity for different values of damping exponent, N . A value of $N = 1.0$ represents the linear viscous damper. Figure 2.10 shows the hysteretic loops for both linear and nonlinear viscous dampers. Structural dampers usually have N values ranging from 0.3 – 1.0. The main advantage of the linear viscous dampers is that there is very little interaction between damper forces and structural forces. Maximum structural forces occur at maximum displacement, at which the damper forces are zero because the deformational velocity in the damper is near zero.

On the other hand, maximum damper forces occur at maximum velocity, at which the structural forces are near zero. The problem associated with linear viscous dampers is that the forces developed in these dampers and in the structure, they are connected to, can be beyond their capacities. Accordingly, the use of nonlinear viscous fluid dampers, with N around 0.5, is more appropriate in these cases because the damper force at high deformational velocity is limited.

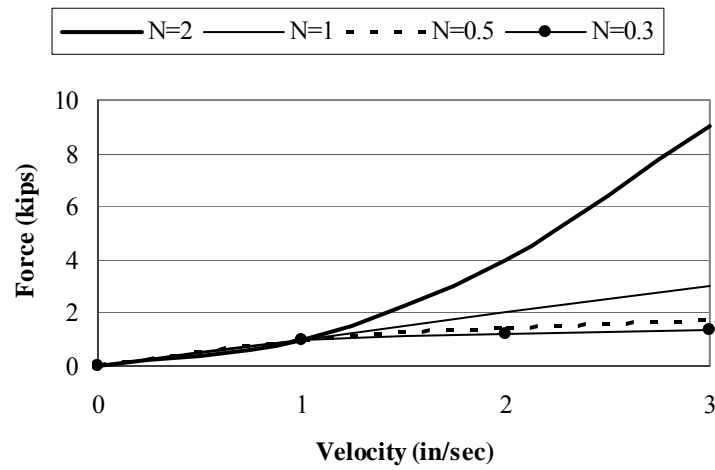


Figure 2.9: Force against velocity for different values of the damping exponent, N (C is constant)

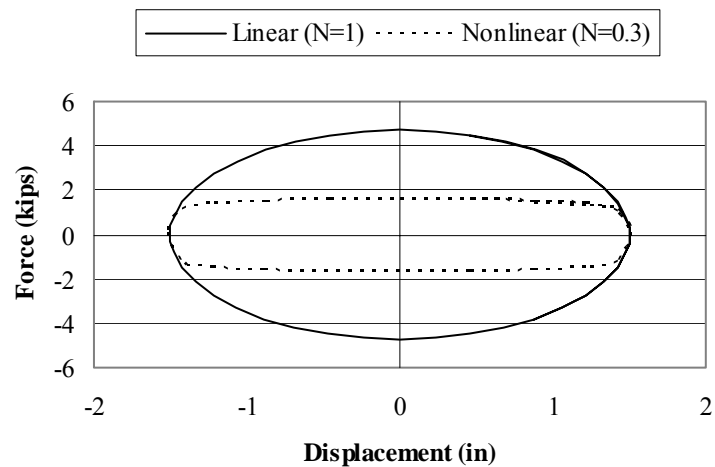


Figure 2.10: Hysteretic loops for linear and nonlinear dampers (C is constant).

Martinez-Rodrigo and Romero (2003) investigated the effect of linear and nonlinear viscous dampers on the response of a six-story, three-bay moment resisting steel frame under seismic loads. A pair of dampers was installed in the middle bay of each story. They presented a simple methodology for the optimal retrofitting of the structures with nonlinear viscous dampers. First, the optimality of linear viscous damper was based on achieving good performance in terms of FEMA 274 [FEMA (1997)] target displacement levels and minimizing the axial forces developed in the damper. Then, the optimality of nonlinear viscous dampers was based on the equal energy dissipation approach. According to the results of the nonlinear response history analysis, they observed that for large values of the nonlinear parameter, N , about 0.8 or 0.9, the envelope of the response remained almost constant while the damper forces were reduced from the linear damper case. They also concluded that if these devices are designed with moderate nonlinearity level ($N \cong 0.8$ to 0.9), the same good performance can be obtained as the case of linear viscous dampers but with a reduction of the damper forces more than 35 %.

Oesterle (2003) compared between linear and nonlinear viscous fluid dampers to determine which is most suitable for structures subjected to certain ground motions (near-field or far-field). He used the Incremental Dynamic Analysis (IDA) approach to assess the performance of fluid viscous dampers when attached to structures subjected to ground motions. Damping exponent values of 0.5, 1.0 and 1.5 were used in the analysis. Structures with each type of damper were subjected to nonlinear inelastic time history analysis for 12 different ground motions. The following observations were obtained:

- Linear viscous dampers improved the structural response for both near-field and far-field ground motions.
- For structures with nonlinear dampers ($N=1.5$), when braces were not allowed to yield, dampers reduced drifts and damage, however, substantial increase in base shear demands was obtained.
- For structures where braces were not allowed to yield, nonlinear dampers ($N=0.5$) produced the least drifts and damage in most cases. Also, nonlinear dampers, with $N=0.5$, were the most effective in limiting the base shear produced when dampers were used.

- For structures with yielding braces, dampers with $N=1.5$ became less effective in reducing drifts. No detrimental effect was obtained for dampers with $N=0.5$ upon allowing brace yielding.

2.2.2.3 Effectiveness of Viscoelastic and Viscous Fluid Dampers

Both viscoelastic and fluid viscous dampers improve the response of structures under different dynamic loads. Viscoelastic dampers provide stiffness and damping while viscous fluid dampers provide damping only under conditions of low-frequency movement.

Chang et al (1991) showed that viscoelastic dampers are very effective in reducing the response of tested structures due to the seismic excitations. They noticed that at 77°F, the viscoelastic dampers reduced the response by 80 %, while at higher temperatures (107°F) the dampers were still able to reduce the response by 40 %.

Viscoelastic dampers are typically placed in structures in temperature-controlled environment so the performance of viscoelastic dampers will not be affected due to environmental temperature change.

Munshi (1997) studied the effect of viscoelastic dampers on the hysteretic response, ductility and energy dissipation of reinforced concrete elements. He carried out parametric studies using the fiber element of the DRAIN-2DX [Powell (1973)] program to simulate the stiffness degradation, strength decay and pinching effects of the reinforced concrete elements. The study was based on SDOF systems with periods of 0.5, 1.0 and 2.0 seconds. The viscoelastic damper behavior was simulated by using Munshi's nonlinear element based on the fractional derivative approach. The results of the study showed that the viscoelastic dampers significantly decrease the curvature demand of the plastic hinges which helps in reducing the effect of the stiffness degradation, strength decay and pinching on the reinforced concrete elements. He found that increasing the viscous damping ratio of the system reduces the energy dissipation demand on the reinforced concrete elements. The study indicated that increasing the viscous damping

ratio is beneficial to a certain limit beyond which it has no effect on the energy dissipated by the viscoelastic dampers. It was noticed that the optimum damping ratio depends on the period and the design ductility ratio of the system.

To compare viscoelastic dampers and viscous fluid dampers, Fu and Kasai (1998) derived mathematical expressions for viscoelastic and viscous damper-brace components. They studied the seismic performance of a 10-story steel frame incorporating viscoelastic or viscous dampers. They found that the systems with viscoelastic dampers gained both stiffness and damping, whereas the systems with viscous dampers gained damping under conditions of low frequency movement. The results showed that both systems had the same effect on column axial force if they provided the same damping ratio. They found that if exposed to the same deformations, viscously damped systems perform slightly better than systems with viscoelastic dampers because viscous fluid dampers can deform more than viscoelastic dampers. However, for the same added damping ratio, systems with viscoelastic dampers perform better.

Lin et al. (1991) conducted an experimental investigation to determine the effectiveness of viscoelastic dampers. The experiment was performed using a $\frac{1}{4}$ -scale model structure to simulate the MDOF frame structure. By proper bracing, a SDOF was also simulated. The results showed that for the SDOF case, the response reduction was 87 % for the relative displacement and 60 % for the absolute acceleration, while for the MDOF with the best damper configuration, the reduction was 80 % for the relative displacement, 70 % for the story drift and about 50 % for the absolute acceleration. The results indicated the dependency of the properties and the effectiveness of the viscoelastic damper on the environmental temperature. Regarding the damper positioning, they concluded that the diagonal placement is the best for the SDOF systems while for MDOF systems they recommended considering the optimal placing of a limited number of viscoelastic dampers.

Lin and Chopra (2003) investigated the earthquake response of elastic SDOF systems with nonlinear viscoelastic damper. The damper consisted of a nonlinear fluid viscous

damper connected in series with a linear elastic brace. They found that the nonlinear viscoelastic dampers were advantageous because they provided the same reduction in the response but with much smaller damper forces comparing to the linear dampers. The reduction in the response depended on the bracing stiffness. They presented a procedure to estimate design values of structural deformations, structural forces, base shear and damper forces directly from the earthquake design (or response) spectrum. Also, they presented a procedure to determine the damper and braces properties necessary to limit the structural deformations to predetermined design values.

2.2.2.4 Optimization of Viscoelastic and Viscous Fluid Dampers

Over the past few years, many researchers considered the optimization of viscous and viscoelastic dampers in order to get the best performance of structures using these dampers. Zhang and Soong (1992) developed a sequential procedure for optimally placing viscoelastic dampers in structures. The method was based on the concept of degree of controllability. They verified the method experimentally through a five-story steel model structure [Chang et al. (1991)]. To apply the method, they carried out a numerical example of a ten-story steel frame. It was shown that for the ten-story frame, a saving of 2-5 dampers could be obtained when considering the story drifts as the criterion of the response reduction. According to the results of the experimental and numerical examples, they found that the economical use of the viscoelastic dampers could be obtained by placing the dampers at the optimal locations found by the procedure. They presented a design procedure that can determine the damper dimensions, number and locations needed to achieve the desired additional damping according to the structural parameters, and the structural response reduction requirements. They presented a design for the viscoelastic dampers for a 24-story steel frame as an example for the design procedure. The distribution of the viscoelastic dampers is shown in Figure 2.11.

From practical point of view, there are many uncertainties to validate a certain optimum placement of dampers in structures. The optimization in dampers configurations is based on a certain ground motion that will not occur again. Moreover, the structure is assumed to behave elastically, which will almost certainly not be true especially under strong ground motions.

Shukla and Datta (1999) investigated the control of the seismic response of multistory building frames using optimally placed viscoelastic dampers. The responses were obtained in the frequency domain using spectral analysis for narrow and broadband stationary random ground motions. To determine the optimal location of the dampers, a controllability index, based on the root-mean-square value of the inter-story drift, was used. They considered three mathematical models for the viscoelastic dampers, which are linear, Kelvin and Maxwell models. Three alternative schemes of damper placement were

studied. To apply the proposed strategy of optimization, they considered twenty-story shear frame models with the viscoelastic dampers. The results showed that the scheme with optimally placed dampers provides more reduction in story drifts than other schemes. They found that the optimal placement of dampers was sensitive to the nature of the excitation force, total quantity of viscoelastic material used, and the modeling of the viscoelastic damper.

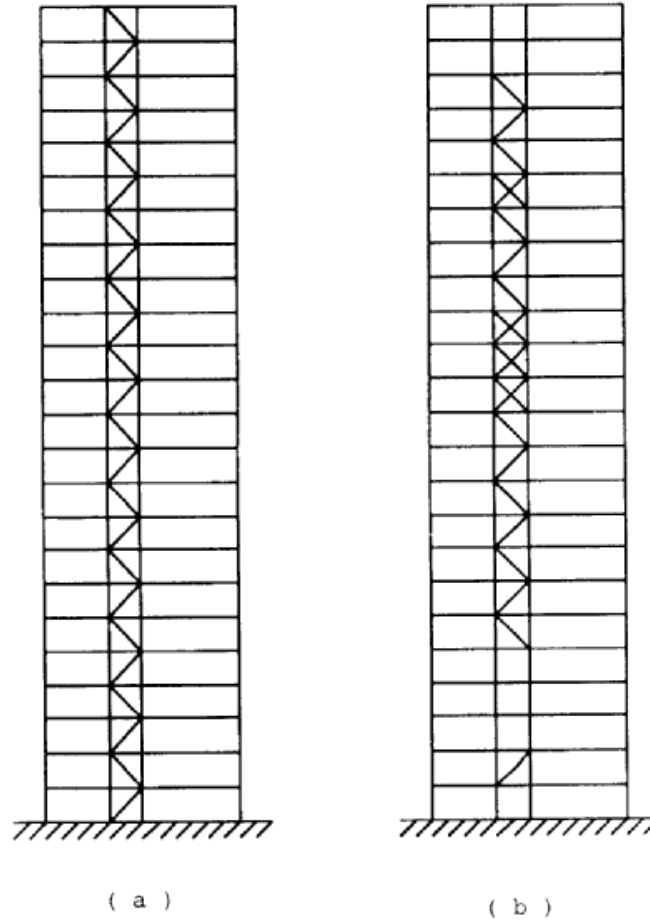


Figure 2.11: Distribution of viscoelastic dampers: a) fully damped; and b) 22 optimally placed

Singh and Moreschi (2001) presented a method to obtain the amount of viscous and viscoelastic damping required for an elastic structure to obtain the desired response reduction. The required supplemental devices were also optimally distributed in the structure. The method was based on a gradient-based optimization approach. To check the applicability of the proposed method, numerical results of a 24-story building were

presented. The reduction of response was expressed in terms of inter-story drift, base shear, or floor acceleration.

Singh and Moreschi (2002) presented a genetic algorithm to determine the optimal size and location of the frequency-dependent and independent viscous dampers as well as the viscoelastic dampers. The genetic approach was used to calculate the required number of a given capacity dampers and their optimal placement locations in a building to achieve the desired reduction in the structural response. According to the genetic approach presented, the response reduction can be expressed in terms of many functions such as base shear, bending moment at column bases, or floor acceleration. To illustrate the applicability of the genetic approach, they presented some numerical results for a shear-building model and torsional-building model with three types of damping devices. The shear building was a 24-story building with non-uniform structural properties. The details of this building are shown in Chang et al. (1991). The second building was six-story torsional building. The stiffness and mass center of the building were not coinciding. The structures were assumed to be elastic assuming the added viscoelastic dampers were designed to prevent inelastic deformations.

Xu and Teng (2002) investigated the optimal placement and optimal parameters of active and passive control devices using the linear quadratic performance index as an objective function. They suggested the suboptimal control gain to compute the seismic response of a tall building with a certain amount of control devices at their optimal positions. They investigated an 18-story two-dimensional linear elastic shear building under N-S 1940 El-Centro earthquake and the artificial Shanghai ground acceleration, which contains significant energy at low frequencies. According to the results of the numerical examples, the suggested approach was considered accurate and effective in determining the optimal parameters of the control devices when limiting the number of removed control devices to a certain range.

It is worth noting that in most of the attempts for optimizing the behavior and placement of dampers, the structures were assumed to be elastic assuming the use of adequate

dampers. This assumption may be valid for low levels of vibrations. However, for relatively large levels of vibrations, some structural elements will undergo inelastic deformations. Also, the optimized placement of dampers under certain ground motion may not be good for other ground motions. Accordingly, from practical point of view, the traditional distribution of dampers, e.g. devices placed at all levels, is usually used.

2.2.2.5 Some Applications of Viscoelastic and Viscous Fluid dampers

Due to the effectiveness of the viscous fluid and viscoelastic dampers in reducing the response due to the seismic excitations and the wind loads, many buildings were constructed with these dampers. One of the most famous buildings in the world, the World Trade Center, New York 1969, had about 20,000 viscoelastic dampers in the two towers. The viscoelastic dampers were used to increase the resistance of the tubular steel frame against the wind-induced building oscillations. The dampers were distributed throughout the building from the 10th to the 110th floor. Mahmoodi et al (1987) presented the configuration and the position of these dampers.

Another use of the viscoelastic damper was in the Columbia Seafirst Building [Keel and Mahmoodi (1986)]. This 76-story building rises to a height of 940 ft above ground. To reduce the wind-induced motions, 260 viscoelastic dampers were installed alongside the main diagonal bracing members in the core of the buildings.

A three-story reinforced concrete structure was upgraded by viscoelastic dampers [Soong et al. (1997)]. The building is located in San Diego, CA. The lateral load resisting system was based on 8-in. reinforced concrete walls on the perimeter of the building. The results of seismic analysis of the building showed insufficiency of resisting against expected seismic loads. Accordingly, a seismic upgrade with an objective of reducing story drifts was carried out using 64 viscoelastic dampers. Each damper consisted of four dampers forming a *K*-brace configuration.

In 1995, viscous fluid dampers were used in the base isolation systems for the San Bernardino Medical Center in California. The five-story building is close to two major faults. One hundred and eighty six nonlinear fluid dampers having an output force of 315 kips and stroke of ± 24 in. were used [Soong et al. (1997)].

Uriz and Whittaker (2001) studied the use of linear fluid viscous dampers for the seismic retrofit of a three-story, pre-Northridge steel-framed building. Ten earthquake histories representing design-earthquakes shaking in Los Angeles and two earthquake histories

representing maximum-earthquake shaking in Los Angeles were used for the nonlinear dynamic analysis. The performance objective used for the retrofitted building was zero plastic rotation in the beam during the design earthquake shaking as given by the 1997 NEHRP recommended provisions [FEMA-274 (1997)]. They concluded that using fluid viscous dampers only for retrofitting the steel frames does not eliminate beam plastic rotation unless excessive levels of damping are added to the structure. The addition of approximately 40 % damping to the steel frame led to substantial reduction in displacements and plastic rotations but resulted in large increase in story shears and column axial forces.

A total of 170 viscous damping walls were used for seismic protection in a building in Shizuka City, Japan [Miyazaki and Mitsusaka (1992)]. The building consists of a 14-story above-ground steel frame structure, along with a two-story reinforced concrete basement. The effective damping ratio of the building was increased to approximately 27%. Based on time history dynamic analysis, the damping walls reduced floor displacements by 70-80%.

2.2.3 Dampers Installation in Structures

2.2.3.1 Different Locations of Dampers

The dampers can be installed in different locations in a building in order to improve the performance under different dynamic loads. The possible locations of the dampers in structures are:

A) In parallel with base isolators

This is useful for structures where there are large displacements at the base.

B) Diagonal member

The damper can be installed like a conventional diagonal brace. This type is effective for refurbishments.

C) Chevron brace

The damper can be installed in both legs of a chevron brace. This configuration has the same effects as the diagonal members.

D) Horizontally at the top or bottom of a chevron brace

The damper can be installed horizontally to a conventional chevron brace, whether at the top or bottom of the brace.

E) Horizontally between adjacent structures.

If there are two structures very close to each other, the damper can be installed horizontally between them to prevent pounding.

F) Toggle brace

The basic idea behind this system is that the damper is placed diagonally and linked to two steel linkage elements, which are not collinear. Accordingly, any small interstory drift is amplified in the direction of the damper, which increases the effect of the dampers (Figure 2.12). Toggle-brace-damper systems were used recently in the United States. Reverse-toggle-brace-damper systems were used in the 37-story Yerba Buena tower in San Francisco and the 37-story Millennium Place in Boston for reducing the wind-induced vibrations [Constantinou et al. (2001)]. Charney and McNamara (2002) applied the same idea in order to reduce the dynamic response of 39-story office building by using viscous fluid dampers in a toggle-brace configuration.

G) Scissor-Jack configuration

This configuration utilizes also the idea of amplifying the deformations in the direction of the damper drift in order to increase its effectiveness [Sigaher and Constantinou (2003)]. The configuration of this system is shown in Figure 2.12. They performed experimental test on a steel frame with the scissor-jack-damper system. The frame was subjected to sinusoidal movement with different frequencies and amplitudes at the beam-column connection. Amplification factors of 2.9 (damper is under compression) and 2.5 (damper is under tension) were obtained under low loading frequency (quasi-static conditions; $\omega = 0.01$ HZ). Under high loading frequency, dynamic conditions, amplification factors were reduced to be 1.9 and 1.6 when the damper was under compression and tension, respectively. A half-scale one-story steel model frame with the scissor-jack-damper system was tested on the earthquake simulator under different ground motions. The results showed significant increase in the damping ratio, which led to a reduction in drift and acceleration responses. The scissor-jack-damper system caused an increase in the frame stiffness as well.

2.2.3.2 Comparison between the Effectiveness of Dampers for Different Placements

Same dampers can have different effects on structural response under vibrations if they are placed differently. A comparison was made theoretically between the different placements of a viscous fluid damper in a single-story steel frame as shown in Figure 2.12 [Constantinou et al. (2001) and Sigaher and Constantinou (2003)].

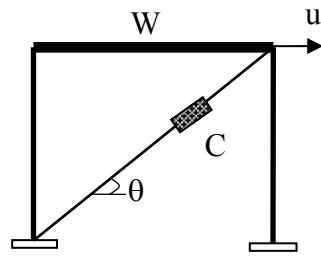
Assuming the interstory drift is denoted by u , the relative displacement developed in the damper can be obtained from:

$$u_D = f u \quad (2-11)$$

where f is the amplification factor.

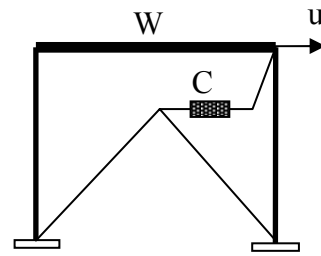
The horizontal component of the damper force exerted on the frame is F , where

$$F = f F_D \quad (2-12)$$



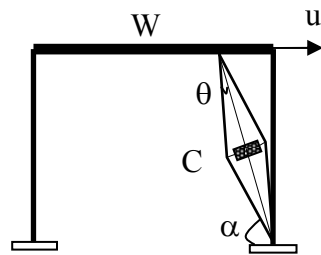
$$\begin{aligned}\theta &= 37^\circ \\ f &= \cos\theta = 0.80 \\ \beta &= 0.03\end{aligned}$$

a) Diagonal



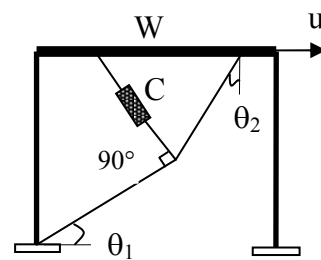
$$\begin{aligned}f &= 1.0 \\ \beta &= 0.05\end{aligned}$$

b) Chevron



$$\begin{aligned}\theta &= 9^\circ, \alpha = 70^\circ \\ f &= \frac{\cos\alpha}{\tan\theta} = 2.16 \\ \beta &= 0.23\end{aligned}$$

c) Scissor Jack



$$\begin{aligned}\theta_1 &= 31.9^\circ, \theta_2 = 43.2^\circ \\ f &= \frac{\sin\theta_2}{\cos(\theta_1 + \theta_2)} + \sin\theta_1 \\ f &= 3.19, \beta = 0.51\end{aligned}$$

d) Upper Toggle

Figure 2.12: Different damper placements and their effectiveness

where F_D is the damper force, which can be obtained from:

$$F_D = C \dot{u}_D \quad (2-13)$$

where C is the damping constant of the viscous damper.

Then,

$$F_D = C f^2 \dot{u} \quad (2-14)$$

Hence, the damping ratio can be obtained from:

$$\beta = \frac{C f^2 g T}{4\pi W} \quad (2-15)$$

where W is the weight of the structure.

Figure 2.12 shows the different amplification factors and damping ratio of the structure with different damper placements [Sigaher and Constantinou (2003)]. The calculations were based on assuming 5 % critical damping in the case of horizontal damper (Chevron brace) and the damping ratios of the other systems were calculated relative to this value.

Although toggle-brace configuration has the largest damping ratio, its efficiency may be dropped because of the phase difference between the deformational velocity in the device and the story velocity, to which the device is connected. Accordingly, the damping forces are not 90° out of phase with the structural forces. This leads to developing large axial forces in linkages, which develops high forces in the structure itself.

According to this comparison, the placement of the damper in the scissor-jack leads to a significant increase in the damping ratio compared to the conventional configurations (horizontal or diagonal) due to the amplification of the story drift. The same idea is utilized in the visco-plastic device, which is presented in this research. However, in the visco-plastic device, a viscoelastic material is sandwiched between two pre-buckled steel shapes to amplify the deformations developed along the device axis. The energy is dissipated through amplified axial strains in the viscoelastic material in addition to the yielding of the steel elements, when exposed to large deformations.

2.3 Summary

One of the main goals of designing passive energy systems is to obtain an optimum balance of added damping and stiffness. Unfortunately, it may be difficult to obtain such a balance because the damping and stiffness component of the device may not be

independently controlled by the designer. The device proposed in this research overcomes this disadvantage by providing a sufficient number of parameters such that both the stiffness and the energy dissipative characteristics of the device can be controlled. Moreover, the visco-plastic device shares many of the advantages of existing passive damping devices, such as the fabrication in existing shops from readily available materials, dissipating energy under different levels of vibrations through amplified strains and interstory-drift amplification. It works as a viscoelastic damper at low levels of excitation, and for extreme levels of vibration, operates as a combined viscoelastic and metallic yielding device.

Chapter 3: Rubber Compounds

3.0 Introduction

Rubber has many advantages that made it useful in a variety of engineering applications such as tires, building foundation, dampers, base isolators, and automotive engine components. Rubber can deform elastically to very large deformations and return to its original shape after load removal. Moreover, rubber has the ability to dissipate energy when exposed to dynamic strains.

Crude rubber, obtained from rubber trees, is not a good material to be used in its natural form. It needs chemical processing as well as incorporating some additives to enhance its different properties. In this section, some rubber processes (compounding and vulcanization) are defined briefly. Also, different rubber compounds are presented showing their advantages and disadvantages as well as the suitable application for each compound. Finally, the properties of fillers, mainly carbon black, and how they can enhance the rubber properties to achieve the desired performance are discussed.

3.1 Compounding

Compounding is the process by which crude rubber is modified to obtain required properties and be suitable for specific applications. Compounding is basically conducted through:

- Curing or vulcanization
- Adding certain fillers

Compounded rubber has many important characteristics, such as high elasticity, high damping capabilities and abrasion resistance.

3.2 Vulcanization

Vulcanization is related to Vulcan, the Roman God of fire. It is the process by which soft compounded rubber materials are converted to high-quality engineering products. In this process, the permanent deformation after load removal is decreased. Hence it increases rubber elasticity and reduces rubber plasticity.

The process is conducted by inserting crosslinks between adjacent polymer chains in the compound. The crosslink is typically a group of sulfur atoms in a chain, or a single sulfur atom. The vulcanization is carried out by heating the rubber mixed with sulfur, as vulcanizing agent, in a mold under pressure. The rubber compounds that are subjected to this process are called rubber vulcanizates.

3.3 Properties and Application of Basic Crude Rubber Types

There are different types of crude rubber. Each type has its own advantages and disadvantages and accordingly is used for specific applications. The attention is directed towards the most widely used types; natural rubber, styrene butadiene rubber and neoprene.

3.3.1 Natural Rubber (NR)

NR is available in various types and grades including air-dried and smoked sheets. NR vulcanizates are well known for their high tensile strength over a wide hardness range. Accordingly, NR can be used in unfilled compounds. Also, NR vulcanizates have very low heat buildup because of the very high resilience. Moreover, NR has many other advantages like good resistance to abrasion, tear, and fatigue, as well as low compression set and stress relaxation. On the other hand, NR is susceptible to atmospheric ozone attack and has low resistance to petroleum-based oils and fuels. In general, NR elastomers are the best choice for applications that require low heat buildup such as tires, vibration mounts and shock absorbers.

3.3.2 Styrene Butadiene Rubber (SBR)

SBR is a copolymer of butadiene and styrene. Generally, SBR can be compounded in the same way as NR. The tensile strength of unfilled SBR compounds is very poor (about 10-15 % of NR compounds tensile strength). However, higher tensile strength can be obtained through reinforcing by fillers. Comparing to NR, SBR compounds have higher abrasion and lower fatigue resistance. Like NR, SBR vulcanizates have low resistance to atmospheric ozone attack and petroleum based oils.

In general, SBR can be used as an alternative for NR in many applications. However, for applications, which require low heat buildup, SBR compounds are not recommended.

3.3.3 Neoprene (CR)

Neoprene is a homopolymer of chloroprene. Neoprene is a versatile synthetic rubber that was originally developed as an oil-resistant substitute of NR. Neoprene compounds typically contain carbon black, mineral fillers or both. Neoprene has good resistance to ozone and weather. Also, it resists burning inherently and remains useful over a wide range of temperatures. In general, neoprene is inferior to NR regarding the mechanical properties, while it is superior in chemical properties. Neoprene elastomers are used in adhesives, hoses, shock absorbers, seals, and vibration mounts.

Table 3.1 shows different properties for natural rubber, styrene butadiene and neoprene. [Freakley (1978)]

Table 3.1: Comparison between rubber compounds

Property	Rubber Compound		
	Natural Rubber	Styrene Butadiene Rubber	Neoprene
Density (kip/in. ³)	0.0336	0.034	0.0444
Tensile strength for unfilled compound (ksi)	3.0	0.4	3.0
Tensile strength for filled compound (ksi)	3.0	3.0	3.0
% Elongation at break for unfilled compound	800	700	800
% Elongation at break for filled compound	< 600	500	< 600
Hardness	20-90	40-90	20-95
Tear resistance	Excellent	Fair	Good
Abrasion resistance	Excellent	Good	Excellent
Heat resistance	Good	Good	Excellent
Cost ratio (relative to SBR)	1.0-1.5	1.0	2.5

3.4. Rubber Reinforcement

Unfilled rubber is rarely used in engineering applications. Fillers usually increase the ultimate properties, such as tear, tensile strength and abrasion resistance. Moreover, filled rubber has higher modulus of elasticity. Many types of fillers, like silica, silicate, clays and other mineral fillers, are used to enhance rubber properties. However, the most well-known reinforcing filler is carbon black.

Carbon black is an industrial manufactured colloidal carbon material with spherical form. It is manufactured by thermal decomposition or by complete combustion of carbon hydrogen compounds. A brief description of the main carbon black properties and how they affect the rubber properties are presented in the following section.

3.4.1 Carbon Black Properties

There are many carbon black properties that affect the properties of an elastomer. These properties include the porosity, the aggregate size and the aggregate shape. However, according to Donnet et al. (1993), the main properties that determine its effect on the elastomer properties include:

- Particle size
- Surface area
- Hydrogen content
- Oxygen content

A brief description of each property as well as how it affects the elastomer properties will be presented.

3.4.1.1 Particle Size

Carbon black is commercially available with a wide range of particle sizes. This range may vary from particle size less than 200 Å as in super abrasion furnace (SAF) to particle size with diameter over 3000 Å as in medium thermal black (MT). The smaller the particle size of carbon black is, the more reinforcement provided to an elastomer. However it is hard to process the finer carbon blacks in the rubber factory.

There are many procedures to determine the particle size. One of the procedures that give improved measurements and now is a part of the ASTM D3849 method [ASTM (1990)] is the cellulose acetate butyrate procedure (CAB) [McDonald and Hess (1983)]. In this procedure, extensive breakdown of the carbon black aggregate occurs, which reduces the aggregate irregularity.

The average particle diameter, d , for each individual aggregate is derived as

$$d = \alpha \left(\frac{\pi A}{P} \right) \quad (3-1)$$

where A is the projected aggregate area, P is the perimeter, $\pi A/P$ represents the mean chord or average width of aggregate, and α function is determined from the circulatory factor, P^2/A .

The number of particles in each aggregate may be approximated as [Donnet et al. (1993)]

$$n = \frac{V_A}{V_P} \quad (3-2)$$

where V_A is the calculated aggregate volume and V_P is the particle volume assuming spherical shape.

3.4.1.2 Surface Area

The effect of carbon black on rubber properties is controlled by the total area of carbon black surface that is exposed to the polymer, its activity per unit area of the sulphur towards the polymer and its ingredients. Surface area can be calculated from the electron microscope procedure (ESMA) [ASTM (1990)]. In this procedure, the specific surface area is derived directly from the surface mean diameter, d_{sm} , as:

$$S(m^2 / g) = \frac{6000}{\rho d_{sm}} \quad (3-3)$$

where S is the specific surface area in m^2/g , ρ is the carbon black density in gm/cm^3 , and d_{sm} in nanometers.

3.4.1.3 Hydrogen Content

High temperatures are used in the formation of carbon black which yields to the dehydrogenation of the fuel and the newly formed carbon black properties. Hydrogen content varies in different carbon black types. It can be as low as 0.07 % like in acetylene black while it may reach 0.6 % as easy processing channel (EPC) carbon black. However, the hydrogen content normally ranges from 0.2 to 0.35 % by weight. As the hydrogen content increases, the chemical reactivity per unit of carbon black surface toward oxygen and sulphur increases [Studebaker (1957)]. Oxygen content reduces the reactivity of the carbon black toward further reaction with oxygen. For a sample of carbon black with a particular specific area after a given type of treatment, the hydrogen content determines its oxygen content.

3.4.1.4 Oxygen Content

The oxygen content is determined by the specific area of the carbon black, the hydrogen content and the history of the sample, e.g. the temperature and the period of the time under which it has been exposed to oxidizing gases [Kraus (1965)]. Around 25% of the oxygen is present as quinone-type oxygen, which controls the carbon black behavior towards vulcanizing agents. This type of oxygen is very important in determining the modulus properties.

3.5 Effect of Carbon Black on Rubber Properties

3.5.1 Modulus

Young's modulus is defined as the slope of the stress-strain curve in the linear elastic range. In rubber compounds, the stress-strain curve is linear for small strains (usually less than 15 %). Accordingly, for higher strains, other moduli are used to describe the stress-strain relationship. Commonly, there are two moduli used when considering rubber compounds. These moduli are the modulus of first extension, normally at high elongation like 300%, and the final modulus, which indicates the extent of crosslinking. Hence, the term "modulus" refers to the stress required to obtain certain strain of say 100 % or 300 %. Carbon black vulcanizates are permanently softened by extension and this

phenomenon is known as “the Mullins effect” [Mullins (1948) and Mullins (1950)]. As the filler loading (filler parts per hundred parts of rubber by weight) increases, more softening occurs. However, the first modulus is higher than that of the unfilled rubber compound. For filled rubber, the reason behind the lower modulus of the successive stretches can be related to [Donnet et al. (1993)]:

- Breakdown of secondary filler network
- Dewetting (deattachment) of rubber molecules from the filler surface.
- Rupture of the short chains between filler particles.
- Movement of aggregate, rotationally and otherwise.

In general, some observations were obtained regarding the effect of fillers, like carbon black, on the modulus values. These observations are [Kraus (1965)]:

- As the filler loading increases, the modulus increases rapidly. The relationship is nonlinear.
- The modulus decreases with decreasing carbon black particle size. This is more obvious in the 300% modulus than the 100% modulus values.
- Modulus value decreases with the increase in the oxygen content, especially the quinone-type oxygen content.

Figure 3.1 shows the relationship between the carbon black loading and Young’s modulus for natural rubber [Freakley (1978)].

Many attempts have been made to obtain a relationship between the modulus of unfilled and filled rubbers. Guth and Gold [Guth and Gold (1938)] proposed the following equation for young’s modulus using Einstein’s viscosity equation

$$E = E_g (1 + 2.5\phi + 14.1\phi^2) \quad (3-4)$$

where E and E_g are young’s modulus of filled rubber and gum, respectively and ϕ is the filler loading.

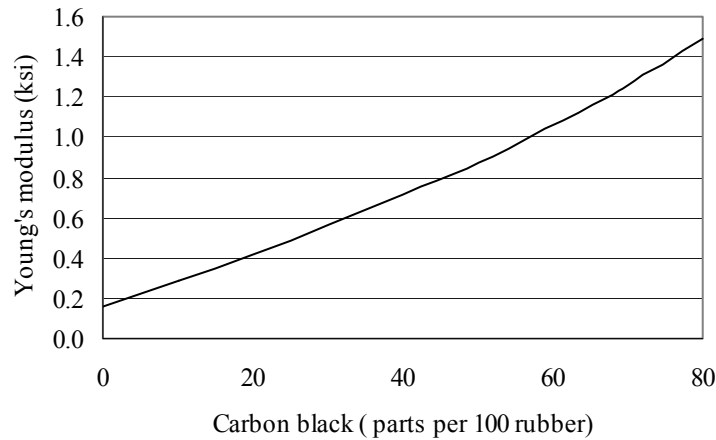


Figure 3.1: Effect of carbon black loading on Young's modulus for natural rubber

The equation is inadequate for reinforcing fillers, especially at filler loadings used in practice since it is based on spherical, well wetted particles ignoring any interaction between particles. Also, the effect of elastomer characteristics is not considered in the equation.

Guth (1945) proposed another equation to suit the practical applications assuming rod-shaped particles.

$$E = E_g (1 + 0.67 f \phi + 1.62 f^2 \phi^2) \quad (3-5)$$

where f is a shape factor. Many attempts [Meinecke and Taftaf (1995) and Ravey et al. (1970)] were done to get f values but no agreement was obtained.

3.5.2 Tensile Strength

The loading of carbon black has almost the same effect on tensile strength as does its surface area. As the carbon black loading increases, the tensile strength increases up to a certain level then drops at high loading values. The concentration at which the maximum tensile strength is obtained depends mainly on the particle size of the carbon black. For smaller particle sizes, maximum tensile strength is obtained at lower loading values. On the other hand, the higher the carbon black loading, the lower elongation at break is

obtained. The effect of carbon black loading on the tensile strength and elongation at break for natural rubber are shown in Figures 3.2 and 3.3, respectively [Freakley (1978)].

Regarding the crack growth, the filler plays a very important role in retarding cracks and dissipating energy since the crack path is increased. Cracks have to move around filler particles and this dissipates more energy. Carbon black surface is covered by a strong rubber shell, which gives it advantage over other fillers.

To achieve high strength, it is recommended that the interaggregate distance is not so large in order to allow developing harmless cracks with a small size within the matrix before another aggregate is met. This will dissipate more energy, which leads to higher strength. [Donnet et al. (1993)]

3.5.3 Energy Dissipation through Dynamic Strains

Rubber compounds are widely used in applications that are exposed to vibrations or dynamic loads in order to dissipate energy. The energy dissipation is mainly related to the rubber reinforcement. The energy is dissipated in rubber compounds due to both of the stress-softening effect and the dynamic strains.

For an elastomer subjected to a sinusoidal axial strain, the strain, ε and stress, σ can be expressed by

$$\varepsilon = \varepsilon_0 \sin(\omega t) \quad (3-6)$$

$$\sigma = \sigma_0 \sin(\omega t + \delta) \quad (3-7)$$

where ε_0 is the strain amplitude, ω is the stretching frequency, σ_0 is the stress amplitude, and δ is the phase angle between the stress and strain.

The stress can be expressed as in phase and out of phase stresses as

$$\sigma = \sigma_0 \sin(\omega t) \cos(\delta) + \sigma_0 \cos(\omega t) \sin(\delta) \quad (3-8)$$

The stress can be also expressed using the in phase modulus or elastic modulus, E' , and out of phase or viscous modulus, E'' , as:

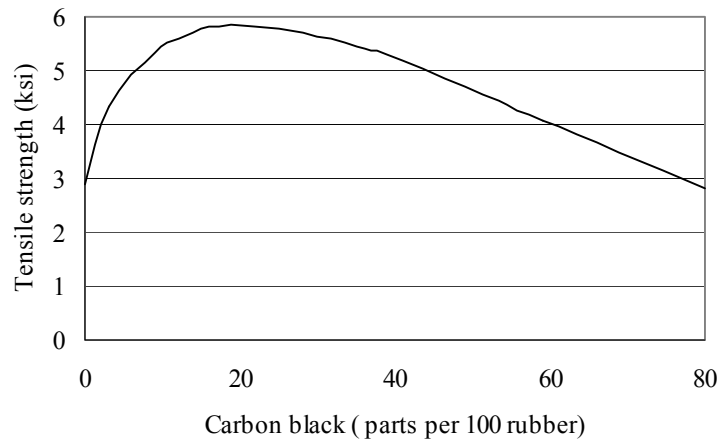


Figure 3.2: Effect of carbon black loading on tensile strength for natural rubber

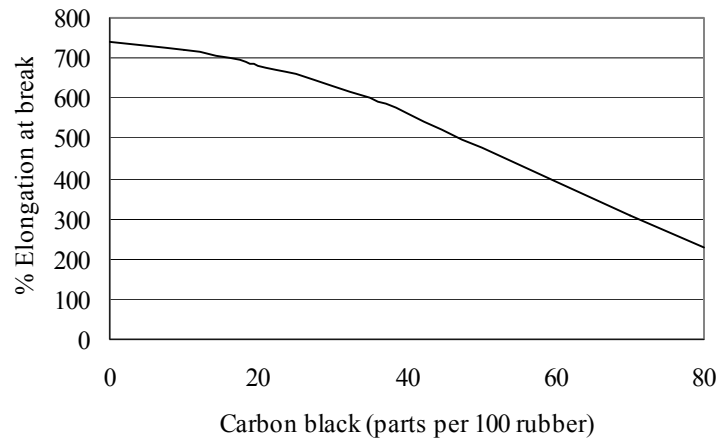


Figure 3.3: Effect of carbon black loading on elongation at break for natural rubber

$$\sigma = \varepsilon_0 E' \sin(\omega t) + \varepsilon_0 E'' \cos(\omega t) \quad (3-9)$$

where

$$E' = \frac{\sigma_0}{\varepsilon_0} \cos \delta \quad (3-10)$$

$$E'' = \frac{\sigma_0}{\varepsilon_0} \sin \delta \quad (3-11)$$

The energy loss is related to the viscous modulus, E'' . Accordingly, it is termed as loss modulus. The energy loss during one strain cycle per unit volume of the material, ΔE , is obtained from

$$\Delta E = \int \sigma d\varepsilon = \int_0^{2\pi\omega} \frac{\sigma d\varepsilon}{dt} dt \quad (3-12)$$

Accordingly,

$$\Delta E = \omega \varepsilon_0^2 \int_0^{2\pi\omega} (E' \sin \omega t \cos \omega t + E'' \cos^2 \omega t) dt \quad (3-13)$$

$$\Delta E = \pi \varepsilon_0^2 E'' \quad (3-14)$$

Thus,

$$\Delta E = \pi \sigma_0 \varepsilon_0 \sin \delta \cong \pi \sigma_0 \varepsilon_0 \tan \delta \quad (3-15)$$

with $\tan \delta = \frac{E''}{E'}$

Then,

$$\Delta E = \frac{\pi \sigma_0^2 E''}{E'^2 + E''^2} \quad (3-16)$$

According to the last equations, under constant strain amplitude, ε_0 , the energy loss is proportional to loss modulus, E'' , (equation 3-14) while under constant energy input, $\sigma_0 \varepsilon_0$, the energy loss is proportional to $\tan \delta$ (equation 3-16).

Considering the effect of fillers on the energy dissipation of rubber compounds, fillers increase both E' and E'' considerably. Since E'' represents the viscous modulus, equation (3-4) can theoretically be applied to E'' . However, that equation was based on hydrodynamics effects only while E'' represents other sources of energy dissipation such as interaggregate interaction, which depends on strain amplitude, filler loading and filler properties [Donnet et al. (1993)].

3.6 High-damping rubber

The need for a rubber compound with enough inherent damping led to the development of a high-damping rubber compounds by the Malaysian Rubber Producers' Research Association (MRPRA) of the United Kingdom in 1982 [Derham et al. (1985)]. The compound is obtained by adding extra fine carbon black, oils or resins, and other proprietary fillers to the natural rubber. The same method of vulcanization is used.

The inherent damping of high-damping rubber compounds may reach as high as 20 % at 100 % shear strains with a corresponding high hardness of 70-75 durometer and high shear modulus of 0.2 ksi.

Since developed in 1982, high-damping rubber compounds were used in many structures for seismic protection all over the world. The first building in the world to use high-damping rubber bearings for seismic isolation was the Foothill Communities Law and Justice (FCLJC) in the United States in 1984 [Tarics et al. (1984)]. The building is 13 miles away from the San Andreas Fault. The building is four-story with a full basement and it was designed to withstand an 8.3 magnitude earthquake. Ninety-eight bearings were used for base isolation.

Twenty eight high-damping rubber bearings were used in The Emergency Operations Center (EOC) in Los Angeles County. The building is two-story braced frame structure. The Los Angeles City Hall, constructed in 1928, is a 28-story steel frame. The total floor area is around 890,000 square foot. The hall was damaged in the 1994 Northridge earthquake. The building was retrofitted using 475 high-damping isolators in combination with 25 fluid viscous dampers for the isolation system and 12 fluid viscous dampers for the superstructure [Naeim and Kelly (1999)].

3.7 Energy Dissipation through Axial and Shear Strains

In most applications of rubber compounds in energy dissipation, like base isolators and viscoelastic dampers, the energy is dissipated through shear strains. In the proposed visco-plastic device, the rubber block is placed such that it is exposed to amplified axial strains. Hence, it is important to compare the energy dissipation through shear strains to that dissipated through amplified axial strains. According to equation (3-14), the energy dissipation per unit volume for one cycle of sinusoidal axial strain can be calculated from:

$$\Delta E = \pi \varepsilon_0^2 E'' \quad (3-17)$$

The loss modulus, E'' , can be obtained from equation (3-11), accordingly:

$$\Delta E = \pi \varepsilon_0^2 \frac{\sigma_0}{\varepsilon_0} \sin \delta \quad (3-18)$$

For small displacements (less than 100 %), the term $\frac{\sigma_0}{\varepsilon_0}$ can be replaced by the initial modulus of elasticity, E_0

$$\Delta E = \pi \varepsilon_0^2 E_0 \sin \delta \quad (3-19)$$

The total energy dissipation through one cycle of sinusoidal axial strain, E_a , can be obtained from:

$$E_a = \pi \varepsilon_0^2 E_0 \sin \delta V_a \quad (3-20)$$

where V_a is the volume of viscoelastic material exposed to axial strains.

Similarly, considering a rubber specimen under shear test, the shear stress and strain may be written as:

$$\gamma = \gamma_0 \sin(\omega t) \quad (3-21)$$

$$\tau = \tau_0 \sin(\omega t + \delta) \quad (3-22)$$

The shear stress can be re-written as:

$$\tau = \gamma_0 G' \sin(\omega t) + \gamma_0 G'' \cos(\omega t) \quad (3-23)$$

where G' and G'' are the storage modulus and loss modulus, respectively.

Accordingly, as before in axial strains, the energy dissipation per unit volume for one cycle under sinusoidal shear strain, ΔE_{sh} , can be calculated from:

$$\Delta E_{sh} = \pi \gamma_0^2 G'' \quad (3-24)$$

Hence, as shown before in the axial strains, the total energy dissipation through one cycle of sinusoidal shear strain, E_{shear} , can be obtained from:

$$E_{sh} = \pi \gamma_0^2 G_0 \sin \delta V_{sh} \quad (3-25)$$

where G_0 is the initial shear modulus, and V_{sh} is the volume of viscoelastic material exposed to shear strains.

Accordingly, for the same viscoelastic material, the ratio between the energy dissipated through axial strains per one cycle to that dissipated through shear strains per one cycle can be obtained from:

$$\frac{E_a}{E_{sh}} = \frac{\varepsilon_0^2 E_0 V_a}{\gamma_0^2 G_0 V_{sh}} \quad (3-26)$$

The relation between the initial modulus of elasticity and shear modulus is

$$E_0 = 2(1 + \nu)G_0 \quad (3-27)$$

where ν is the Poisson ratio; $\nu=0.5$ for rubber compounds.

Then,

$$\frac{E_a}{E_{sh}} = 3.0 \frac{\varepsilon_0^2 V_a}{\gamma_0^2 V_{sh}} \quad (3-28)$$

In order to compare the visco-plastic device, where energy dissipated through amplified axial strains, to the conventional viscoelastic dampers, where energy is dissipated through shear strains, assume both dampers are exposed to a horizontal harmonic deformation with amplitude of d_{HL} . Accordingly, the maximum shear strain developed in the viscoelastic damper is

$$\gamma_0 = \frac{d_{HL}}{t} \quad (3-29)$$

where t is the thickness of the viscoelastic material in the viscoelastic damper. Typical thickness of the viscoelastic material in these dampers is about 1.0 in.

Now, consider the visco-plastic device is deformed horizontally by d_{HL} , as shown in Figure 3.4, assuming an amplification factor of 2.5 is obtained, the maximum axial strain at the middle of the device (assuming uniform strains in the whole material) is obtained from:

$$\varepsilon_0 = \frac{5d_{HL}}{h} \quad (3-30)$$

where h is the thickness of the viscoelastic material at the middle of the device. As shown in the next chapter, h was selected to be 16 in.

Applying the last two equations with the mentioned values for the thickness of the viscoelastic material in both types of dampers in equation (3-28) results in:

$$\frac{E_a}{E_{sh}} = 0.29 \frac{V_a}{V_{sh}} \quad (3-31)$$

Given the fact that the volume of the viscoelastic material in the visco-plastic device is several times larger than the volume of the viscoelastic material in the conventional configuration of the viscoelastic dampers, the energy dissipated through axial strains may reach 2-3 times the energy dissipated through shear strains. Accordingly, placing the viscoelastic material in the proposed configuration is much more effective compared to its placing in the conventional configuration.

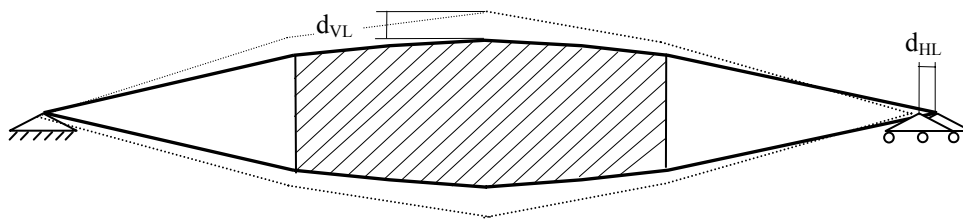


Figure 3.4: Deformations in the visco-plastic device (under compression)

3.8 Summary

In general, filled rubber compounds have better physical properties than unfilled rubbers. Many types of fillers can be used in reinforcing rubber, such as silica, silicate and clays. However, the most-used filler is the carbon black. There are many properties that affect the properties of filled rubber, such as the type of filler, filler loading, particle size and surface area of the filler.

In the visco-plastic device, a block of rubber is sandwiched between two steel shapes. Under low levels of vibrations, the energy dissipation through the device is mainly due to the axial strains in the rubber block only, however under higher levels of vibrations, the energy is dissipated through the steel yielding in addition to the axial strain in the rubber block. Accordingly, the device efficiency in energy dissipation depends primarily on the selection of the rubber type and its filler. Recently, high-damping rubber has been used in many applications due to its higher ability to dissipate energy compared to other filled rubber, when exposed to dynamic strains. The inherent damping ratio of high-damping rubber compounds can reach 20 %. Accordingly, the high-damping rubber compounds are recommended for this device.

The following properties should be considered in selecting the rubber compound for the visco-plastic device:

- Tensile strength
- Elongation at break
- Modulus of elasticity at different strains
- Cost.

Chapter 4: Detailed Description of the Device

4.0 Introduction

The visco-plastic device proposed in this research combines and enhances many of the proven characteristics of both displacement-dependent and velocity-dependent devices. The device is fabricated from readily available materials. Moreover, the device dissipates energy under all levels of vibrations. At low levels of excitation, the device works as a viscoelastic damper and the energy is dissipated through amplified axial strains. The strains are amplified due to the pre-buckled shape of the device. For high levels of vibration, it operates as a combined viscoelastic and metallic yielding device. In addition to the energy dissipation, the device provides stiffness to structures through the steel elements and the storage stiffness of the viscoelastic material. There are many parameters can be manipulated to enhance the device effectiveness.

The idea of amplifying the displacement is utilized by Constantinou et al. (1997) in a toggle brace system. The basic idea behind the toggle-brace system is that the damper is placed diagonally and linked to two steel linkage elements, which are not collinear. Accordingly, any small interstory drift is amplified in the direction of the damper, which increases the effect of the dampers. Charney and McNamara (2002) applied the same idea in order to reduce the dynamic response of 39-story office building. Viscous fluid dampers were utilized in a toggle brace configuration. The idea of displacement amplifying was also used in the scissor-jack-damper configuration by Sigaher and Constantinou (2003), which was discussed in the previous chapter.

The same bent configuration was used before in Euler vibration isolator [Winteflood (2002) and Chin et al. (2004)] instead of the traditional vertical isolators. For traditional linear-spring isolator, no buckling occurs until the load reaches a certain value, known as the critical load, after which buckling starts. Hence, a static energy is stored in the system. On the other hand, bent configuration doesn't store energy before the operating range. Accordingly, the required mass to operate the isolator is minimized, which increases the resonant frequency of the spring elements. As a result of that, a broader isolation bandwidth is obtained.

4.1 Device Description

The device consists of a viscoelastic solid material bonded into place between two steel plates or shapes, bent as shown in Figure 4.1. When the device is exposed to a compressive force along the longitudinal axis of the device, a shortening with amount, δ will take place. A vertical expansion in the middle of the device is accompanied by this shortening. Due to the bent configuration of the plates, the transverse expansion of the device is several times the axial shortening. This expansion is quantified as $\eta \cdot \delta$, where η is a geometric amplification factor. When the transverse dimension of the proposed visco-plastic device expands or contracts, the entire volume of viscoelastic material is subjected to a near-uniform axial strain. For practical seismic displacement demands, there is sufficient curvature in the steel elements to prevent the “straightening out” of the plates when the device is in tension.

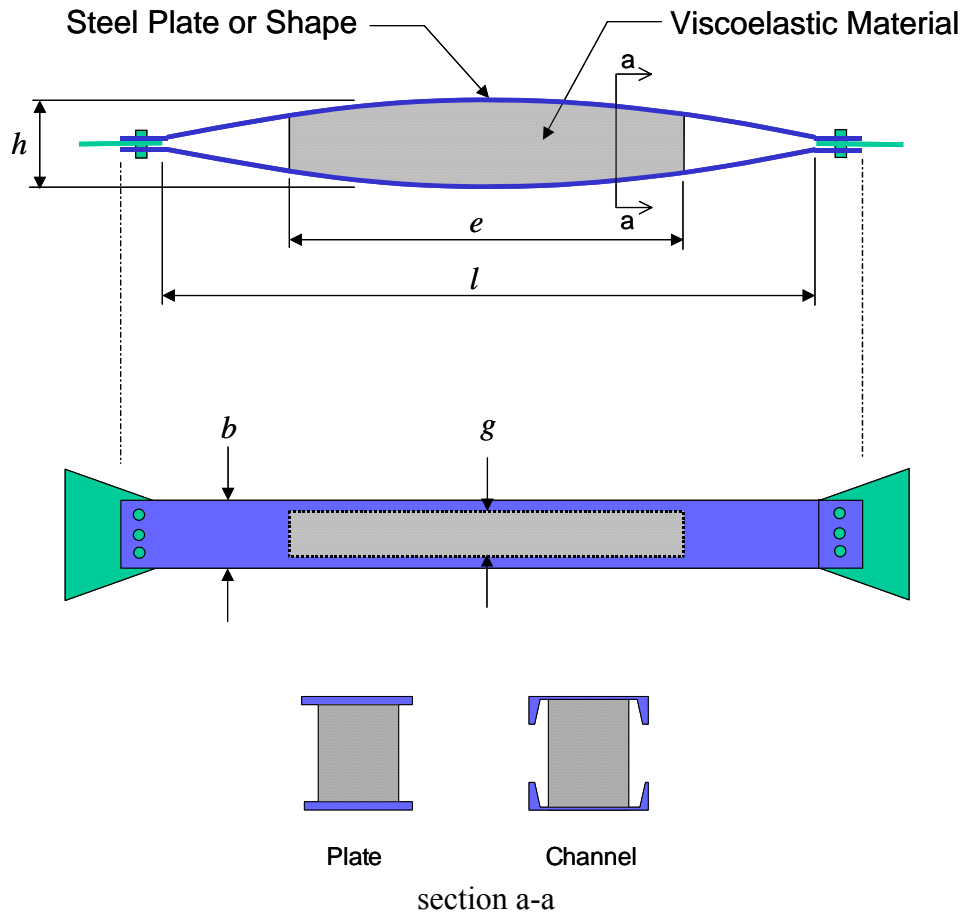


Figure 4.1: Details of visco-plastic device

For low-level seismic vibrations, the energy is dissipated through tensile and compressive strains in the viscoelastic material. The steel elements will remain elastic and no energy is dissipated through steel yielding. Accordingly, the vibration suppression is provided by the axial stiffness of the steel elements and the damping characteristics of the viscoelastic material. It should be noted that, due to the “pre-buckled” bent shape of the plates, the axial stiffness of the device is significantly less than the stiffness that would be obtained if the same plates were used in a straight configuration. This is an advantage of the visco-plastic device because excessive added stiffness may act as a “seismic attractor,” increasing base shears and increasing response accelerations, which result in damage to contents and nonstructural components.

For high level seismic vibrations, an additional significant source of energy dissipation in the device is provided by axial-flexural yielding of the steel elements. This yielding occurs when the device is in tension or compression. When the device is in compression, the pre-buckled symmetry of the plates and the rigidity of the viscoelastic material will prevent uncontrolled inelastic buckling of the steel elements. Additionally, a restraining mechanism may be placed in the device which limits the amount of transverse expansion that may occur when the device is under compression. When placed into a structural system it is expected that the devices would be used in pairs, where one device is in tension and the companion device is in compression.

There are a number of parameters that may be manipulated to control the behavior of the device. These parameters include:

- Length (l), thickness (h) and breadth (b) of the device
- Aspect ratio, (h/l) of the device
- Initial bent shape of the device (circular, parabolic, transcendental)
- Size and shape of steel sections (plate, channel, tee)
- Type of steel (mild or high-strength steel)
- Dimension of the viscoelastic material

- Solidity of viscoelastic material. To reduce stiffness holes may be cored into the material
- Type of viscoelastic material (filled, unfilled materials)
- Bonding of the viscoelastic material to the plates (bonded vs. unbonded)

The visco-plastic device is constructed from readily available materials, can be assembled in most structural steel fabrication plants, is projected to have a relatively low cost, and should require little if any maintenance. Unlike many other passive energy dissipation devices, the visco-plastic device should operate without need for replacement for all applications except the most extreme seismic loading.

In the next chapter, a preliminary analysis of the device using SAP2000 program [Computers and Structures Inc. (2002)] is described. In this analysis, the effect of different parameters on the device response was investigated. The viscoelastic material was modeled using discrete springs and dashpots while the steel elements were modeled using beam elements. The analysis considered large displacement and P-delta effects. After that, the devices were attached to different types of structures and the effectiveness of the devices were determined by analyzing these structures with the devices under different ground excitations. The device effectiveness was compared to the effectiveness of the conventional viscoelastic dampers.

Chapter 5: Preliminary Analysis of the Device

5.0 Introduction

There are many parameters that control the behavior of the visco-plastic device. Hence, it is important to investigate how these parameters affect the behavior of the device and its effect on the response of structures under different dynamic loads. A simplified model was developed to be used in analysis of structures using SAP2000 [Computers and Structures (2003)]. First, the device was attached to one-bay single-story steel frame to study the effect of the different parameters. After that, a detailed investigation was carried out on a multi-bay multi-story steel structure with the device attached to each story of the frame. The response of the structure was studied without and with the device. Also, a comparison was made between the effect of the device and the conventional viscoelastic damper. Finally, a different arrangement of the device in the structure was studied to show the need for optimizing the device in order to get the best results out of using it.

5.1 Device Modeling

The device was modeled using SAP2000. Frame elements were used to represent the bent steel elements. The steel elements were assumed to behave linearly elastic during the analysis. The inelastic behavior of steel elements is considered in the finite element analysis of the device in Chapter 6, and in the simplified device models in Chapters 7 and 8.

Several discrete vertical dashpots were used to represent the viscoelastic material. Kelvin models were used for the viscoelastic materials. The Kelvin model consists of a linear dashpot in parallel with a spring. This was modeled in SAP2000 using NLINK elements (which are in fact Maxwell model) in parallel with linear springs. The Maxwell model was converted to a true dashpot using a large value for the spring component of the model. The model of the device is shown in Figure 5.1 a.

Different parameters of the device were investigated including the damping constant of the dashpots, stiffness of the linear springs, cross section of the steel elements and the

aspect ratio of the device. A wide range of the damping constant and spring stiffness was selected to present reasonable values that can be obtained practically according to the properties of different rubber compounds.

First, in order to estimate the damping constant of the discrete dashpots used in the model of the device, the energy dissipation under axial strains through one cycle of harmonic strains is needed. The total energy dissipated during one cycle can be estimated (as shown in the previous chapter) from:

$$E_T = \pi \varepsilon_0^2 E' V \tan \delta \quad (5-1)$$

where E' is the elastic modulus, which can be approximated by the initial Young's modulus for relatively small axial strains (less than 100 %), and V is the volume of the material that is represented by the dashpot. Assuming the phase angle of the rubber compound is 15° , the energy dissipated during one cycle is:

$$E_T = 0.842 \varepsilon_0^2 E_0 V \quad (5-2)$$

where E_0 is the initial Young's modulus.

The axial strain, ε_0 , can be calculated from

$$\varepsilon_0 = \frac{U_{\max}}{h} \quad (5-3)$$

where U_{\max} is the total vertical displacement of the dashpot, and h is the length of the dashpot.

Accordingly, the energy dissipated during one cycle is:

$$E_T = 0.842 \left[\frac{U_{\max}}{h} \right]^2 E_0 V \quad (5-4)$$

For a SDOF viscously-damped structure subjected to simple harmonic loading, the total energy dissipation through one cycle can be calculated from:

$$E_T = \pi \omega C U_{\max}^2 \quad (5-5)$$

where C is the damping constant of the dashpot, and ω is the forcing frequency.

Equating equation (5-4) and equation (5-5) yields to:

$$C = \frac{0.842 E_0 V}{\pi \omega h^2} \quad (5-6)$$

For the device model, the dashpot length is 16 in. approximately (corresponding to h in Figure 4.1), the material volume, V , that the dashpot represents is (8*16*12 in.), and the loading frequency is equal to π , hence the damping constant can be estimated as:

$$C = 0.512E_0 \text{ (k-sec/in.)} \quad (5-7)$$

The initial modulus of elasticity can vary according to the rubber compound. Typically, it can range from 0.1 to 1.0 ksi. Accordingly, three values of the damping constant were chosen; 0.1, 0.3 and 0.5 k-sec/in to represent reasonable values that can be obtained practically.

Second, the spring constant can be estimated from:

$$K = \frac{E_0 A}{h} \quad (5-8)$$

where A is the cross sectional area and h is the thickness of the material, which is represented by the spring. The cross sectional area of the material is (8*12 in.) and the thickness of the material is 16 in. Then,

$$K = 6E_0 \text{ (kip/in.)} \quad (5-9)$$

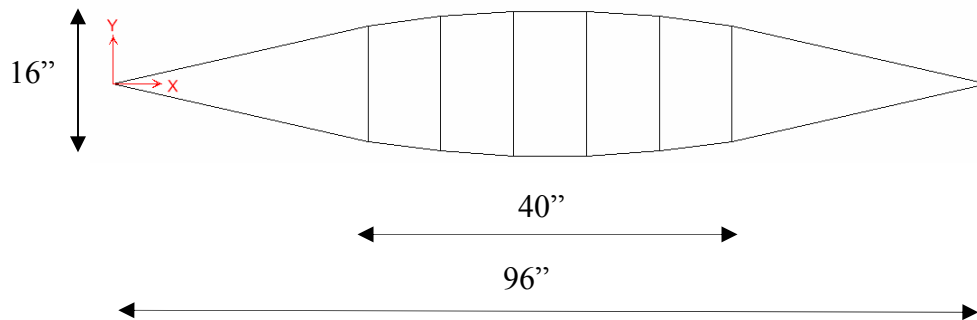
In order to increase the energy dissipation through the device, some holes can be punched in the rubber block in order to reduce its stiffness to allow larger axial strains. Accordingly, three values of the spring stiffness were selected; 0.4, 1.0 and 4.0 kip/in. to cover a reasonable range of values that can be obtained.

The device was attached to a single-story structure and a nine-story five-bay steel frame to consider the parameters that control the device behavior, in addition to the effect of the device on different structures.

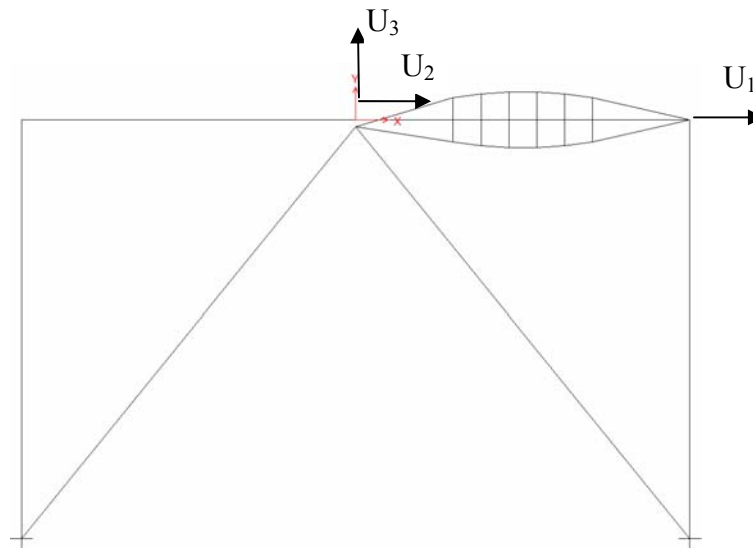
5.2 Single-Story Structure

A nonlinear response history analysis was performed on a one-bay single-story steel frame with a single visco-plastic device attached to it. The frame has a span and a height of 16 and 12 feet, respectively. The model of the steel frame with the device is shown in Figure 5.1 b. There are effectively three degrees of freedom, denoted by U_1 , U_2 , and U_3 . The instantaneous horizontal deformation in the device is ($U_1 - U_2$). The analysis was

performed using the SAP2000 program. The inherent damping of the structure was assumed to be 3 % critical damping. A parametric study was carried out through several runs on a steel frame with the device under harmonic excitations. The frame was exposed to a harmonic excitation with acceleration of $100 \sin(\pi t)$ for three quarters of a cycle and then left for free vibration. Table 5.1 shows the different parameters considered, ground excitations and earthquakes and their symbols to be used in this chapter.



a: Device model



b: Single-story steel frame with the device

Figure 5.1: Models; a: Device, b: single-story steel frame with the device

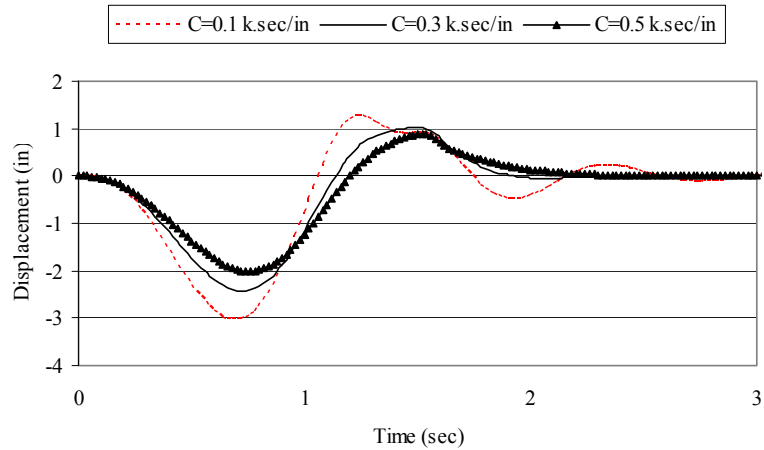
Table 5.1: General symbols for the analysis.

Damping Constant	C=0.1 kip-sec/in.	C=0.3 kip-sec/in.	C=0.5 kip-sec/in.
Symbol	C1	C2	C3
Stiffness Constant	K=0.4 kip/in.	K=1.0 kip/in.	K=4.0 kip/in.
Symbol	K1	K2	K3
Aspect Ratio h/l *	$h/l = 0.083$	$h/l = 0.125$	$h/l = 0.167$
Symbol	H1	H2	H3
Cross Section	C10x20	C12x25	C15x50
Symbol	S1	S2	S3
Ground Excitation	Harmonic	EI Centro	Northridge
Symbol	H	E	NR
Large Disp. And P-delta	Not considered	Considered	
Symbol	N	LP	

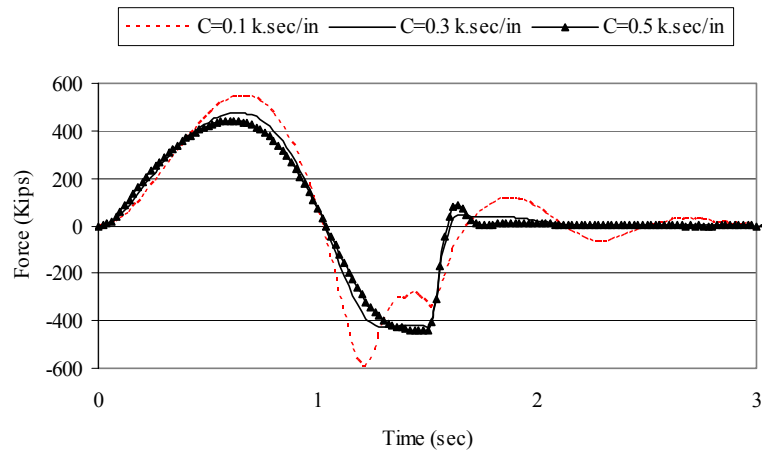
* h is the middle thickness of the viscoelastic material and l is the length of the device (See Figure 4.1).

5.2.1 Effect of the Damping Constant of the Dashpots

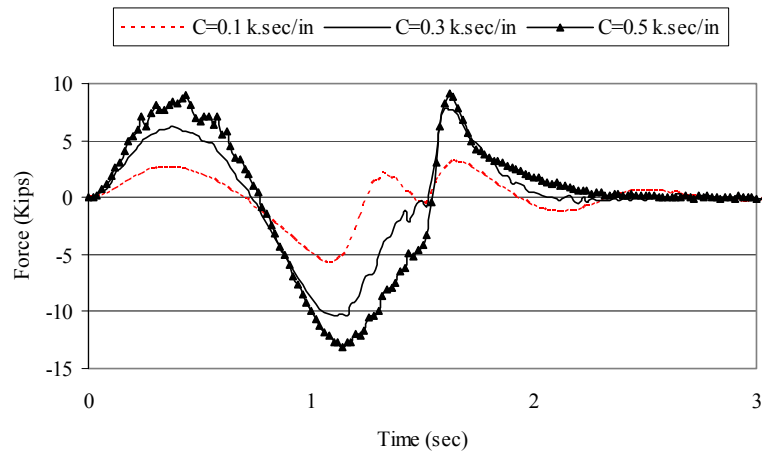
One of the most important parameters that should be considered is the damping constant of the dashpots. The viscoelastic material is typically one of the rubber compounds. The damping constant depends on different factors, such as the rubber compound, cross sectional area and the thickness of that material. Three runs were performed to understand the effect of damping on the response of the frame under the harmonic excitation. The damping constants of the dashpots were chosen to be 0.1, 0.3 and 0.5 kip-sec/in. The results of the response history analysis of the three cases are shown in Figure 5.2. It is shown that increasing the damping constant from 0.1 to 0.5 k-sec/in. reduces the floor displacement and consequently reduces the base shear. The force in the device was nonlinearly proportional to the damping constant since the velocity of the vertical motion in the device (parallel to h) was reduced upon increasing the damping constant. The damping constant was set to be 0.3 kip-sec/in. for the rest of the analyses. Note that the terms that were held constant in this comparison are given in the caption of Figure 5.2, which are the spring stiffness, K1, steel cross section, S2, and the device aspect ratio, H3.



a) Floor horizontal displacement.



b) Base shear.



c) Axial force of the dashpot in the middle of the device.

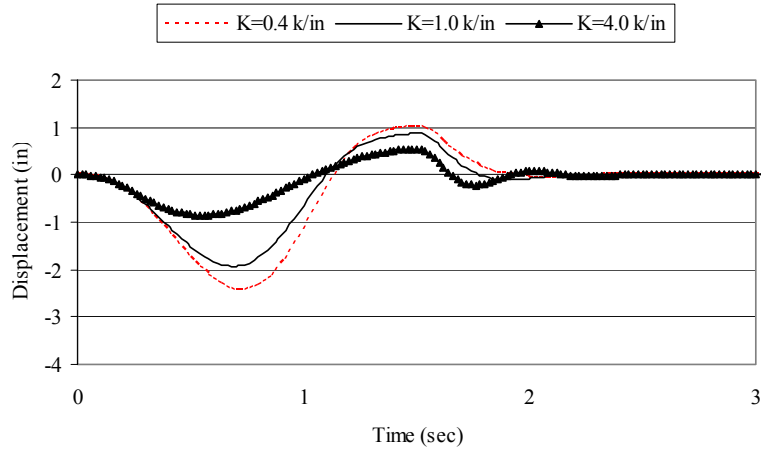
Figure 5.2: Effect of damping constant on the response of the single-story frame under harmonic excitation. (K1-S2-H3-LP-H)

5.2.2 Effect of the Stiffness of the Linear Springs

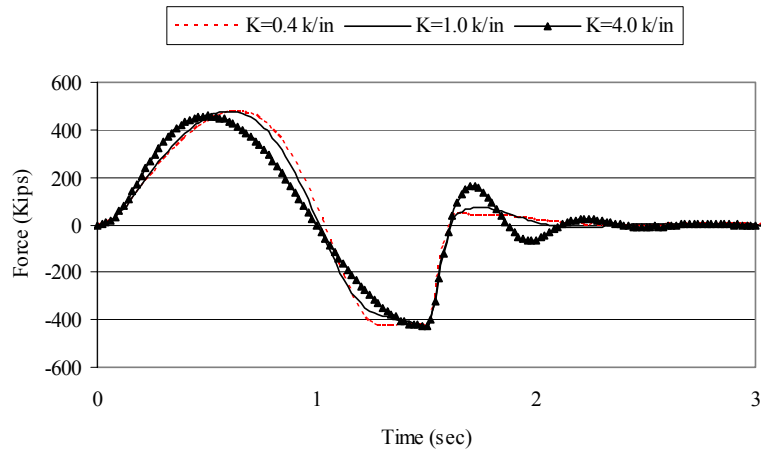
The second parameter to be investigated was the spring stiffness. Many parameters affect the spring stiffness, such as the modulus of elasticity, the cross sectional area and the thickness of the viscoelastic material. The dimension of the device material can be adjusted easily to obtain the required value of the stiffness, while the modulus of elasticity depends on the material type. There is a wide range for the values of the modulus of elasticity for the rubber materials that may range from 0.1 to 1 ksi. Three values of spring stiffness were chosen as 0.4, 1.0 and 4.0 kip/in. The effect of the spring stiffness on response of the structure is shown in Figure 5.3. From this Figure, it is shown that increasing the spring stiffness from 0.4 kip/in. to 4.0 kip/in. reduces the maximum floor displacement by a factor of 3 approximately while it has a smaller effect on the base shear. Although increasing the spring stiffness reduces the maximum displacement but it restricts the amplification of the displacement through the device. Accordingly, a relatively small value of the spring stiffness is better to maintain the high damping provided by the device. A value of 0.4 kip/in. was selected for the spring stiffness for the rest of analyses. During this step, the parameters that were kept constant were the damping constant, C2, steel cross section, S2 and the device aspect ratio, H3.

5.2.3 Effect of the Cross Sections of the Steel Elements

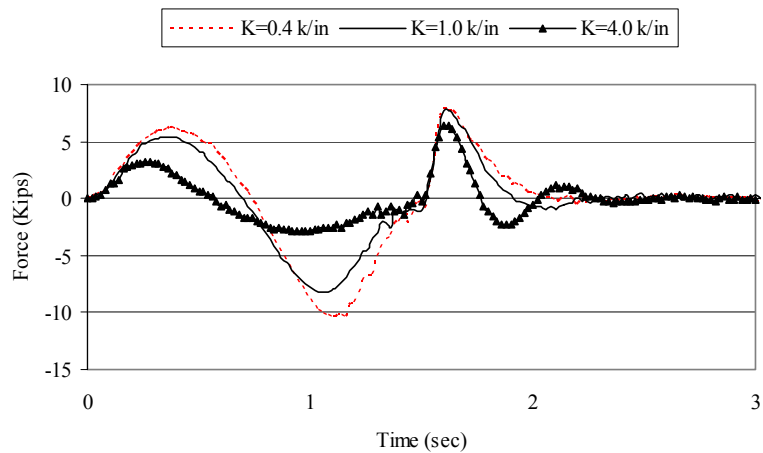
Three different cross sections were chosen as C10x20, C12x25 and C15x50. Figure 5.4 shows the effect of the steel cross section of the device. According to the results of this analysis, it is shown that the larger the cross section selected, the smaller the floor displacement obtained since the steel elements increases the horizontal stiffness of the frame. On the other hand, increasing the cross section reduces the vertical displacement at the middle of the device, which reduces the damping ratio provided by it. Also, although having a large cross section reduces the maximum floor displacement by a factor of 1.6 approximately, it almost has no effect on the base shear. This is due to the increase in the axial forces in the braces upon using larger cross section, which leads to almost the same base shear even with the reduction in the shear forces in the columns. During this step, the parameters that kept constant were the damping constant, C2, spring stiffness, K1 and the device aspect ratio, H3.



a) Floor horizontal displacement.

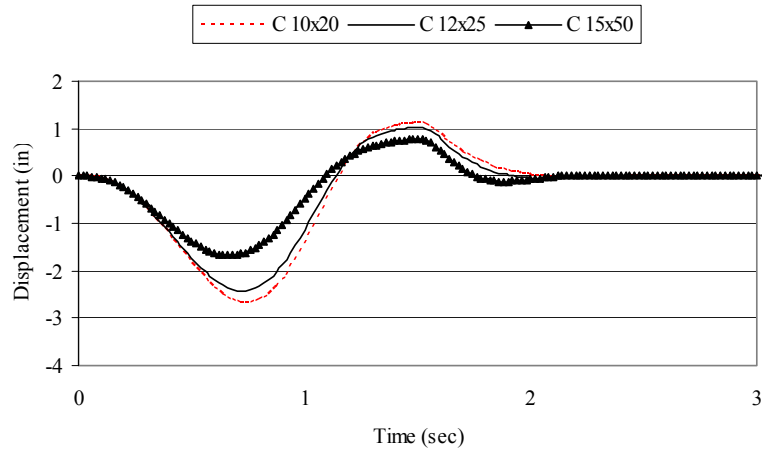


b) Base shear.

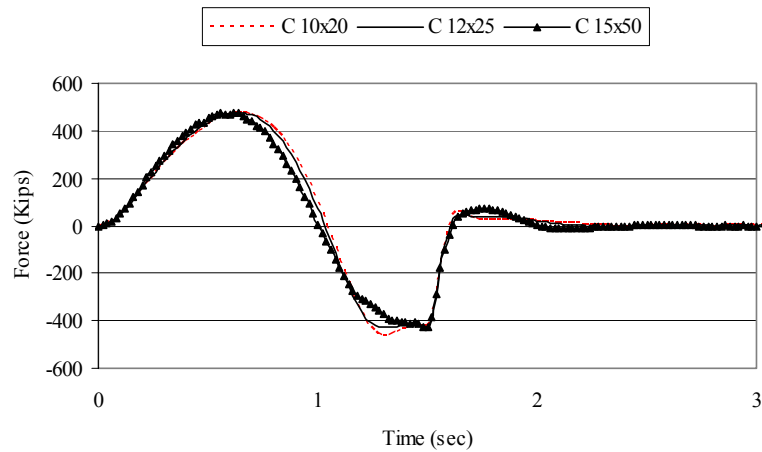


c) Axial force of the spring in the middle of the device.

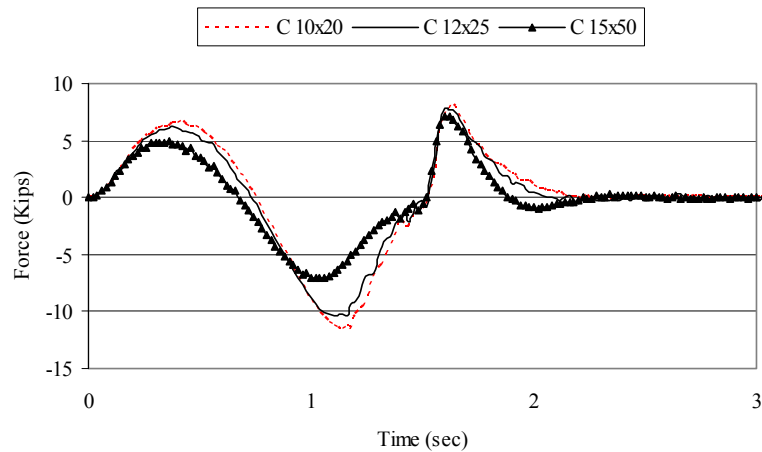
Figure 5.3: Effect of spring constant on the response of the single-story frame under harmonic excitation. (C2-S2-H3-LP-H)



a) Floor horizontal displacement.



b) Base shear.

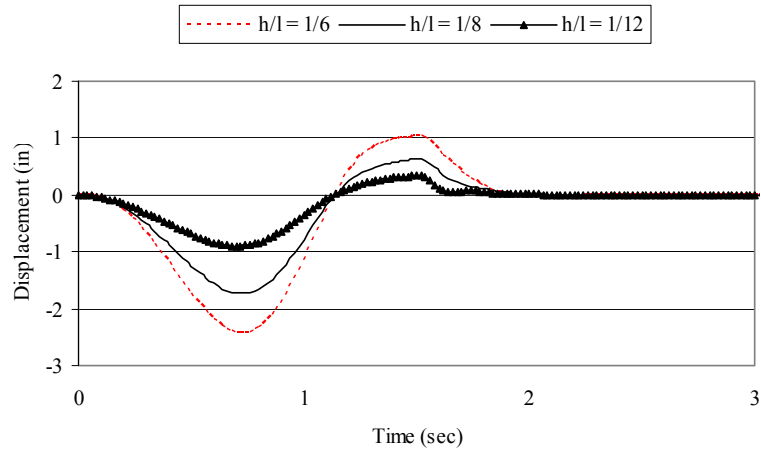


c) Axial force of the dashpot in the middle of the device.

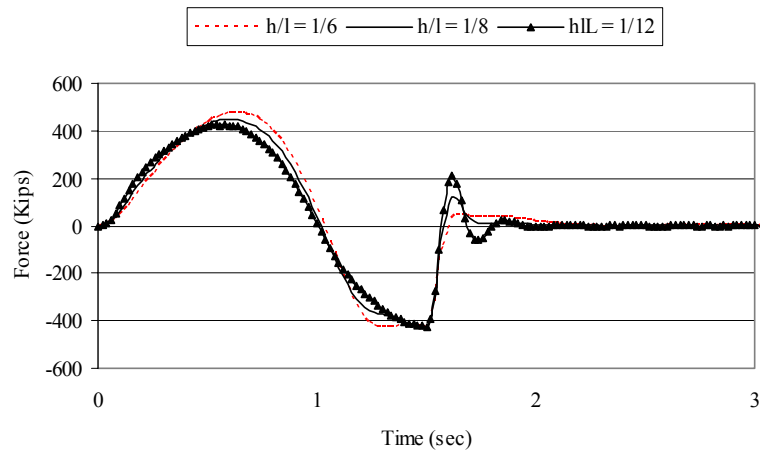
Figure 5.4: Effect of the device cross-section on the response of the single-story frame under harmonic excitation. (C2-K1-H3-LP-H)

5.2.4 Effect of the Device Aspect Ratio

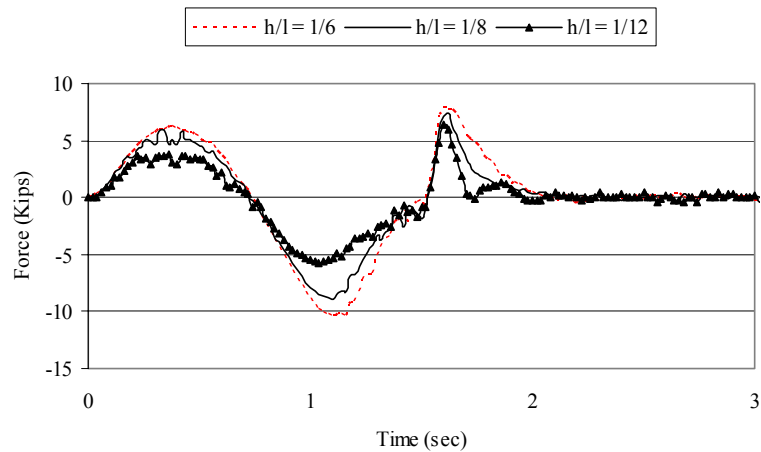
The last parameter in this investigation that affects the behavior of the device is its shape. Three cases were studied with aspect ratio, h/l , of $1/6$, $1/8$ and $1/12$, where h is the thickness of the viscoelastic material and l is the device length. As the aspect ratio increases, the horizontal stiffness provided by the device is reduced while the damping ratio is increased. The results of this analysis are shown in Figure 5.5. An aspect ratio of $1/12$ was chosen for the rest of the analyses. The parameters damping constant, C_2 , spring stiffness, K_1 and steel cross section, S_2 were kept fixed for this comparison.



a) Floor horizontal displacement.



b) Base shear.



c) Axial force of the dashpot in the middle of the device.

Figure 5.5: Effect of the aspect ratio of the device on the response of the single-story frame under harmonic excitation. (C2-K1-S2-LP-H)

5.2.5 Effect of the Device on the Response of the Single-Story Structure

Now, after determining the best design parameters according to the simple parametric study, it is necessary to check the efficiency of the device by comparing the results of the nonlinear response history analysis of the frame with and without the device under harmonic excitations as well as real records of El Centro and Northridge earthquakes. The accelerations and the 5% damped pseudoacceleration response spectrum of El Centro and Northridge earthquakes are shown in Figure 5.6 and 5.7, respectively. The peak ground acceleration is 0.35 g and 0.6 g, respectively.

According to the results shown in Figure 5.8, the device introduces great improvement of the response of the frame under the harmonic excitation in addition to the El Centro and Northridge earthquakes. The maximum floor displacement was reduced from 4.12 to 2.43 in. under harmonic excitation, from 3.6 in. to 1.2 in. under El Centro earthquake and from 6.8 to 2.9 in. under Northridge earthquake. In other words, the reduction of the floor displacement was 41.0 %, 66.8 % and 57.6 % under harmonic, El Centro earthquake and Northridge earthquakes respectively.

In the all-mentioned analyses, the large displacement and P- δ effects were included in the nonlinear response history analyses. The steel members were assumed to behave linearly elastic in the all analyses.

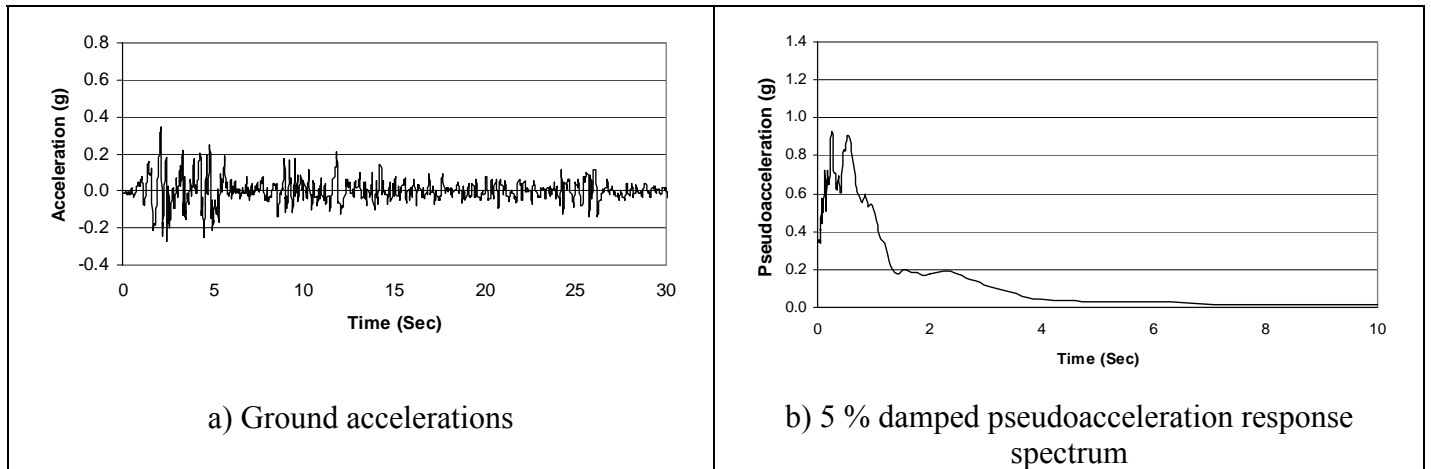


Figure 5.6: El Centro earthquake

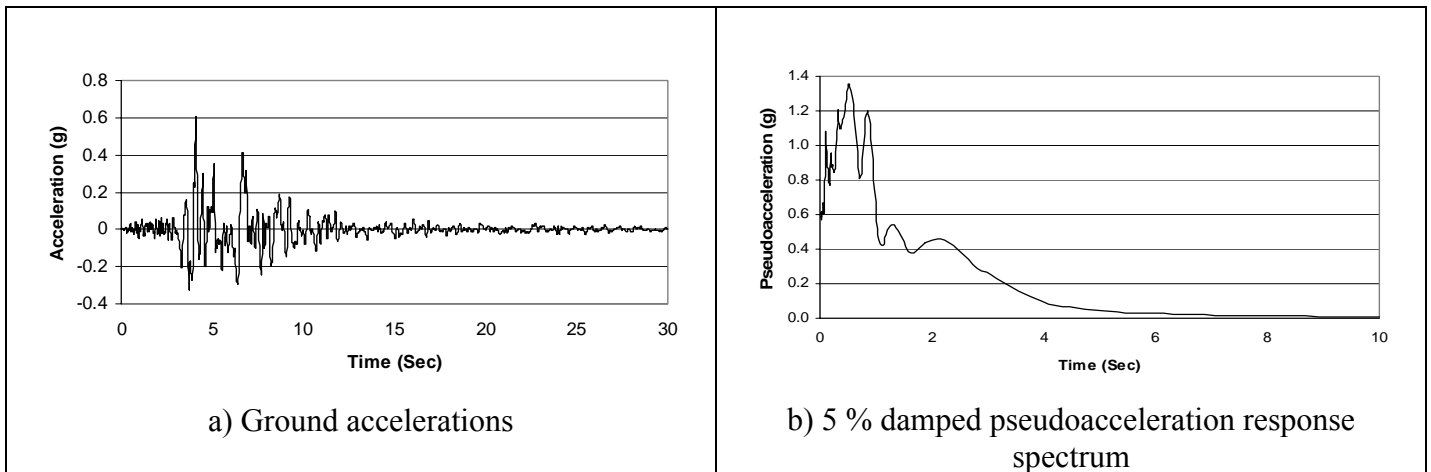
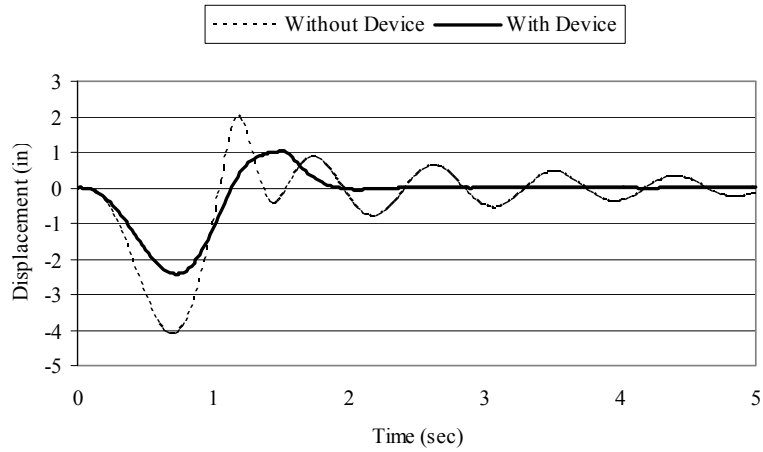
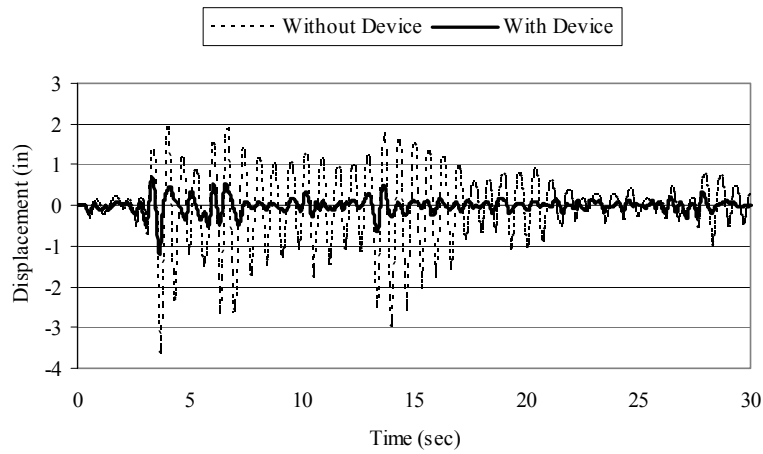


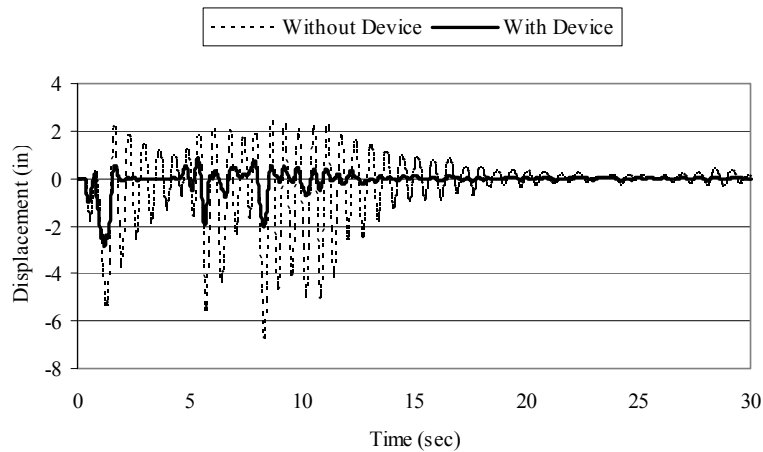
Figure 5.7: Northridge earthquake



a) Floor displacement under harmonic excitation



b) Floor displacement under El Centro earthquake



c) Floor displacement under Northridge earthquake

Figure 5.8: Effect of the analysis type on the response of the single-story Frame. (C2-K2-H3-S3-LP)

5.3 Multi-Bay Multi-Story Steel Frame

Now, after observing the effectiveness of the device through the analysis of a single-story steel frame under different ground excitations, it is important to study the effect of the device on the response of a real multi-story structure. In order to do so, a model of five-bay nine-story steel frame designed for the SAC building project (Gupta and Krawinkler, 1999) was chosen. The periods of vibrations of the first four modes of the structure are 1.595, 0.593, 0.345 and 0.229 seconds, respectively. The frame was analyzed under harmonic excitation as well as the real records of El Centro and Northridge earthquakes. Large displacement and P- δ effects were considered for the whole analysis. One device was attached to each floor. The details of the frame are shown in Figure 5.9 while the model of the frame and the arrangement of the devices are shown in Figure 5.10. The periods of vibrations of the first four model of the structure with devices are 1.579, 0.581, 0.345 and 0.236 seconds, respectively. The reason behind the small change in the periods of vibrations of the structure with the devices from that of the structure without devices is due to the bent shapes of the steel elements, which reduces the stiffness provided to the structure significantly. In order to show the effect of the aspect ratio of the steel elements, h/l , on their stiffness, two steel channels, C15x50, bent to have a shape of $\frac{h}{2} \sin \frac{\pi x}{96}$ were exposed to a static load to calculate their stiffness. Different configurations were considered to have an aspect ratio from zero to 1/6. As shown in Figure 5.11, as the aspect ratio increases, the stiffness of the steel elements are reduced significantly.

As before, a parametric study was carried out to choose the different parameters of the device in order to optimize its effect on the response of the frame under different ground excitations. The parametric study was performed by analyzing the frame under harmonic excitation. The damping constant, spring stiffness and the cross section of the steel elements of the device were considered in this parametric study.

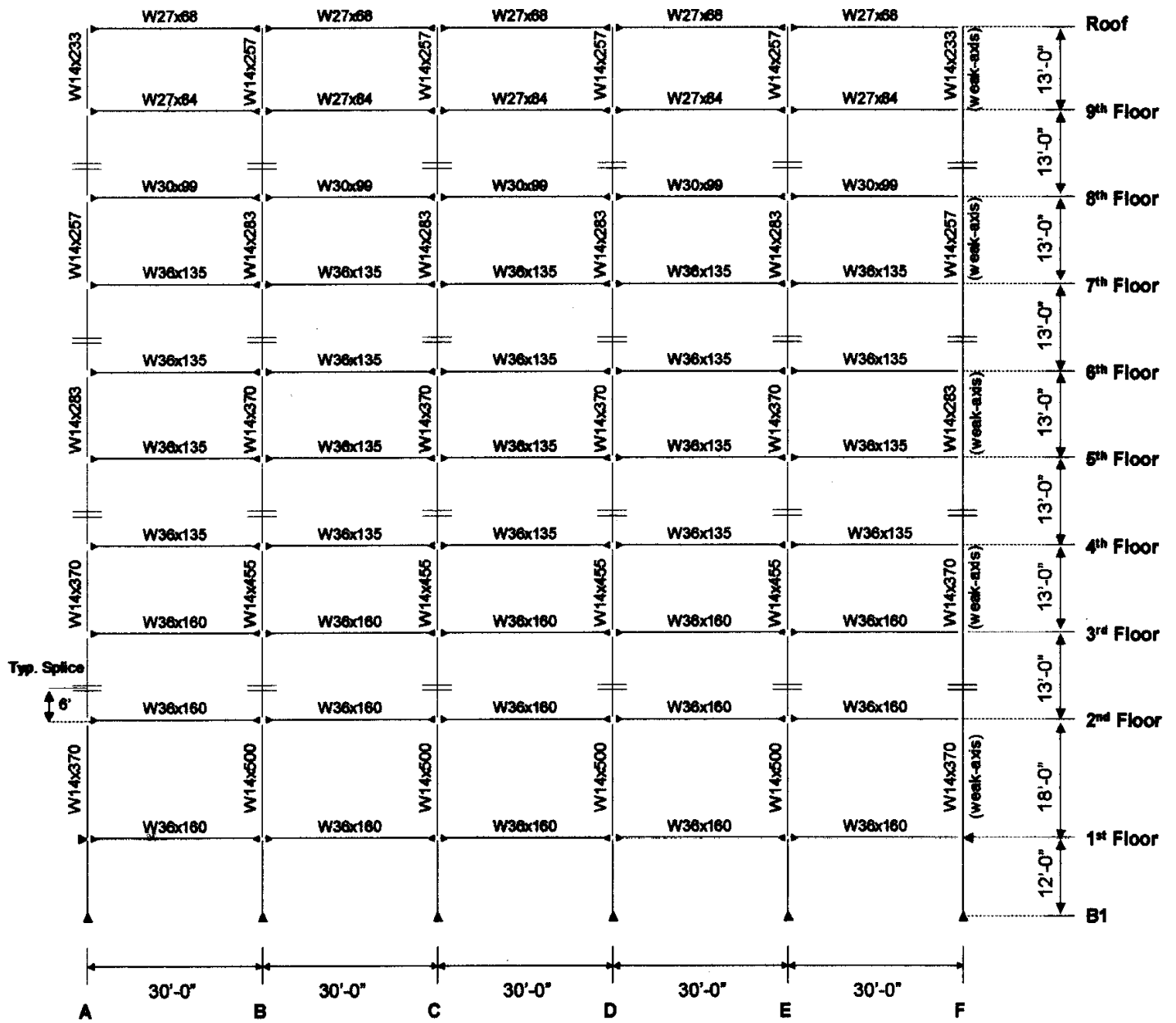


Figure 5.9: Details of the Nine-story five-bay used in the analysis

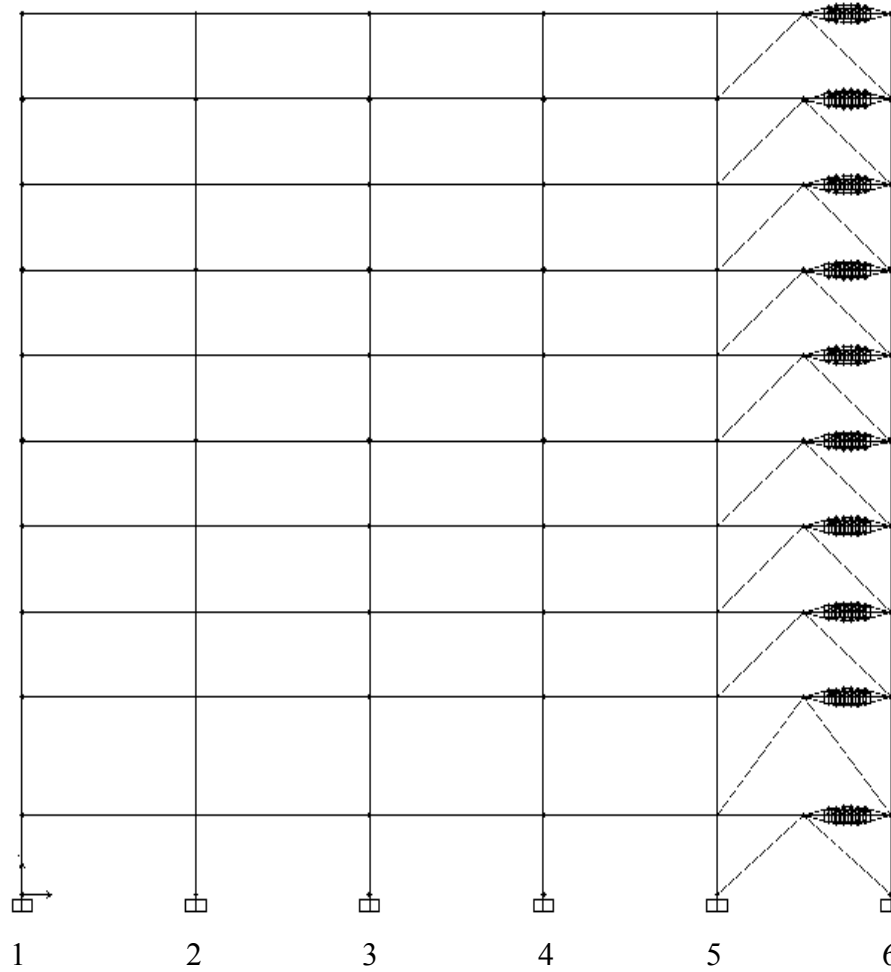


Figure 5.10: Model of the analyzed nine-story steel frame with the devices (See Figure 5.1 for details of the device model).

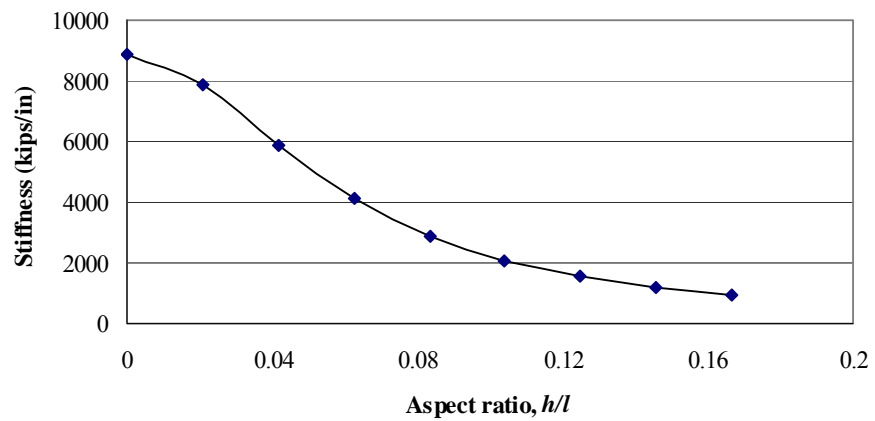
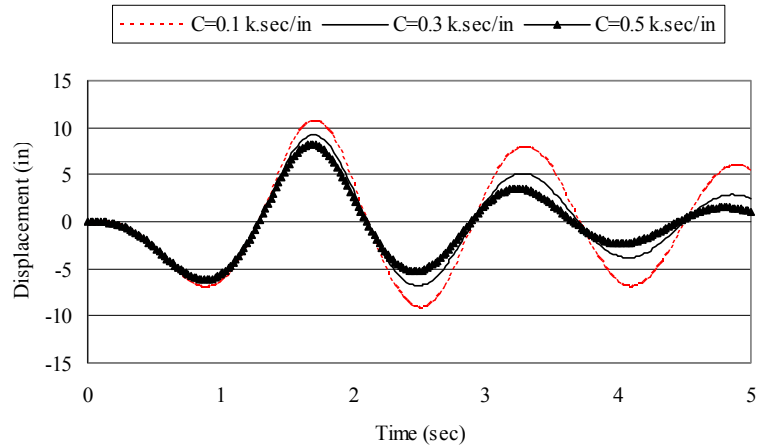


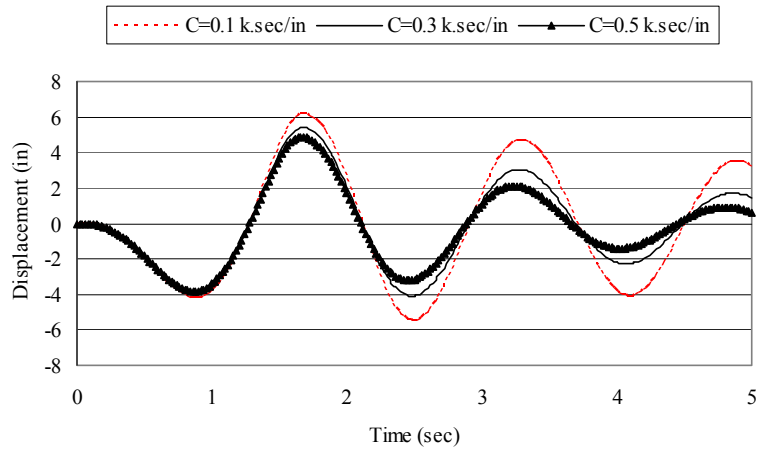
Figure 5.11: Effect of the aspect ratio of the steel elements on their stiffness (VE material not included).

5.3.1 Effect of Device Parameters on the Structural Response

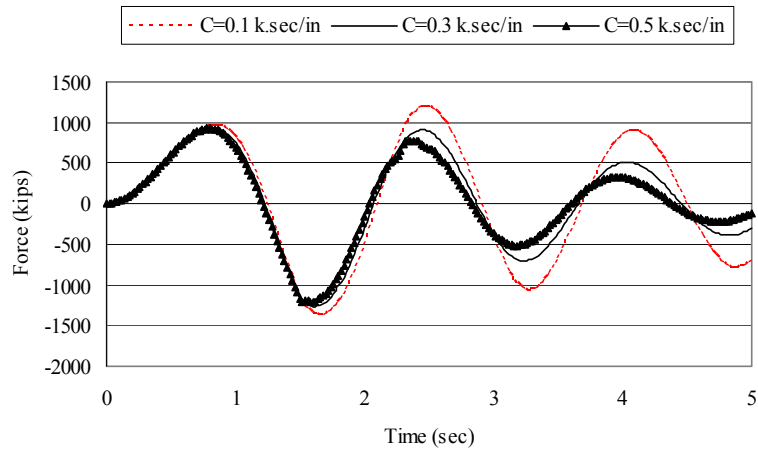
Figure 5.12 shows the effect of the damping constant of the device on the response of the steel frame. It is obvious that increasing the damping constant from 0.1 kip-sec/in. to 0.5 kip-sec/in. reduced the floor displacements and the total base shear by a considerable amount. Regarding the spring constant, the results show that having a small spring constant results in higher damping ratio. The effect of the spring constant on the response of the frame under the harmonic excitation is shown in Figure 5.13. The effect of the steel cross section on the steel frame response is shown in Figure 5.14. The response of the frame was almost unchanged using cross sections of C10x20, C12x25 and C15x50. The reason behind that may be due to the fact that the chosen cross sections have a relatively small stiffness compared to the five-bay nine-story steel frame structure. However, using more devices per floor may lead to more clear effect of the cross section of the steel elements. It is worth noting that the stiffness provided by the device depends on the stiffness of the viscoelastic material as well as the stiffness of the steel elements. According to the results of these analyses, a damping constant of 0.5 kip-sec/in., spring stiffness of 0.4 kip/in. and a cross section of C15x 50 were chosen for the rest of the analyses.



a) Top floor horizontal displacement.

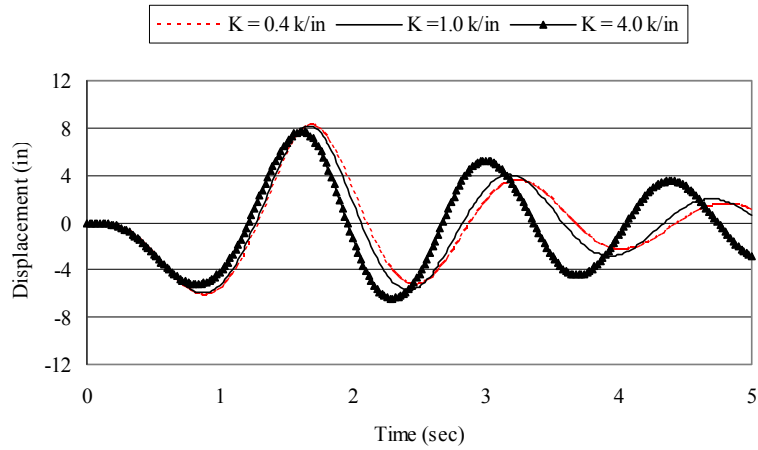


b) Fifth floor horizontal displacement.

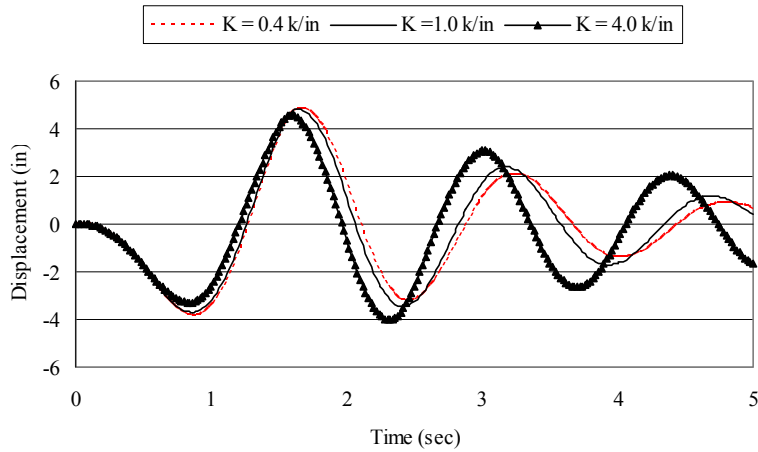


c) Total base shear.

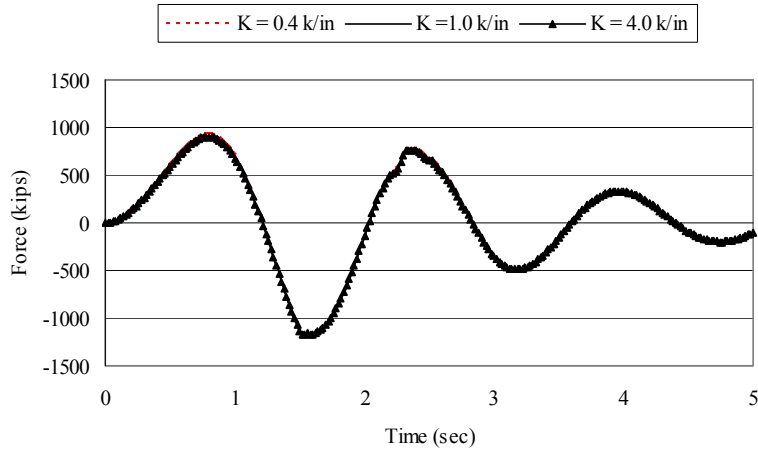
Figure 5.12: Effect of damping constant on the response of the nine-story frame under harmonic excitation (K1-S1-H3-LP-H).



a) Top floor horizontal displacement.

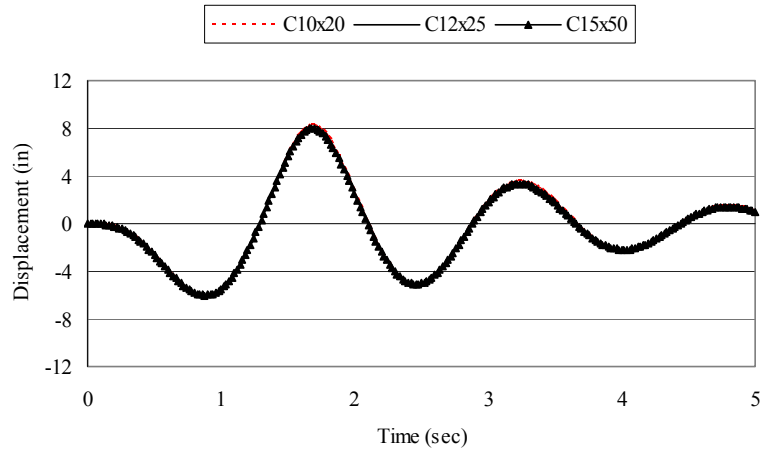


b) Fifth floor horizontal displacement.

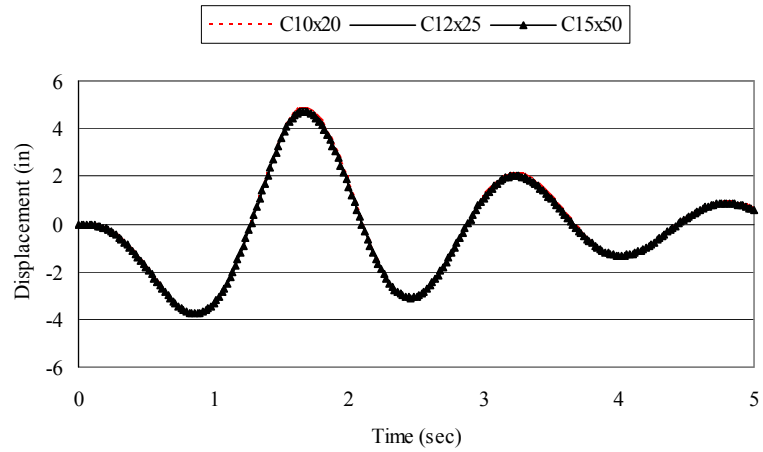


c) Total base shear.

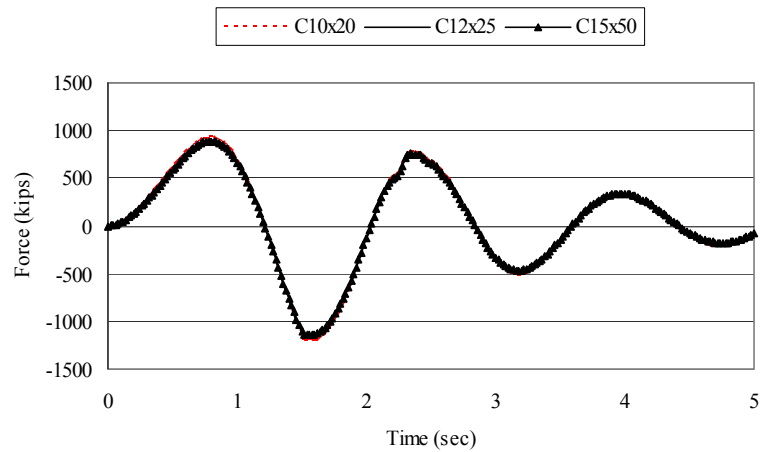
Figure 5.13: Effect of spring constant on the response of the nine-story frame under harmonic excitation. (C3-S1-H3-LP-H)



a) Top floor horizontal displacement.



b) Fifth floor horizontal displacement.



c) Total base shear.

Figure 5.14: Effect of device cross-section on the response of the nine-story frame under harmonic excitation. (C3-K1-H3-S1-LP-H)

5.3.2 Effect of the Device on the Response of the Multi-story Structure

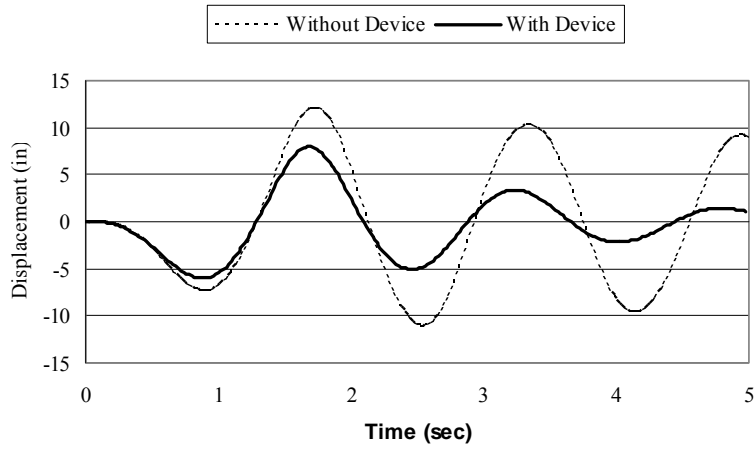
Now, after setting the different device parameters for the nine-story steel frame, a detailed investigation is needed to determine the effect of the device on the response of the frame under different ground excitations. The model of the structure was analyzed with and without the device. Figures 5.15 and Figure 5.16 show the response of the frame in both cases under harmonic excitation. The maximum top floor displacement was reduced from 11.8 in. to 8.0 in. with a reduction percentage of 32.5 %. The maximum fifth floor displacement was reduced from 6.8 in. to 4.7 in. with a reduction percentage of 30.4 %. The maximum total base shear was reduced from 1354.4 kips to 1144.1 kips with a reduction percentage of 15.5 %. As shown in Figure 5.16, using the device has a great effect on the story displacements. At maximum top floor displacement, the average reduction in story displacements 28.9 %. The bending moments at column bases were greatly reduced due to the use of the device. The average reduction in the bending moments at column bases was 20.7 %.

The frame was analyzed again under real unscaled records of El Centro earthquake for the both cases, with and without the device. The results of the two cases are shown in Figure 5.17 and Figure 5.18. The maximum top floor displacement was reduced by 44.2 % while the reduction in the maximum fifth floor displacement was 41.6 %. The maximum base shear was reduced due to the use of the device from 1083.8 kips to 628.0 kips with a reduction percentage of 42.1 %. Due to the use of the device, the floor displacements were highly reduced. At the maximum top floor displacement, the average reduction in the story displacements was 38.9 %. Using the device resulted in a considerable reduction in the bending moments at column bases for all columns. The average reduction in the bending moments at column bases was 27.5 %.

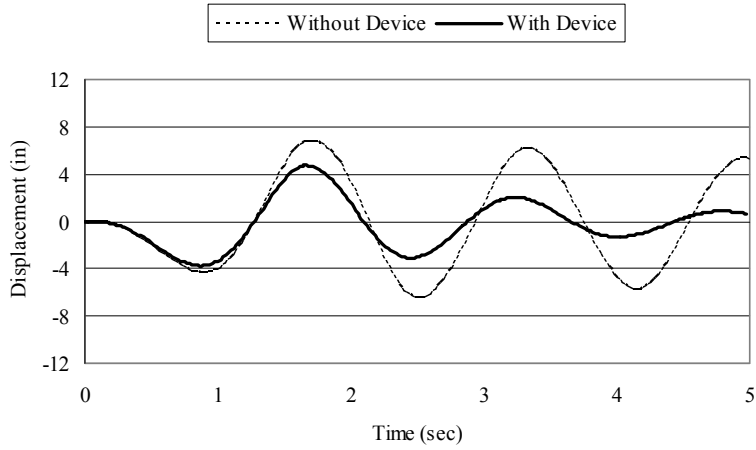
Figure 5.19 and Figure 5.20 show the effect of the device on the response of the nine-story steel frame under real unscaled records of Northridge earthquake. The maximum top floor displacement was reduced from 16.2 in. to 9.9 in. with a reduction percentage of 39.0 %. The maximum fifth floor displacement was reduced by 27.8 %. The maximum base shear was reduced by 29.2 %. At the maximum top floor displacement, the story

displacements were reduced with an average percentage of 20.4 %. The average reduction in the bending moments at column bases was 10.8 %.

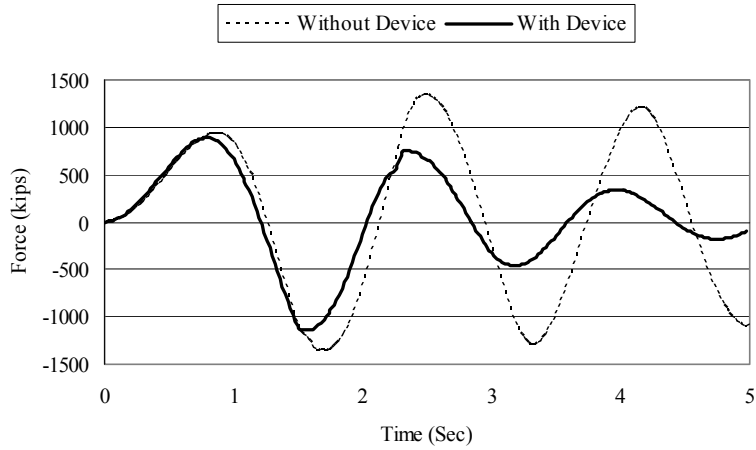
During the previous analyses, the steel frame behaved elastically under different ground excitations. To encounter the geometric nonlinearities, large displacement and P- δ effects were considered in the analyses



a) Top floor horizontal displacement.

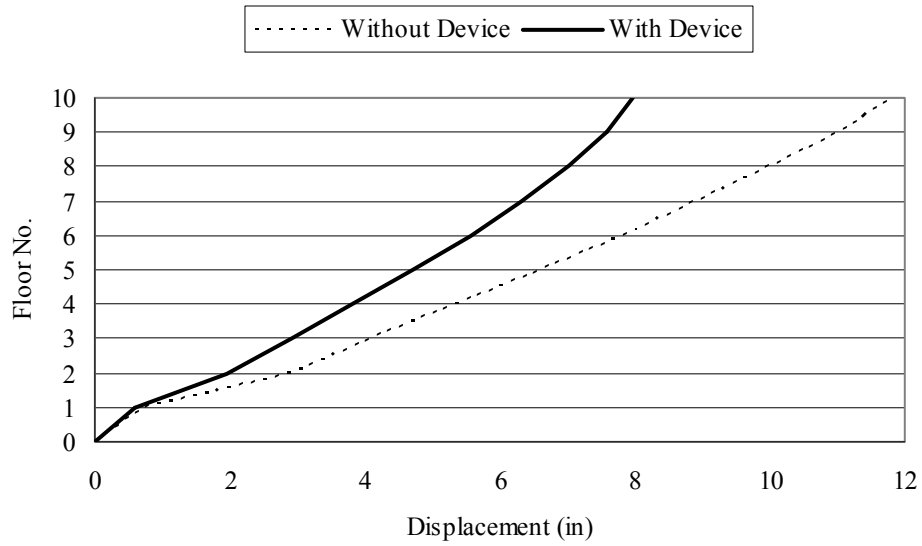


b) Fifth floor horizontal displacement.

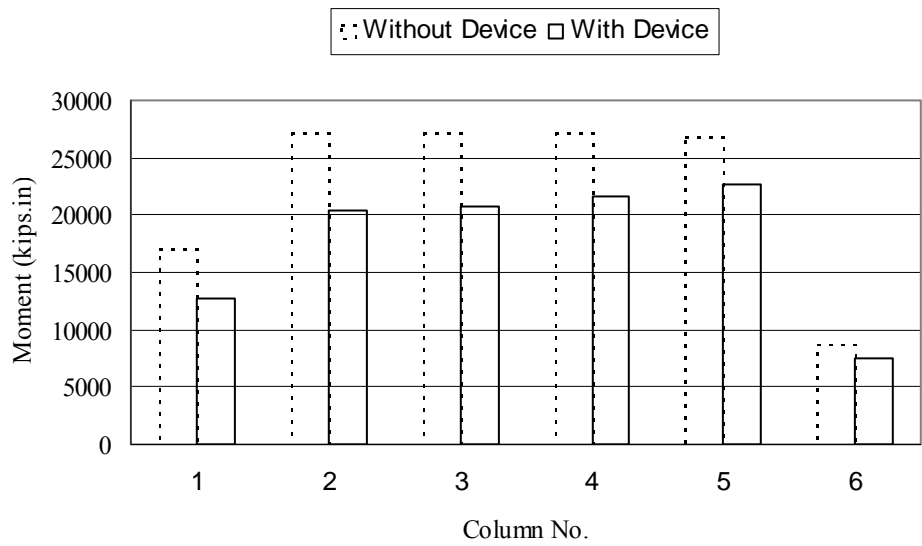


c) Total base shear.

Figure 5.15: Effect of the device on the response of the nine-story frame under harmonic excitation. (C4-K1-H3-S1-LP-H)

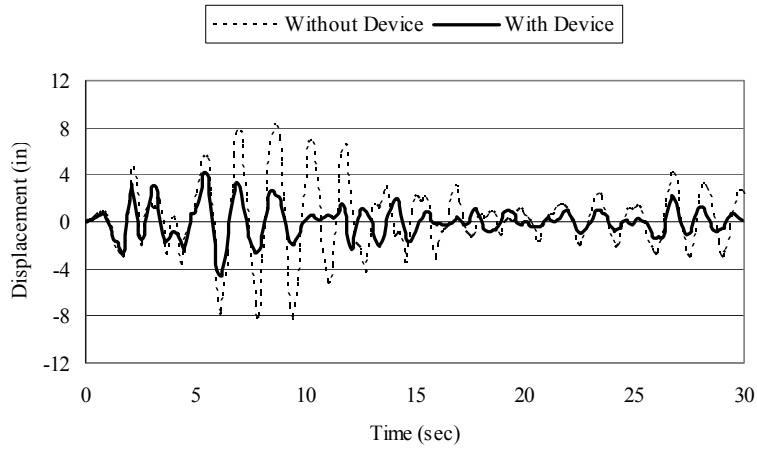


a) Story displacements at maximum top floor displacement.

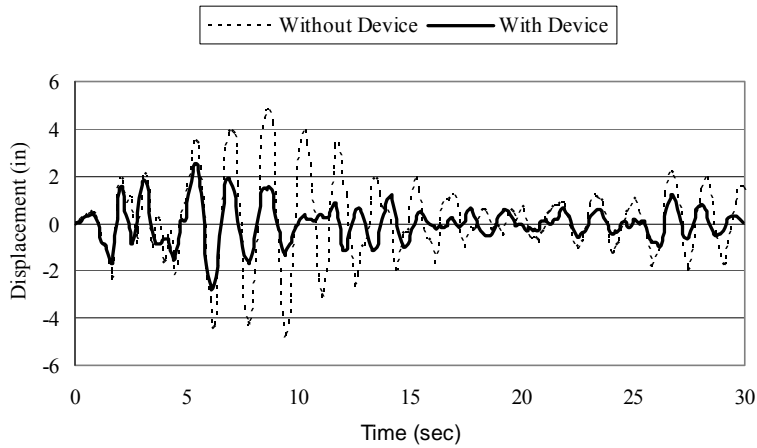


b) Bending moment on the column bases at maximum top floor displacement.

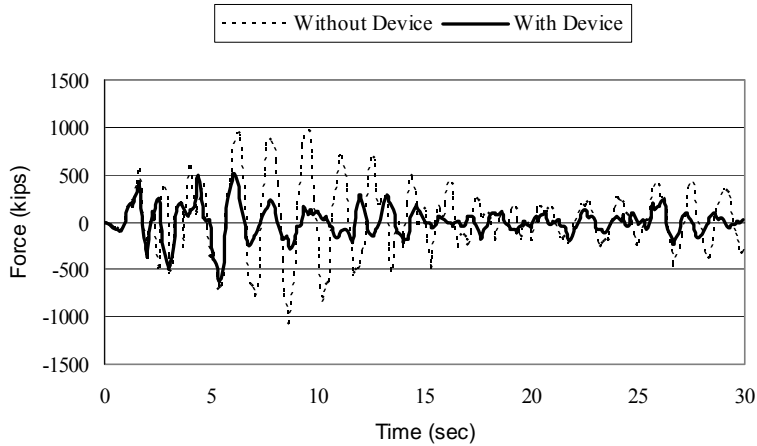
Figure 5.16: Effect of the device on the floor displacements and bending moments at column bases of the nine-story frame under harmonic excitation. (C3-K1-H3-S1-LP-H)



a) Top floor horizontal displacement.

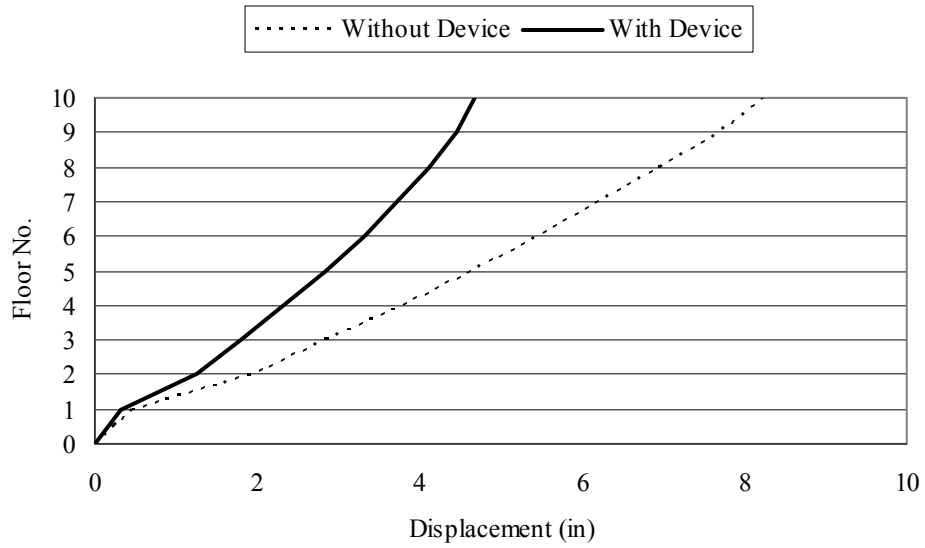


b) Fifth floor horizontal displacement.

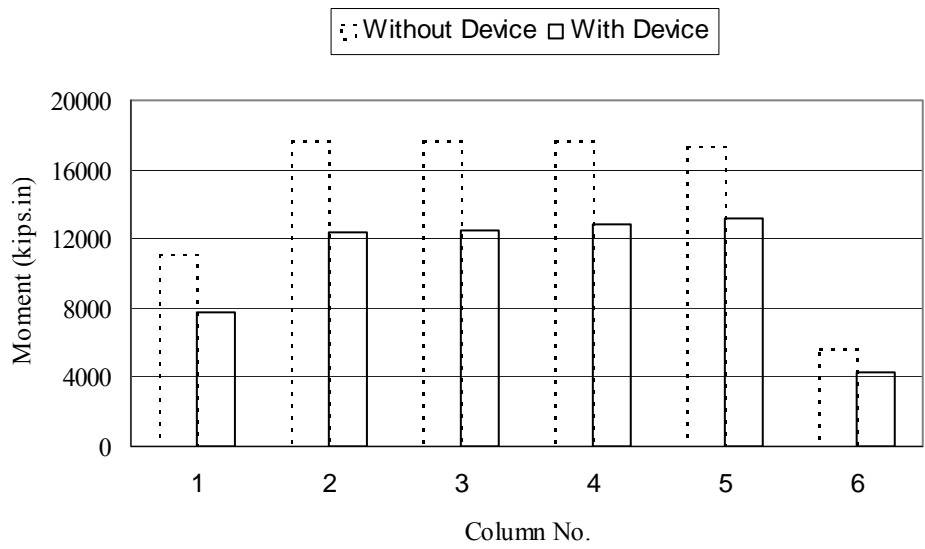


c) Total base shear.

Figure 5.17: Effect of the device on the response of the nine-story frame under El Centro earthquake. (C4-K1-H3-S1-LP-E)

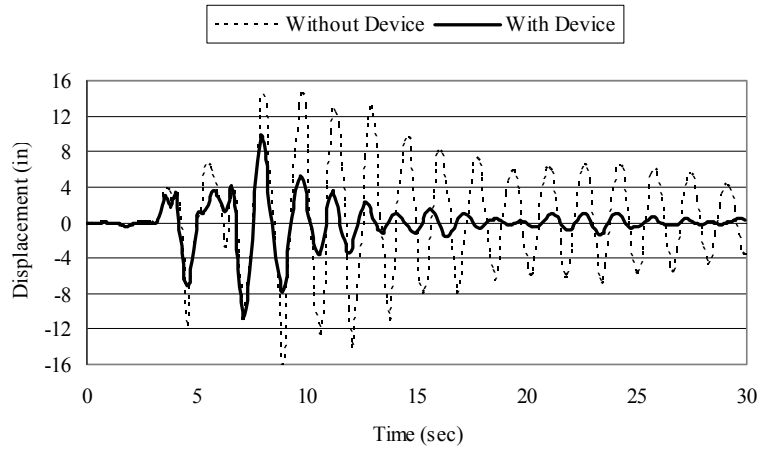


a) Story displacements at maximum top floor displacement.

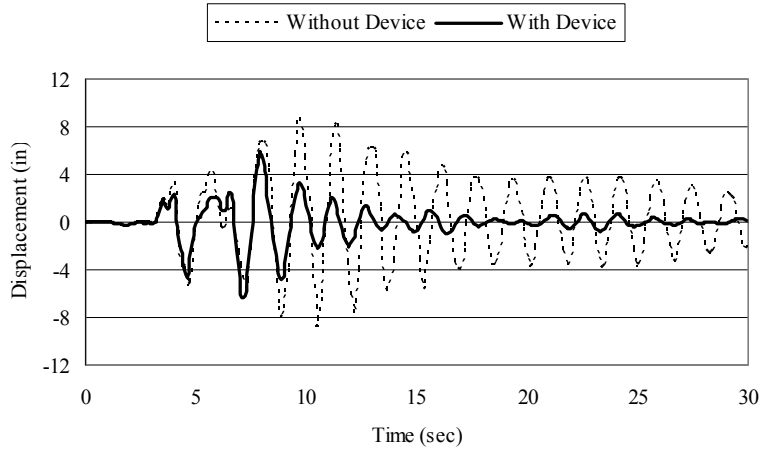


b) Bending moment on the column bases at maximum top floor displacement.

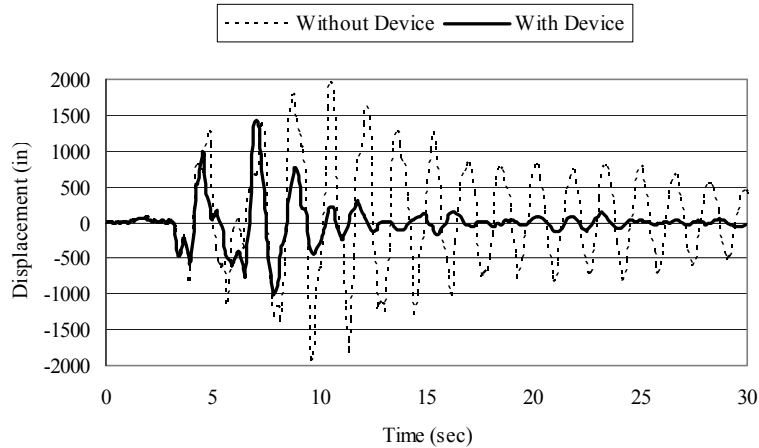
Figure 5.18: Effect of the device on the floor displacements and bending moments at column bases of nine-story frame under El Centro earthquake (C3-K1-H3-S1-LP-E)



a) Top floor horizontal displacement.

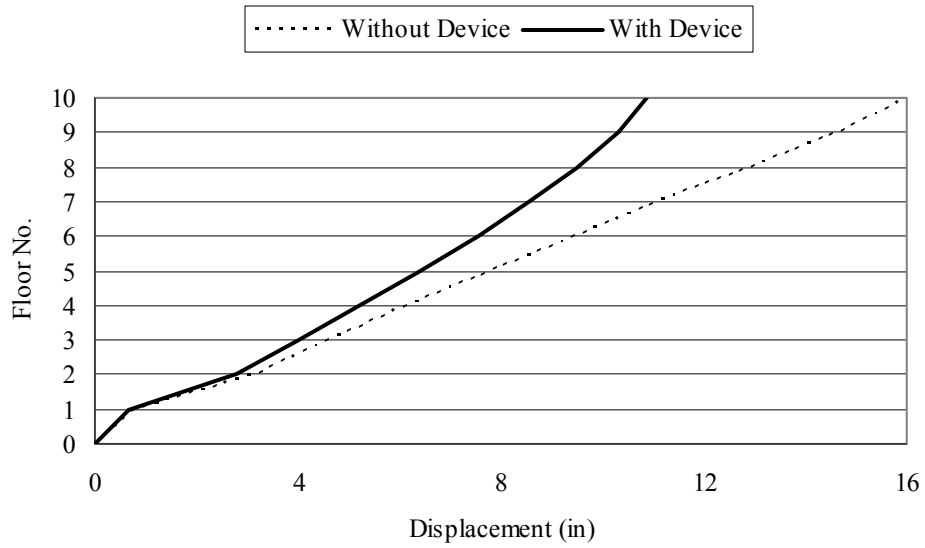


b) Fifth floor horizontal displacement.

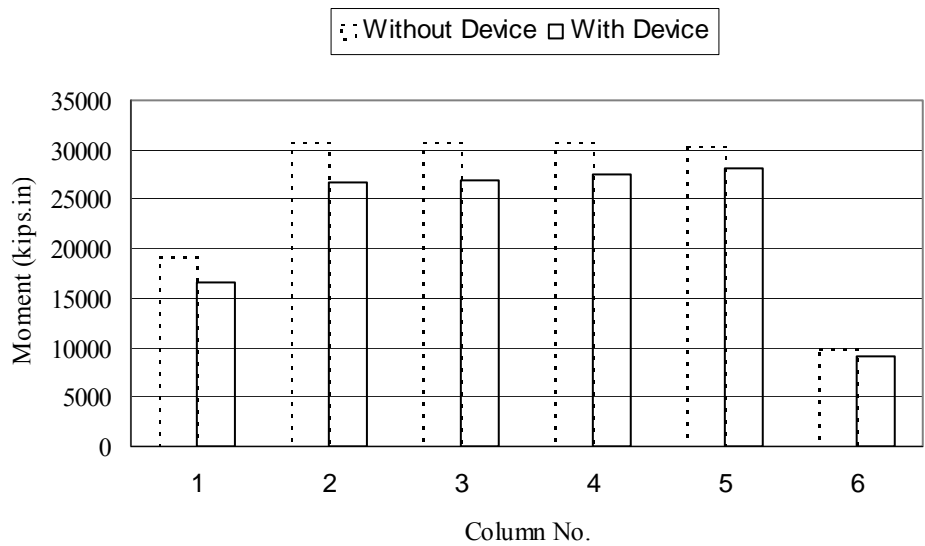


c) Total base shear.

Figure 5.19: Effect of the device on the response of the nine-story frame under Northridge earthquake. (C4-K1-H3-S1-LP-NR)



a) Story displacements at maximum top floor displacement.



b) Bending moment on the column bases at maximum top floor displacement.

Figure 5.20: Effect of the device on the floor displacements and bending moments at column bases of the nine-story frame under Northridge Earthquake. (C3-K1-H3-S1-LP-NR)

5.3.3 Comparison between Visco-plastic Device and Conventional Viscoelastic Dampers

In most of the viscoelastic damper applications, the conventional damper is relying on obtaining the damping through the shear strains developed in the material. In this device, the damping is mainly obtained through the tensile and compression strains. Now, it is important to compare the efficiency of this device with the conventional type of the viscoelastic dampers. To model this device, the vertical viscous dashpot and springs were replaced by one horizontal dashpot and one horizontal spring having the damping constant, C , equal to the summation of the damping constants of the vertical dashpots and the spring stiffness, K , equal to the summation of the stiffness of the vertical springs.

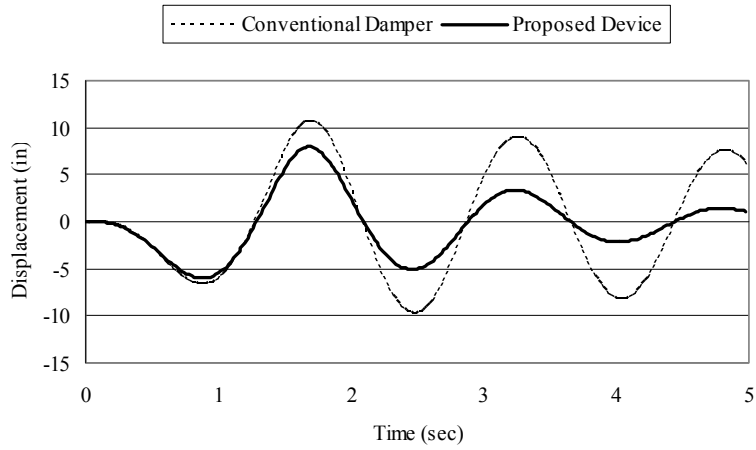
The responses of the nine-story steel frame with the conventional type and with the new device under harmonic excitation are shown in Figure 5.21 and Figure 5.22. The results show the superiority of the new device over the conventional viscoelastic damper regarding its effect on the response of the nine-story frame. The maximum top floor displacement was reduced from 10.7 in. in the conventional damper case to 8.0 in. in the new device case with a reduction percentage of 25.5 %. The maximum fifth floor displacement was reduced by 24.1 %. As depicted from the figures, the reduction increases in the next cycles. This indicates that more energy was dissipated per cycle by the new device. According to Figure 5.22a, the new device enhanced the structural response regarding the story displacements much more than the conventional damper. At the maximum top floor displacement, using the new device instead of the conventional damper resulted in an average reduction of story displacements of 21.8 %. Using the new device resulted in lower values of bending moments at column bases, as shown in Figure 5.22b. The average reduction in the bending moments at column bases was 10.9 %.

The same comparison was conducted on the two cases but this time having the steel frame subjected to El Centro earthquake. Figure 5.23 and Figure 5.24 present the results of this analysis. The maximum displacement was reduced in the case of the new device by 34.2 % and 36.9 % in the top floor and fifth floor respectively. The maximum base shear was reduced from 1118.4 kips to 628.0 kips with a reduction percentage of 43.8 %.

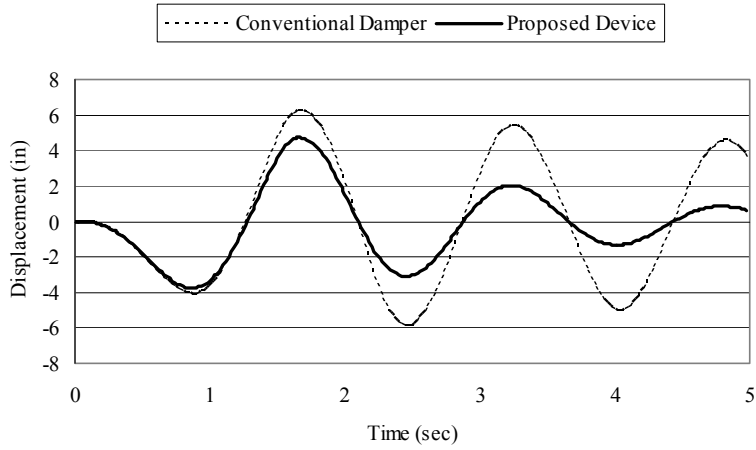
Figure 5.24 shows the superiority of the new device in its effect on the story displacements and bending moments at column bases, at the maximum top floor displacement. The story displacements were considerably reduced especially in the upper stories. The average reduction in floor displacements was 28.0 %. The bending moments at column bases were reduced in all columns. The average reduction in bending moments was 16.2 %.

In order to check the effect of both dampers on the response of the steel frame under different ground excitations, the two cases were studied again under Northridge earthquake. The results of this analysis are shown in Figure 5.25 and Figure 5.26. Due to the use of the new device instead of the conventional damper, the maximum top floor displacement was reduced by 27.6 % while the fifth floor displacement was only reduced by 18.7 %. The maximum base shear was reduced from 1963.5 kips to 1405.2 kips with a reduction percentage of 28.4 %. At the maximum top floor displacement, the floor displacements were reduced by an average of 15.9 % while the bending moments at column bases were reduced by an average of 6.2 %.

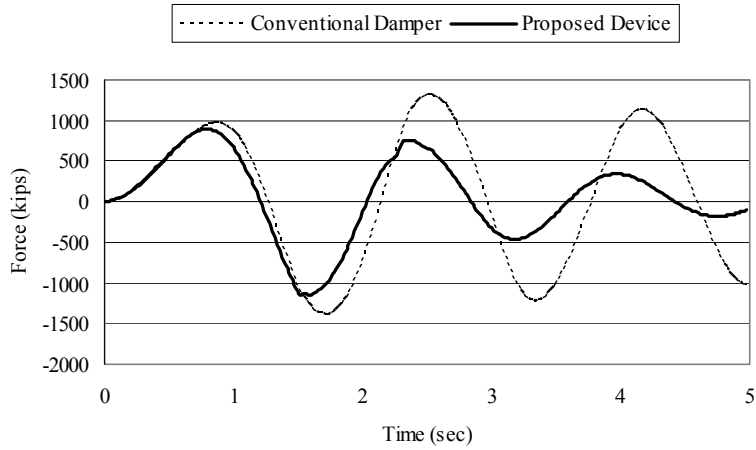
Of course, an improvement in the performance of the conventional viscoelastic damper can be obtained by picking higher values for the damping constant and spring stiffness, but the comparison was made according to the same values of these parameters in both cases. Also, the new device provides higher stiffness in both directions because of the steel elements of the device as well as the larger volume of the viscoelastic material sandwiched between these steel elements.



a) Top floor horizontal displacement.

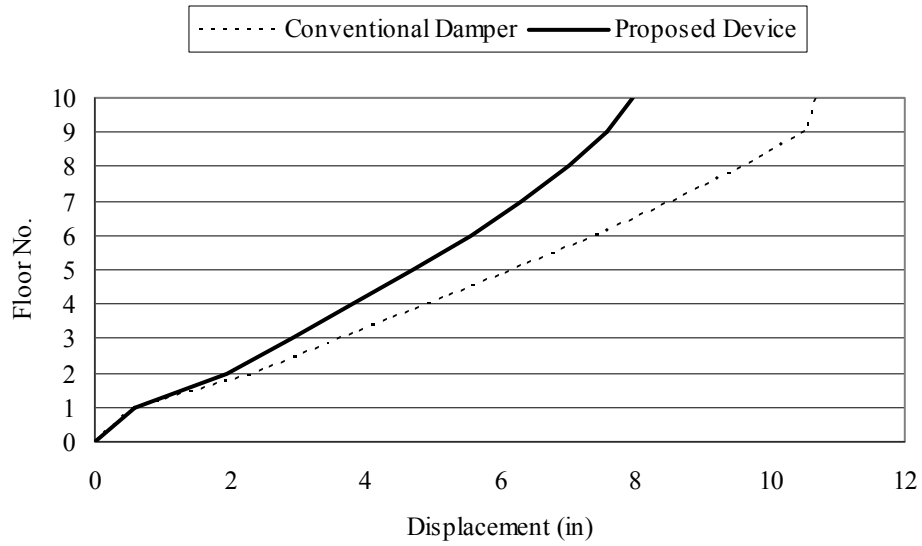


b) Fifth floor horizontal displacement.

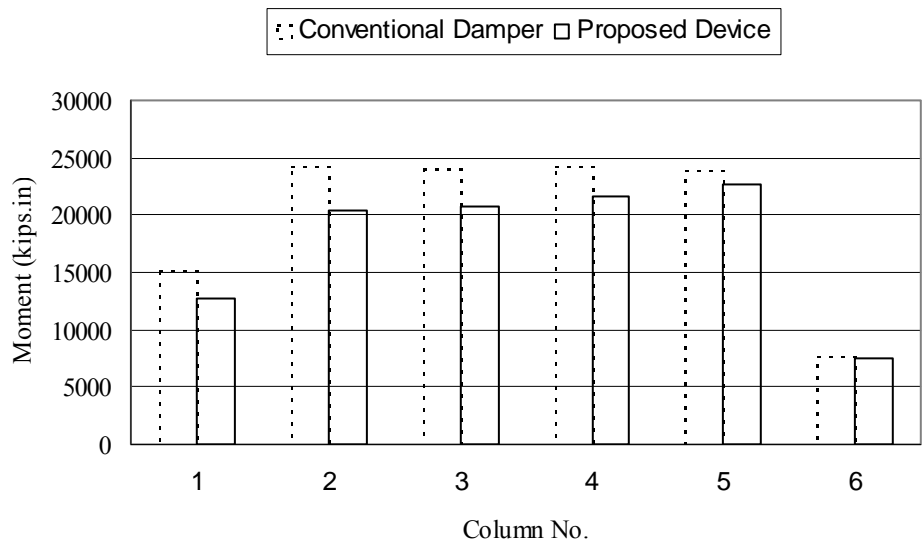


c) Total base shear.

Figure 5.21: Effect of using the new device instead of the conventional damper on the response of the nine-story frame under harmonic excitation. (C4-K1-H3-S1-LP-H)

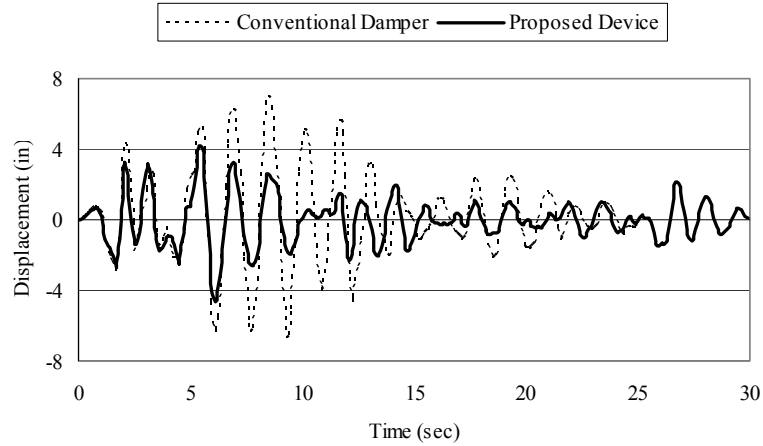


a) Story displacements at maximum top floor displacement.

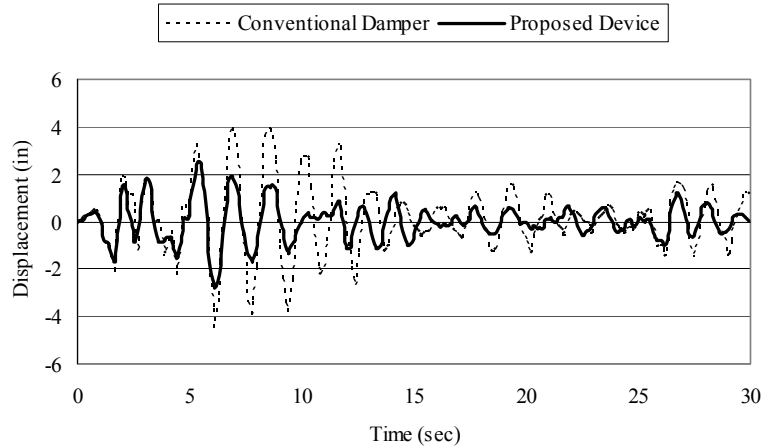


b) Bending moment on the column bases at maximum top floor displacement.

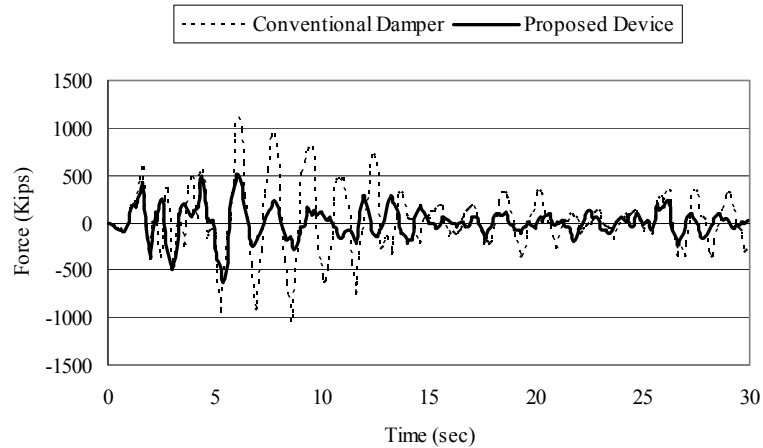
Figure 5.22: Effect of using the new device instead of the conventional damper on the floor displacements and bending moments at column bases of the nine-story frame under harmonic excitation. (C4-K1-H3-S1-LP-H)



a) Top floor horizontal displacement

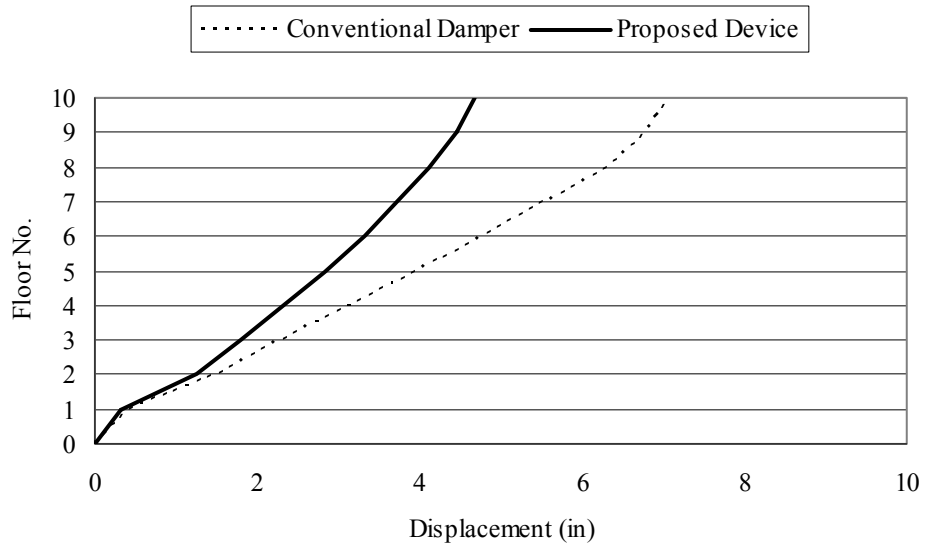


b) Fifth floor horizontal displacement.

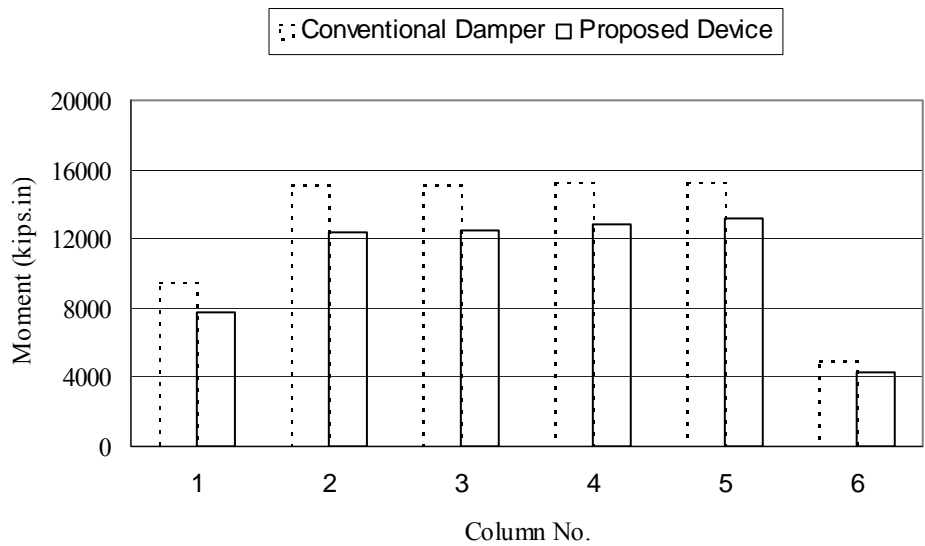


c) Total base shear.

Figure 5.23: Effect of using the new device instead of the conventional damper on the response of the nine-story frame under El Centro earthquake. (C4-K1-H3-S1-LP-E)

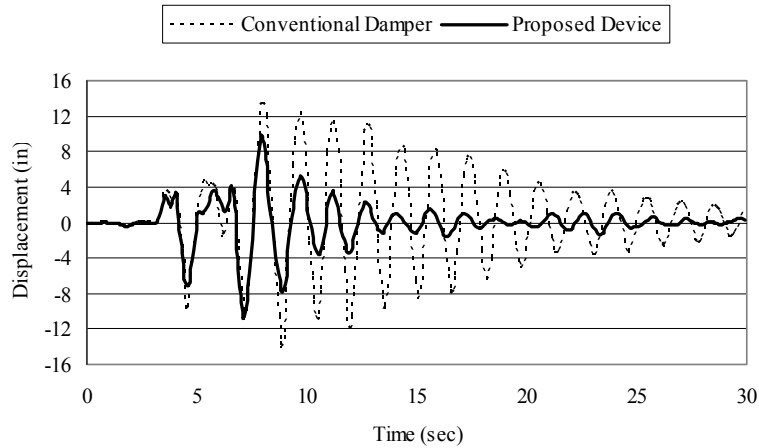


a) Story displacements at maximum top floor displacement.

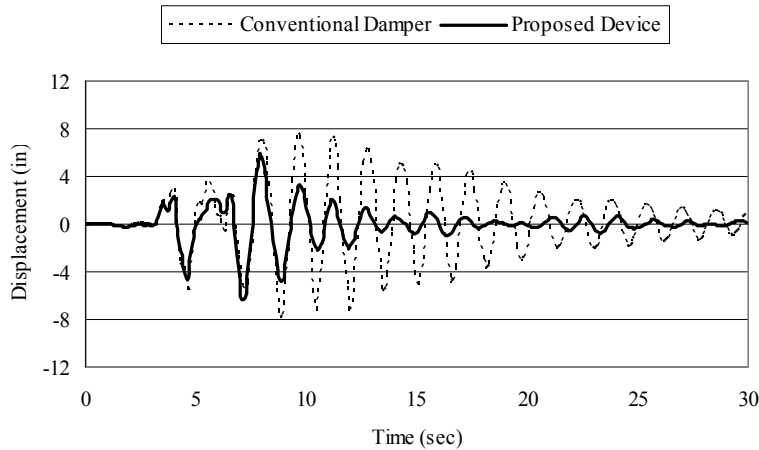


b) Bending moment on the column bases at maximum top floor displacement.

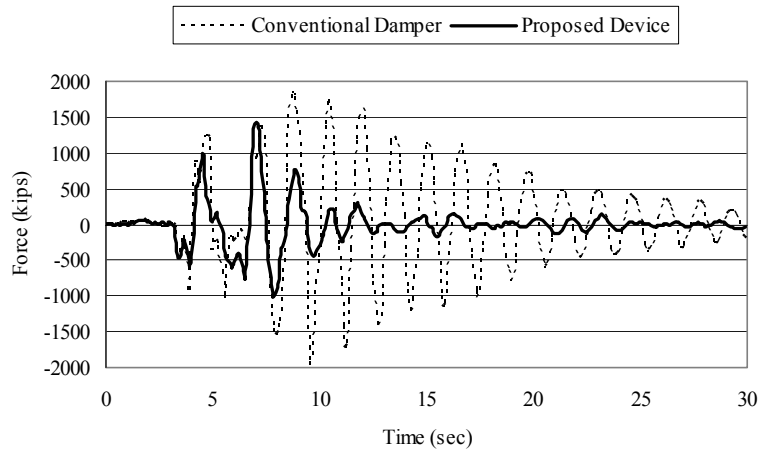
Figure 5.24: Effect of using the new device instead of the conventional damper on the floor displacements and bending moments at column bases of the nine-story frame under El Centro earthquake. (C4-K1-H3-S1-LP-E)



a) Top floor horizontal displacement

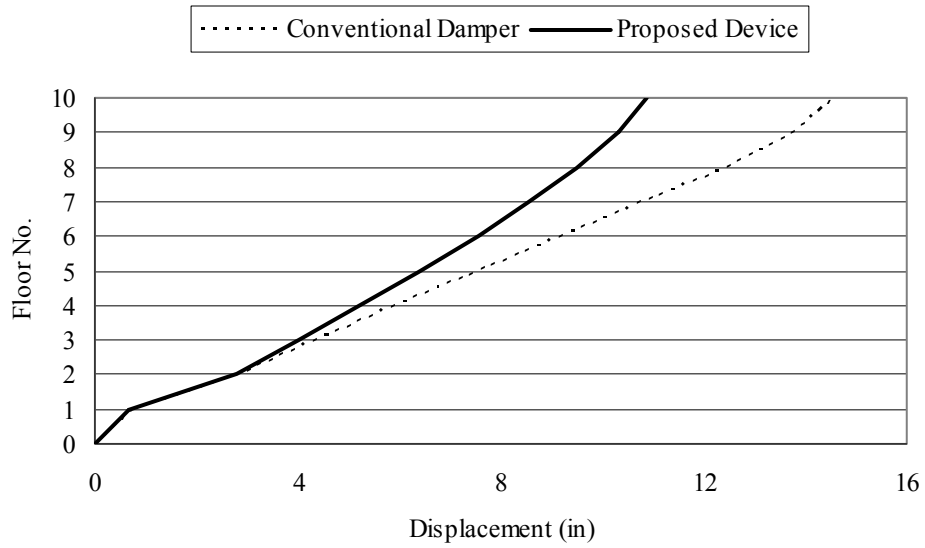


b) Fifth floor horizontal displacement.

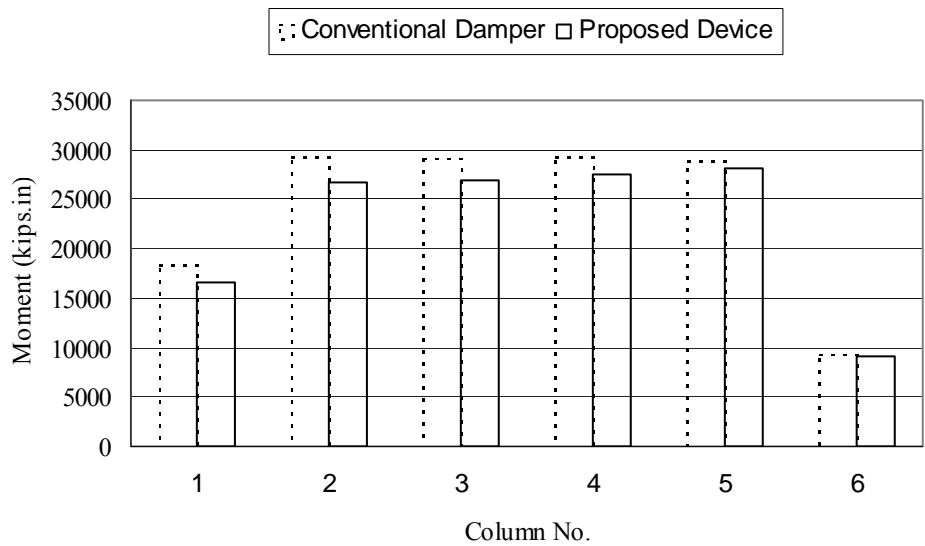


c) Total base shear.

Figure 5.25: Effect of using the new device instead of the conventional damper on the response of the nine-story frame under Northridge earthquake. (C4-K1-H3-S1-LP-NR)



a) Story displacements at maximum top floor displacement.



b) Bending moment on the column bases at maximum top floor displacement.

Figure 5.26: Effect of using the new device instead of the conventional damper on the floor displacements and bending moments at column bases of the nine-story frame under Northridge earthquake. (C4-K1-H3-S1-LP-NR)

5.3.4 Different Arrangement of the Devices in the Multi-Story Structure

After showing the great improvement introduced by the new device to the response of the nine-story steel frame under different ground excitations and its superiority over the conventional viscoelastic damper, another arrangement of the device was tried to check the possibility of optimizing the device effect on the response of the nine-story steel frame. As shown in Figure 5.27, the new arrangement was chosen to be two devices per story. Now, a response history analysis of this new model under different ground excitations was conducted and the results were compared to the results of the steel frame without any devices.

First, the new model was analyzed under harmonic ground excitation. Figure 5.28 and Figure 5.29 show the comparison between both models. The results show great enhancement on the structural response due to the new arrangement. The maximum top floor displacement was reduced by 68.3 % while the maximum fifth floor displacement was reduced by 62.7 %. The maximum total base shear was reduced by 24.4 %. As shown in Figure 5.29, the new arrangement of the devices had a great effect in reducing the story displacements and bending moments at column bases. At the maximum top floor displacement, the average reduction introduced by the new arrangement regarding the floor displacements was 62.3 %. The bending moments at column bases were significantly reduced by an average percentage of 45.1 %.

Both cases were compared upon analyzing the nine-story steel frame under unscaled real records of El Centro earthquake. Figure 5.30 and Figure 5.31 show the results of this analysis. Due to the use of two devices per story, the maximum top floor displacement was reduced by 66.9 % while the maximum fifth floor displacement was reduced by 62.7 %. The new arrangement had a great effect on the story displacements and bending moments at column bases, as shown in Figure 5.31. The average reduction in story displacements was 60.1 %. The bending moments at column bases were significantly reduced by the new arrangement. The average reduction in the bending moments at column bases was 38.1 %.

Finally, the nine-story steel frame with two devices per floor was analyzed under Northridge earthquake and compared to the results of the steel frame without devices under the same earthquake. Upon using this new arrangement, the maximum top floor displacement was reduced from 16.18 in. to 7.5 in. with a reduction percentage of 56.4 % while the maximum fifth floor displacement was reduced from 8.9 in. to 4.4 in. with a reduction percentage of 50.5 %. The maximum base shear was reduced by 53.3 %. At maximum top floor displacement, the bending moments at column bases were reduced in all columns with an average reduction percentage of 11.8 %. The new arrangement of the devices reduces effectively the story displacements. At maximum top floor displacement, the average reduction of the story displacements was 44.3 %. The results of this analysis are shown in Figure 5.32 and Figure 5.33.

According to the previous analyses relevant to the arrangement of the devices throughout the structure, it was shown that the improvement that the device can introduce to the response of multi-story frames can be optimized if their arrangement was chosen carefully. Of course, the suggested arrangement is not the only possible one in this regard. On the other hand, the maximum number of devices to be attached to a structure is governed also by the economic factors although the cost of the devices is not expected to be high since the device is made from readily available materials.

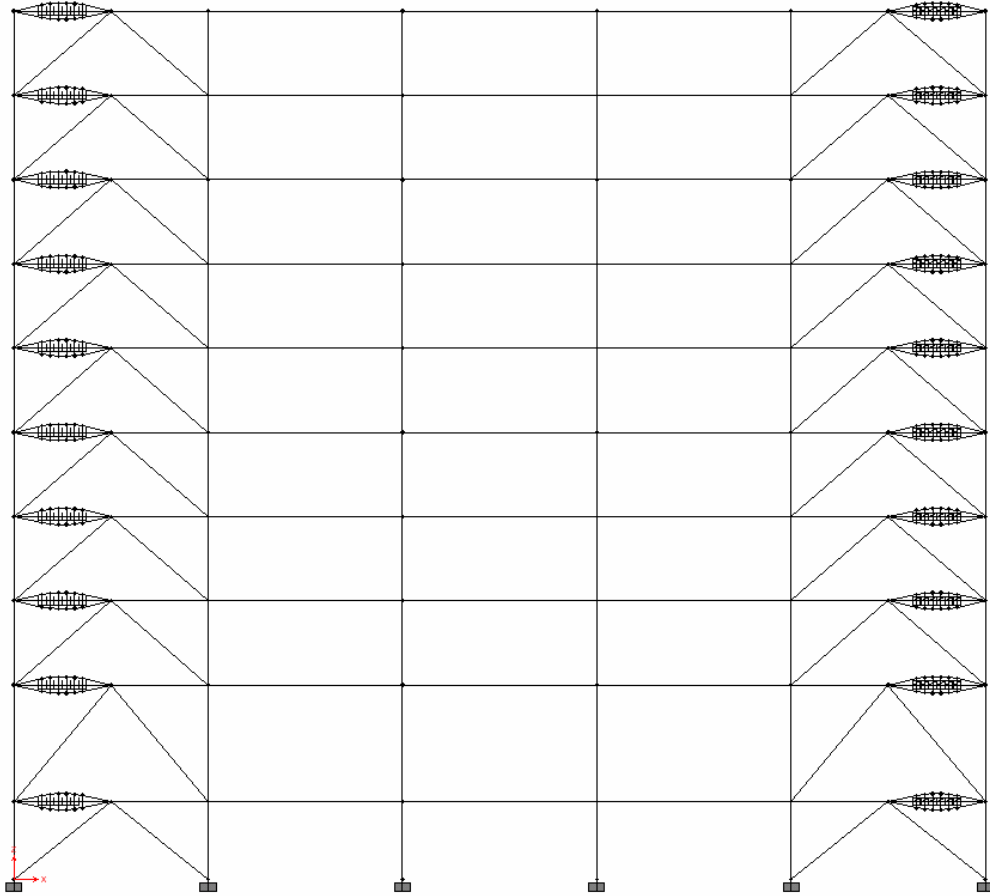
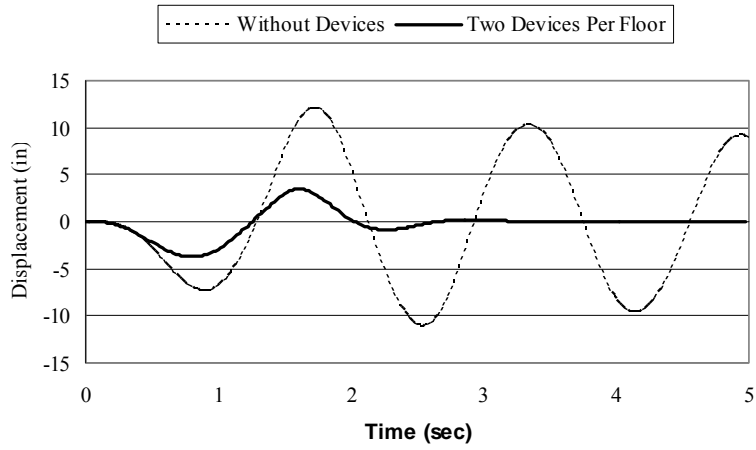
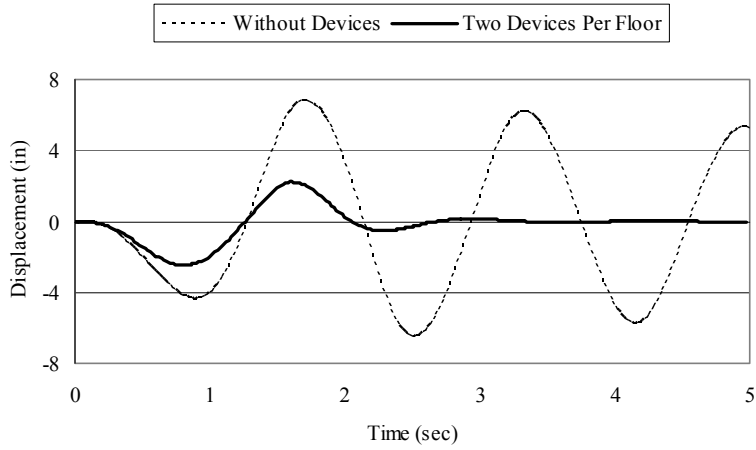


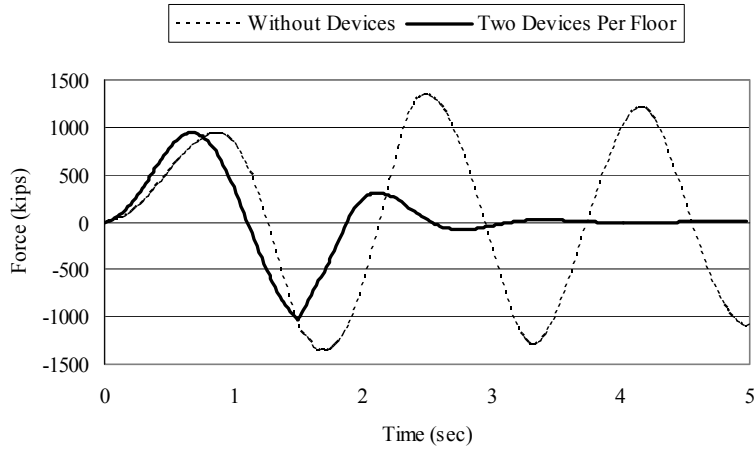
Figure 5.27: The nine-story five-bay steel frame with two devices per floor.



a) Top floor horizontal displacement.

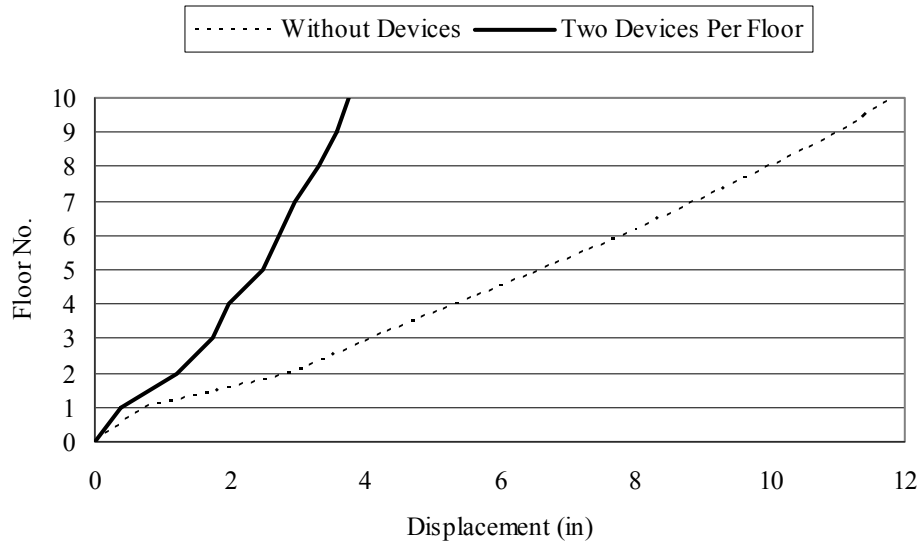


b) Fifth floor horizontal displacement.

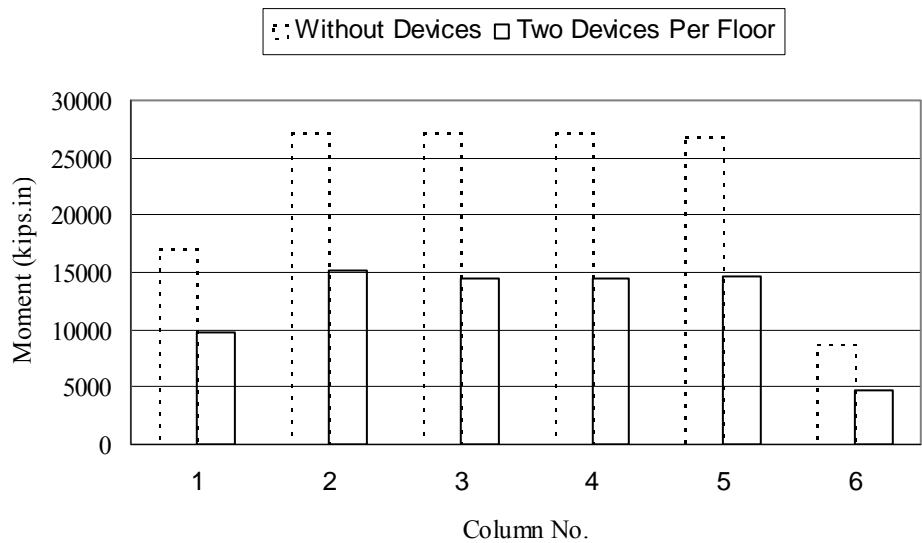


c) Total base shear.

Figure 5.28: Effect of using two devices per floor on the response of the nine-story frame under harmonic excitation. (C4-K1-H3-S1-LP-H)

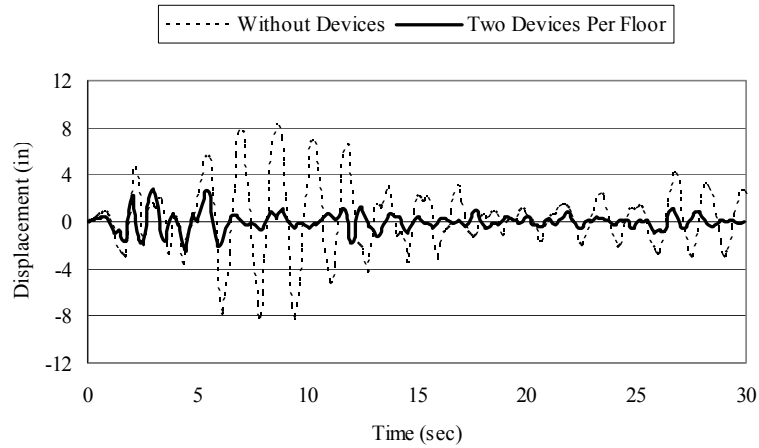


a) Story displacements at maximum top floor displacement.

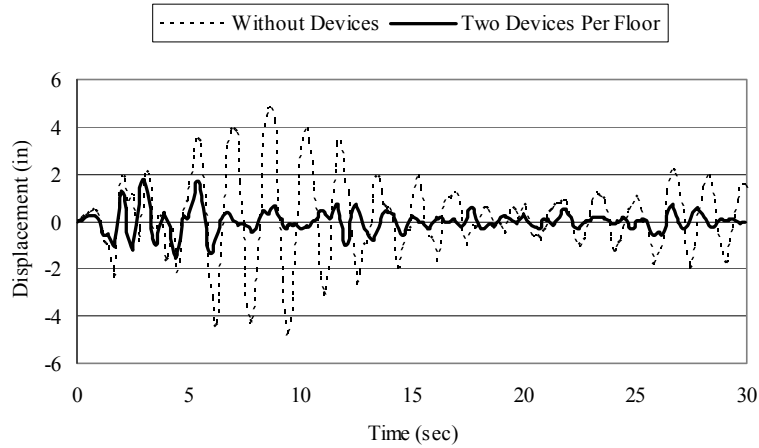


b) Bending moment on the column bases at maximum top floor displacement.

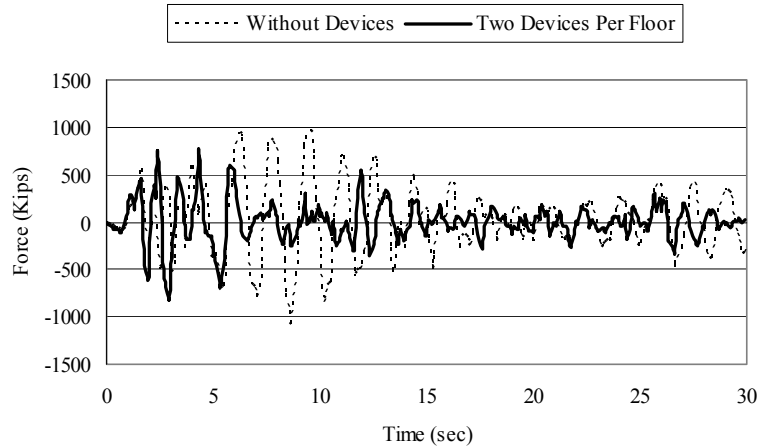
Figure 5.29: Effect of using two devices per floor on the floor displacements and bending moments at column bases of the nine-story frame under harmonic excitation. (C4-K1-H3-S1-LP-H)



a) Top floor horizontal displacement.

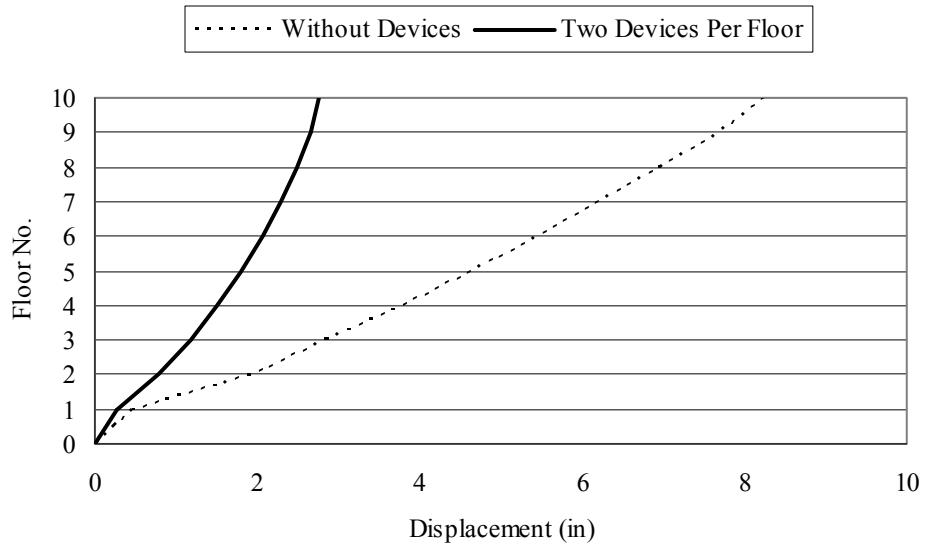


b) Fifth floor horizontal displacement.

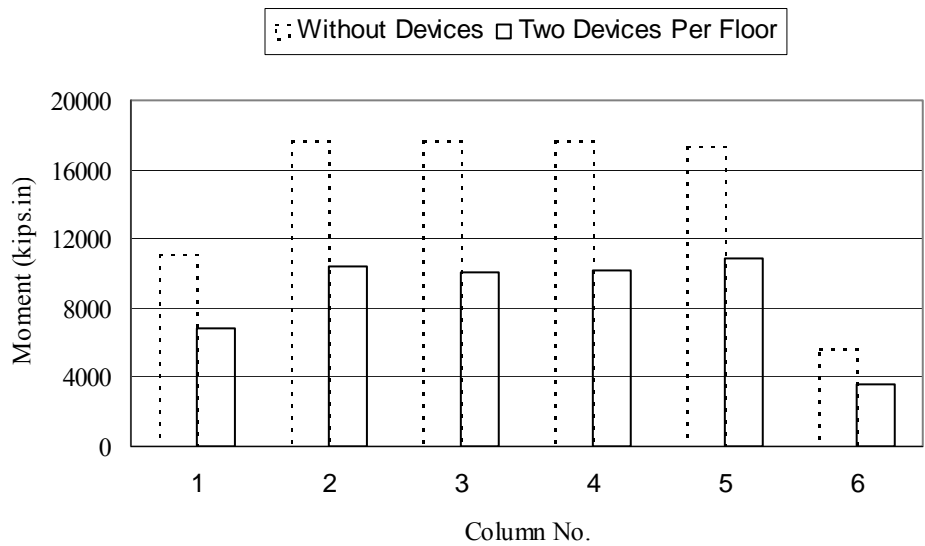


c) Total base shear.

Figure 5.30: Effect of using two devices per floor on the response of the nine-story frame under El Centro earthquake. (C4-K1-H3-S1-LP-E)

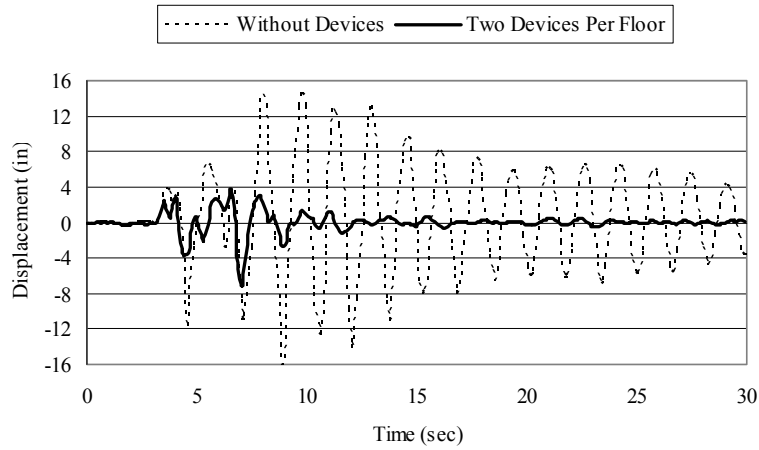


a) Story displacements at maximum top floor displacement.

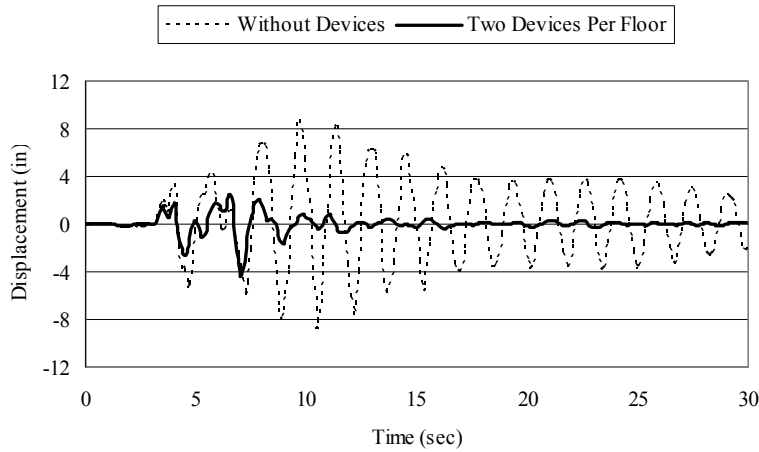


b) Bending moment on the column bases at maximum top floor displacement.

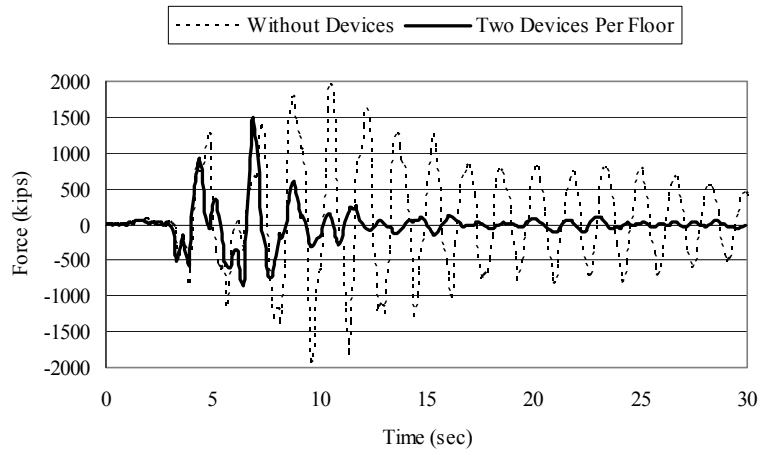
Figure 5.31: Effect of using two devices per floor on the floor displacements and bending moments at column bases of the nine-story frame under El Centro earthquake. (C4-K1-H3-S1-LP-E)



a) Top floor horizontal displacement.

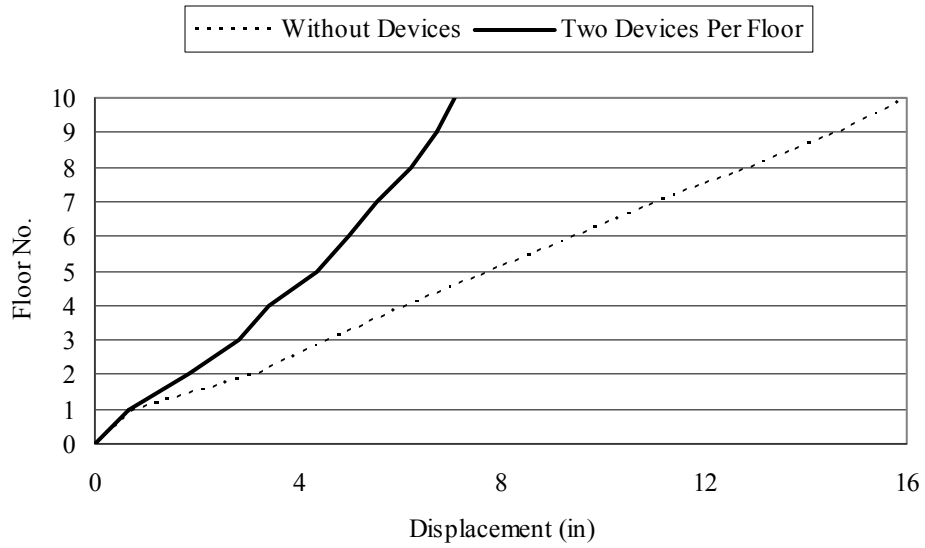


b) Fifth floor horizontal displacement.

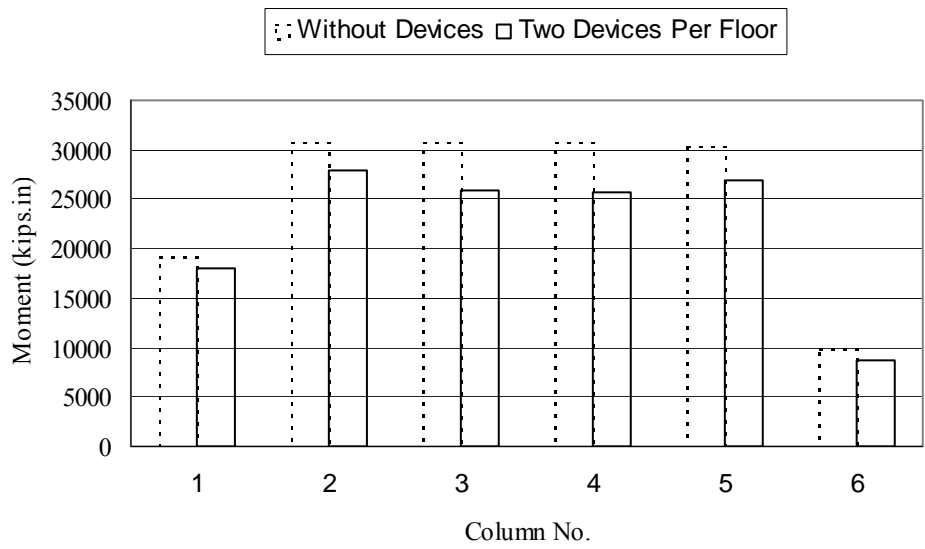


c) Total base shear.

Figure 5.32: Effect of using two devices per floor on the response of the nine-story frame under Northridge earthquake. (C4-K1-H3-S1-LP-NR)



a) Story displacements at maximum top floor displacement.



b) Bending moment on the column bases at maximum top floor displacement.

Figure 5.33: Effect of using two devices per floor on the floor displacements and bending moments at column bases of the nine-story frame under Northridge earthquake. (C4-K1-H3-S1-LP-NR)

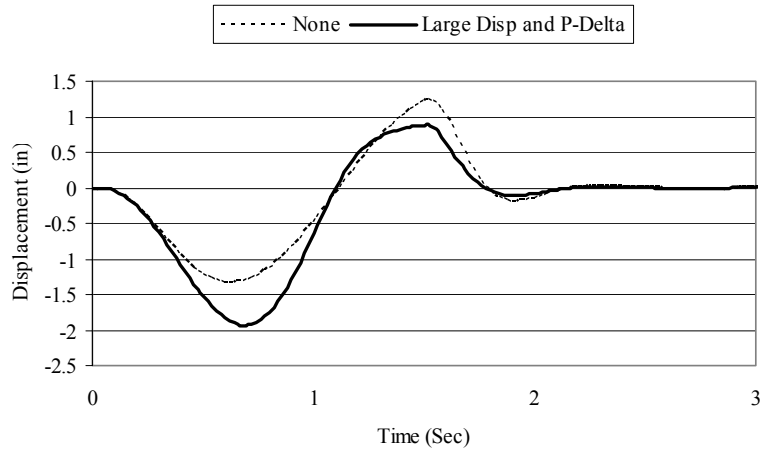
5.4 Comments on the device modeling using SAP2000

5.4.1 Material Modeling

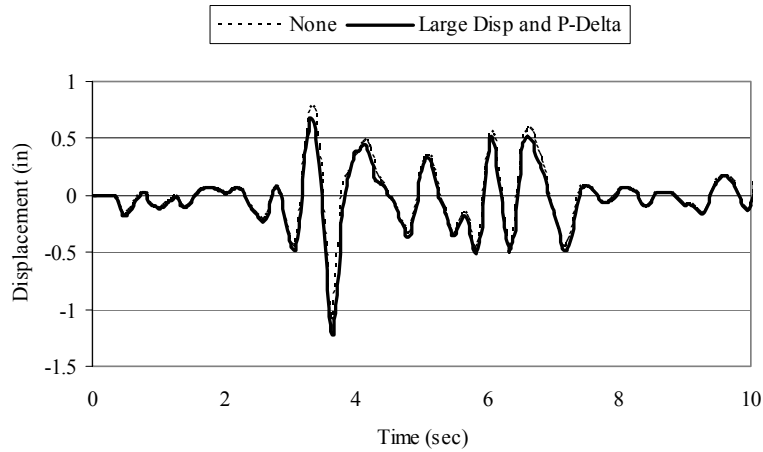
Throughout the analyses performed so far, the steel elements of the device were assumed to behave linearly elastic. However, it is expected that these elements undergo inelastic behavior under moderate and strong ground excitations. Considering this behavior will result in dissipating higher energy through the device, which improves the structural performance under different ground excitations. At the same time, steel yielding causes a reduction in the device stiffness, which may lead to a small increase in floor displacements. This behavior is discussed in detail in the next chapter through the finite element analysis of the device.

5.4.2 Analysis Type

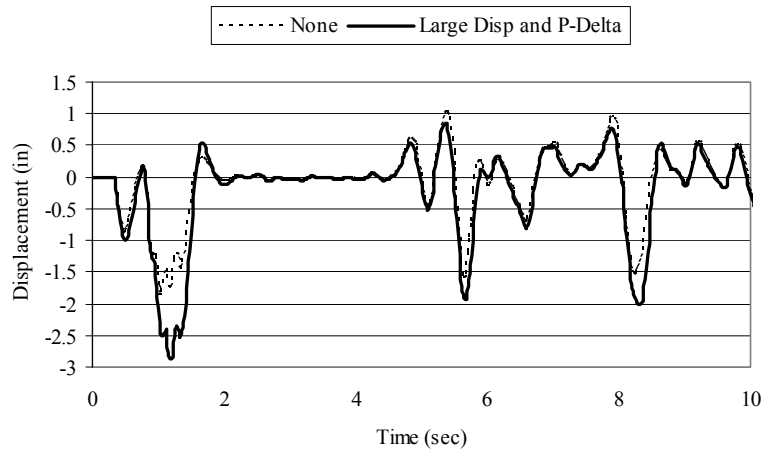
During all of the previous analyses, a time integration method was used to determine the response of the structure under different types of excitations. To encounter the geometric nonlinearities, large displacement and P- δ effects were considered in the analyses. To show the importance of considering these effects on the results, the single-story steel frame with the device was analyzed under harmonic excitation and real records of El Centro and Northridge earthquakes ignoring the geometric nonlinearities. As shown in Figure 5.34, considering the geometric nonlinearities affects the results considerably, especially when the structure experiences relatively large floor displacements. Considering the large-displacement P- δ effects in the analysis is important for the device behavior. In the next chapter, large displacement and P- δ effects are considered in the detailed finite element analysis of the device.



a) Floor displacement under harmonic excitation.



b) Floor displacement under El Centro earthquake.



c) Floor displacement under Northridge earthquake.

Figure 5.34: Effect of analysis type on the response of the single-story frame. (C2-K2-H3-S3)

5.5 Conclusions

The device is very controllable since it has many design parameters that should be considered in order to optimize the use of this device in dissipating energy in different structures. These parameters include the aspect ratio of the device, h/l , dimensions of the viscoelastic material, type and cross section of the steel elements, type of the viscoelastic material (which reflects the values of the damping and stiffness) and the arrangement of the devices. The optimum use of this device is generally obtained through the maximum amplification of the horizontal displacement to get the maximum vertical displacement at the middle of the device within the allowable values of the tensile and compression strains of the viscoelastic material. The material should be picked carefully to satisfy the different requirements of the analyses especially the allowable strains and the required damping. According to the previous analyses, it was shown that the device provided a significant reduction of the response of different types of frames, single-story single-bay and nine-story five-bay structures under harmonic excitation in addition to the real records of El Centro and Northridge earthquakes. The device showed a much better improvement than the conventional type of viscoelastic dampers.

In order to obtain accurate results, the inelastic behavior of the steel elements should be modeled using the Von Mises yield criterion. The viscoelastic material should be modeled as three-dimensional solid elements considering the hyperelastic behavior of the material since the material is expected to be exposed to large tensile and compressive strains. Throughout the preliminary analyses, the damping constant of the viscoelastic material was assumed to be constant regardless the strains developed within the material as well as the excitation frequency, which contradicts the actual behavior of viscoelastic materials. These shortcomings were eliminated in the accurate finite element analysis.

In chapter 6, a detailed parametric study was carried out using the finite element analysis program, ABAQUS [Hibbitt, Karlsson, and Sorensen, Inc. (2002)], to determine the different device parameters in order to enhance its behavior and consequently its effectiveness on the response of structures. The device parameters included in this study were the aspect ratio, rubber width, steel cross section and steel type. The device was

analyzed under different dynamic loads, including quasi-static tension, quasi-static compression, and harmonic loads.

Chapter 6: Detailed Finite Element Analysis

6.0 Introduction

In the previous chapter, the device was preliminarily modeled using the SAP2000 program. The viscoelastic material was modeled using discrete linear springs in parallel to nonlinear NLINK elements. The NLINK element consists of a nonlinear spring in series with a dashpot, which represents the Maxwell model. The steel elements were modeled using beam elements and were assumed to behave linearly elastic during the whole preliminary analyses.

In this chapter, a detailed finite element analysis was conducted to determine the actual behavior of the device. The viscoelastic material was modeled using three-dimensional solid elements. The viscoelastic and hyperelastic properties were considered. The steel elements were modeled using quadrilateral shell elements. The inelastic behavior of these elements was considered using the Von Mises yield criterion. The device was modeled taking in consideration the large displacement and p-delta effects.

First, the material modeling of the rubber and steel will be presented in detail. Then, the geometric modeling of the device, including the types of meshing elements for rubber block and steel will be explained. Finally, a detailed parametric study will be conducted on the device to determine the different parameters that control its behavior and how they can be properly selected to enhance the device behavior. The device will be analyzed under different types of dynamic loads, include tension, compression and harmonic loads.

6.1 Material Modeling

6.1.1 Modeling Rubber Block

6.1.1.1 Hyperelasticity

Elastomers, like rubber and foam, are classified as hyperelastic materials. Hyperelastic materials have the ability to deform elastically up to large strains. The stress-strain curve is highly nonlinear but elastic. Typical hyperelastic behavior of rubber is shown in Figure 6.1.

ABAQUS assumes the following assumptions for hyperelastic material

- Material behavior is isotropic.
- Material behavior is elastic.
- Material is incompressible by default (unless specified).
- Analysis includes nonlinear geometric effects.

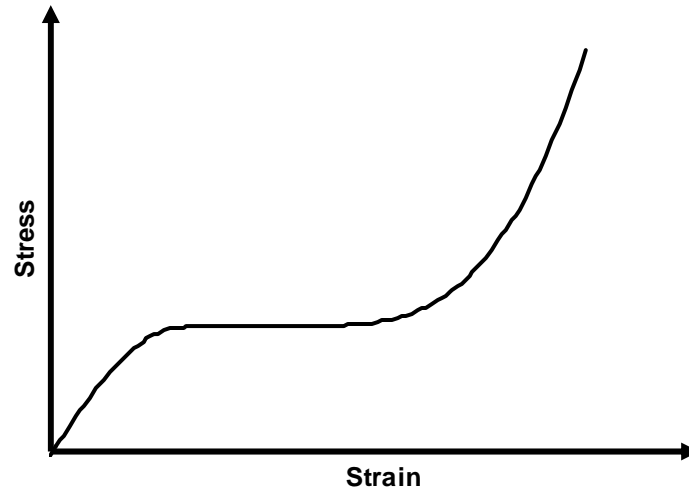


Figure 6.1: Typical stress-strain curve for hyperelastic material

6.1.1.1.1 Hyperelastic models

To define the hyperelastic behavior of a material, a stored strain energy function, $U(\varepsilon)$ is introduced. This function defines the strain energy stored in a material per unit volume. The stress-strain relationship of a hyperelastic material can be obtained from this function through the following relation:

$$\sigma_{ij} = \frac{\partial U(\varepsilon)}{\partial \varepsilon_{ij}} \quad (6-1)$$

where σ_{ij} and ε_{ij} are the stress and strain component, respectively.

Depending on the form of this function, there are many models or forms used to model the hyperelasticity, such as Arrude-Boyce, Van der Waals, Mooney-Rivlin, Neo-Hookean, Ogden, Polynomial, Reduced polynomial and Yeoh forms. Most of these

models are special cases from the polynomial form [Raos (1992) and Hibbitt, Karlsson, and Sorensen, Inc. (2002)].

Raos (1992) investigated four models, Van der Waals, Mooney-Rivlin, Neo-Hookean, and Ogden models in order to check the possibility of predicting the experimental results by these models. The experimental results were obtained from uniaxial and biaxial tension and compression tests on SBR rubber vulcanizate. These tests covered a wide range of deformations (extension ratio, λ , from 0.5 to 4.0). According to the results of this analysis, it was observed that Neo-Hookean and Mooney-Rivlin models can predict experimental results in compression and moderate tension only (extension ratio, λ less than 1.8) while Van der Waals and Ogden model can predict experimental results for the whole range considered with satisfactory approximation.

In this chapter, the polynomial model is described as well as the Ogden model, which is used in modeling the hyperelastic behavior of the viscoelastic material used in the device.

6.1.1.1.1 Polynomial Model

The polynomial strain energy function per unit original volume, $U(\varepsilon)$, is defined as

$$U(\varepsilon) = \sum_{i+j=1}^N C_{ij} (\bar{I}_1 - 3)^i (\bar{I}_2 - 3)^j + \sum_{i=1}^N \frac{1}{D_i} (J^{el} - 1)^{2i} \quad (6-2)$$

where C_{ij} and D_i are temperature-dependent material parameters and \bar{I}_1 and \bar{I}_2 are the 1st and 2nd deviatoric strain invariants obtained from:

$$\bar{I}_1 = \bar{\lambda}_1^2 + \bar{\lambda}_2^2 + \bar{\lambda}_3^2 \quad (6-3)$$

$$\bar{I}_2 = \frac{1}{\bar{\lambda}_1^2} + \frac{1}{\bar{\lambda}_2^2} + \frac{1}{\bar{\lambda}_3^2} \quad (6-4)$$

And,

$$\bar{\lambda}_i = J^{-\frac{1}{3}} \lambda_i \quad (6-5)$$

where λ_1 , λ_2 and λ_3 are the principal stretches obtained from dividing the current length over the initial one, $\bar{\lambda}_i$ are the deviatoric stretches, and J is the total volume ratio.

$$J = \frac{\lambda_1 \lambda_2 \lambda_3}{V_0} \quad (6-6)$$

where V_0 is the original volume, $J=1$ for incompressible material, J^{el} is the elastic volume ratio; $J^{el} = \frac{J}{J^{th}}$ and J^{th} is the thermal volume ratio obtained from:

$$J^{th} = (1 + \varepsilon^{th})^3 \quad (6-7)$$

where ε^{th} is the linear thermal expansion strain.

It is worth noting that most elastomers are almost incompressible. This means that the material volume almost doesn't change when it is stressed unless exposed to thermal effects. This assumption is satisfactory for applications in which the material is not highly confined. Accordingly, experimental data obtained from simple deformations tests are used to define the material parameter, C_{ij} assuming material incompressibility

6.1.1.1.2 Ogden Model

In this model, the strain energy function is defined as:

$$U = \sum_{i=1}^N \frac{2\mu_i}{\alpha_i^2} (\bar{\lambda}_1^{\alpha_i} + \bar{\lambda}_2^{\alpha_i} + \bar{\lambda}_3^{\alpha_i} - 3) + \sum_{i=1}^N \frac{1}{D_i} (J^{el} - 1)^{2i} \quad (6-8)$$

where μ_i , α_i and D_i are temperature-dependent material parameters and $\bar{\lambda}_i$ are deviatoric principal stretches, which can be obtained from:

$$\bar{\lambda}_i = J^{-\frac{1}{3}} \lambda_i \quad (6-9)$$

where λ_i are the stretches in the principal directions.

The initial shear modulus, μ_0 , can be obtained from

$$\mu_0 = \sum_{i=1}^N \mu_i \quad (6-10)$$

The bulk modulus, K_0 , is given by

$$K_0 = \frac{2}{D_1} \quad (6-11)$$

6.1.1.1.2 Modeling the Hyperelasticity in ABAQUS

To obtain the hyperelastic material parameters that are necessary for defining the material behavior, results of experimental tests are needed. ABAQUS can use the test data from the following deformation modes:

- Uniaxial tension and compression
- Biaxial tension and compression
- Planar tension and compression
- Volumetric tension and compression

The schematic of these deformations are shown in Figure 6.2.

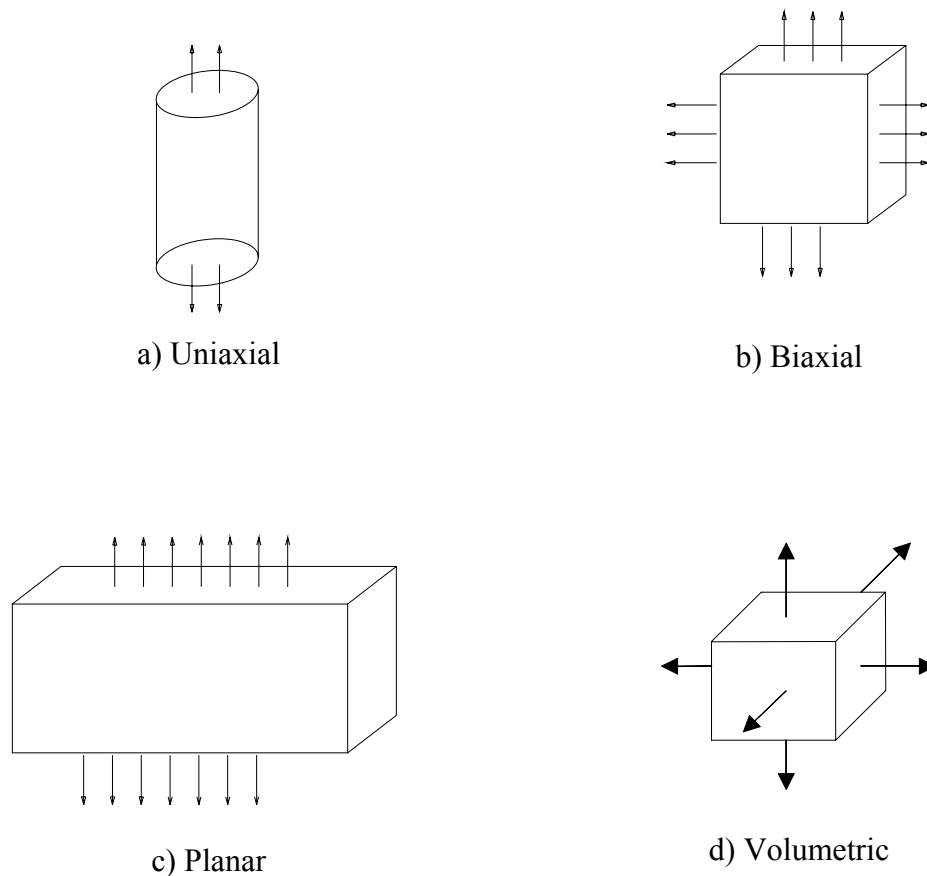


Figure 6.2: Schematic of deformations in different tests used to model hyperelasticity.

Assuming material incompressibility and isothermal response, then,

$$\lambda_1 \lambda_2 \lambda_3 = 1.0 \quad (6-12)$$

Accordingly,

$$\bar{I}_1 = \lambda_1^2 + \lambda_2^2 + \lambda_3^2 \quad (6-13)$$

$$\bar{I}_2 = \frac{1}{\lambda_1^2} + \frac{1}{\lambda_2^2} + \frac{1}{\lambda_3^2} \quad (6-14)$$

where $\lambda_i = 1 + \varepsilon_i$ and ε_i is the principal nominal strain.

The principal stretch, λ_i , is defined according to the deformation mode or in other words the experimental test.

Uniaxial tests

For uniaxial tension or compression test,

$$\lambda_1 = \lambda_u \quad (6-15)$$

$$\lambda_2 = \lambda_3 = \frac{1}{\sqrt{\lambda_u}} \quad (6-16)$$

where, λ_u is the stretch in the loading direction and

$$\varepsilon_u = \lambda_u - 1 \quad (6-17)$$

Biaxial tests

For biaxial tension or compression test,

$$\lambda_1 = \lambda_2 = \lambda_B \quad (6-18)$$

$$\lambda_3 = \frac{1}{\lambda_B^2} \quad (6-19)$$

where, λ_B is the stretch in the two perpendicular directions and

$$\varepsilon_B = \lambda_B - 1 \quad (6-20)$$

Planar tests

For planar tension or compression test,

$$\lambda_1 = \lambda_s \quad (6-21)$$

$$\lambda_2 = 1 \quad (6-22)$$

$$\lambda_3 = \frac{1}{\lambda_s} \quad (6-23)$$

where, λ_s is the stretch in the loading directions and

$$\varepsilon_s = \lambda_s - 1 \quad (6-24)$$

The following steps summarize how the parameters of a hyperelastic material are obtained and accordingly, how the stress-strain relationship is developed:

- Define number of terms to be used, N . In this model, $N=3$ was used. ($N=1$ is sufficient for strains up to 100 %).
- According to the deformation mode or (experimental test), the principal stretch, λ_i , is defined based on equations from (6-15) to (6-23).
- The strain energy function is obtained according to the model used in the analysis. The Ogden model was used for modeling the viscoelastic material in the device. The material was assumed incompressible. Hence, the second term in the strain energy function was set to be zero. Hence, the strain function for Ogden model was obtained from:
$$U = \sum_{i=1}^N \frac{2\mu_i}{\alpha_i^2} (\bar{\lambda}_1^{\alpha_i} + \bar{\lambda}_2^{\alpha_i} + \bar{\lambda}_3^{\alpha_i} - 3)$$
- Based on the results of experimental test, ABAQUS determines the material parameters in the last equation using a regression analysis, which is a statistical technique applied to data to determine, for predictive purposes, the degree of correlation of a dependent variable with one or more independent variables.
- The stress component can be obtained using equation (6-1).

6.1.1.1.3 Modeling the Hyperelasticity of Rubber Block

In order to model the hyperelastic behavior of rubber in ABAQUS, results of uniaxial and biaxial tension-compression tests are required. Yoshida et al. (2004) presented experimental results of uniaxial tension and biaxial tension tests conducted on high-damping rubber (HDR-A). In order to better model the hyperelastic behavior of the rubber block, results of a compression test conducted on high-damping rubber specimen is needed. Amin et al. (2002) presented the results of uniaxial compression test on high-

damping rubber. The different experimental results used in modeling the hyperelastic behavior of rubber block are shown in Figures 6.3 and 6.4. Note that rubber compounds in general can deform to large deformations in tension (strains up to 400 % to 500%), however they can not develop more than 50 % strains in compression. Typically, the rubber block is expected to experience around 50 % strains under tension and compression, as shown later in the results.

6.1.1.2 Viscoelasticity

Considering a specimen of rubber under loading, tension, compression or shear, the specimen response differs according to the loading rate. If the load develops slowly, larger strains are expected. Also, the strains increase gradually under the sustained loads and this phenomenon is known as the material creep, which is a characteristic of viscoelastic materials. To explain the viscoelastic material behavior, consider a rubber specimen exposed to tensile stresses applied suddenly at time $t=0$. The material will respond elastically with an elongation, OA , as shown in Figure 6.5. If the stress remains constant for a time period, T , then the deformation increases with time, as shown by curve segment AB . The rate of the increase in deformation depends on the magnitude of the stress. If the load is removed suddenly at time $t=T$, the elastic deformation will be instantaneously recovered and after that a gradual recovery will take place, part BDE . At some point in time, the residual elongation will be zero.

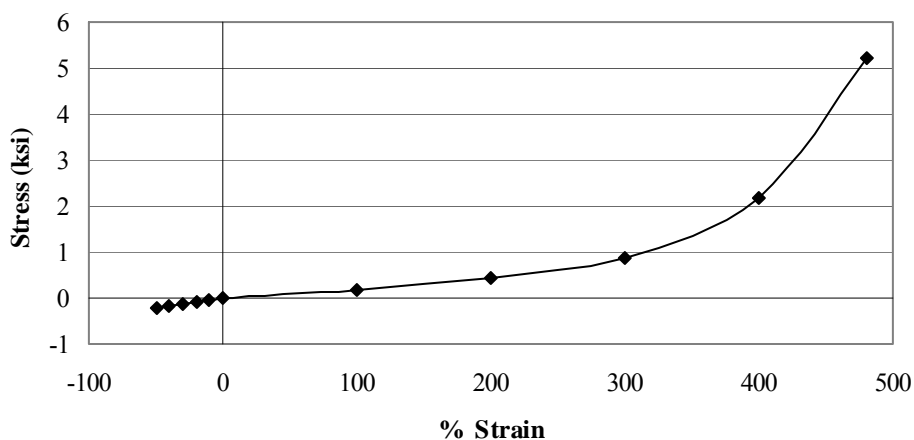


Figure 6.3: Uniaxial tension-compression tests on high-damping rubber

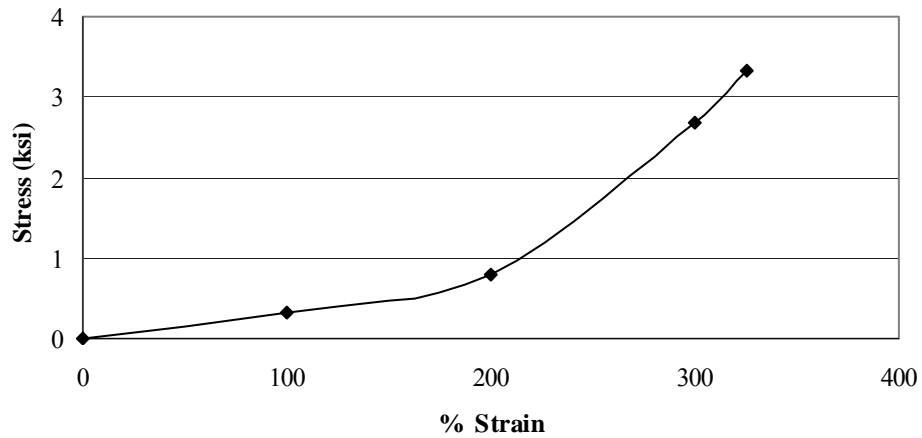


Figure 6.4: Biaxial tension test on high-damping rubber

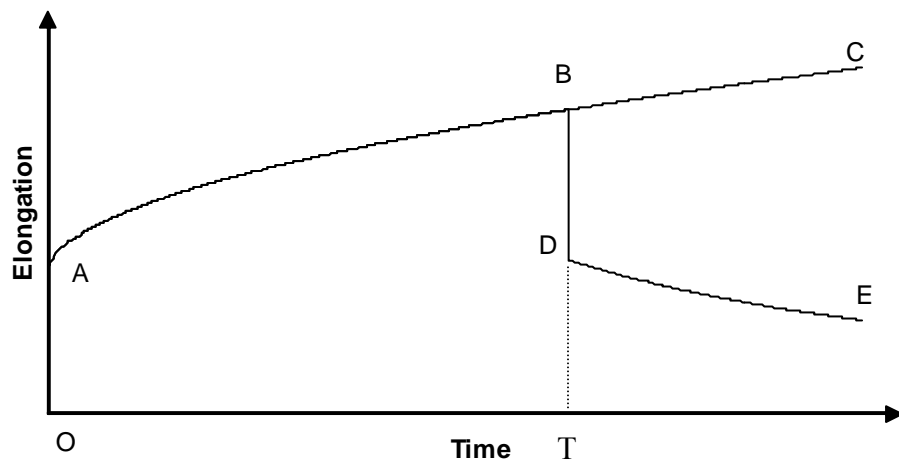


Figure 6.5: Creep and recovery for a viscoelastic material

6.1.1.2.1 Viscoelastic Model

ABAQUS provides an isotropic rate-dependent viscoelastic material model. This model can be used in large-strain problems and in conjunction with the hyperelastic material behavior.

To define the model, consider a rubber specimen, which is exposed to a sudden small shear strain, $\gamma(t)$ at time $t=0$ and then the strain is kept constant for a certain time. Accordingly, the corresponding shear stress can be defined as

$$\tau(t) = \int_0^t G_R(t-s) \dot{\gamma}(s) ds \quad (6-25)$$

where $G_R(t)$ is the time-dependent shear relaxation modulus, which characterizes the response of the material.

The time-dependent shear relaxation modulus, $G_R(t)$, can be written in a non-dimensional form:

$$g_R(t) = \frac{G_R(t)}{G_0} \quad (6-26)$$

where $g_R(t)$ is the time-dependent dimensionless shear modulus and G_0 is the instantaneous shear modulus.

Thus,

$$\tau(t) = G_0 \int_0^t g_R(t-s) \dot{\gamma}(s) ds \quad (6-27)$$

Similarly, for large shear strains, the shear stress, $\tau(t)$, can be obtained by the integration by parts as:

$$\tau(t) = G_0 \left[(\gamma - \int_0^t \dot{\gamma}(s) ds) g_R(t-s) + \int_0^t \dot{\gamma}(s) \tau_0(t-s) ds \right] \quad (6-28)$$

Or,

$$\tau(t) = \tau_0(t) - \int_0^t \dot{g}_R(s) \tau_0(t-s) ds \quad (6-29)$$

where: $\tau_0(t)$ is the instantaneous shear stress at time t .

Accordingly, to define the viscoelastic material behavior, it is necessary to define the dimensionless shear relaxation modulus, $g_R(t)$. ABAQUS assumes that the modulus can be defined by a prony series expression as:

$$g_R(t) = 1 - \sum_{i=1}^N g_i (1 - e^{-t/\tau_i}) \quad (6-30)$$

where g_i and τ_i are material constants, and $i=1, 2, \dots, N$

Accordingly, for small shear strains

$$\tau(t) = G_0 (\gamma - \sum_{i=1}^N \gamma_i) \quad (6-31)$$

where:

$$\gamma_i = \frac{g_i}{\tau_i} \int_0^t e^{-s/\tau_i} \gamma(t-s) ds \quad (6-32)$$

The corresponding creep strain can be calculated from:

$$\gamma^{cr} = \sum_{i=1}^N \gamma_i \quad (6-33)$$

6.1.1.2.2 Modeling the Viscoelasticity in ABAQUS

There are four ways to determine the viscoelastic material parameters in ABAQUS.

These methods are

- Direct specification of Prony series parameters
- Creep test data
- Relaxation test data
- Frequency-dependent data obtained from sinusoidal oscillation experiment

6.1.1.2.3 Modeling the Viscoelasticity of Rubber Block

For the device model, the viscoelastic behavior of rubber was modeled using the experimental results of relaxation shear test conducted on a high-damping rubber specimen (HDR-A) by Yoshida et al. (2004). The specimen was exposed to three-step

relaxation experiment. First, the specimen was stressed until 50% shear strains were developed and then relaxed for 10 minutes. Then the specimen was stressed to develop 150 % shear strains. The specimen was relaxed again for 10 minutes before stressing it again to 250 % shear strains then it was relaxed for the third time. ABAQUS uses only one-step relaxation test to model the viscoelasticity of any material. Accordingly, the first step (relaxation for the first 10 minutes) was used to model the viscoelasticity of the rubber block. The experimental results of the shear relaxation test on the high-damping rubber specimen for the first 10 minutes, which are used in modeling the viscoelasticity, are shown in Figure 6.6.

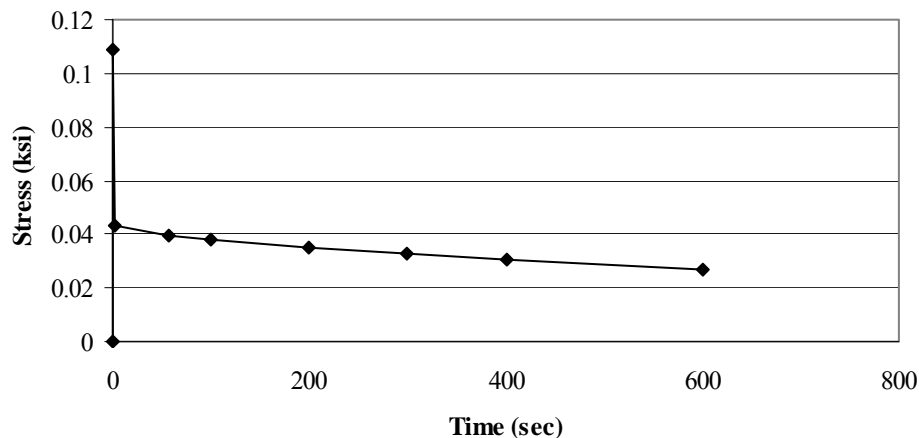


Figure 6.6: Relaxation shear test on high-damping rubber

6.1.2 Steel Elements

6.1.2.1 Stress-Strain Curve for Steel Elements

Typical stress-strain curve for steel under tension is shown in Figure 6.7. The same curve is obtained under compression if support is provided to prevent buckling. The stress is defined as the load per original cross-sectional area of the steel specimen. This stress is known as the engineering stress or the nominal stress. Similarly, the strain is obtained by dividing the total elongation (or contraction in compression test) over the original length. This strain is known as the nominal strain. The relationship between the stress and strain is proportional up to a point, known as the yielding point, before which the steel behaves

linearly elastic. The ratio between the stress and strain in the elastic part is known as the modulus of elasticity or Young's modulus, E , which equals approximately 29,000 ksi for structural steels. After yielding, the strain increases up to 15-20 times the maximum elastic strain while the stress remains constant. This part of the curve is known as the plastic range or yield plateau. For larger strains, the stress increases with the increase in strains but with a much smaller rate than the original elastic one. The increase in stress is known as strain hardening. This stress increase continues up to the maximum stress, after which the stress falls off with the increase in the strain until the failure occurs.

6.1.2.2 The Von Mises Yield Criterion

Von Mises yield surface allows isotropic yielding. The uniaxial yield stress can be obtained in terms of the three principal stresses as:

$$\sigma_y^2 = \frac{1}{2} [(\sigma_1 - \sigma_2)^2 + (\sigma_2 - \sigma_3)^2 + (\sigma_3 - \sigma_1)^2] \quad (6-34)$$

where σ_1 , σ_2 and σ_3 are the tensile or compressive stresses that act in the three principal directions and σ_y is the yield stress. The principal stresses act in the three mutually perpendicular planes that have zero shear stress. The Von Mises yield surface assumes that the yielding is independent of the equivalent stress.

6.1.2.3 Modeling the inelastic behavior of the steel

One of the advantages of modeling the device in ABAQUS is the availability of considering the inelastic behavior of the steel elements. In order to do so, the elastic-plastic behavior of steel was considered. To model the plasticity in ABAQUS, true stress and true strain must be used instead of the nominal stress and strain.

The nominal strain is defined as:

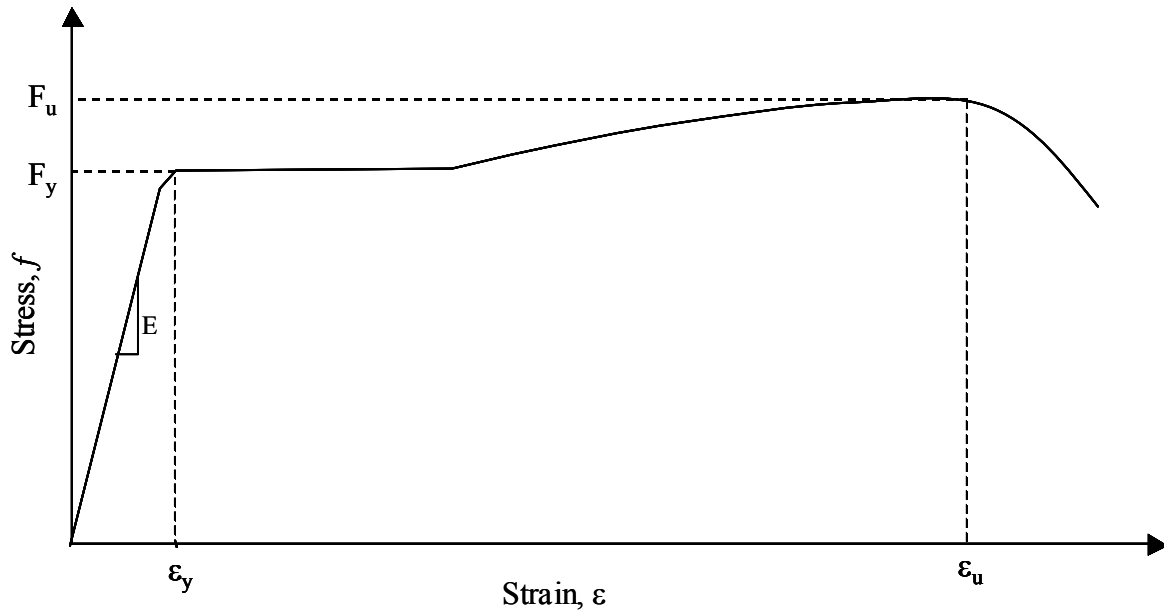


Figure 6.7: Typical stress-strain curve for steel

$$\varepsilon_{nom} = \frac{l - l_0}{l_0} = \frac{l}{l_0} - 1 \quad (6-35)$$

Accordingly, true strain, ε , can be obtained from:

$$\varepsilon = \ln \frac{l}{l_0} = \ln(1 + \varepsilon_{nom}) \quad (6-36)$$

Assuming the incompressibility of the material, its volume remains constant.

$$l_0 A_0 = l A \quad (6-37)$$

So, the actual area, A , is calculated from:

$$A = A_0 \frac{l_0}{l} \quad (6-38)$$

Now, the relation between the true stress and nominal stress is defined as

$$\sigma = \frac{F}{A} = \frac{Fl}{A_0 l_0} = \sigma_{nom} \frac{l}{l_0} \quad (6-39)$$

$$\sigma = \sigma_{nom} (1 + \varepsilon_{nom}) \quad (6-40)$$

The true strain calculated from the aforementioned equations is a combination of elastic strain and plastic strain. According the plastic strain can be obtained from the following equation:

$$\varepsilon_{pl} = \varepsilon_t - \varepsilon_{el} = \varepsilon_t - \frac{\sigma}{E} \quad (6-41)$$

where ε_{pl} is the true plastic strain, ε_t is the true total strain, σ is the true stress, and E is the modulus of elasticity. The true strain curve used in this model for high-strength steel is given in Table 6.1. The true stress-plastic strain curve used by ABAQUS is shown in Figure 6.8.

Table 6.1: Stress and strain for steel

Nominal stress (ksi)	Nominal strain	True stress (ksi)	True strain	Plastic strain
50.00	0.0017	50.05	0.0017	0
50.00	0.0213	51.07	0.0211	0.0193
58.50	0.0500	61.39	0.0488	0.0467
66.20	0.1000	72.77	0.0953	0.0928
70.80	0.1500	81.39	0.1394	0.1366
69.30	0.2000	83.10	0.1823	0.1795
67.70	0.2500	84.61	0.2231	0.2202
66.90	0.3000	87.00	0.2624	0.2594
65.40	0.3500	88.26	0.3001	0.2971

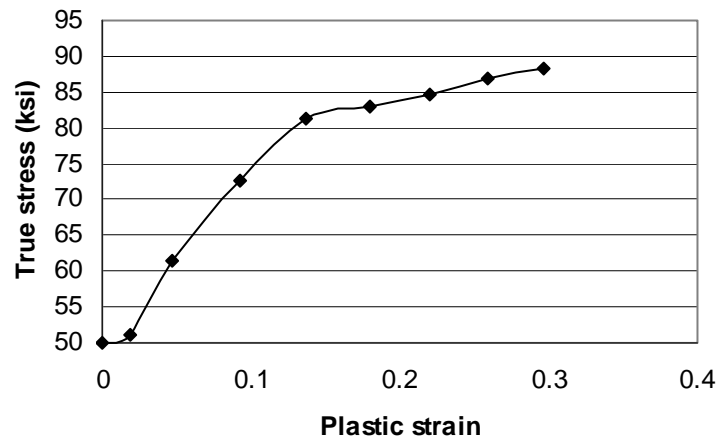


Figure 6.8: Stress-strain curve used by ABAQUS for high-strength steel.

To model the steel hardening, an isotropic hardening model was used. This model assumes that the center of the yield surface remains stationary in the stress space however the size of the yield surface changes uniformly in all directions such that the yield stress varies according to the plastic strains. This model is suitable for dynamic problems with large deformations.

6.2 Geometric modeling of the device

Reduced-integration elements use one fewer integration point in each direction than the fully integration elements. For linear elements, using the reduced integration causes a numerical problem called hourglassing. To explain this problem, consider a linear reduced-integration element is subjected to bending moment, M . An expected deformation mode is shown in Figure 6.9. The dotted lines remain unchanged in the length after deformation. The angle between these lines is unchanged as well. Accordingly, no stress is developed at the single integration point. This means that no stiffness in the element can resist such type of deformations. For coarse meshes with these element types, this deformation mode can propagate through the entire mesh causing poor results. ABAQUS uses an artificial hourglass stiffness to prevent the propagation of these modes. However this affects the accuracy of the results. Accordingly, very fine mesh of linear-reduced integration elements is recommended. Although quadratic reduced-integration elements also have hourglass modes, it is almost impossible for these modes to propagate in a normal mesh and it is rare problem for sufficiently fine mesh. Accordingly, this type of elements is used in the model.

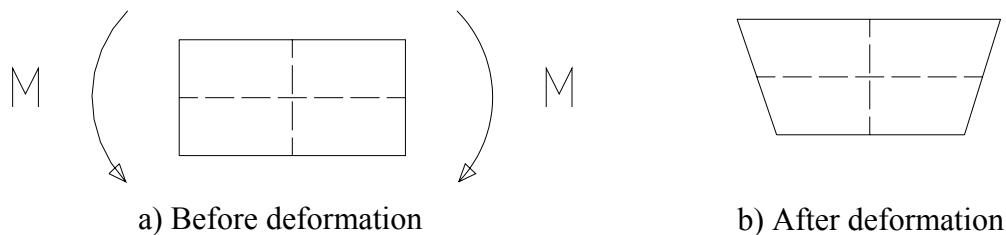


Figure 6.9: Linear reduced-integration element subjected to bending moment, M .

To model the rubber block, C3D20R elements were used. These elements are three dimensional, twenty-node, quadrilateral, reduced-integration hybrid continuum elements,

which are suitable for large-strain analysis. Hybrid elements were used for incompressible materials, like rubber with Poisson ratio as high as 0.5.

The steel elements were modeled as S8R elements, which are eight-node quadrilateral reduced integration shell elements. The finite element model of the device is shown in Figure 6.10. Figure 6.11 and Figure 6.12 show the deformed shape of the device under tension and compression respectively.

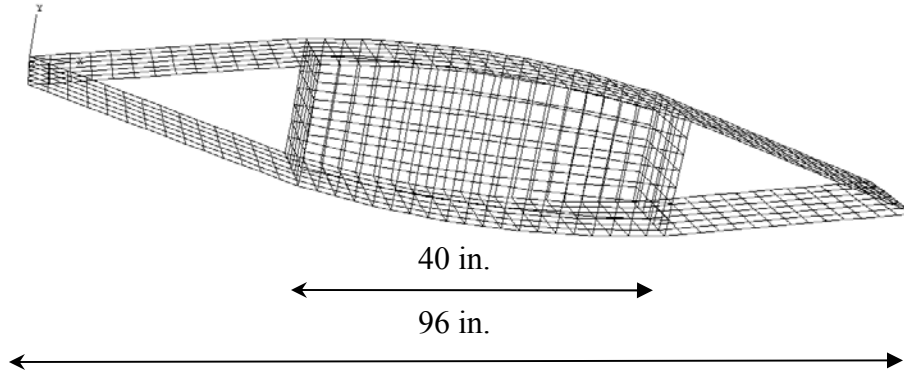


Figure 6.10: Modeling the device in ABAQUS

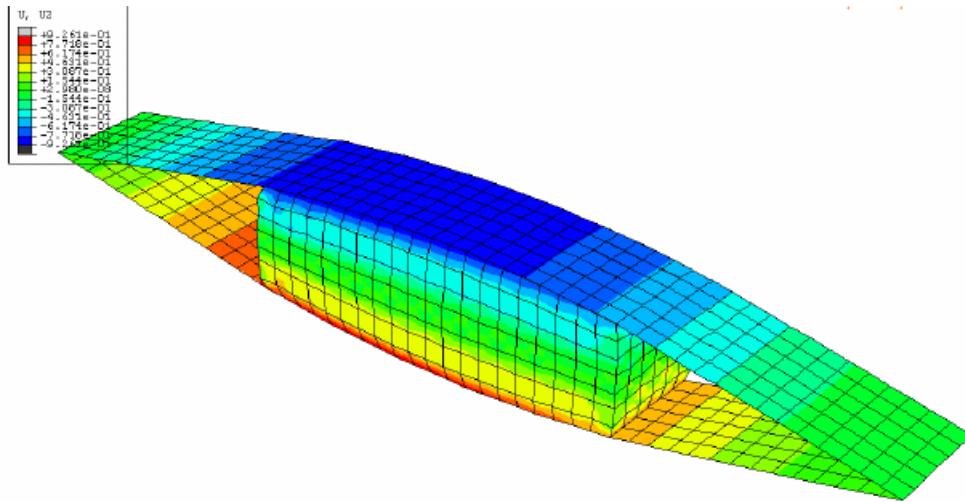


Figure 6.11: Deformation shape of the device under tension

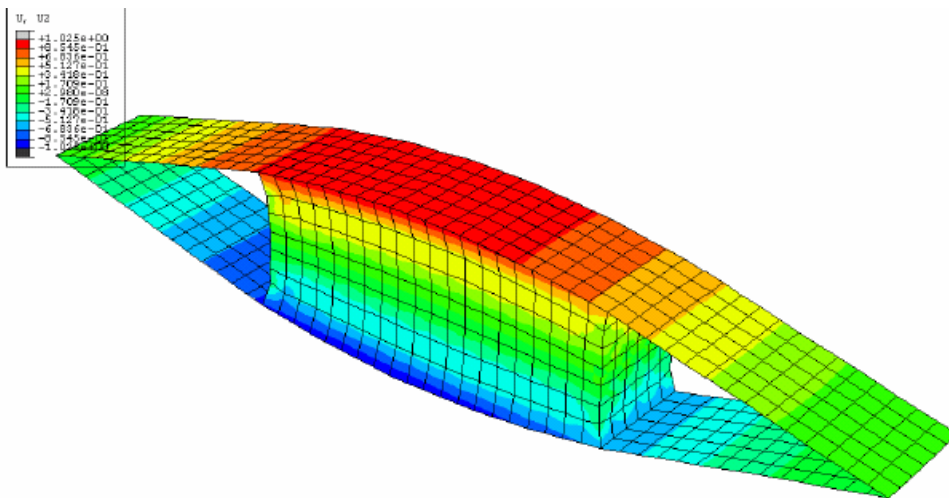


Figure 6.12: Deformation shape of the device under compression

6.3 Parametric study

There are many parameters that control the device behavior. Accordingly, the effectiveness of the device can be improved considerably by the proper selection of each of these parameters.

The parameters considered in this study are:

- Steel type
- Device aspect ratio (h/l , as seen in Figure 4.1)
- Breadth of viscoelastic material (e , as seen in Figure 4.1)
- Cross section of steel elements

During this parametric study, the device was exposed to different types of dynamic loads. These loads are shown in Table 6.2.

Table 6.2: Loading types used in the parametric study

Load Type	Force (kips)	Duration (seconds)
Quasi-static Tension	$F = \frac{t}{360} * 300$	360
Quasi-static Compression	$F = \frac{t}{360} * 300$	360
Harmonic	$F = 300 \sin(2\pi t)$	3

6.3.1 Effect of Steel Type

To determine the effect of steel type on the device behavior, two steel grades were chosen. These grades are A36 and A572 with a yielding stress of 36 ksi and 50 ksi, respectively. During this analysis, the breadth of the viscoelastic material, e , was kept equal to 40 in. The width of the steel plates, g , and the width of the viscoelastic material, b , were kept equal to 12 in. The device aspect ratio, h/l was chosen to be 1/6. The steel elements selected for this analysis were 1.5-in. thick steel plates.

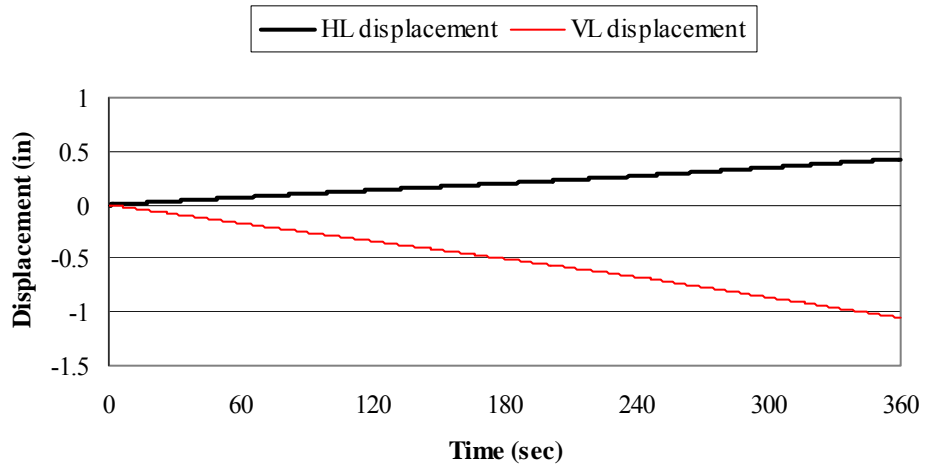
As shown in Figure 6.13 and Figure 6.14, at the end of tensile loading, the horizontal displacement of the device was 0.43 in. for mild steel and 0.37 in. for the high-strength steel. However, the vertical displacement at the middle of the device was 1.05 in. and 0.95 in. for mild and high-strength steel respectively. At the end of loading duration, the energy dissipated through the viscoelastic material and inelastic behavior of steel plates for the mild steel was 23.2 kip-in. and 15.1 kip-in. respectively. On the other hand, the energy dissipated in the high-strength steel case through viscoelastic material and steel yielding was 18.5 kip-in. and 2.0 kip-in. respectively. Figure 6.13c illustrates what is meant by the horizontal and vertical deformations developed in the device.

Under compressive loading, the device was displaced horizontally at its edge by 1.39 in., however the vertical displacement at the middle of the device reached 2.91 in. at the end of the compressive loading. On the other hand for the high-strength steel case, the horizontal displacement reached 0.83 in. at the end of loading while the corresponding vertical displacement at the middle of the device was 1.82 in. The total energy dissipated by the viscoelastic material was 96.9 kip-in. while the energy dissipated through steel yielding was 91.7 kip-in., in the first case. For the high-strength steel case, the energy dissipated at the end of loading duration was 46.5 kip-in. and 26.4 kip-in. by the viscoelastic material and steel elements, respectively. Figure 6.15 and 6.16 show the comparison between the two cases under compression.

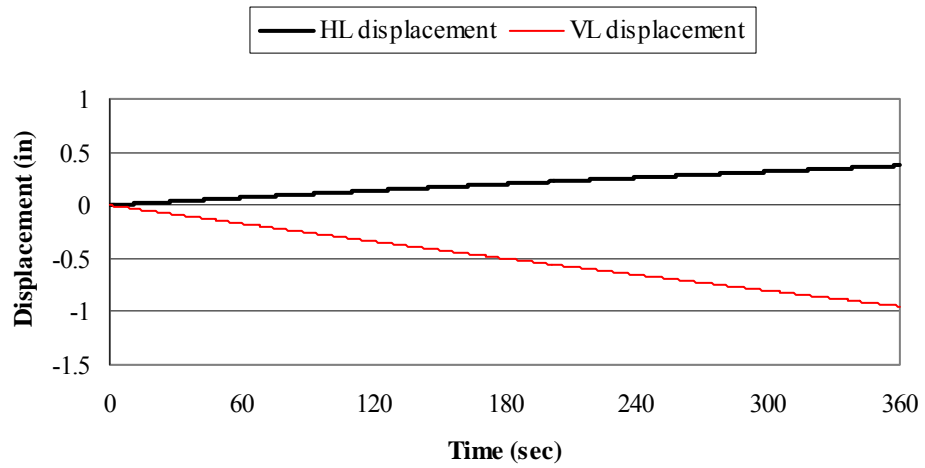
The device was analyzed under harmonic loading. For the mild-steel case, the device was displaced horizontally up to 0.36 in. under tension and 0.75 in. under compression. After three cycles, the viscoelastic material dissipated 260.6 kip-in. while the steel elements dissipated 176.3 kip-in. through yielding. For the high-strength case, due to the higher yielding stress, the device experiences lower levels of yielding, which results in lower deformations developed in the device compared to the mild-steel case. The horizontal displacement reached 0.32 in. and 0.57 in. under tension and compression respectively. The energy dissipated in this case through the viscoelastic material was 202.4 kip-in. while the energy dissipated through steel yielding was 26.0 kip-in. after three complete cycles of harmonic loading.

The energy dissipation through the mild steel was much higher than that dissipated through the high-strength steel due to the severe yielding developed in the mild-steel plates. The results of both cases under harmonic excitation are shown in Figure 6.17 and Figure 6.18.

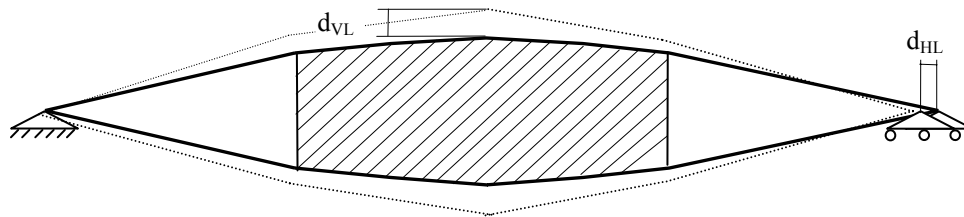
From the previous results, it can be noticed that devices with mild-steel elements dissipate more energy through yielding. However, steel yielding occurs under relatively small deformations. Moreover, devices with mild-steel experienced excessive yielding when exposed to moderate deformations, which reduces the device strength and its ability to undergo large deformations. Although displacement-dependent dampers such as metallic dampers depend on the energy dissipation through mild steel elements, these dampers have no way to dissipate energy other than metallic yielding. However, the new visco-plastic device introduces another source of energy dissipation, which is the viscoelastic material dissipation through tensile and compressive strains. The viscoelastic dissipation is the primary source of energy dissipation under small deformations. This supports the idea of using the high-strength steel elements instead of mild-steel elements. Accordingly, high-strength steel elements are selected for the device.



a) Mild steel

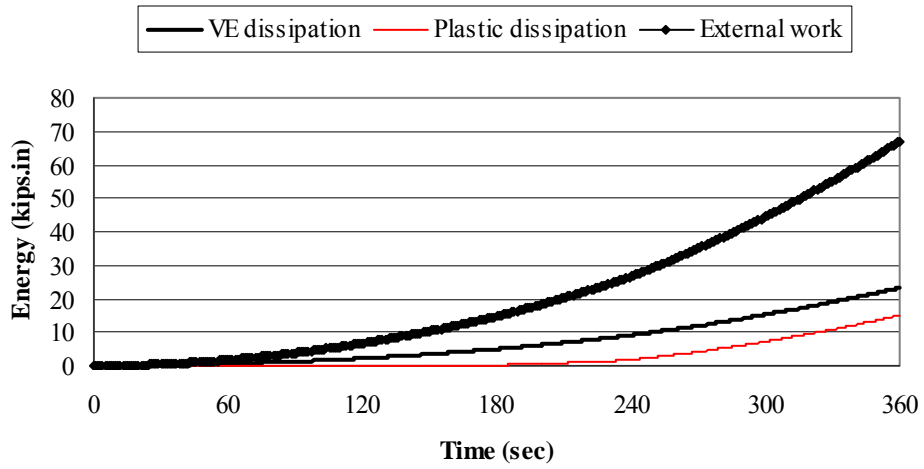


b) High-strength steel

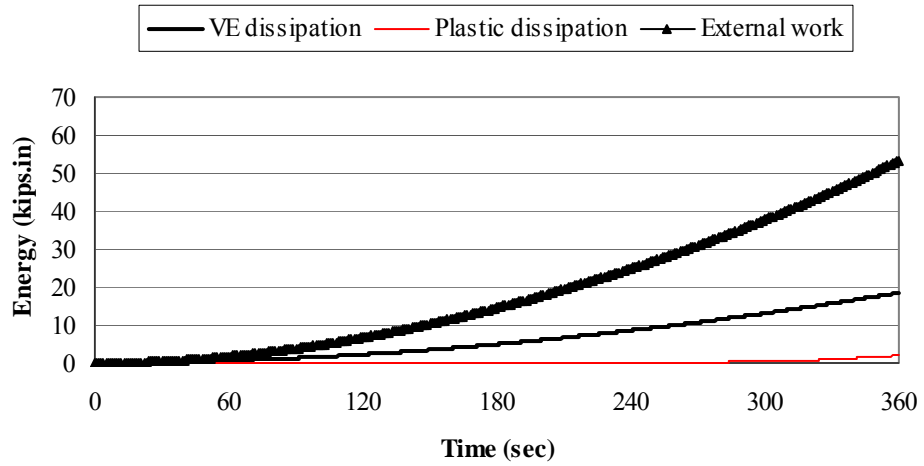


c) Schematic representation of deformed shape of the device (Solid line: before deformation; dotted line: after deformation)

Figure 6.13: Effect of steel type on the deformations of the device under tensile loading.

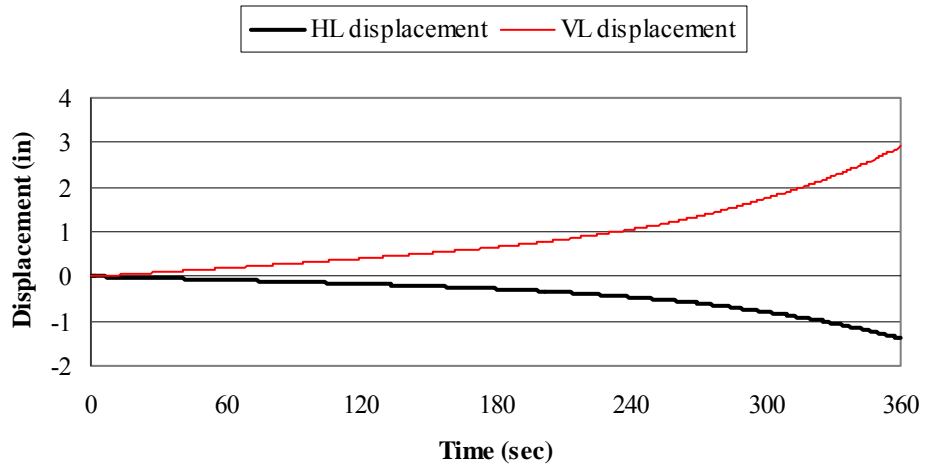


a) Mild steel

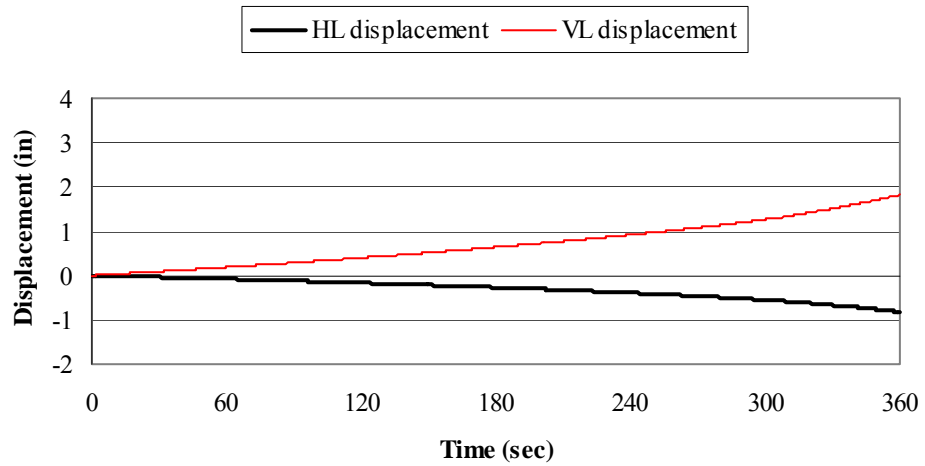


b) High-strength steel

Figure 6.14: Effect of steel type on the energy dissipation of the device under tensile loading.

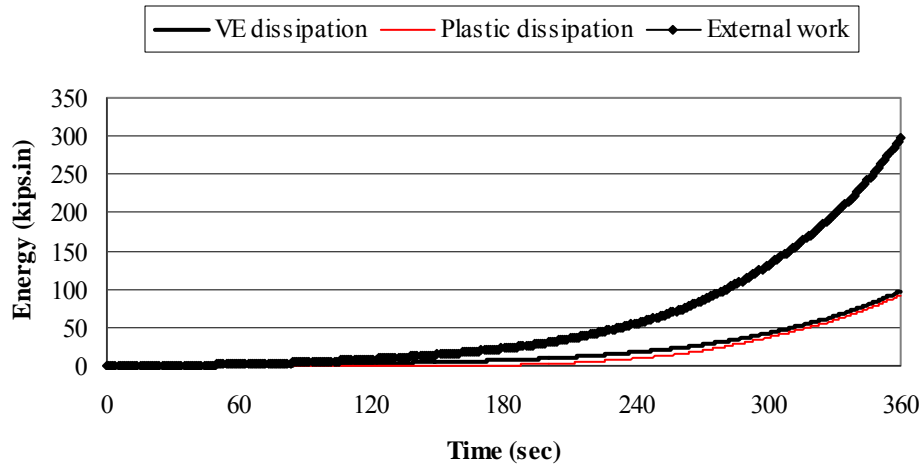


a) Mild steel

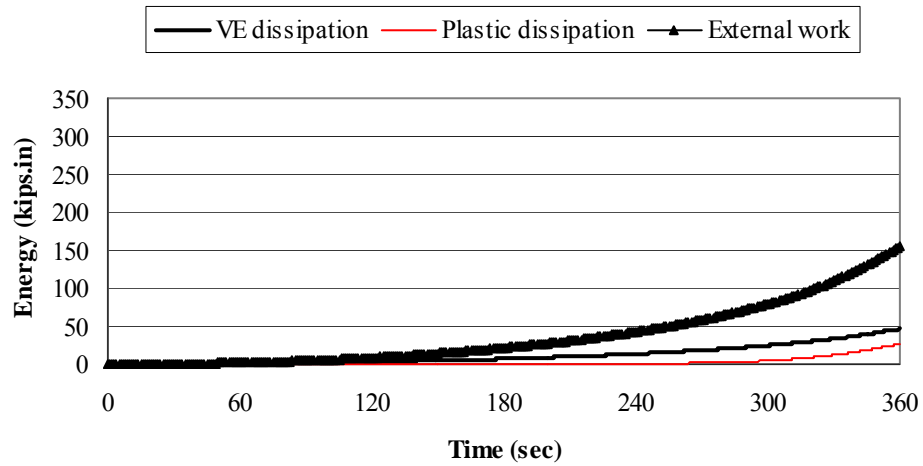


b) High-strength steel

Figure 6.15: Effect of steel type on the deformations of the device under compressive loading.

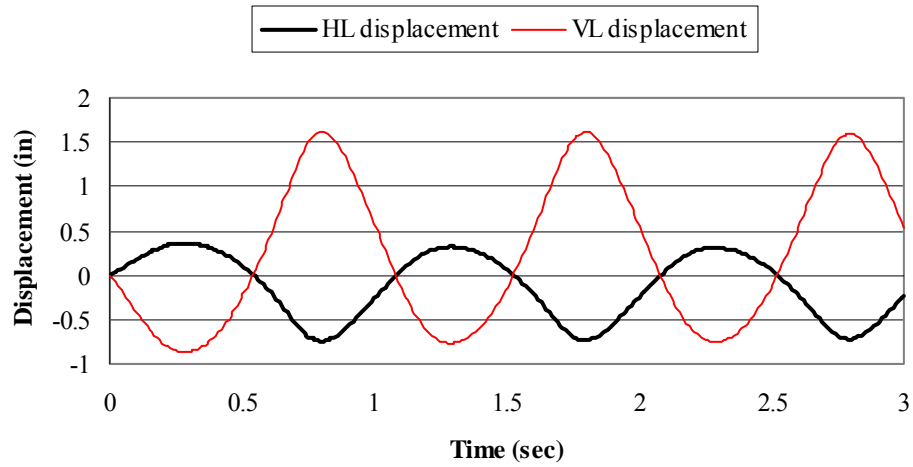


a) Mild steel

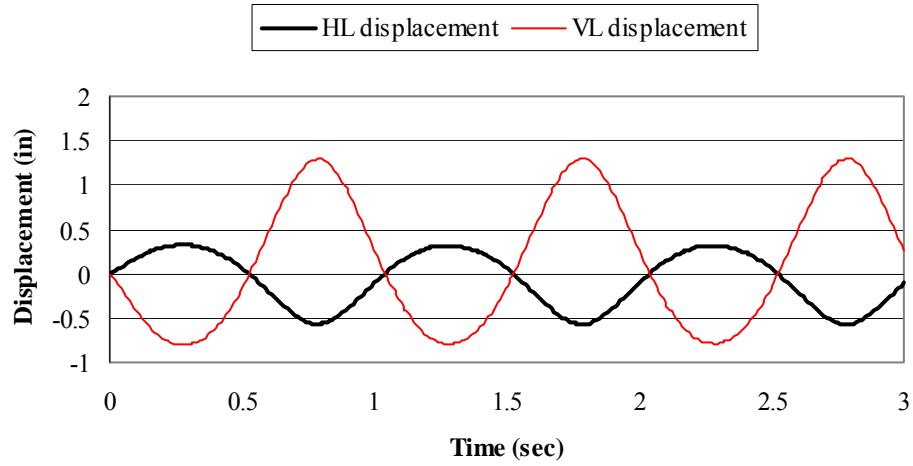


b) High-strength steel

Figure 6.16: Effect of steel type on the energy dissipation of the device under compressive loading.

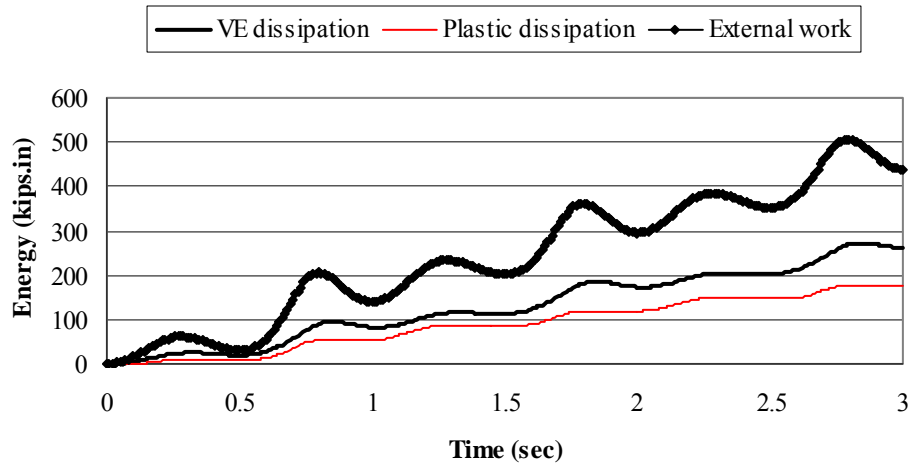


a) Mild

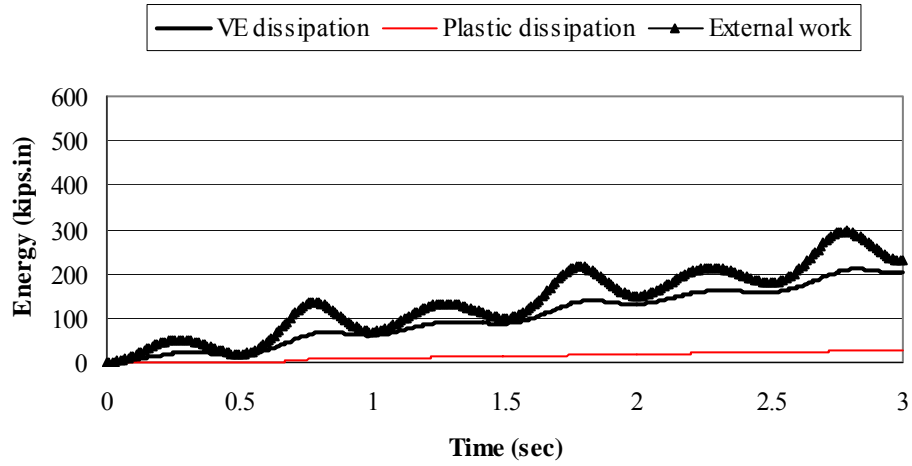


b) High-strength steel

Figure 6.17: Effect of steel type on the deformations of the device under harmonic loading.



a) Mild



b) High-strength steel

Figure 6.18: Effect of steel type on the energy dissipation of the device under harmonic loading.

6.3.2 Effect of the Aspect Ratio

The second parameter considered in this parametric study that affect the device behavior was the aspect ratio, which is the ratio between the viscoelastic material breadth at the middle of the device and its span. One of the advantages of this device is the amplification of the horizontal deformations into higher vertical deformations due to the geometry of the device. This amplification results in higher tensile and compressive strains in the viscoelastic material, which maximizes the energy dissipation through this material. Also, the device aspect ratio controls the stresses developed in the steel elements and accordingly the energy dissipation through steel yielding.

To check the effectiveness of the aspect ratio on the device behavior, three cases of different aspect ratios were considered to represent different device configurations. These aspect ratios were 1/12, 1/8 and 1/6 respectively. The device had a span of 96 in., which reflects viscoelastic material thickness at the middle of the device of 8, 12 and 16 in., respectively. High-strength steel plates with a thickness of 1.5 in. were chosen with a bent shape on the form $\frac{h}{2} \sin\left(\frac{\pi x}{l}\right)$, where h is the viscoelastic material thickness at the middle of the device; x is the distance from the device left side and l is the device length. The rubber breadth, e , was kept equal to 40 in. in this part of analysis while the width of the steel plates, g , and viscoelastic material, b , was 12 in.

First, the three cases were investigated under tensile loading. The corresponding results are shown in Figure 6.19 and Figure 6.20. At the end of loading, the horizontal displacement of the device was 0.08, 0.19 and 0.37 in. for the cases of aspect ratio, h/l equals to 1/12, 1/8 and 1/6, respectively. The vertical displacement at the middle of the device was 0.29, 0.59 and 0.95 in. for the three cases, respectively. The compressive strains at the middle of the device can be estimated by dividing the total vertical deformation (two times of the vertical displacement at the middle of the device) over the original thickness of the viscoelastic material at the middle of the device. Accordingly, the compressive strains for the three cases can be estimated as $2*0.29/8$, $2*0.59/12$ and $2*0.95/16$ or 7.3 %, 9.8 % and 11.9 %, respectively. The energy dissipation through the

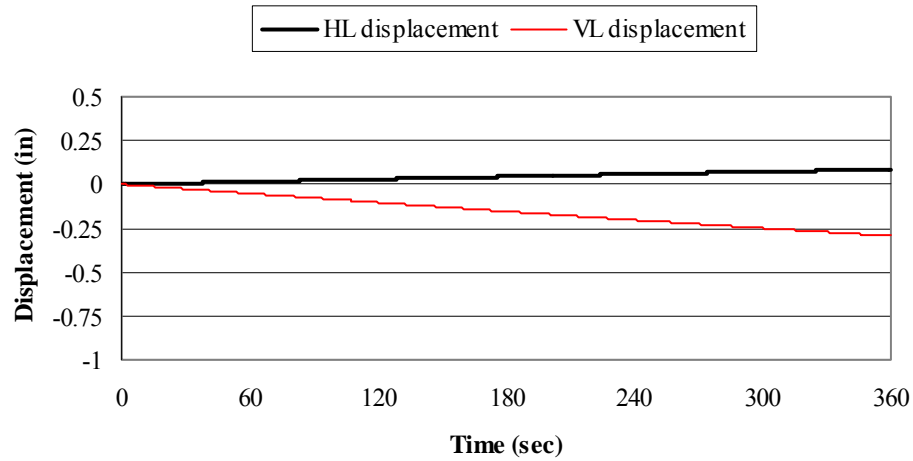
viscoelastic material at the end of tensile loading was 2.6, 9.9 and 18.5 kip-in. for the three cases, respectively. No yielding occurred in the first and second cases, however for the third case, the energy dissipation through the inelastic behavior of the steel plates was 2.0 kip-in.

Three devices with the previously mentioned aspect ratios were analyzed under quasi-static compressive loading. The results of this analysis are shown in Figure 6.21 and Figure 6.22. The horizontal displacement of the device was 0.12, 0.32 and 0.83 in. for device aspect ratios of 1/12, 1/8 and 1/6, respectively. The vertical displacement at the middle of the device was 0.46, 0.96 and 1.96 in., respectively, which reflects an estimate of tensile strains of 11.5 %, 16.0 % and 24.5 % at the end of loading duration for the three aspect ratios, respectively. The energy dissipated through the viscoelastic material at the end of loading was 4.7 kip-in., 19.1 kip-in. and 46.5 kip-in., respectively. No yielding occurred in the first while the energy dissipated through yielding was 0.9 kip-in. and 26.4 kip-in. for the second and third cases, respectively. Accordingly, the total energy dissipation in the three cases was 4.7, 20.0 and 72.9 kip-in., respectively.

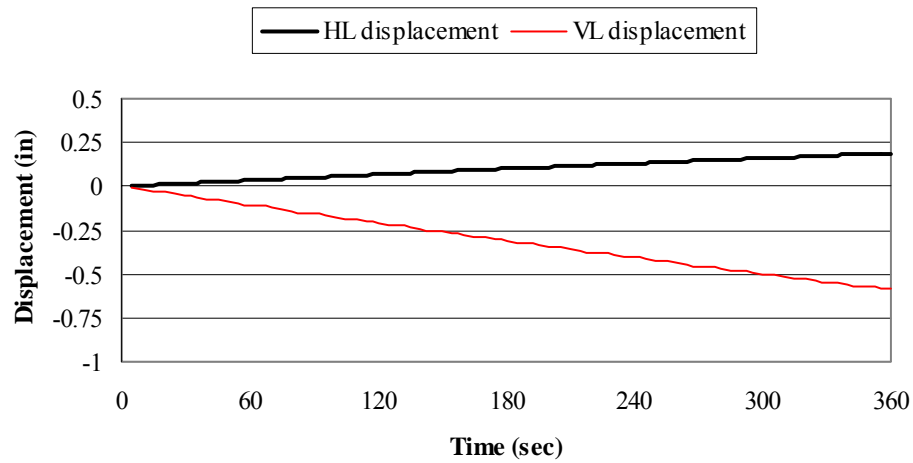
The three devices with the different aspect ratios were analyzed under harmonic loading. As shown in Figure 6.23, the horizontal displacement ranged from 0.07 in. under tension and 0.09 in. under compression in the first case. For the second case, the horizontal displacement reached 0.16 under tension and 0.25 under compression. As before, the third case experienced the largest deformations in the device. The horizontal displacement ranged from 0.32 in. under tension to 0.57 in. under compression. The energy dissipation through the viscoelastic material was 2.4, 96.2 and 202.4 kip-in. while the energy dissipation through yielding was zero, 0.6 and 26.0 kip-in., respectively. The total energy dissipated was 2.43, 96.8 and 228.4 kip-in. for the three cases, respectively. The plots of the energy dissipation through the different cases are shown in Figure 6.24 and Figure 6.25.

It can be noticed from the results of devices with different aspect ratios under different types of loading that the energy dissipation through the viscoelastic material increases

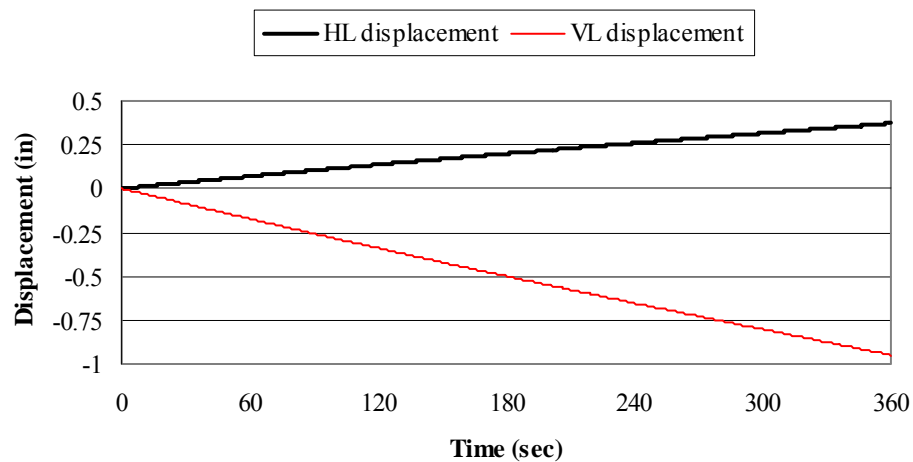
with the increase in the device aspect ratio, which can be explained by the higher axial strains developed in the viscoelastic material upon increasing the aspect ratio. Also, higher aspect ratios result in higher energy dissipation through the steel elements as well due to the higher deformations developed in steel elements. On the other hand, devices with lower aspect ratios provide higher stiffness. Although higher device stiffness may lead to smaller structural deformations but on the other hand, excessive added stiffness may act as a “seismic attractor,” increasing base shears and increasing response accelerations, which result in damage to contents and nonstructural components. Accordingly, high aspect ratio is recommended for the device. An aspect ratio of 1/6 was selected for the rest of the analyses.



a) Aspect ratio = 1/12

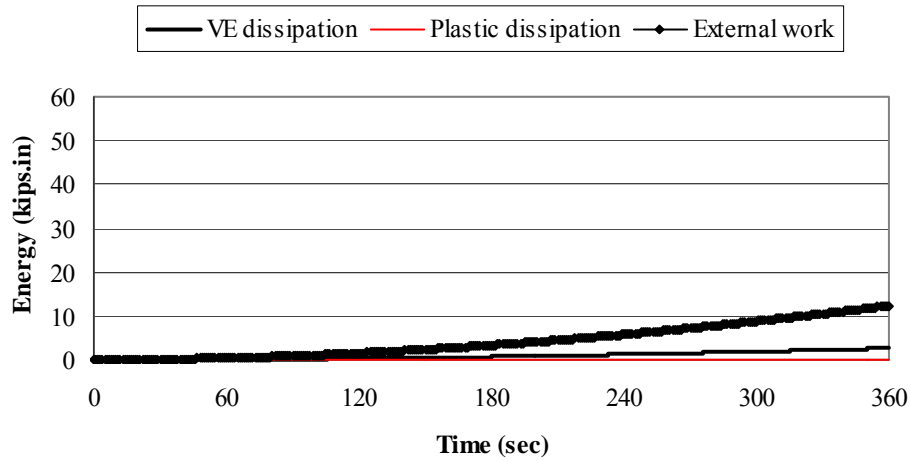


b) Aspect ratio = 1/8

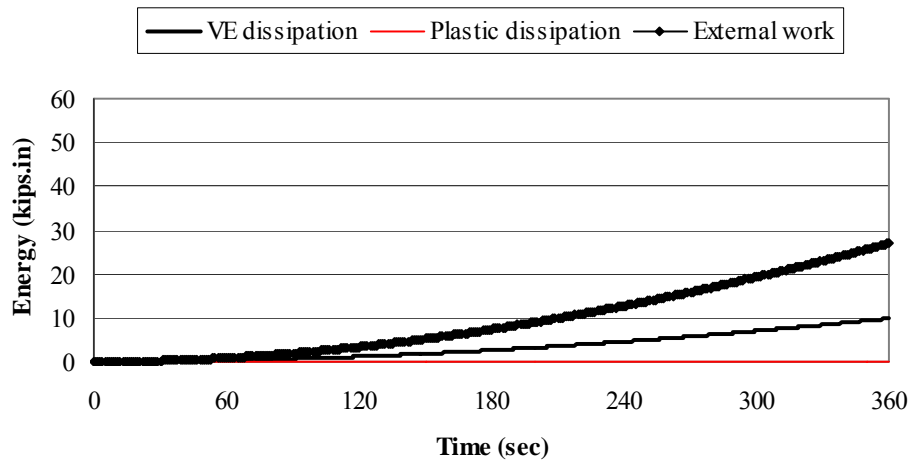


c) Aspect ratio = 1/6

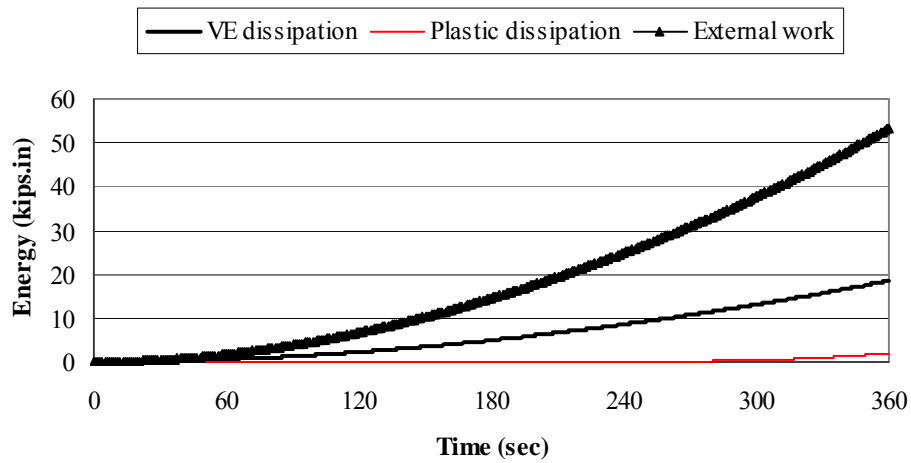
Figure 6.19: Effect of the device aspect ratio on the deformations of the device under tensile loading.



a) Aspect ratio = 1/12

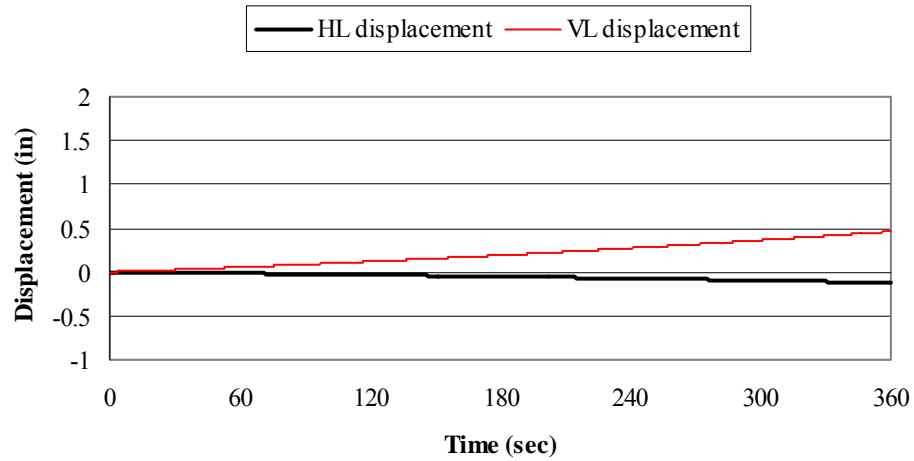


b) Aspect ratio = 1/8

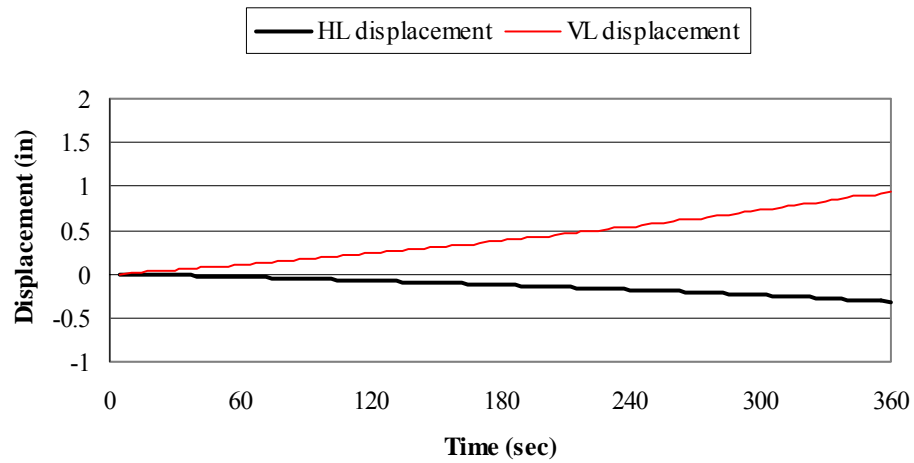


c) Aspect ratio = 1/6

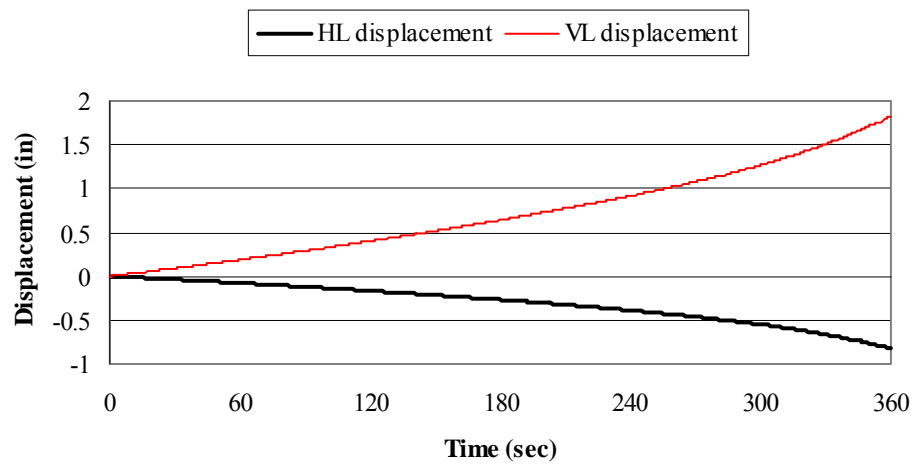
Figure 6.20: Effect of the device aspect ratio on the energy dissipation under tensile loading.



a) Aspect ratio = 1/12

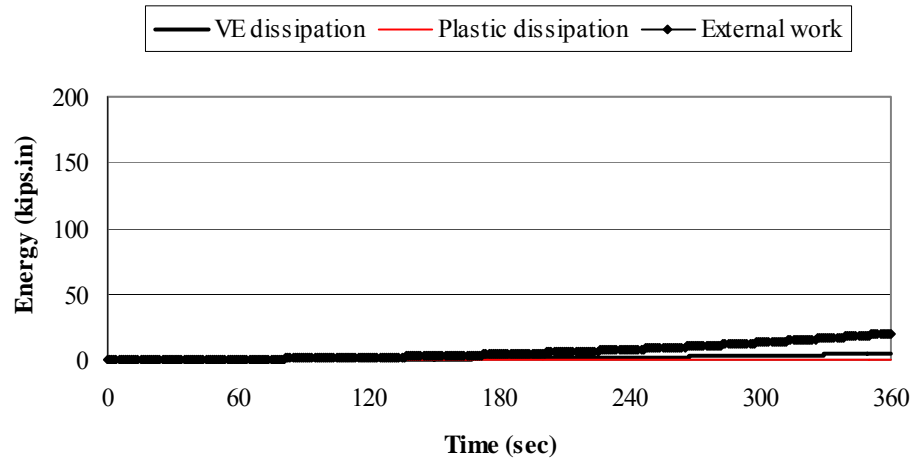


b) Aspect ratio = 1/8

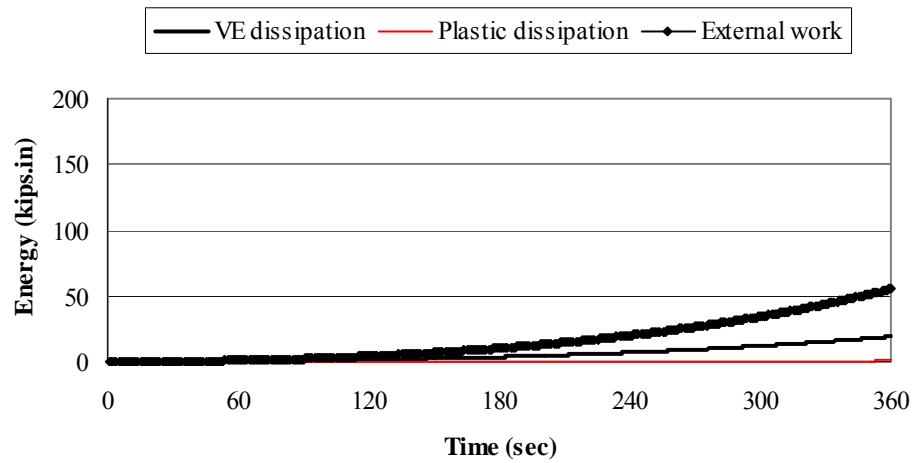


c) Aspect ratio = 1/6

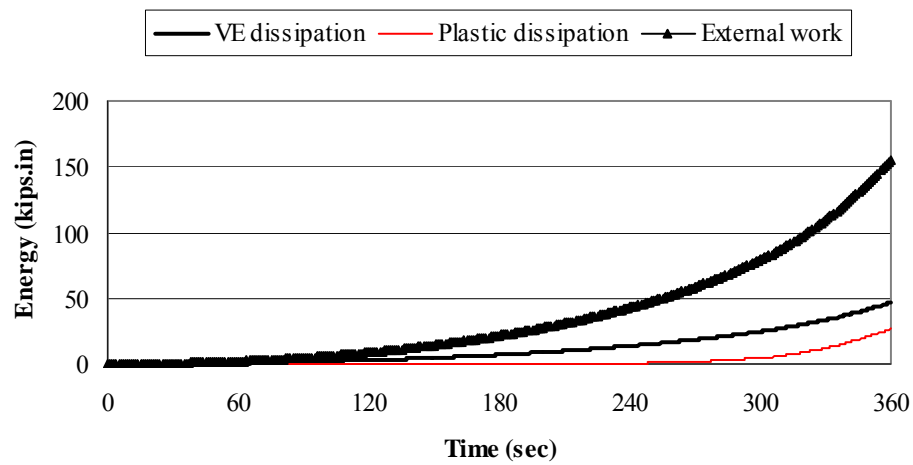
Figure 6.21: Effect of the device aspect ratio on the deformations of the device under compressive loading.



a) Aspect ratio = 1/12

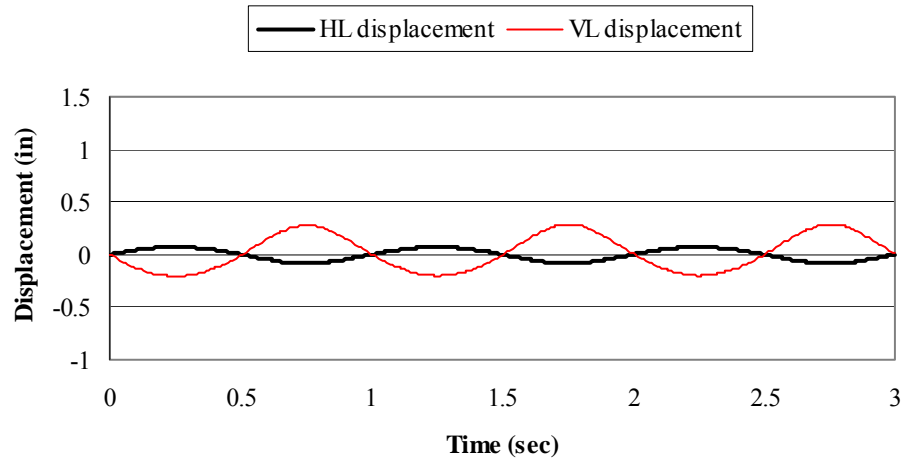


b) Aspect ratio = 1/8

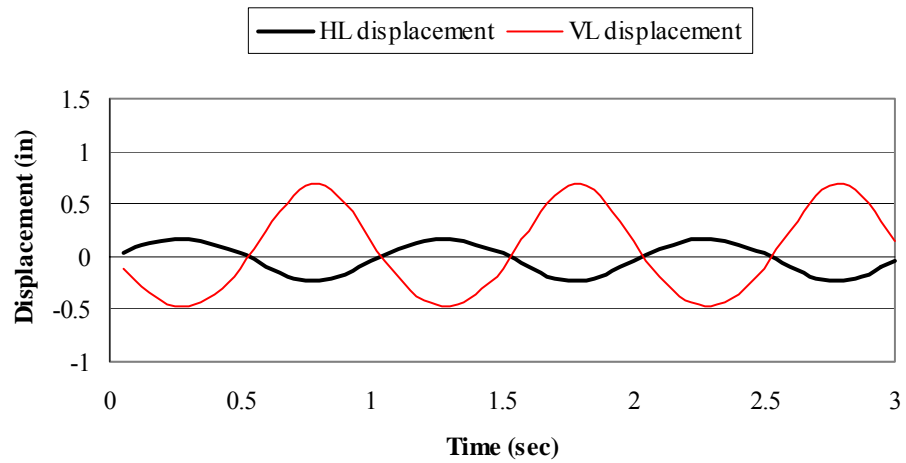


c) Aspect ratio = 1/6

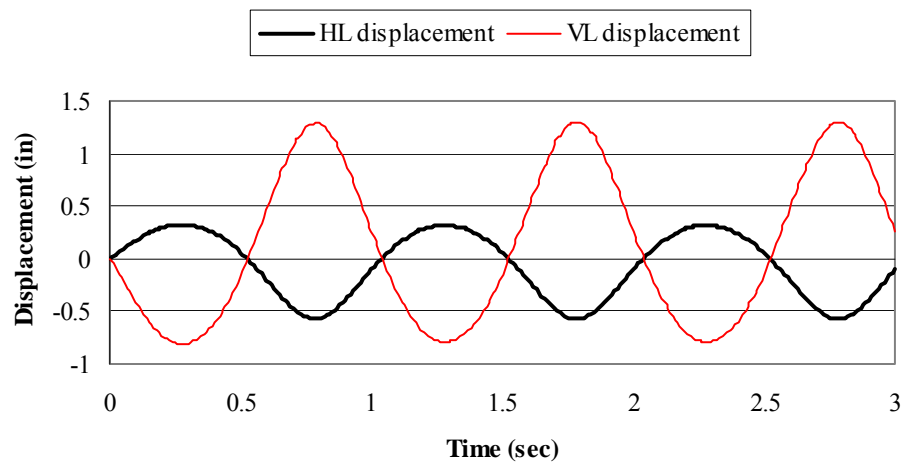
Figure 6.22: Effect of the device aspect ratio on the energy dissipation under compressive loading.



a) Aspect ratio = 1/12

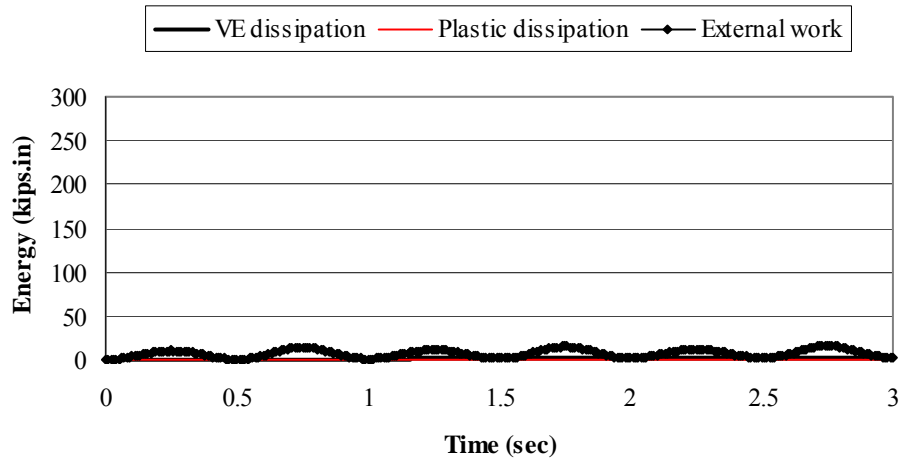


b) Aspect ratio = 1/8

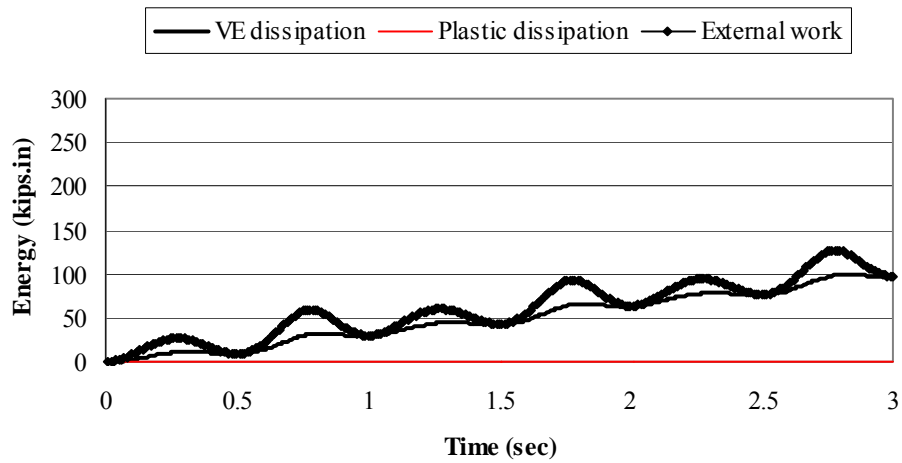


c) Aspect ratio = 1/6

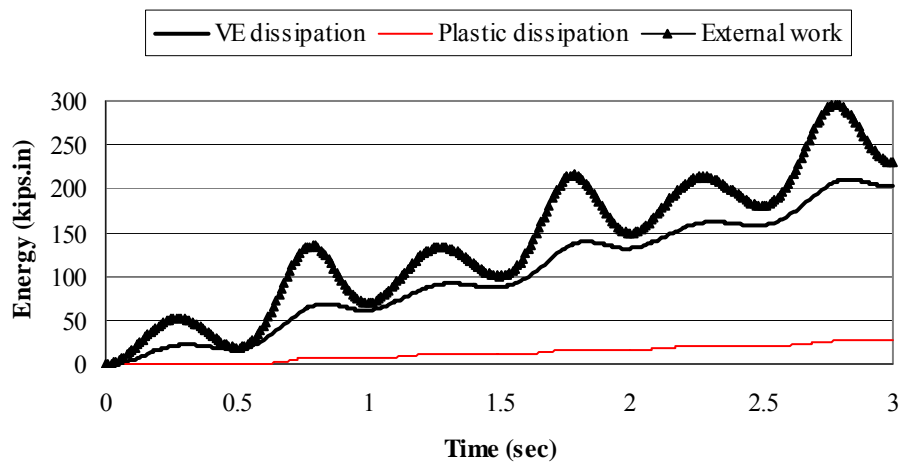
Figure 6.23: Effect of the device aspect ratio on the deformations of the device under harmonic loading.



a) Aspect ratio = 1/12



b) Aspect ratio = 1/8



c) Aspect ratio = 1/6

Figure 6.24: Effect of the device aspect ratio on the energy dissipation under harmonic loading.

6.3.3 Effect of Rubber Breadth

The third parameter considered in this parametric study was the breadth of the viscoelastic material. This is the dimension, e , in Figure 4.1. The viscoelastic material breadth controls the deformations in the device and consequently the energy dissipation through the viscoelastic material as well as the steel elements. Also, the stiffness provided by the device depends on the dimensions of the viscoelastic material. To determine the appropriate breadth of rubber and its effect on the overall performance of the device, three devices with different breadths of rubber block were studied. These rubber breadths chosen were 30, 40 and 50 in. while the length of the device was kept equal to 96 in. The width of the rubber block was 12 in. An aspect ratio of 1/6 was selected for the three cases. The steel elements were chosen to be a plate with thickness of 1.5 in.

The three cases were first analyzed under tensile loading. The results are shown in Figure 6.26 and Figure 6.27. At the end of loading, the horizontal displacement was 0.41, 0.37 and 0.33 in. in the three cases, respectively. The vertical displacement at the middle of the device, which indicated the ability of amplifying the horizontal deformation for each case, was 1.06, 0.95 and 0.84 in., respectively. The energy dissipation through the viscoelastic material was almost the same under the three cases due to the small deformations developed in the viscoelastic material. The energy dissipation through the inelastic behavior of the steel plates was 4.2, 2.0 and 0.9 kip-in., respectively.

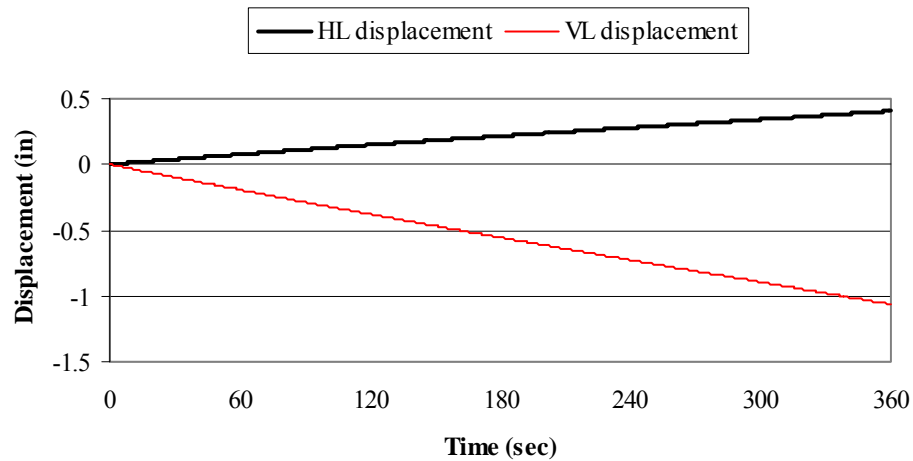
The three cases were analyzed again under compressive loading. In this analysis, the device experiences large deformations and consequently the effect of rubber breadth on the device behavior was obvious. The maximum horizontal displacement was 1.12, 0.83 and 0.63 in. while the maximum at the middle of the device was 2.41, 1.82 and 1.46 in. for the three cases, respectively. The deformations developed in the device for the three cases under compression are shown in Figure 6.27. The energy dissipation through the viscoelastic material was 56.4, 46.5 and 37.6 kip-in., for the three cases, respectively, while the energy dissipation through the yielding of steel plates was 62.8, 26.4 and 10.7

kip-in. respectively. The plots of the energy dissipations for the three cases are shown in Figure 6.28

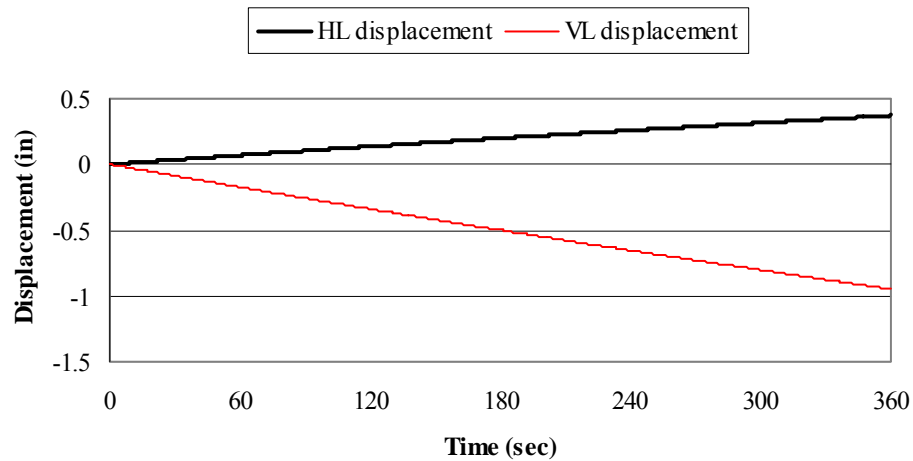
Devices with rubber breadths of 30, 40 and 50 in. were analyzed under harmonic loading. The results of this analysis are shown in Figure 6.29 and 6.30. Considering the first case, the horizontal displacement of the right side of the device reached 0.35 in. under tension and 0.73 in. under compression. For the second case, the horizontal displacement ranged between 0.32 in. under tension and 0.57 in. under compression. The maximum horizontal displacement was 0.28 in. under tension and 0.46 in. under compression for the third case. After three cycles of harmonic loading, the energy dissipation through the viscoelastic material was 216.8, 202.4 and 176.7 kip-in., for the three cases, respectively, while the energy dissipation through the inelastic behavior of the steel plates was 83.8, 26.0 and 10.3 kip-in., respectively.

According to the results of the devices with different viscoelastic material breadths under different types of dynamic loadings, it can be noticed that the viscoelastic material breadth has a considerable effect on the deformations developed in the device as well as the energy dissipation through the viscoelastic material and the steel elements. The energy dissipation through the viscoelastic material increases by the increase of the axial deformations in the viscoelastic material as well as the increase in its volume. The axial deformations have a larger effect on the viscoelastic energy dissipation of the device than the material volume. The smaller the viscoelastic material breadth, the larger the strains obtained in the device and accordingly the higher the energy dissipation through the viscoelastic and steel materials. On the other hand, smaller viscoelastic material breadth results in lowering the displacements supply of the device, which can lead to excessive inelastic deformation in steel elements under relatively small deformations. Increasing the viscoelastic material breadth leads to limiting the deformations developed in the device, which reduces significantly the total energy dissipation. Accordingly, reasonable viscoelastic material breadth is recommended to provide a balance between the stiffness and energy dissipation provided by the device and to ensure having devices with large-

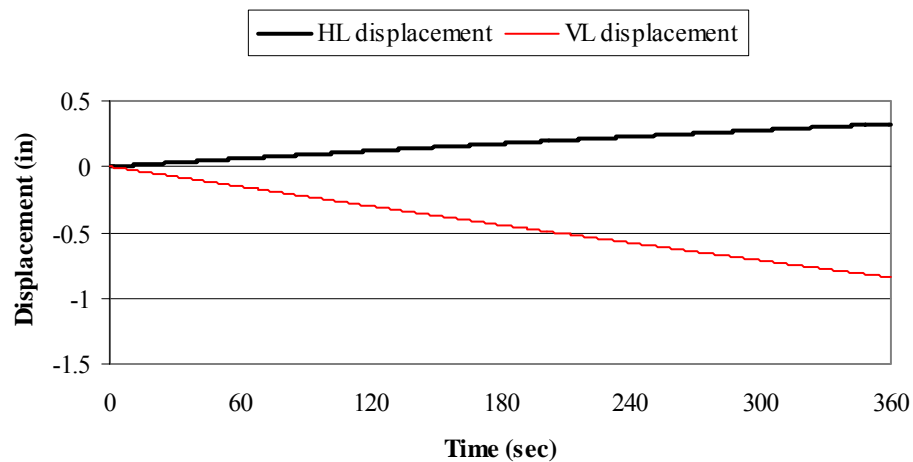
displacement supplies. As a result of these analyses, a rubber breadth of 40 in. is recommended with a ratio between rubber breadth and device span around 0.4.



a) Rubber breadth = 30 in.

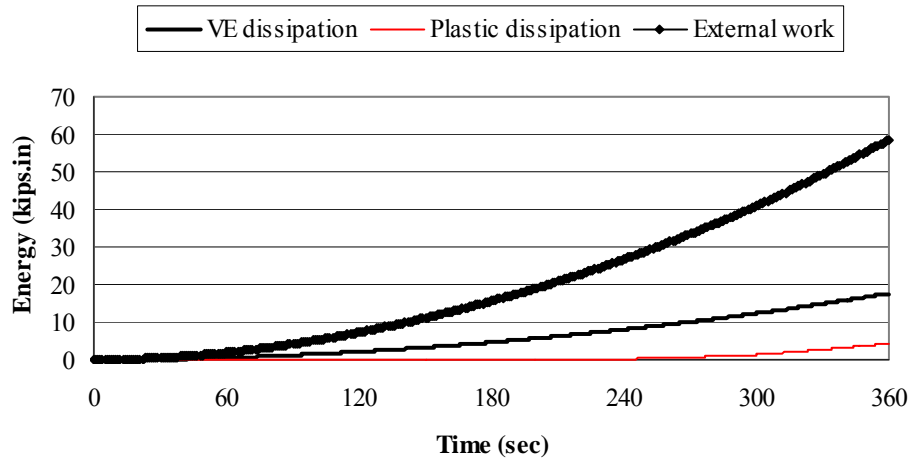


b) Rubber breadth = 40 in.

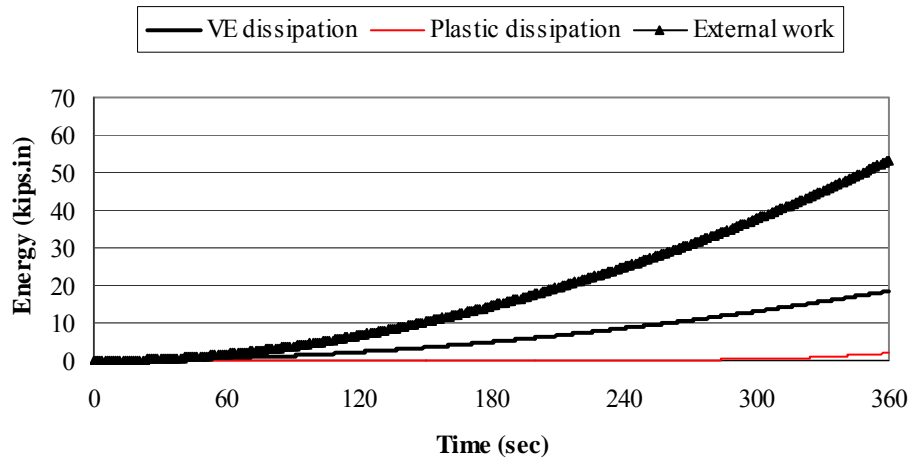


c) Rubber breadth = 50 in.

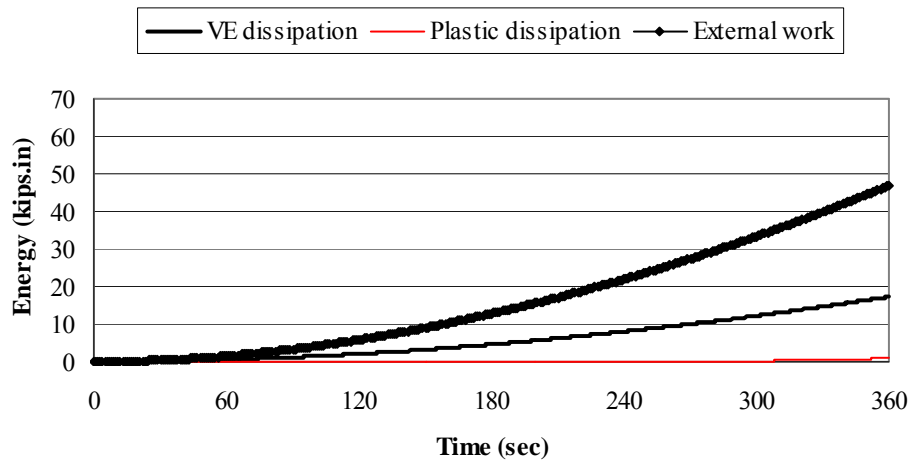
Figure 6.25: Effect of the rubber breadth on the deformations of the device under tensile loading.



a) Rubber breadth = 30 in.

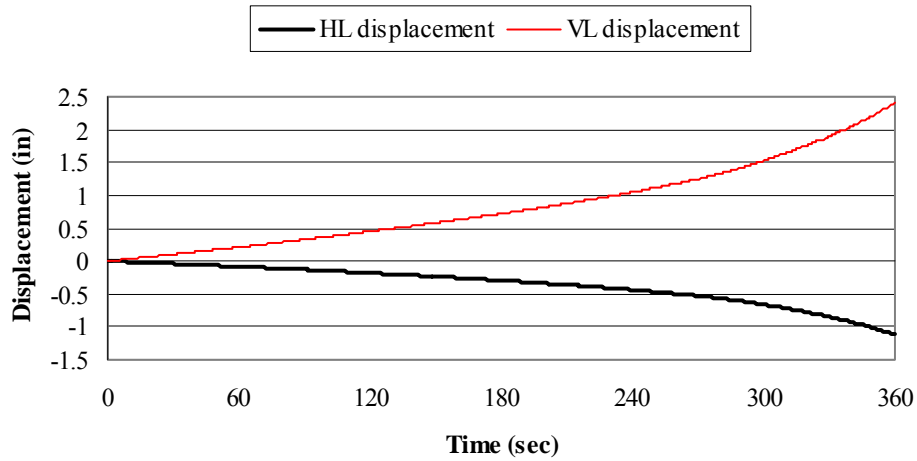


b) Rubber breadth = 40 in.

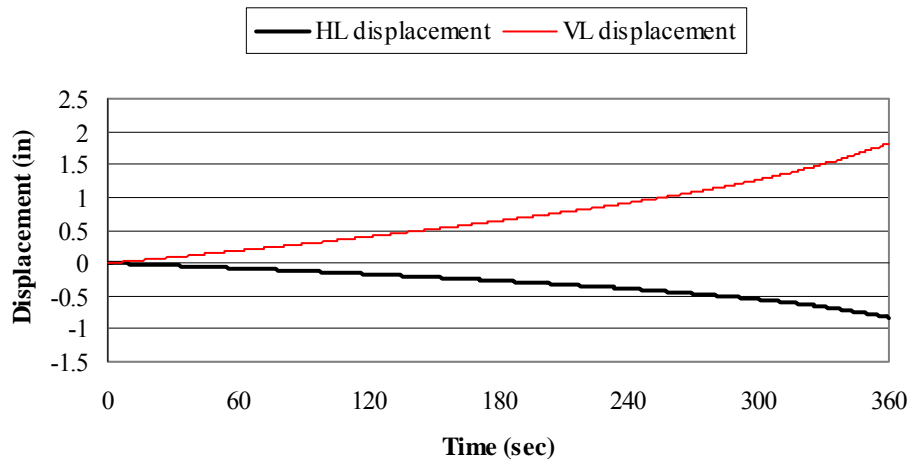


c) Rubber breadth = 50 in.

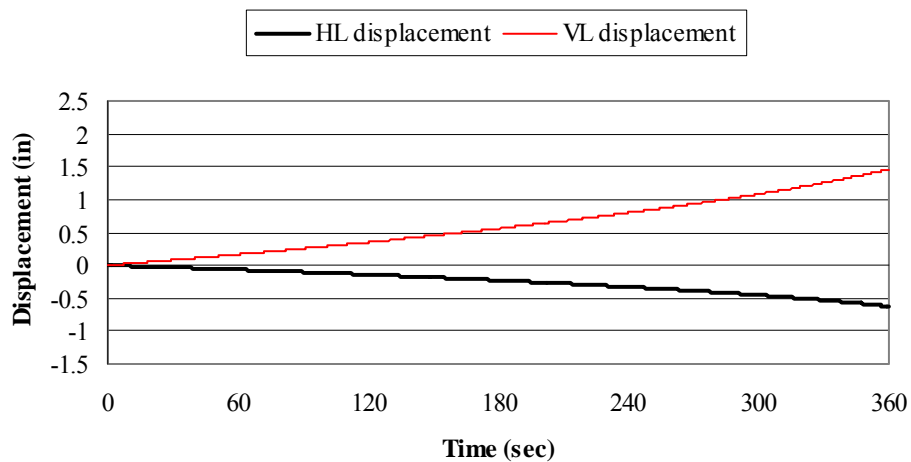
Figure 6.26: Effect of the rubber breadth on the energy dissipation under tensile loading.



a) Rubber breadth = 30 in.

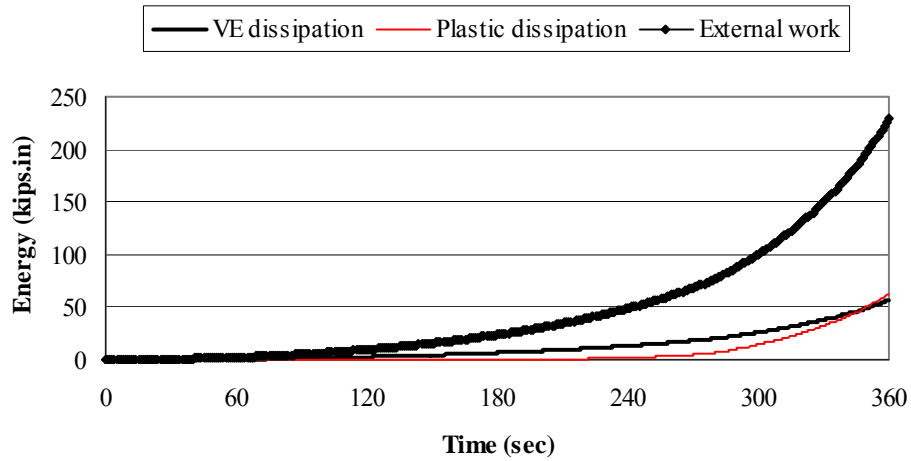


b) Rubber breadth = 40 in.

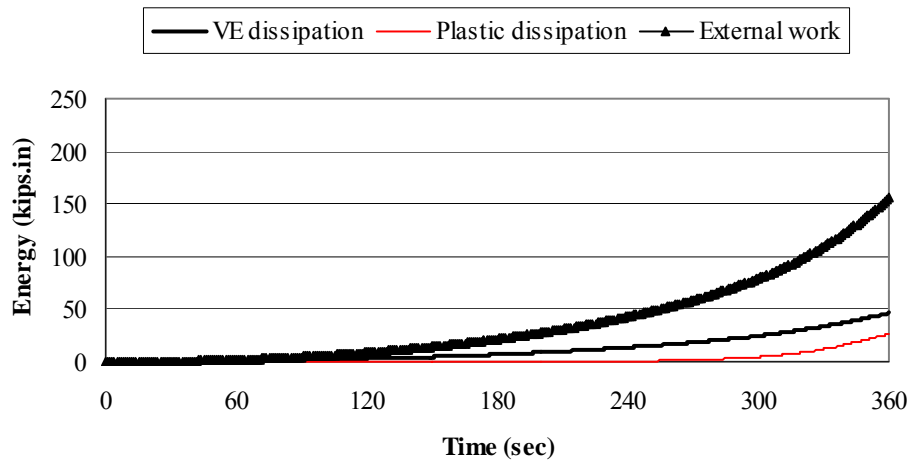


c) Rubber breadth = 50 in.

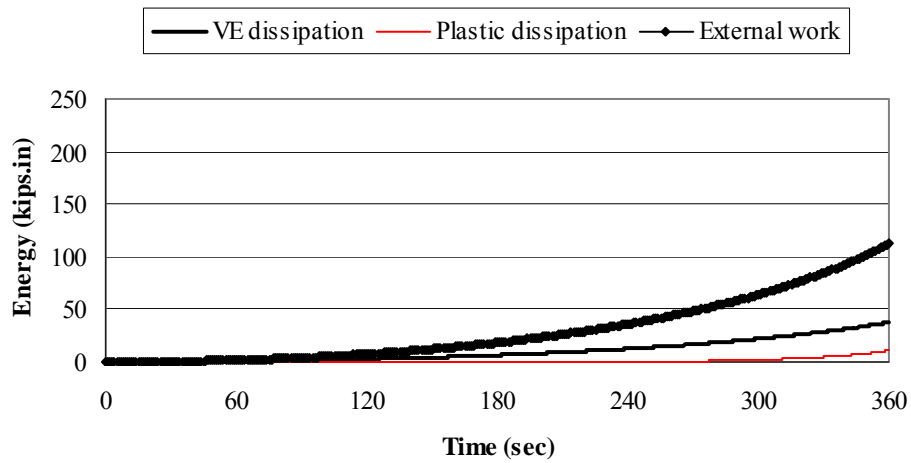
Figure 6.27: Effect of the rubber breadth on the deformations of the device under compressive loading.



a) Rubber breadth = 30 in.

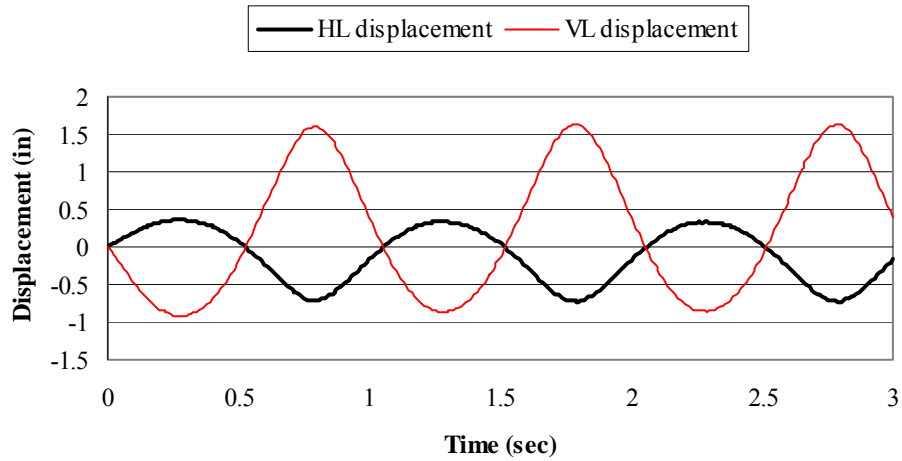


b) Rubber breadth = 40 in.

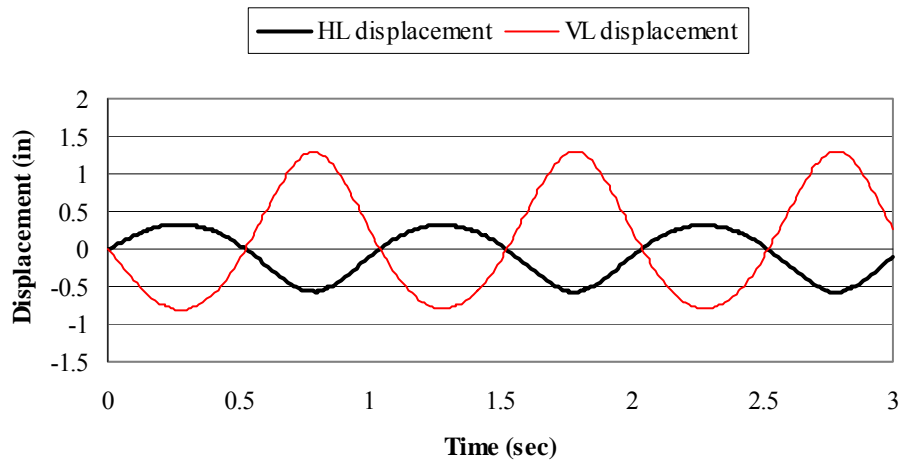


c) Rubber breadth = 50 in.

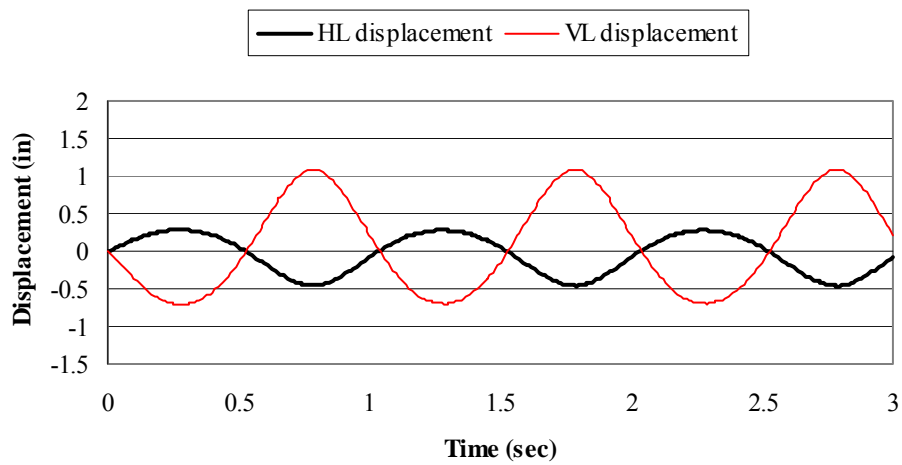
Figure 6.28: Effect of the rubber breadth on the energy dissipation under compressive loading.



a) Rubber breadth = 30 in.

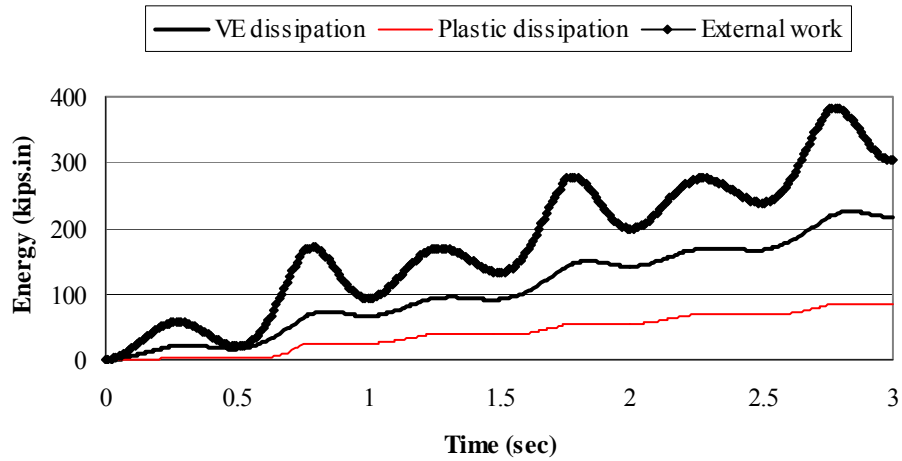


b) Rubber breadth = 40 in.

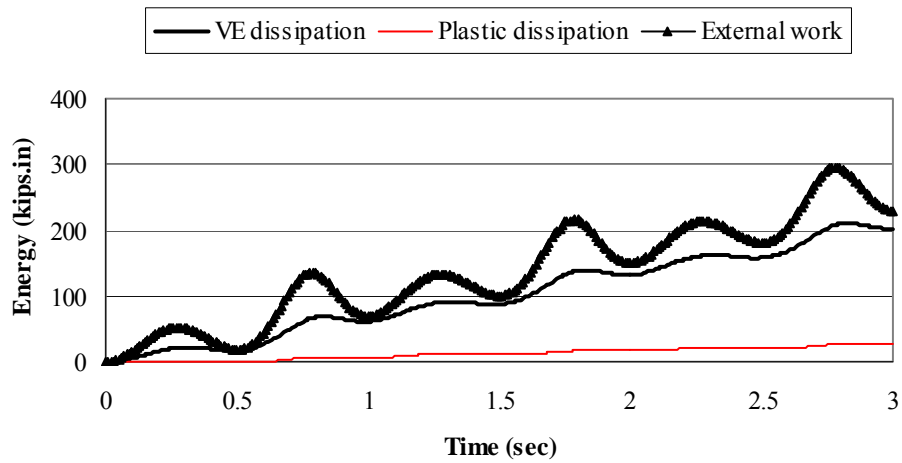


c) Rubber breadth = 50 in.

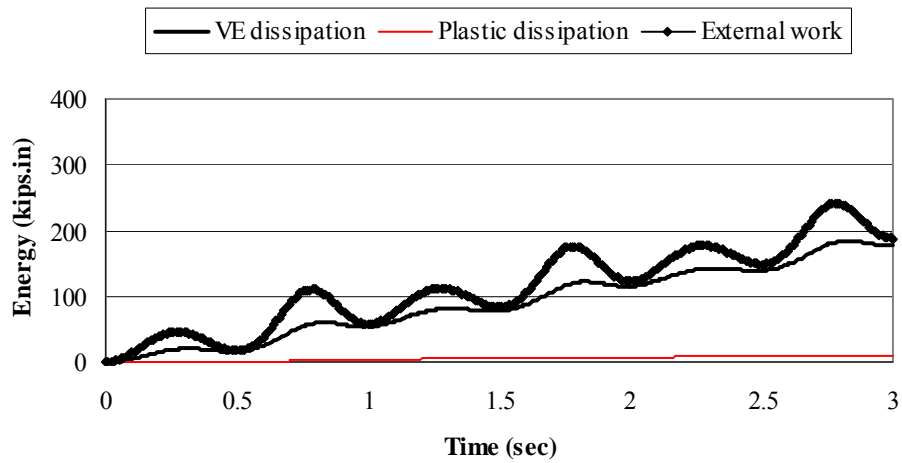
Figure 6.29: Effect of the rubber breadth on the deformations of the device under harmonic loading.



a) Rubber breadth = 30 in.



b) Rubber breadth = 40 in.



c) Rubber breadth = 50 in.

Figure 6.30: Effect of the rubber breadth on the energy dissipation under harmonic loading.

6.3.4 Effect of the Cross Section of Steel Elements

The last parameter in this parametric study that affects the behavior of the device was the cross section of the steel elements. This parameter controls the stiffness, total strength and the energy dissipation of the device. Also, the weight and total cost are greatly dependent on the cross section of the steel elements.

To determine how this parameter affects the device behavior, three different cases with different cross sections are considered. The chosen cross sections are channel, C15x50, 1.5-in. thick and 2.0-in. thick plates. All the cross sections are made from high-strength steel material. The aspect ratio selected was 1/6, while rubber breadth was 40 in. The three cases were analyzed under quasi-static tensile, quasi-static compressive and harmonic forces.

First, devices with aforementioned cross sections were studied under quasi-static tensile forces. The results of this analysis are shown in Figure 6.31 and Figure 6.32. In the first case, steel channels, the maximum horizontal displacement was 0.38 in. while the maximum vertical displacement at the middle of the device was 0.96 in. At the end of loading, the energy dissipation through the viscoelastic material was 23.2 kip-in. and the energy dissipation through steel yielding was 4.3 kip-in. In the second case in which 1.5-in. thick plate was used, the maximum horizontal displacement was 0.37 in. while the maximum vertical displacement at the middle of the device was 0.95 in. At the end of loading, the energy dissipated through viscoelastic material as well as the inelastic behavior of steel plates was 18.51 and 1.96 kip-in., respectively. The maximum horizontal displacement in the case of the 2 in.-thick steel plate was 0.25 in. while the maximum vertical displacement at the middle of the device was 0.63 in. The energy dissipated through the viscoelastic material and steel yielding was 7.8 and 0.5 kip-in., at the end of loading, respectively.

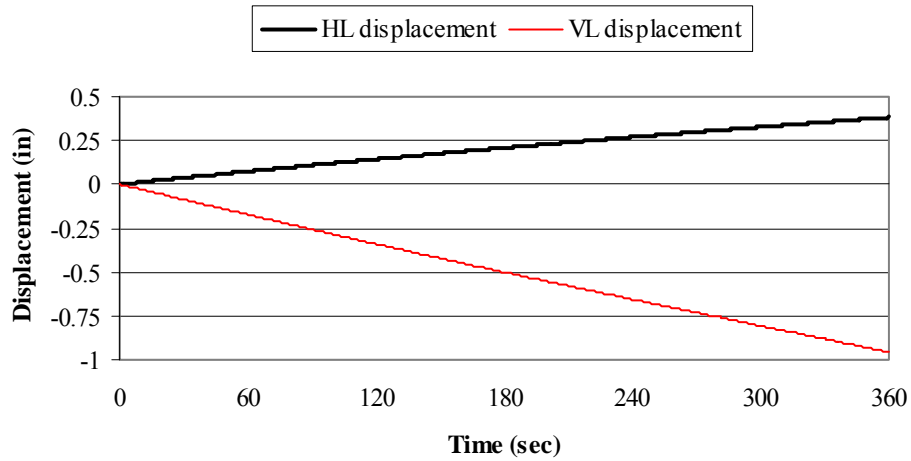
The responses of the device with different cross sections under compression were compared. Devices with channel, C15x50, experienced higher deformations. The maximum horizontal displacement at the device edge and vertical displacement at the

middle of the device were 0.87 and 1.85 in., respectively. At the end of loading, the energy dissipation was 57.8 and 18.3 kip-in. through the viscoelastic material and steel yielding, respectively. The device in the second case was displaced horizontally by 0.83 in. The maximum vertical displacement at the middle of the device was 1.82 in. The viscoelastic material dissipated energy with a value of 46.5 kip-in. while the energy dissipated through steel yielding was 26.4 kip-in. Device with 2-in. thick plate had much higher stiffness and accordingly smaller deformations were developed in the device compared to the other cases. As a result of that, no considerable yielding occurred in the steel plates. The energy dissipated through the viscoelastic material and steel yielding was 11.3 and 2.9 kip-in. The corresponding horizontal displacement at the device edge and vertical displacement at the middle of the device were 0.41 and 0.96 in., respectively, which are much less the deformations in the other cases. The results of this analysis are shown in Figure 6.33 and Figure 6.34.

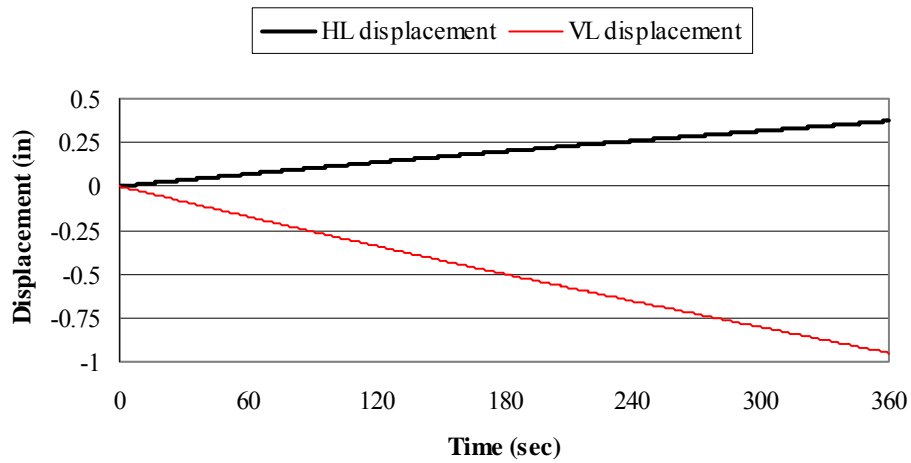
The same trend of results was obtained under harmonic loading. The deformations of the first two cases are much higher than the deformations developed in the third case. The horizontal displacement ranged from 0.36 in. under tension to 0.69 in. under compression, 0.32 in. under tension to 0.57 in. under compression and 0.23 in. under tension and 0.32 in. under compression for the three cases, respectively. The total energy dissipation was 309.6, 228.4 and 84.0 kip-in., respectively. The results of this analysis are shown in Figure 6.35 and Figure 6.36.

From the previous results under tensile, compression and harmonic loadings, it was obvious that the devices with C15x50 channels experienced larger deformations than the other cases due to the small cross sectional area of the channels compared to the area of the steel plates. Large deformations in the visco-plastic device lead to the increase in energy dissipation through the viscoelastic material as well as the steel elements. Small cross sections results in reducing the device cost in addition to its total weight, which add more advantages to the device. Despite the relatively small cross sectional area of the selected channels, their second moment of inertia around both axis are high, which

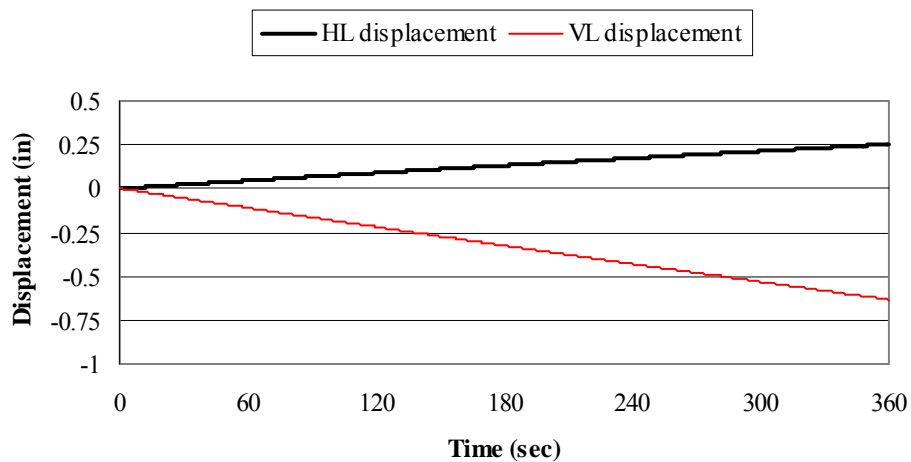
increases the device strength and its ability to undergo large deformations. Accordingly, the channels, C15x50 were selected for the device.



a) Channel; C15x50

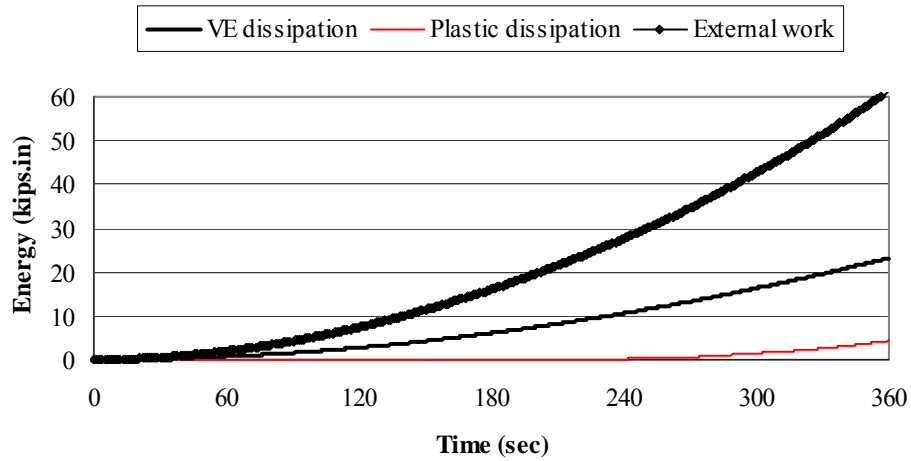


b) Plate; 1.5-in. thick

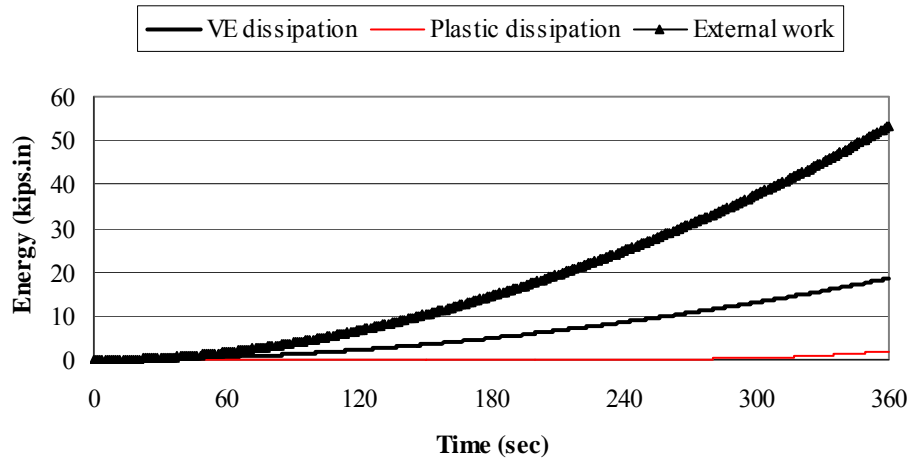


c) Plate; 2.0-in. thick

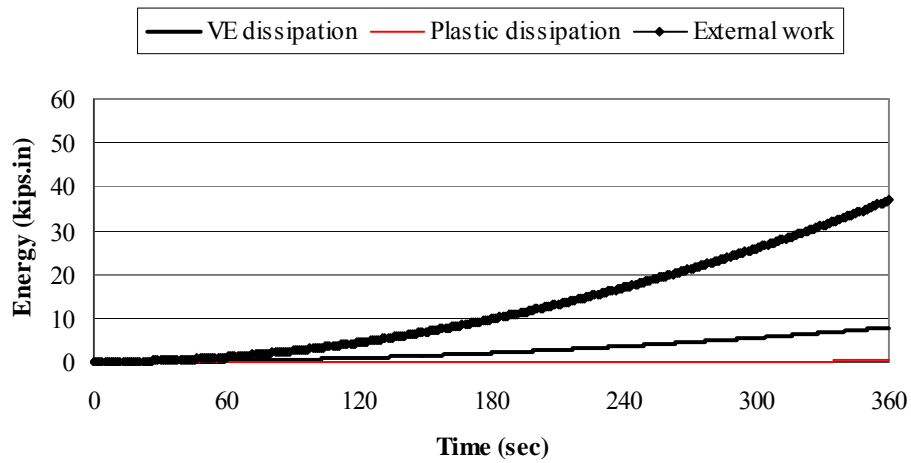
Figure 6.31: Effect of steel cross section on the deformations of the device under tensile loading.



a) Channel; C15x50

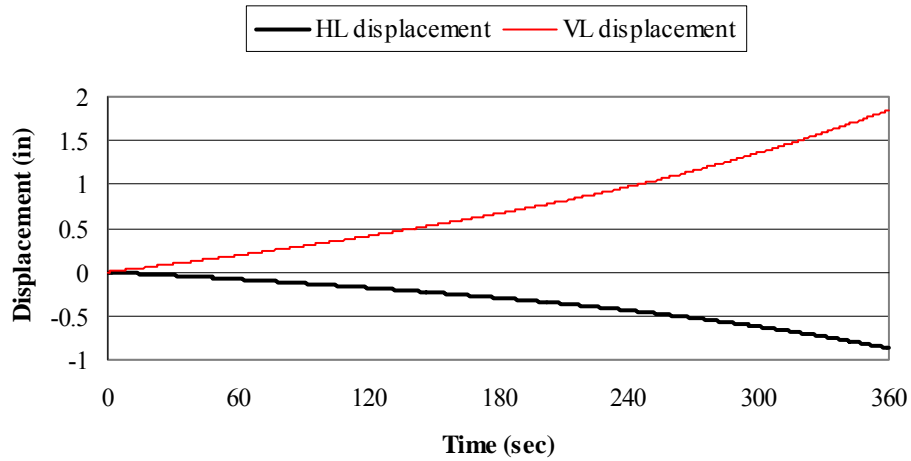


b) Plate; 1.5-in. thick

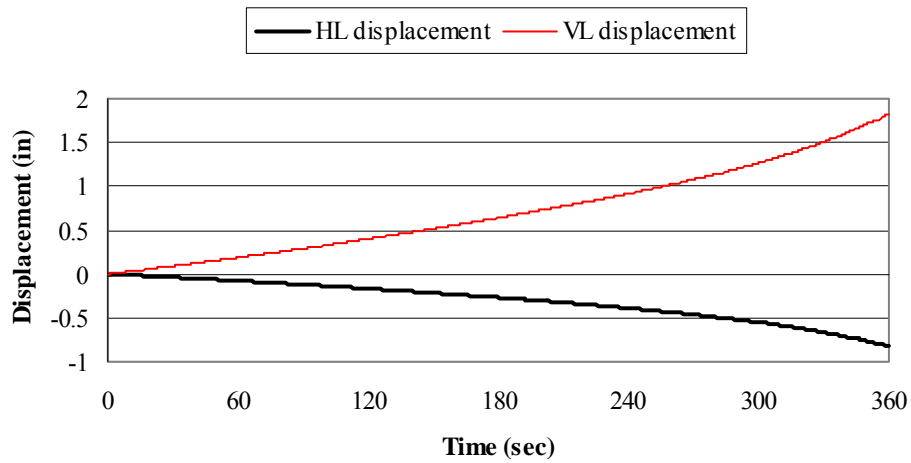


c) Plate; 2.0-in. thick

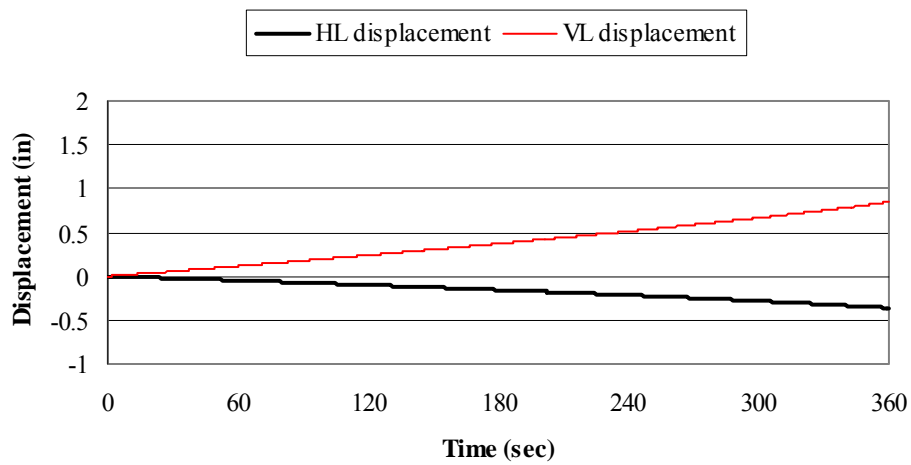
Figure 6.32: Effect of steel cross section on the energy dissipation under tensile loading.



a) Channel; C15x50

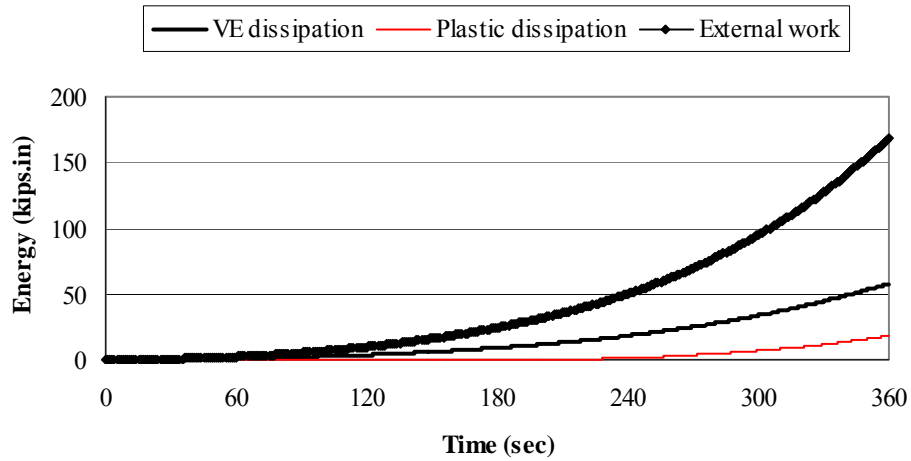


b) Plate; 1.5-in. thick

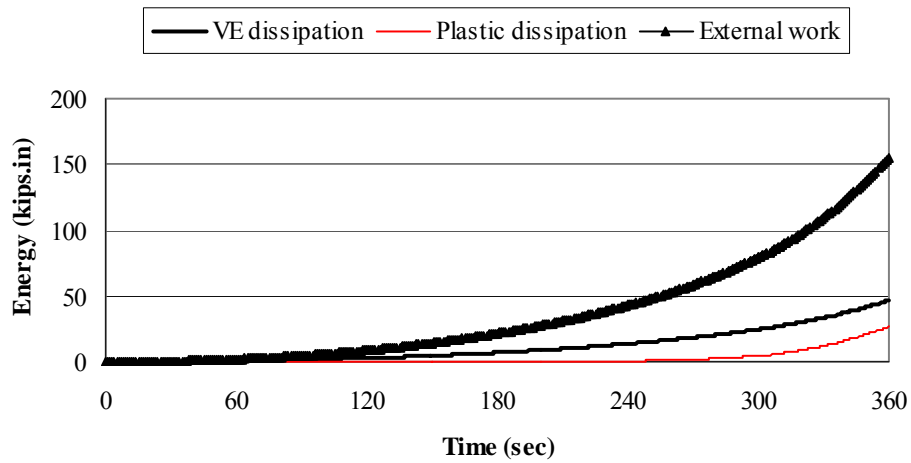


c) Plate; 2.0-in. thick

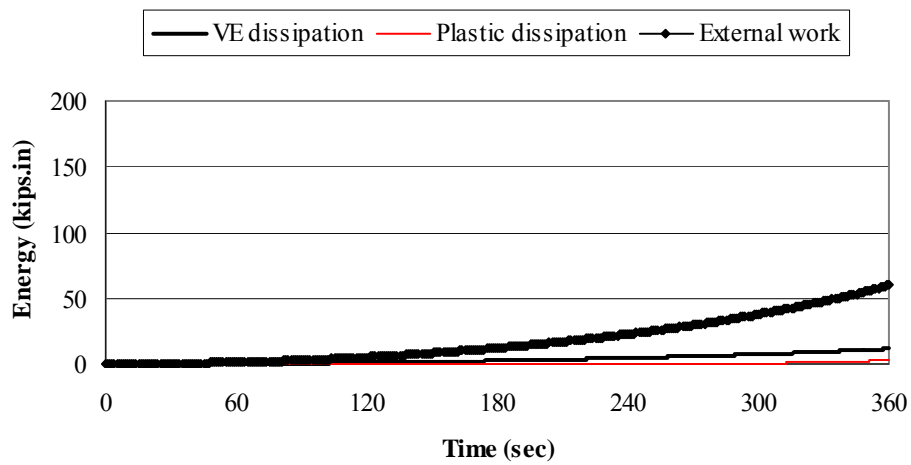
Figure 6.33: Effect of steel cross section on the deformations of the device under compressive loading.



a) Channel; C15x50

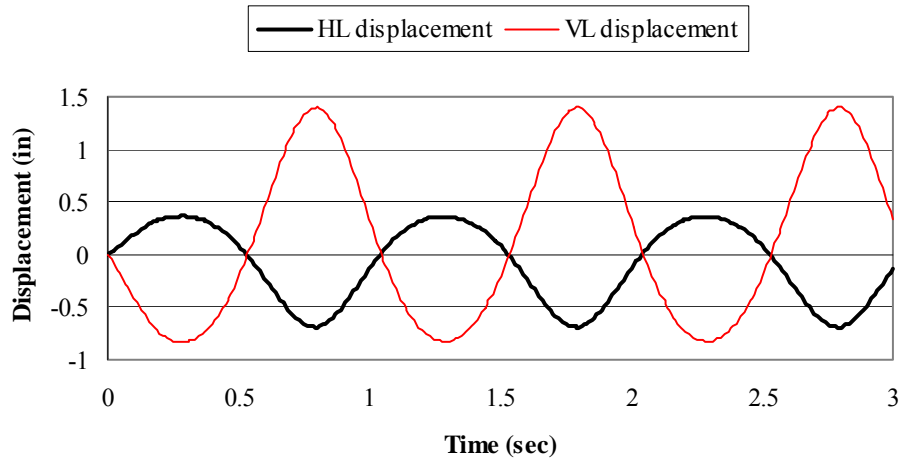


b) Plate; 1.5-in. thick

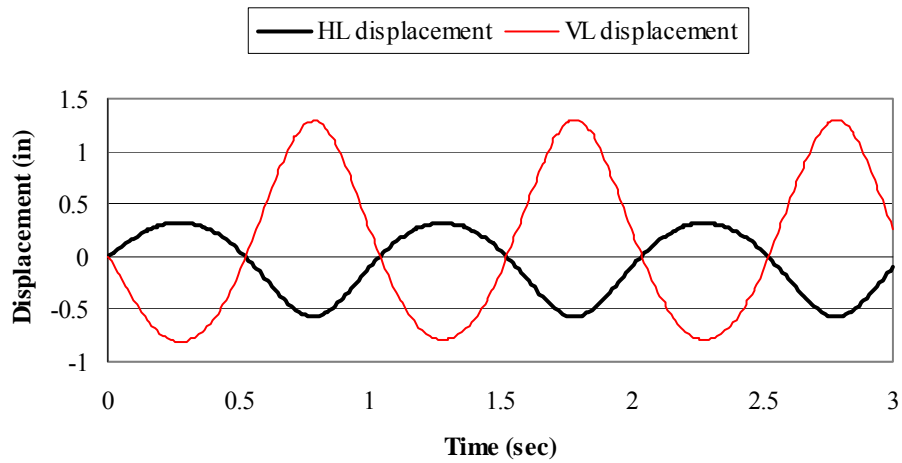


c) Plate; 2.0-in. thick

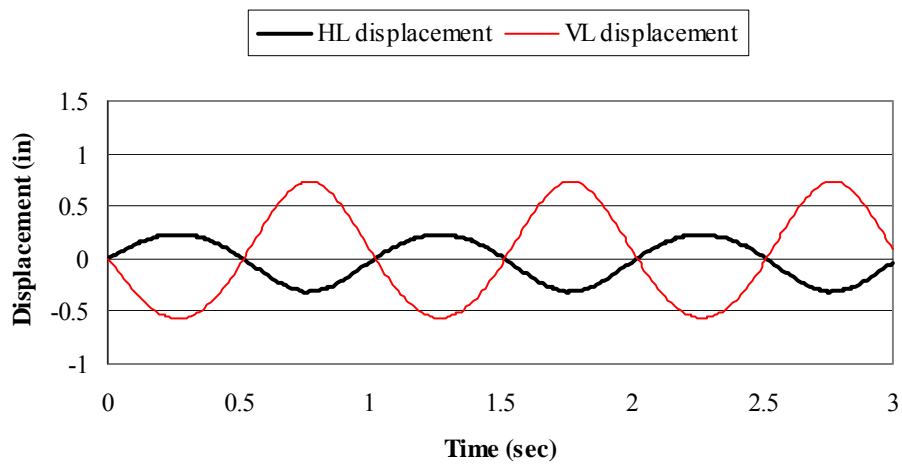
Figure 6.34: Effect of steel cross section on the energy dissipation under compressive loading.



a) Channel; C15x50

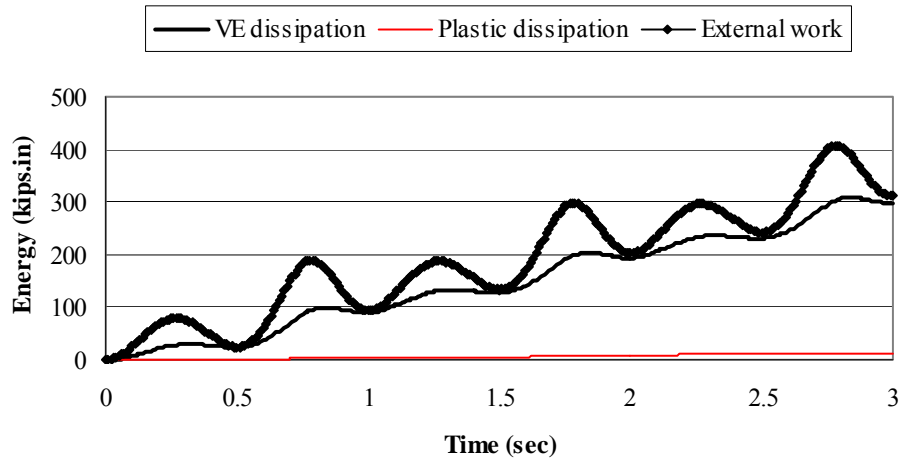


b) Plate; 1.5-in. thick

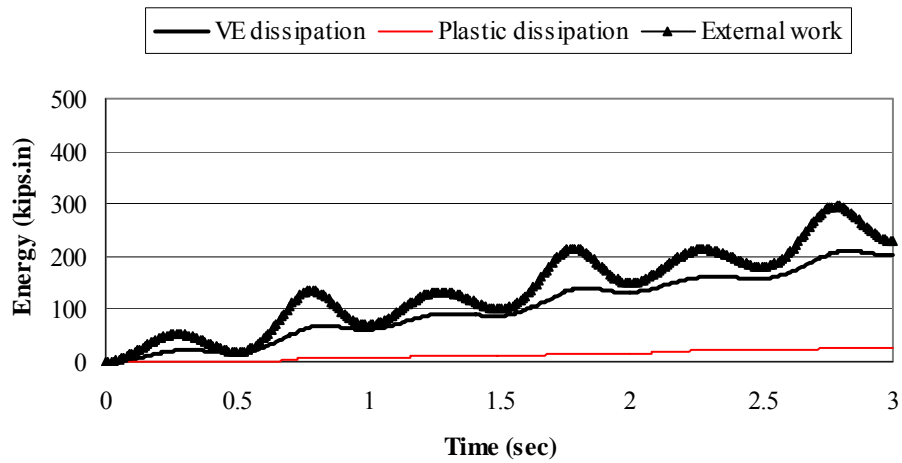


c) Plate; 2.0-in. thick

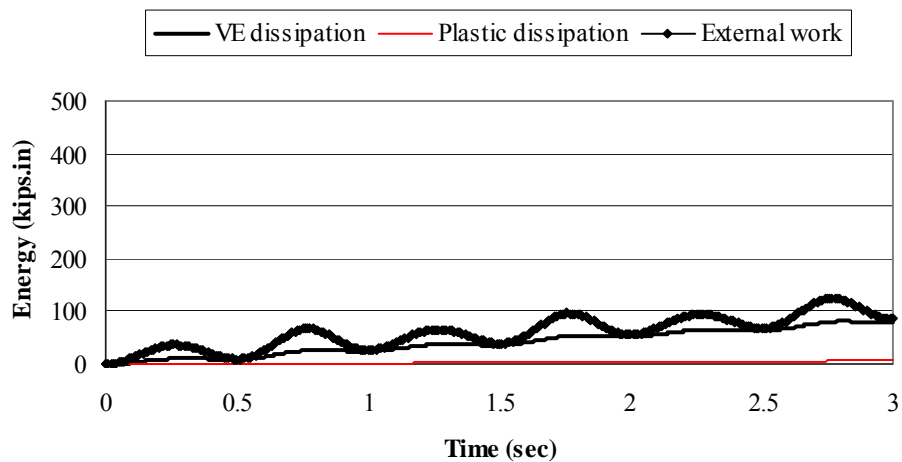
Figure 6.35: Effect of steel cross section on the deformations of the device under harmonic loading.



a) Channel; C15x50



b) Plate; 1.5-in. thick



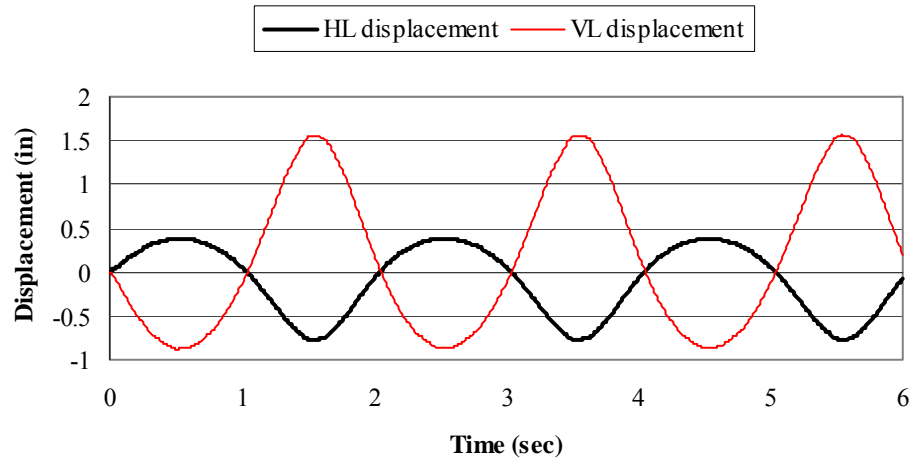
c) Plate; 2.0-in. thick

Figure 6.36: Effect of steel cross section on the energy dissipation under harmonic loading.

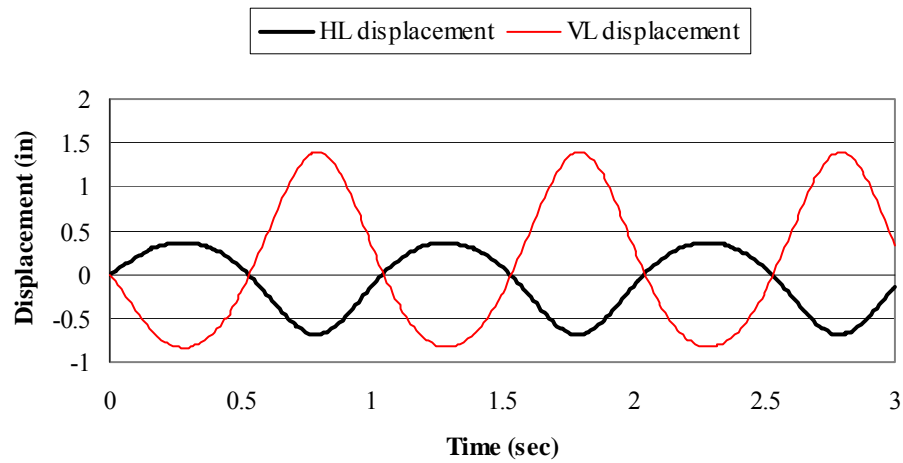
6.4 Performance of the Visco-Plastic Device under Different Loadings

According to the previous analyses of the visco-plastic device with different parameters under different types of dynamic loadings, a 40-in. breadth high-damping rubber block was selected to be sandwiched between two high-strength steel channels, C15x50. Device aspect ratio was chosen to be 1/6. It is important to investigate the device performance under different loading frequencies and different displacement amplitudes. The visco-plastic device with the selected parameters was analyzed under different loading frequencies that cover a reasonable range of frequencies of seismic excitations. Three different harmonic loadings with the same loading amplitude were selected; $300 \sin(\pi t)$, $300 \sin(2\pi t)$, and $300 \sin(4\pi t)$. The response of the device under these loadings in three cycles is shown in Figure 6.37 and Figure 6.38. As the loading frequency increases, the deformations in the device are reduced. However, the viscoelastic energy dissipation is increased by the increase in the loading frequency. The energy dissipation through the inelastic behavior of steel elements is slightly affected by the loading frequency due to the variations in the deformations developed in the device. It can be noticed that the visco-plastic device performed well under different loading frequencies.

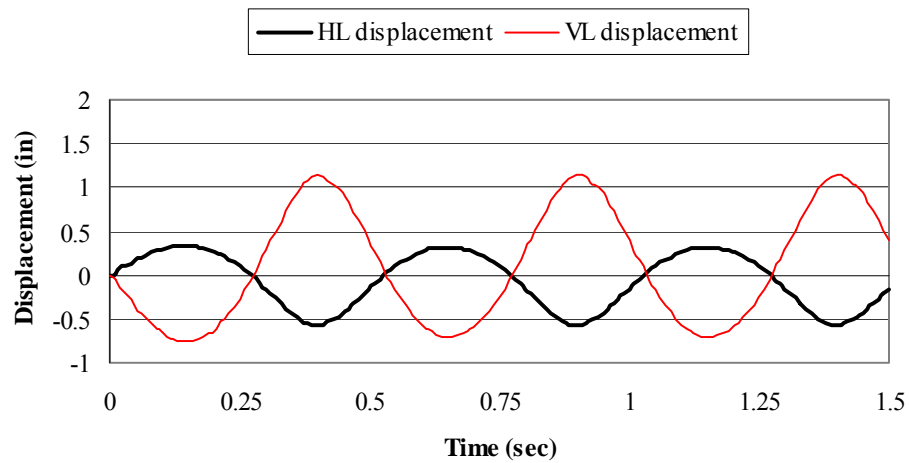
To show the performance of the visco-plastic device under different displacements amplitudes, the device was exposed to different harmonic horizontal excitations; $0.5 \sin(2\pi t)$, $1.0 \sin(2\pi t)$, and $1.5 \sin(2\pi t)$. The results of these analyses are shown in Figure 6.39 and 6.40. From these results, it can be observed that the device behaved as a viscoelastic device under low-level excitations in the matter that the energy was dissipated through the viscoelastic material only and the steel elements were kept elastic. Under higher levels of excitations, the energy was dissipated through the viscoelastic material and the steel channels. The amplification factor, the ratio between the vertical displacement at the middle of the device and the horizontal displacement at the device edge, is higher for high-level excitations due to the reduction in the stiffness of the steel elements upon yielding.



a) Load = $300 \sin(\pi t)$



b) Load = $300 \sin(2\pi t)$



c) Load = $300 \sin(4\pi t)$

Figure 6.37: Effect of the loading frequency on the deformations of the device

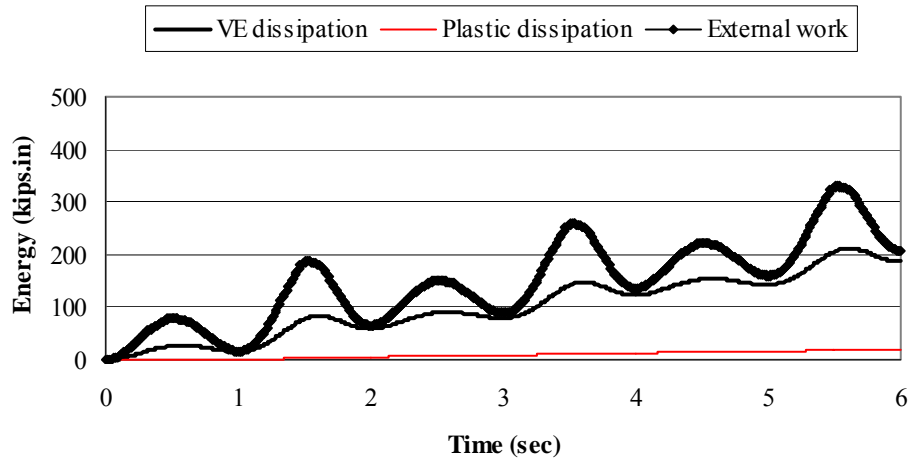
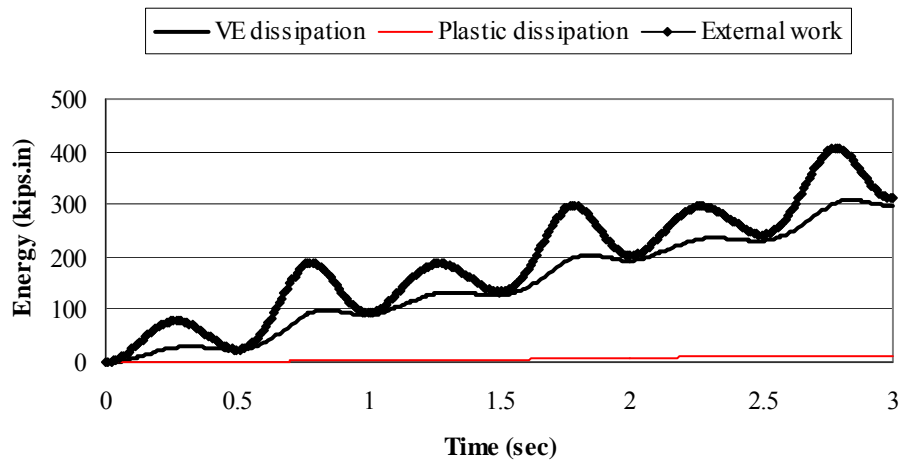
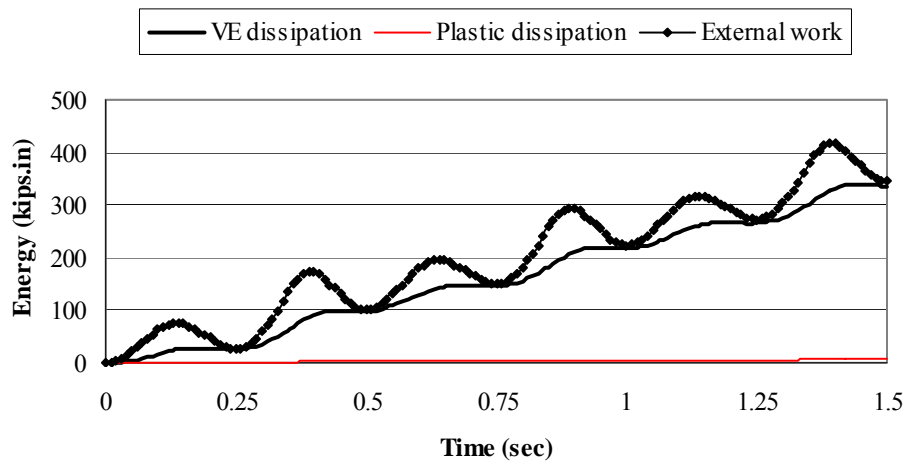
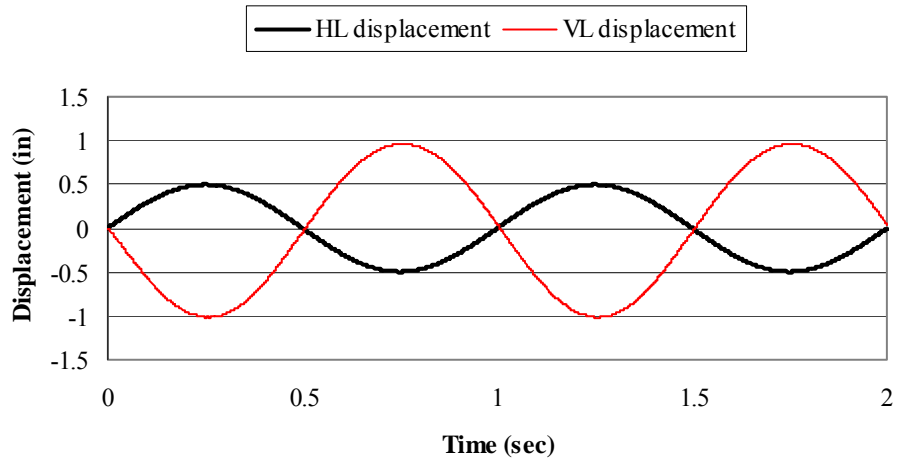
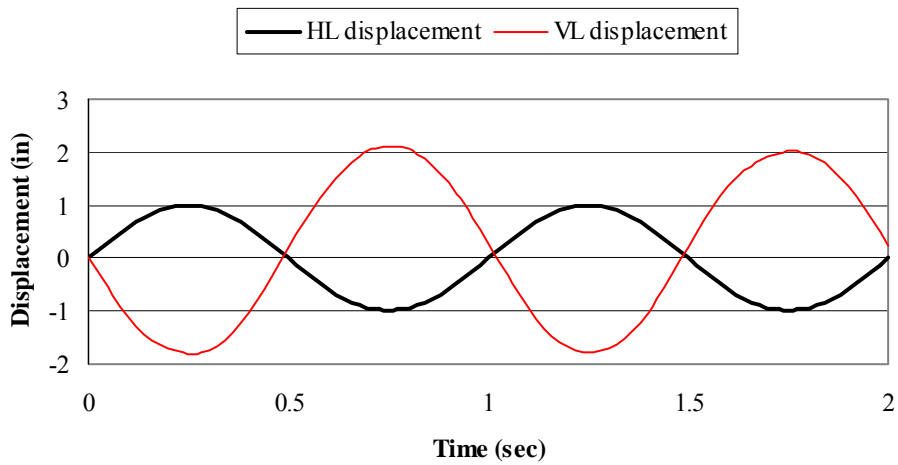
a) Load = $300 \sin(\pi t)$ b) Load = $300 \sin(2\pi t)$ c) Load = $300 \sin(4\pi t)$

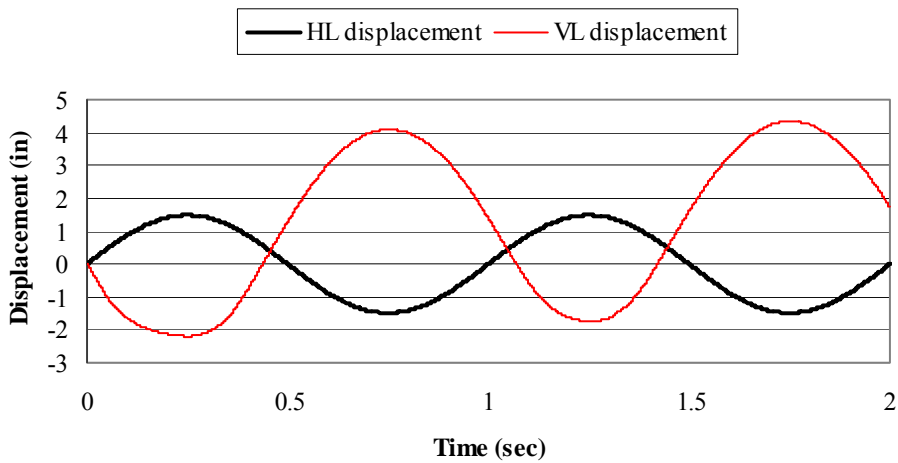
Figure 6.38: Effect of the loading frequency on the energy dissipation by the device.



a) Displacement; $0.5 \sin(2\pi t)$

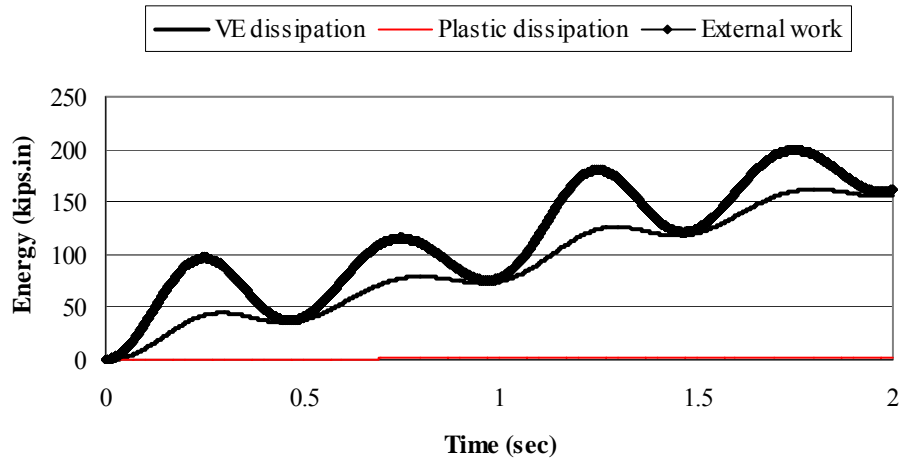


b) Displacement; $1.0 \sin(2\pi t)$

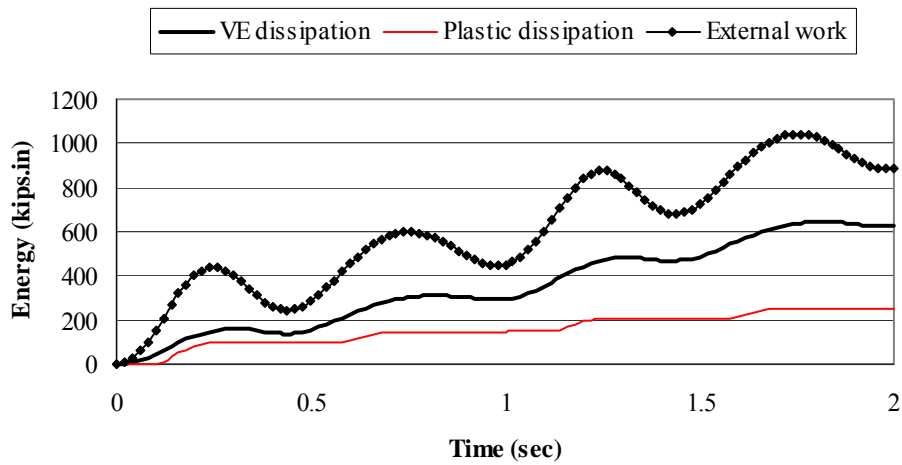


c) Displacement; $1.5 \sin(2\pi t)$

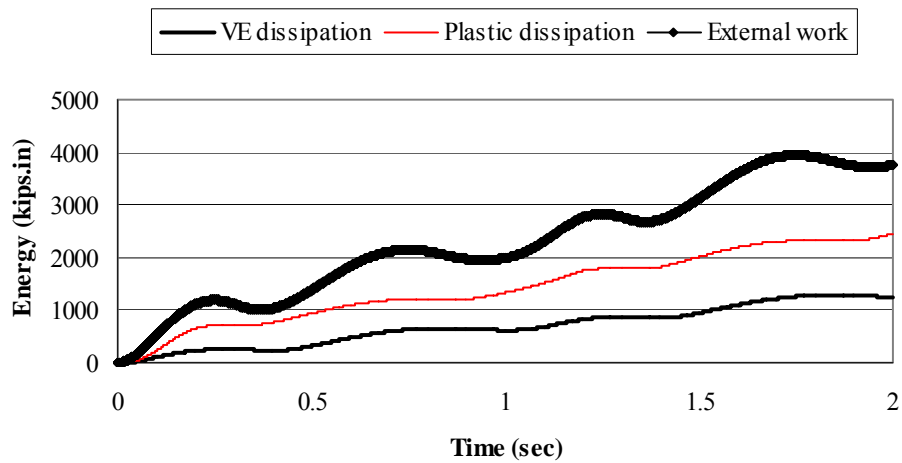
Figure 6.39: Response of device under different displacement amplitudes



a) Displacement; $0.5 \sin(2\pi t)$



b) Displacement; $1.0 \sin(2\pi t)$



c) Displacement; $1.5 \sin(2\pi t)$

Figure 6.40: Energy dissipation of the device under different displacement amplitudes.

6.5 Summary

A three-dimensional detailed finite element model for the visco-plastic device was developed using ABAQUS. The model considered the hyperelasticity and viscoelasticity of the rubber block. Experimental results of high-damping rubber compounds were used. The rubber block was modeled using three-dimensional 20-node quadrilateral reduced-integration elements solid elements. The inelastic behavior of the steel elements was considered. The steel elements were modeled using 8-node quadrilateral reduced integration shell elements. Large-displacement analysis was conducted.

A parametric study was carried out on the device to investigate the effect of different parameters on the device behavior. Different types of loadings were considered in this study. The parameters considered are:

- Steel type
- Device aspect ratio
- Breadth of rubber block
- Cross section of steel elements

According to the results of the parametric study, the following observations were obtained:

1. Devices with mild-steel elements dissipate more energy through yielding. However, steel yielding occurs under relatively small deformations. Moreover, devices with mild-steel experienced excessive yielding when exposed to moderate deformations, which reduces the device strength and its ability to undergo large deformations.
2. As the aspect ratio increases, the device stiffness is reduced. Accordingly, larger deformations are developed in the viscoelastic material as well as the steel elements, which results in increasing the total energy dissipation through the device. On the other hand, devices with lower aspect ratios provide higher stiffness. Although higher device stiffness may lead to smaller structural deformations but on the other hand, excessive added stiffness may act as a “seismic attractor,” increasing base shears and increasing response accelerations,

- which result in damage to contents and nonstructural components. Accordingly, high aspect ratio is recommended for the device.
3. The smaller the viscoelastic material breadth, the larger the strains obtained in the device and accordingly the higher the energy dissipation through the viscoelastic and steel materials. On the other hand, smaller viscoelastic material breadth results in lowering the displacements supply of the device, the ability of the device to undergo large horizontal displacements, which can lead to excessive inelastic deformation in steel elements under relatively small deformations. Very large viscoelastic breadth leads to limiting the deformations developed in the device, which reduces significantly the total energy dissipation. Accordingly, reasonable viscoelastic material breadth is recommended to provide a balance between the stiffness and energy dissipation provided by the device and to ensure having devices with large-displacement supplies.
 4. Devices with small cross sections of steel elements experience large deformations, which results in more energy dissipation through viscoelastic material and steel elements. However, these devices do not have the ability to undergo large deformations without severe yielding. On the other hand, having large steel sections limits the deformations developed in the device, which reduces the efficiency of the device considerably. Accordingly, reasonable cross sections are recommended for the device in order to develop a balance between stiffness and damping provided by the device.

After selecting the different device parameters based on the parametric study, the device was analyzed under harmonic loading with different amplitudes and loading frequencies. Under low-level of deformations, the device behaved like viscoelastic damper in the way that the energy was dissipated through the viscoelastic material. For high-level of deformations, significant energy dissipation was obtained from the inelastic behavior of the steel elements. The device performed well under different loading frequencies.

Chapter 7: Simplified Device Models

7.0 Introduction

In the previous chapter, the modeling procedure for a detailed finite element analysis of the visco-plastic device using the finite element program, ABAQUS, was presented. The viscoelastic material was modeled using three-dimensional solid elements. The viscoelastic material was assumed to be an incompressible material since the Poisson ratio is as high as 0.5 for rubber. Hybrid elements were used to account for the incompressibility. The hyperelastic and viscoelastic behaviors of the rubber block were modeled using experimental results of uniaxial tension and compression, biaxial tension, and relaxation tests conducted on high-damping rubber compounds. The inelastic behavior of the steel elements was modeled using the Von Mises yield criterion. Large displacement analysis was conducted on the device.

The detailed finite element analysis provided accurate results because it considered every aspect of the device as well as the different properties of steel and rubber. However, it is not practical for designers to use this complicated model in the structural analysis of multi-story buildings. To facilitate the use of this device in protecting structures against seismic excitations as well as structural retrofitting, a simplified physical model of this device is needed. Unfortunately, the approximations in the development of the simplified model may result in less accuracy in the computed response. Accordingly, a balance between the model simplicity and its accuracy is essential. In this chapter, different simplified models are presented in order to determine the simplified model that gives the most satisfactory approximate results.

7.1 Simplified Models

7.1.1 Simple Model, *MI*

Different simplified physical models are presented using the SAP2000 program. The first simplified model used in this analysis is *MI*, which is shown in Figure 7.1. The steel elements are modeled using beam elements. The rubber block is modeled using a multilinear elastic spring to represent the hyperelasticity, and a viscous dashpot to

represent the viscoelasticity of rubber block. The masses are lumped at ten interior nodes, as shown in Figure 7.1.

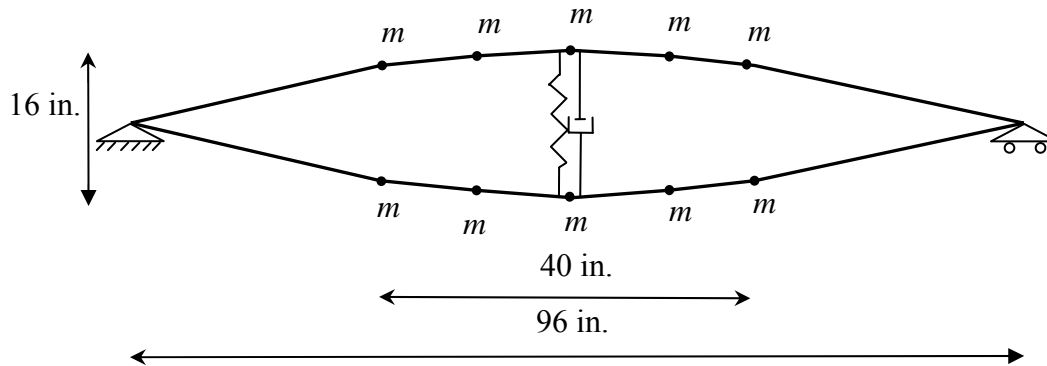


Figure 7.1: Simplified model, $M1$

7.1.1.1 Model Mass

The weight of the visco-plastic device is the summation of the weight of the rubber block and the steel elements. The shape of the steel elements modeled in the previous chapter has a form of $\frac{h}{2} \sin(\frac{\pi x}{l})$ where h is the thickness of the rubber block at the middle of the device and l is the device length. For the finite element model, h and l were taken equal to 16 and 96 in., respectively while the rubber breadth, e , and width, b , were 40 and 12 in., respectively (See Figure 4.1 for details of the device configuration).

Rubber block

The volume of the rubber block can be calculated from:

$$V_r = A_r b \quad (7-1)$$

where A_r is the area of rubber block in the front view and b is the block width.

The area is obtained from:

$$A_r = 2 \int_{28}^{68} \frac{h}{2} \sin\left(\frac{\pi x}{l}\right) dx = -\frac{h \cdot l}{\pi} \cos\left(\frac{\pi x}{l}\right) \Big|_{28}^{68}$$

$$A_r = -\frac{hl}{\pi} \left[\cos\left(\frac{68\pi}{96}\right) - \cos\left(\frac{28\pi}{96}\right) \right]$$

$$A_r = 595.28 \text{ in}^2.$$

Accordingly, the volume of rubber block is:

$$V_r = 7143.31 \text{ in}^3.$$

The weight of rubber block is determined from:

$$W_r = V_r \gamma_r \quad (7-2)$$

$$W_r = 7143.31 * \frac{0.094}{12 * 12 * 12}$$

$$W_r = 0.39 \text{ kips.}$$

Steel elements

The steel elements chosen from the previous chapter are C15x50 steel channels. The shape of the steel channels has a form of $\frac{h}{2} \sin(\frac{\pi x}{l})$. To calculate the weight of the steel channels, the curved length has to be calculated first. The arc length of a sinusoidal shape can be calculated from:

$$l_c = \int \sqrt{\left(\frac{dy}{dx}\right)^2 + 1} dx \quad (7-3)$$

$$l_c = \int_0^{96} \sqrt{\left(\frac{8\pi}{96}\right)^2 \cos^2\left(\frac{\pi x}{96}\right) + 1} dx$$

Using the trapezoidal method to calculate this integral numerically leads to:

$$l_c = 97.63 \text{ in}^2.$$

Accordingly, the weight of the two steel channels can be determined from:

$$W_s = 2 * (97.63 * 14.7) * \frac{0.49}{12 * 12 * 12}$$

$$W_s = 0.81 \text{ kips}$$

The total weight of the device is the summation of the weight of the rubber block and steel elements.

$$W_{device} = W_r + W_s = 1.20 \text{ kips}$$

The device mass can be calculated by dividing the total weight by the ground acceleration, g :

$$m = \frac{1.20}{386.2}$$

$$m = 0.0031 \text{ kip-sec}^2/\text{in.}$$

The mass in the simplified model is lumped in ten nodes.

$$m \text{ (per node)} = 0.00031 \text{ kip-sec}^2/\text{in.}$$

7.1.1.2 Modeling the Hyperelasticity of the Rubber Block

Hyperelastic materials have the ability to deform elastically up to large strains. The stress-strain curve is highly nonlinear but elastic. To model the hyperelasticity in finite element model, experimental results of uniaxial and biaxial tension and compression tests on specimens of high-damping rubber compounds were used. In order to model the hyperelasticity in the simplified model, a vertical multilinear elastic spring is used. The force-displacement curve of this spring is obtained directly from the results of the uniaxial tension and compression tests by multiplying the stress by the plan area of rubber block (40 x 12 in.) and multiplying the strain by the thickness of rubber block at the middle of the device (16 in.). The results of the uniaxial tension and compression tests and the force-displacement relationship of the spring used in this model are shown in Figure 7.2 and Figure 7.3, respectively.

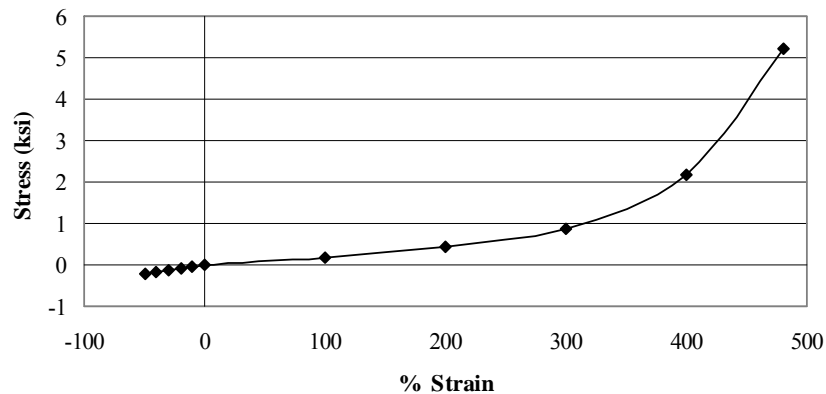


Figure 7.2: Stress-strain curve obtained from the uniaxial tension and compression tests on high-damping rubber specimen.

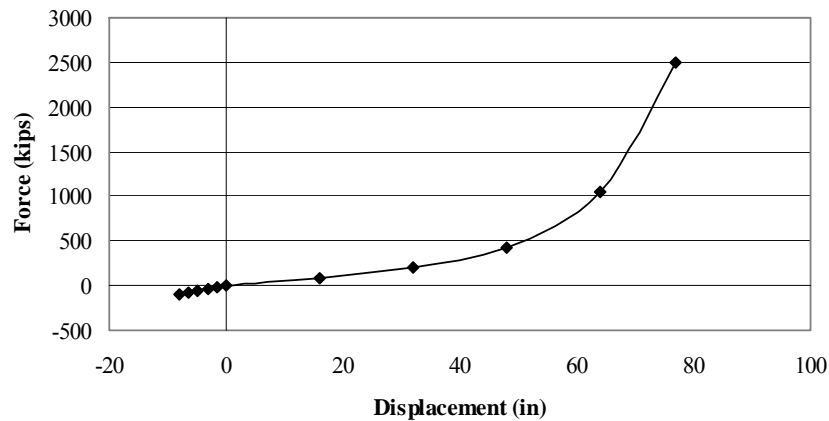


Figure 7.3: Force-displacement relationship of the multilinear spring representing the rubber hyperelasticity

7.1.1.3 Modeling the Viscoelasticity of the Rubber Block

When the device undergoes horizontal displacements, the viscoelastic material is exposed to amplified axial strains (tensile or compressive). The energy dissipation by the viscoelastic material depends on these axial strains. Filled rubber compounds in general have the ability to dissipate more energy than unfilled rubber compounds. Also, as the viscoelastic material volume increases, more energy is dissipated. Accordingly, the energy dissipation through the viscoelastic material depends primarily on

- Type of viscoelastic material (high-damping, filled or unfilled)
- Axial strains
- Volume of the viscoelastic material

Assuming uniform axial strains developing in the entire block of the viscoelastic material, the energy dissipation per cycle through the viscoelastic material per unit volume can be estimated from equation (3-15) as:

$$\Delta E = \pi \sigma_0 \varepsilon_0 \sin \delta \quad (7-4)$$

where σ_0 and ε_0 are the stress and strain amplitudes, respectively and δ is the phase angle of the rubber compound.

The total energy dissipation through the rubber block per cycle, E_T , can be obtained from:

$$E_T = \Delta E V_r \quad (7-5)$$

where V_r is the volume of the rubber block.

The previous equation was used in a simple way to estimate the energy dissipation through the high-damping rubber block of the device under different harmonic displacements.

First, in order to determine the phase angle of the high-damping rubber compound used in the analysis, a finite element analysis using ABAQUS was conducted on a rubber block with a dimension 4x6x10 in. The rubber block had the same properties used in the finite element analysis of the device. The rubber block was analyzed under three harmonic axial vertical stresses with different amplitudes covering the expected range of axial strains that the rubber block in the device can experience. These stresses were $0.05 \sin(2\pi t)$, $0.10 \sin(2\pi t)$ and $0.15 \sin(2\pi t)$. The model of the rubber block is shown in Figure 7.4. A typical stress-strain curve of a rubber specimen under harmonic strains (tension, compression, or shear) is shown in Figure 7.5.

The phase angle of the rubber compound can be calculated from:

$$\sin \delta = \frac{h1}{h2} \quad (7-6)$$

where $h1$ and $h2$ are the stress at zero strain and the maximum strain, respectively, as shown in Figure A-2.

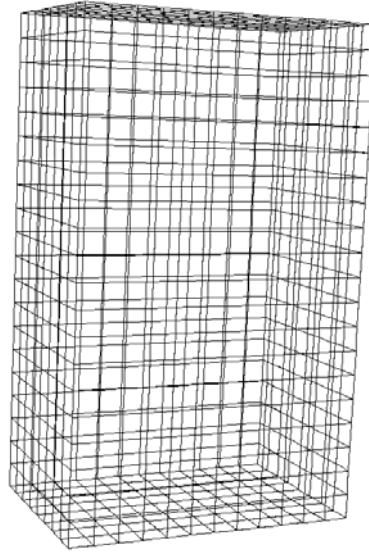


Figure 7.4: Modeling of a high-damping rubber block in ABAQUS

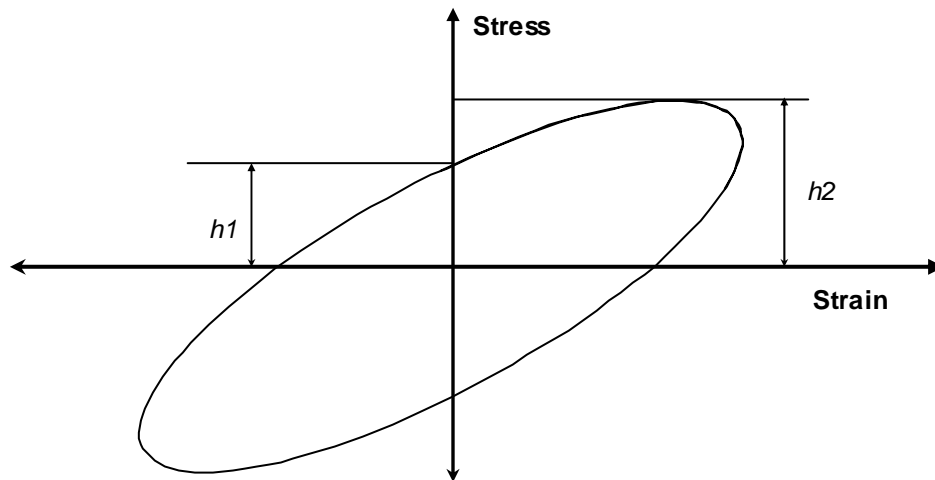


Figure 7.5: Typical stress-strain curve of rubber specimen under dynamic tests.

The stress-strain curve obtained from the finite element analysis of the rubber block under different stress amplitudes are shown in Figure 7.6. The calculation of phase angle, δ , is shown in Table 7.1. The stress, h_1 , is calculated by taking the average in tension and compression. From the results, an average value of $\sin \delta = 0.6263$ was taken. The reason behind the large value of the phase angle, δ , is the use of high-damping rubber

compound, which was not considered in the preliminary analysis of the device in Chapter 5.

Table 7.1: Calculation of the phase angle of the high-damping rubber

Stress (ksi)	Average h_1 (ksi)	h_2 (ksi)	$\sin \delta$
$\sigma = 0.05 \sin (2\pi t)$	0.0313	0.05	0.626
$\sigma = 0.10 \sin (2\pi t)$	0.0626	0.10	0.626
$\sigma = 0.15 \sin (2\pi t)$	0.094	0.15	0.627

The maximum axial strains expected to develop in the rubber block of the device is around 50 %. Accordingly, the stresses developed in the rubber block can be estimated by multiplying the initial modulus of elasticity by the axial strains. Assuming uniform axial strains developing in the entire rubber block, the axial strain can be calculated from:

$$\varepsilon_0 = \frac{2d_{vl}}{h} \quad (7-7)$$

where d_{vl} and h are the vertical displacement and the thickness of the rubber block at the middle of the device, respectively.

The stress amplitude, σ_0 , can be estimated by:

$$\sigma_0 = E_0 \varepsilon_0 \quad (7-8)$$

where E_0 is the average initial modulus of elasticity of rubber since the initial modulus of elasticity is different in tension and compression for rubber.

Applying equations (7-7) and (7-8) in equation (7-5), the total energy dissipation through the entire rubber block in the device under harmonic displacement per cycle can be estimated by:

$$E_T = [\pi E_0 \left(\frac{2d_{vl}}{h}\right)^2 \sin \delta] V_r \quad (7-9)$$

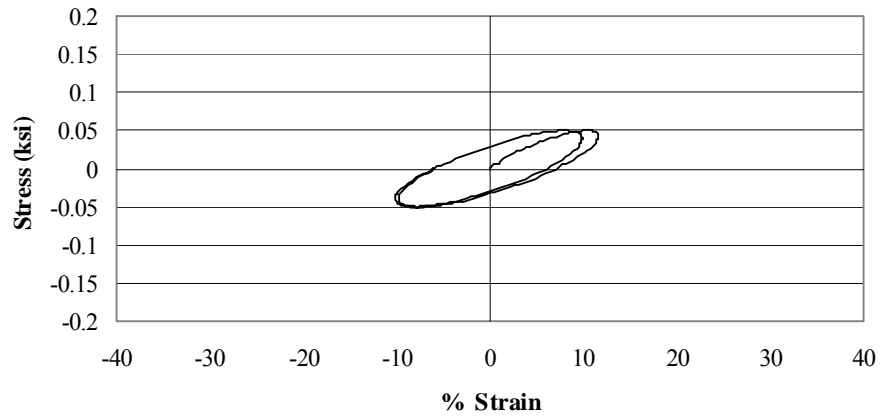
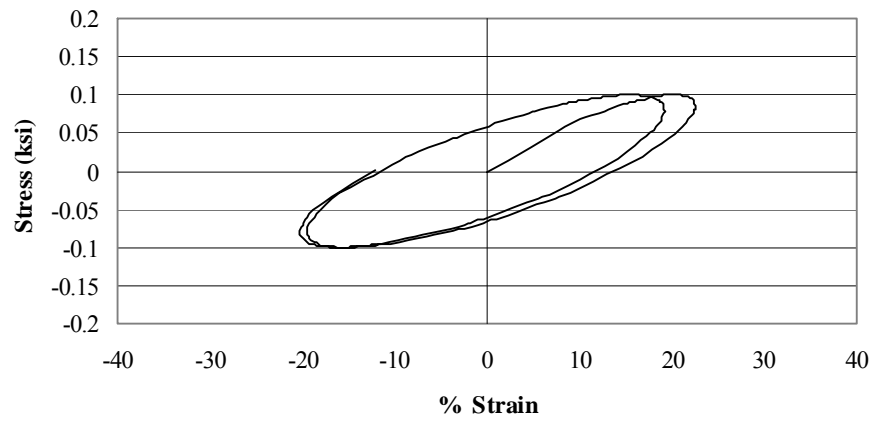
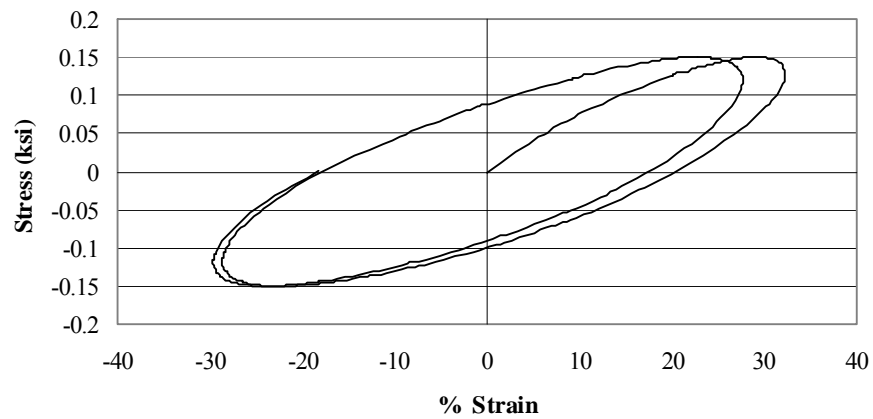
a) Stress; $\sigma = 0.05 \sin(2\pi t)$ b) Stress; $\sigma = 0.10 \sin(2\pi t)$ c) Stress; $\sigma = 0.15 \sin(2\pi t)$

Figure 7-6: Stress-strain curve of high-damping rubber block under different axial harmonic stresses.

For a SDOF viscously-damped structure subjected to simple harmonic loading, the total energy dissipation through one cycle can be calculated from:

$$E_T = \pi\omega CU_{\max}^2 \quad (7-10)$$

where ω is the loading frequency, C is the damping constant and U_{\max} is the displacement amplitude.

Now, by modeling the viscous behavior of the rubber block by a single vertical viscous dashpot, the energy dissipation in equation (7-9) and (7-10) can be equated. The maximum displacement, U_{\max} , in equation (7-10) can be replaced by the total vertical elongation (or shortening) in the vertical dashpot in the simplified model.

$$U_{\max} = 2d_{vt} \quad (7-11)$$

Accordingly, the damping constant of the dashpot can be estimated by:

$$C = \left[\frac{E_0}{\omega h^2} \sin \delta \right] V_r \quad (7-12)$$

The damping constant of the dashpot that was used in the simplified model was calculated based on the results of the detailed finite element. To investigate the accuracy of the previous equation, the damping constant can be calculated from the physical properties of the rubber block and compared to the damping constant that was used in the simplified model. The damping constant can be calculated from:

$$C = \left[\frac{0.325}{2\pi(16)^2} 0.626 \right] * 7143.31$$

$$C = 0.90 \text{ kip-sec/in.}$$

In order to verify the previous method in estimating the damping constant of the dashpot used in the simplified model, the results obtained from the detailed finite element analysis were used. Knowing the energy dissipated through one cycle for different harmonic displacements from the finite element model as well as the vertical displacement at the middle of the device, the damping constant can be estimated from equation (7-10). Table 7.2 summarizes these calculations.

Table 7.2: Damping constant Estimation

Case	Harmonic displacement	U_{\max} (in.)	ω	E_D (kip-in.)	C (kip-sec/in.)
1	$0.5 \sin 2 \pi t$	2.50	2π	74.14	0.956
2	$1.0 \sin 2 \pi t$	4.90	2π	294.44	0.973
3	$1.5 \sin 2 \pi t$	8.96	2π	616.66	0.786

According to the calculations in Table 7.2, the average value of the damping constant is $C=0.91$ kip-sec/in., which is almost the same obtained from equation (7-9). This indicates very good approximation despite the simplicity of the method. From the practical point of view, as mentioned before, the structural designers will not use the complicated finite element analysis in order to estimate the device parameters. Accordingly, the damping constant can be well approximated from equation (7-9) for any visco-plastic device with different physical rubber properties and geometric configuration.

7.1.1.4 Modeling the Steel Elements

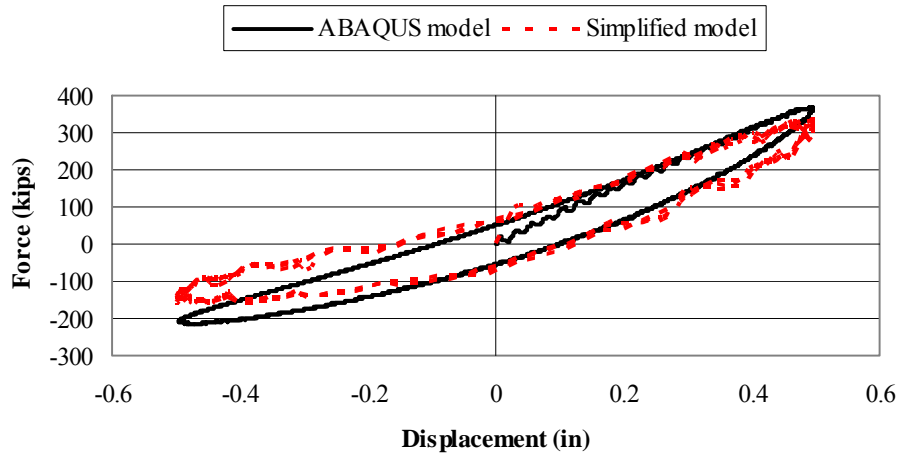
In the simplified model, MI , beam elements were used to model the steel elements (channels C15 x 50). The steel elements were assumed to behave linearly elastic during the analysis.

7.1.1.5 Comparison between ABAQUS Model and the Simplified Model, M1

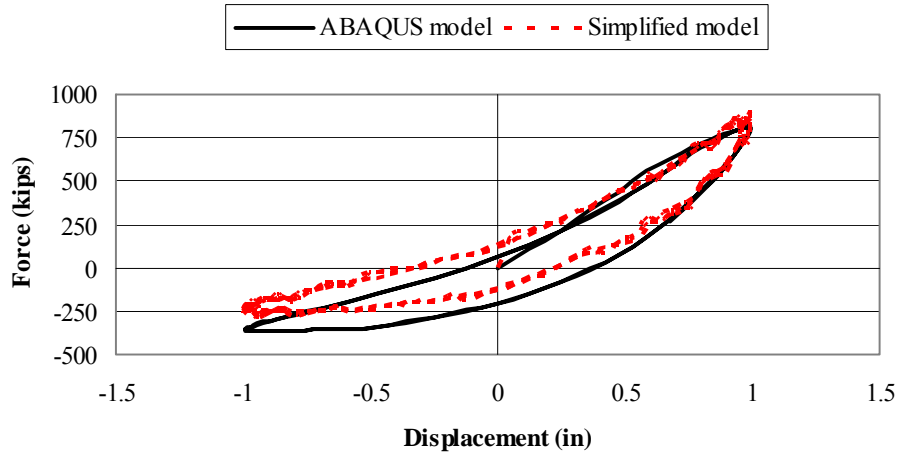
The simplified model was analyzed under harmonic displacements; $0.5 \sin (2\pi t)$, $1.0 \sin (2\pi t)$ and $1.5 \sin (2\pi t)$. A nonlinear response time history analysis was performed on the simplified model. Large-displacement analysis and P- δ effect were considered. The results of the time history analysis on the simplified model were compared to the results of the detailed finite element analysis based on the hysteretic curve of the device as shown in Figure 7.7.

According to the results shown in Figure 7.7, it is clear that there is a good matching between the results of the simplified model and the finite element model under low to moderate levels of harmonic displacements, $0.5 \sin (2\pi t)$ and $1.0 \sin (2\pi t)$. However,

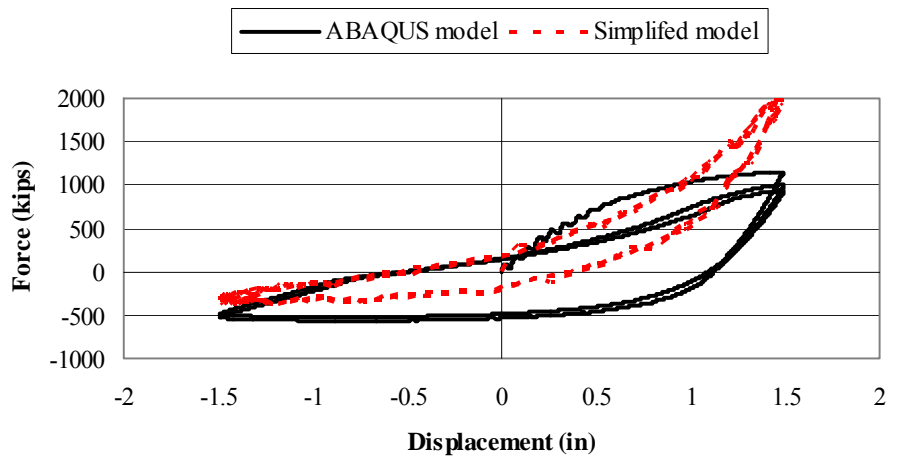
under larger displacements, $1.5 \sin(2\pi t)$, the simplified model has relatively high stiffness and low energy-dissipation ability compared to the finite element model. The reason behind that is the assumed elastic behavior of steel channels, which ignores the stiffness degradation upon steel yielding and the energy dissipation through the inelastic behavior of the steel elements especially when the device is exposed to large deformations. These shortcomings were overcome in the next simplified model, *M2*.



a) Displacement; $0.5 \sin 2\pi t$.



b) Displacement; $1.0 \sin 2\pi t$.



c) Displacement; $1.5 \sin 2\pi t$.

Figure 7.7: Comparison between the results of finite element model and simplified model, $M1$

7.1.2 Simple Model, $M2$

The only difference between this model and the previous one is considering the inelastic behavior of the steel elements. As shown in Figure 7.8, two plastic hinges at the middle of the model at the upper and lower channels were used to account for the energy dissipation as well as the stiffness degradation of the beam elements after yielding. Default flexural hinges in SAP2000, based on FEMA-273 (1997), were used in the beam elements assuming the length of the plastic hinge is 5 % of the beam length. The comparison between the results of the simplified model, $M2$, and ABAQUS model under different harmonic displacements are shown in Figure 7.9.

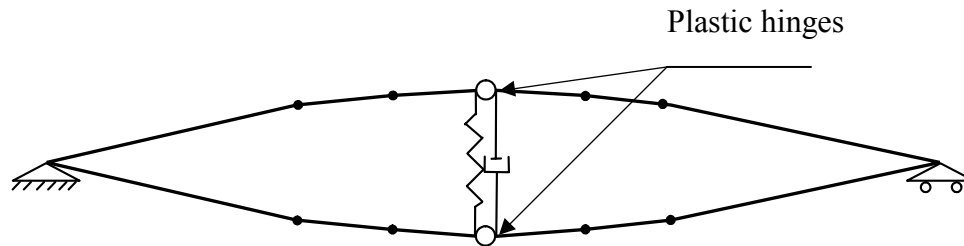
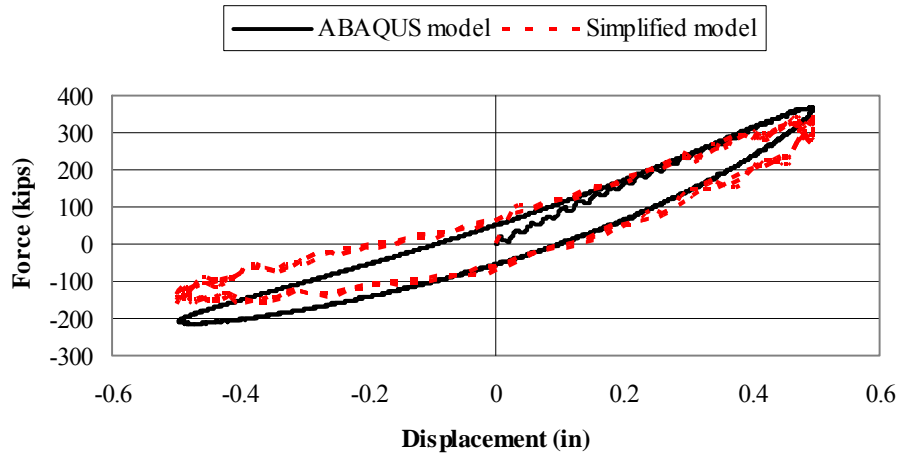
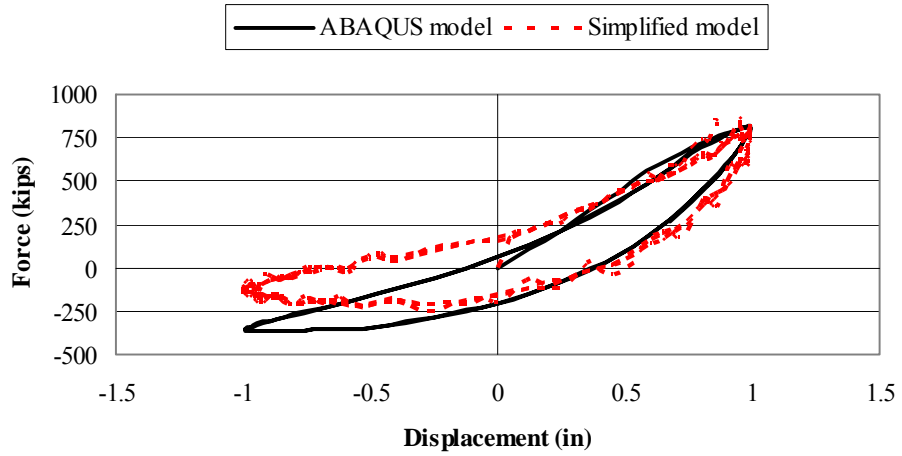


Figure 7.8: Simplified model, $M2$

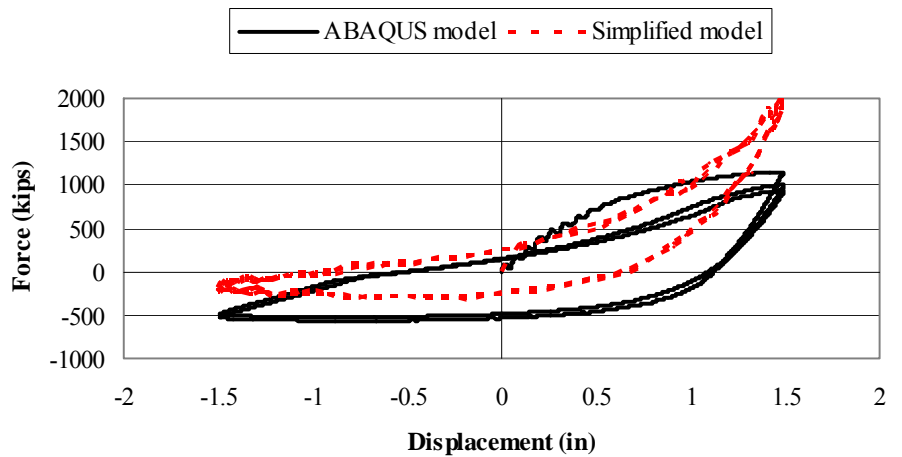
From the results shown in Figure 7.9, it can be observed that introducing plastic hinges in the simplified model, $M2$, enhances the accuracy of the results when the device is exposed to large harmonic displacement, $1.5 \text{ in } (2\pi t)$, regarding the energy dissipation. However, the device stiffness under compression is considerably underestimated by the simplified model under the different considered levels of harmonic displacements. The reason behind this may be due to the modeling of the hyperelastic behavior of the rubber block by a single multilinear spring, which does not represent its actual behavior. Accordingly, the rubber block was modeled using an area sandwiched between the steel channels with a thickness equal to the device width, which was applied in the simplified model, $M3$.



a) Displacement; $0.5 \sin 2\pi t$.



b) Displacement; $1.0 \sin 2\pi t$.



c) Displacement; $1.5 \sin 2\pi t$.

Figure 7.9: Comparison between the results of finite element model and simplified model, $M2$

7.1.3 Simple Model, *M3*

In this model, the hyperelastic behavior of rubber was modeled using an elastic material filling the area sandwiched between the steel channels. The breadth of this material was taken equal to 40 in. The thickness of this material was 12 in., which is equal to the device width. The configuration of the simplified model, *M3*, is shown in Figure 7.10.

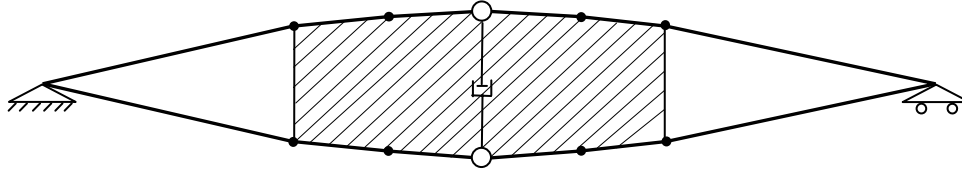


Figure 7.10: Simplified model, *M3*

To define this material in SAP2000, a value of modulus of elasticity and Poisson ratio is needed. The expected range of horizontal displacements to which the device can be exposed in real buildings is less than two in. With an average amplification of 2.0, as shown in most of the finite element analysis, the maximum vertical displacements at the middle of the device may reach 4.0 in. In other words, the maximum axial strains in the entire rubber block may reach around 50 %. Accordingly, as shown in Figure 7.2, the modulus of elasticity of the material used in the simplified model, *M3*, can be estimated as the average initial modulus of elasticity of rubber material used in the device since the initial modulus of elasticity is different in compression and tension. An average initial modulus of elasticity of 0.325 ksi is used in this simplified model. To model the material incompressibility, a Poisson ratio of 0.5 is used.

The viscoelastic behavior of the rubber block was modeled, as in the previous models, using a vertical viscous dashpot and the inelastic behavior of the steel elements was modeled using two flexural plastic hinges. The comparison between this model and the ABAQUS finite element model is shown in Figure 7.8 for different harmonic displacements.

According to the results shown in Figure 7.11, the simplified model, *M3*, provides a satisfactory approximation of the hysteretic behavior of the device under different harmonic displacements. The accuracy of this simplified model is better than the previous models especially when the device experiences large deformations. Moreover, the model is simple and can be easily modified to model any rubber compound used in the real device. Also, the geometry of the model can be easily selected to match the geometry of the device.

7.2 Summary

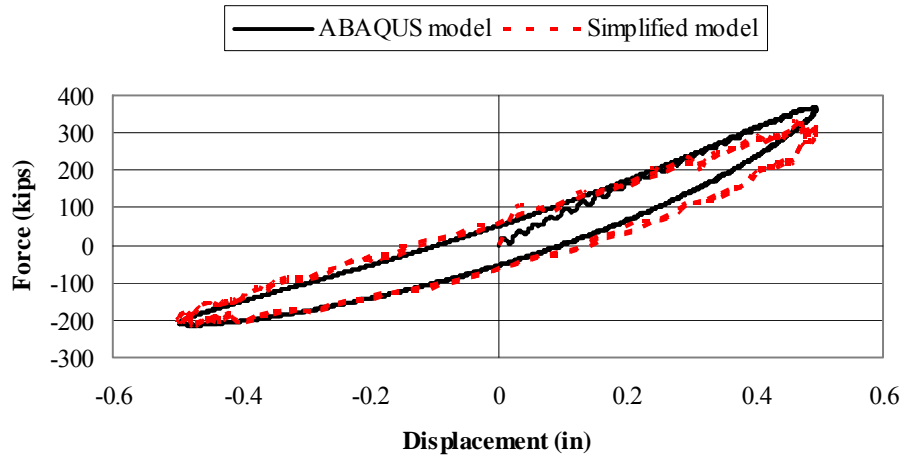
In order to facilitate the use of the visco-plastic device, three simplified models were presented using SAP2000. The results of these models under harmonic loading were compared to the results obtained from the detailed finite element analysis. Based on this comparison, the simplified model, *M3*, was selected.

One of the advantages of the visco-plastic device is the availability of controlling its behavior through different parameters. Accordingly, the structural designer can select the required device parameters in order to suit his structure. The method that was used in developing the simplified model can be used to model any device with different geometric and material properties. The following data is needed to develop a simplified model for any device:

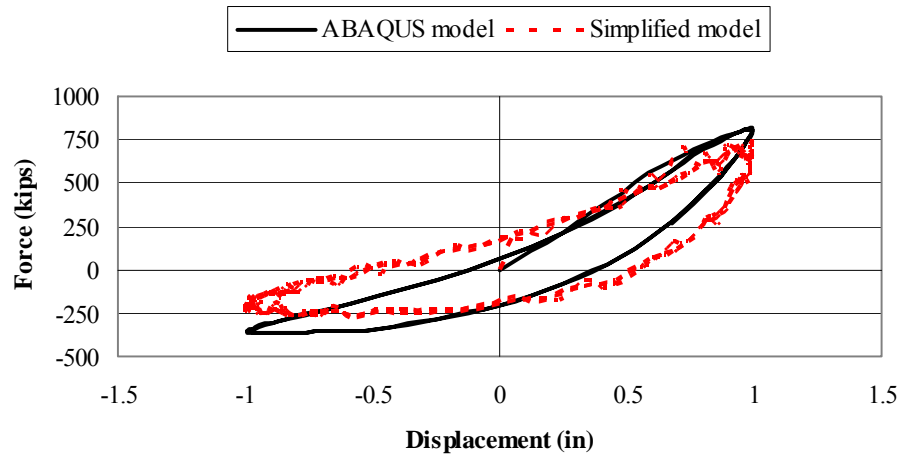
- Geometry of the device
- Cross section of steel elements
- Steel yielding stress
- Volume of rubber block
- Thickness of the rubber block at the middle of the device
- Properties of the rubber compound (initial modulus of elasticity and phase angle)
- The loading frequency (It is recommended to be equal to the natural frequency of the structure, to which the device will be attached)

In the next chapter, the simplified model, *M3*, is used to check the effectiveness of this device on the performance of the nine-story five-bay steel frame, which were used in the

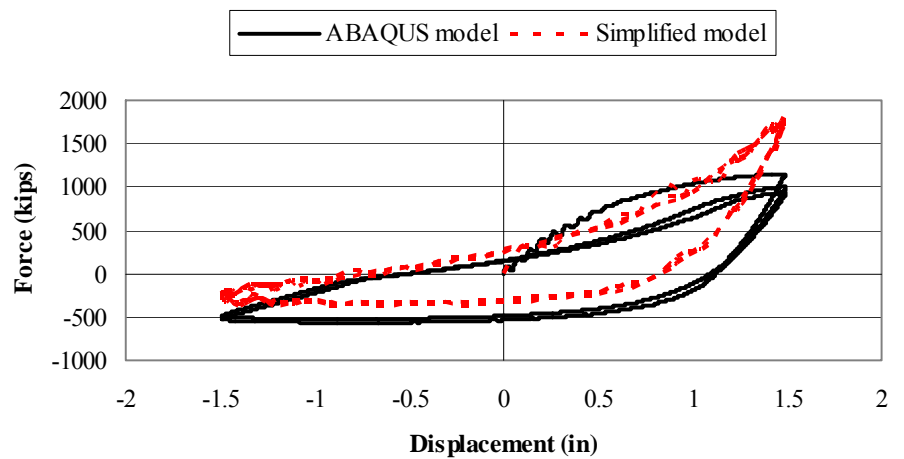
preliminary analysis of the device in Chapter 4, under different seismic excitations. Also, two different arrangements of the devices are investigated



a) Displacement; $0.5 \sin 2\pi t$.



b) Displacement; $1.0 \sin 2\pi t$.



c) Displacement; $1.5 \sin 2\pi t$.

Figure 7.11: Comparison between the results of finite element model and simplified model, $M3$

Chapter 8: Analysis of Multi-Story Structures with Devices using the Simplified Model

8.0 Introduction

In the previous chapter, different simplified models were presented and compared to the detailed finite element analysis of the visco-plastic device. The comparison was based on the hysteretic behavior of the device under different amplitudes of harmonic displacements that the device can experience. The simplified model, *M3*, showed reasonable and satisfactory approximation of the real device behavior. In this model, the steel channels were modeled using beam elements while the rubber block was modeled as an elastic material with a large Poisson ratio to account for the incompressibility. The viscoelastic behavior of the rubber block was modeled using a vertical viscous dashpot. Flexural plastic hinges were used to model the steel yielding. The different model parameters and how they can be calculated were presented in detail in the previous chapter. The simplified model, *M3*, is used in this chapter to determine the actual effectiveness of the device on the response of the nine-story five-bay steel frame, which was described in chapter 5 under different ground excitations. Two arrangements of the devices are considered; one device and two devices per each floor.

8.1 Multi-Story Structure with One Device per Floor

In order to determine the effect of the visco-plastic device on the response of multistory structures under different ground excitations, a visco-plastic device was attached at each floor of a nine-story five-bay steel frame. A visco-plastic device with 180-in. span was used to fit a bay with a span of 360 in. An aspect ratio of 1/6 was selected. The rubber breadth was chosen to be 72 in. to have a ratio of 0.4 between the rubber breadth and the device span. The configuration of the simplified model is shown in Figure 8.1.

The rubber area is calculated from:

$$A_r = 2 \int_{54}^{126} \frac{h}{2} \sin\left(\frac{\pi x}{l}\right) dx = -\frac{h * l}{\pi} \cos\left(\frac{\pi x}{l}\right) \Big|_{54}^{126}$$

$$A_r = -\frac{hl}{\pi} \left[\cos\left(\frac{126\pi}{180}\right) - \cos\left(\frac{54\pi}{180}\right) \right]$$

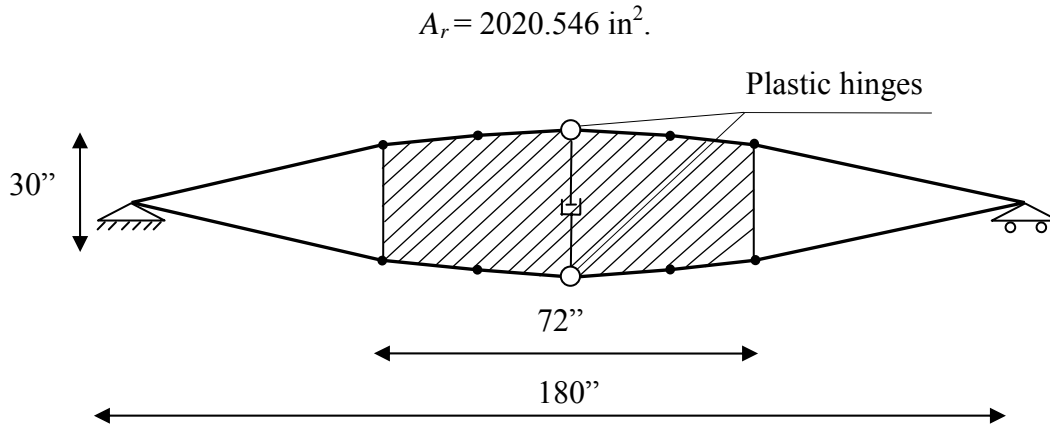


Figure 8.1: Configuration of the simplified model used in the analysis

Having a 12-in. device width, the volume of rubber block is:

$$V_r = 24246.55 \text{ in}^3$$

The weight of rubber block can be calculated from:

$$W_r = 24246.55 * \frac{0.094}{12 * 12 * 12}$$

$$W_r = 1.32 \text{ kips.}$$

To calculate the weight of the steel channels, the arc length of the sinusoidal shape should be calculated first from:

$$l_c = \int \sqrt{\left(\frac{dy}{dx}\right)^2 + 1} dx$$

$$l_c = \int_0^{180} \sqrt{\left(\frac{15\pi}{180}\right)^2 \cos^2\left(\frac{\pi x}{180}\right) + 1} dx$$

Using the trapezoidal method to calculate this integral numerically leads to:

$$l_c = 183.05 \text{ in}^2$$

Accordingly, the weight of the two steel channels can be determined from:

$$W_s = 2(183.05 * 14.7) * \frac{0.49}{12 * 12 * 12}$$

$$W_s = 1.53 \text{ kips}$$

The total weight of the device is the summation of the weight of the rubber block and steel elements.

$$W_{\text{device}} = W_r + W_s = 2.85 \text{ kips}$$

The device mass can be calculated by dividing the total weight over the ground acceleration, g :

$$m = \frac{2.85}{386.2} = 0.0074 \text{ kip-sec}^2/\text{in.}$$

The mass in the simplified model is lumped in ten nodes.

$$m \text{ (per node)} = 0.00074 \text{ kip-sec}^2/\text{in.}$$

The damping constant of the dashpot in the simplified model can be estimated from the relation presented in the previous chapter:

$$C = \left[\frac{E_0}{\omega h^2} \sin \delta \right] V_r$$

Assuming the loading frequency is equal to the natural frequency of the nine-story steel frame used in the analysis, the loading frequency can be calculated from:

$$\omega = \frac{2\pi}{T_0}$$

where the natural period of the nine-story steel structure without the devices is equal to 1.595 seconds.

Accordingly, the damping constant can be estimated from:

$$C = \left[\frac{0.325}{\frac{2\pi}{1.595} (30)^2} \cdot 0.626 \right] * 24246.56$$

$$C = 1.39 \text{ kip-sec/in.}$$

The simplified model of the visco-plastic device was attached to each floor of the nine-story five-bay moment-resisting steel frame. The first time period of the structure is reduced from 1.595 to 1.40 due to the use of the devices. In the preliminary analysis of the device, there was no significant change in the time period due to the devices. The reason behind that is the use of a small value of the modulus of elasticity in the preliminary analysis, which was used in determining the stiffness in the NLINK elements. In the real device, a high-damping rubber material was selected in order to increase the energy dissipation through the device. This material has a relatively high modulus of elasticity, which leads to increase the stiffness of the device. Moreover, in the

simplified model, modeling the viscoelastic material as an area instead of vertical springs, as in the preliminary analysis, provides stiffness to the structure in the horizontal direction as well as the vertical direction. The stiffness provided in the horizontal direction affects the period of the structure more than the stiffness provided in the vertical direction.

The configuration of the steel frame with the simplified model of the devices is shown in Figure 8.2. The frame was analyzed under harmonic excitation and unscaled real records of El Centro and Northridge earthquakes. The response of the steel frame with the devices was compared to the response of the same frame without devices to determine the effect of the devices on the frame response under different ground excitations, which have different excitation characteristics like the frequency content and peak ground accelerations. During the analysis, the steel frame remained elastic under the different ground excitations.

First, the nine-story five-bay steel frame with one device per each floor was analyzed under harmonic excitation. Figure 8.3 and Figure 8.4 show the comparison between the response of the steel frame with and without the devices under the harmonic excitation. The maximum top floor displacement was reduced from 12.0 in. to 7.6 in. with a reduction percentage of 36.7 %. The maximum fifth floor displacement was reduced from 6.8 in. to 4.4 in. with a reduction percentage of 35.8 %. The maximum total base shear is slightly increased from 1354.4 kips to 1398.4 kips with an increasing percentage of 3.2 %. It can be noticed from Figure 8.3 that the total base shear was only increased in the first cycle, however for the consequent cycles the total base shear was reduced considerably due to the energy dissipation through the devices. Using the device has a great effect on the story displacements. At maximum top floor displacement, the average reduction in story displacements was 39.3 %. The bending moments at column bases were significantly reduced due to the use of the device. The average reduction in the bending moments at column bases was 57.6 %.

The steel frame with and without the devices was analyzed again under unscaled real records of El Centro earthquake. The results of the two cases are shown in Figures 8.5 and Figure 8.6. The maximum top floor displacement was reduced from 8.3 in. to 4.6 in. with a reduction percentage of 44.4 %. The maximum fifth floor displacement was reduced from 4.83 in. to 2.62 in. with a reduction percentage of 45.8 %. The maximum base shear was reduced due to the use of the device from 1083.8 kips to 733.3 kips with a reduction percentage of 32.3 %. Due to the use of the device, the floor displacements were highly reduced. At the maximum top floor displacement, the average reduction in the story displacements was 44.6 %. Using the device resulted in a considerable reduction in the bending moments at column bases. The average reduction in bending moments at column bases was 62.3 % at the maximum top floor displacement.

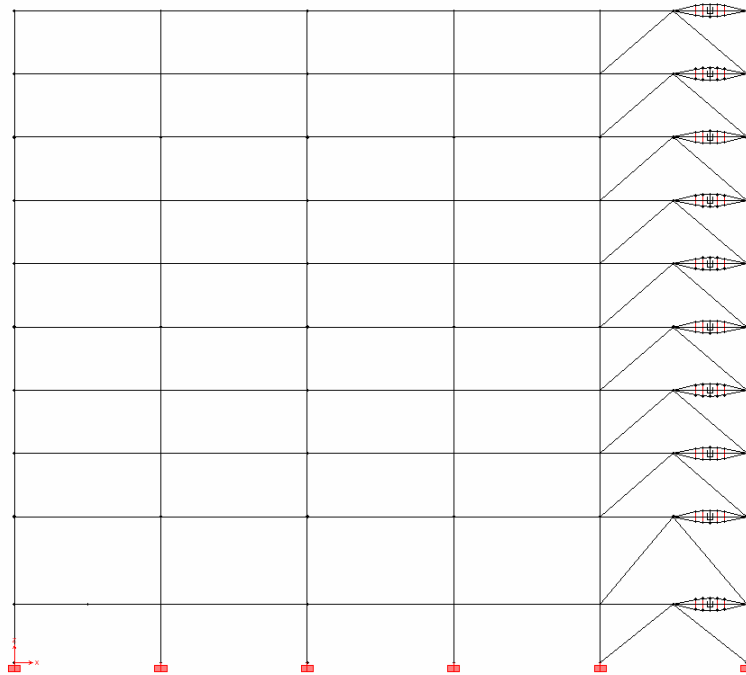
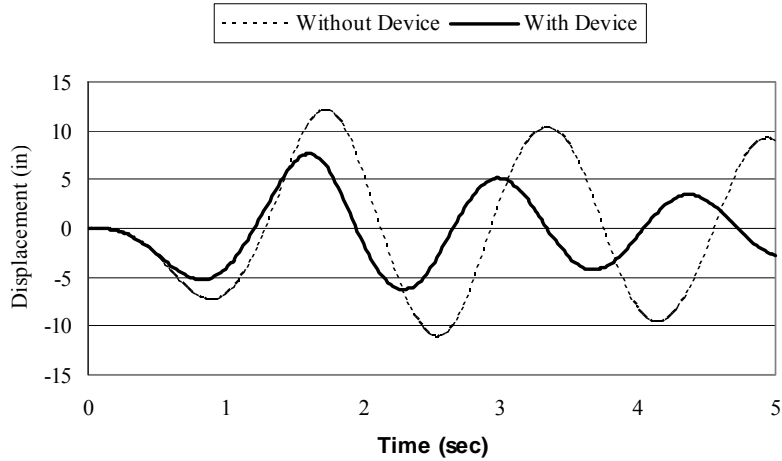


Figure 8.2: The analyzed nine-story frame with simplified model of devices. (One device per floor)

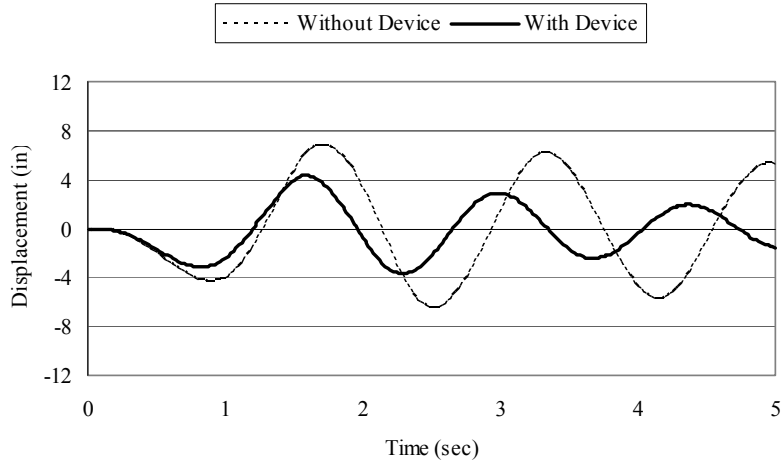
Figure 8.7 and Figure 8.8 show the enhancement of the response of the steel frame due to the use of one device per floor under unscaled real records of Northridge earthquake. The maximum top floor displacement was reduced from 16.2 in. to 12.6 in. with a reduction

percentage of 22.3 %. The maximum fifth floor displacement was reduced from 8.9 in. to 7.0 with a reduction percentage of 21.0 %. The maximum base shear was slightly increased by 6.0 %. As shown in Figure 8.7, although the maximum base shear was slightly increased, the base shear was considerably reduced after 10 seconds of the earthquake due to the significant reduction in floor displacements. At the maximum top floor displacement, the story displacements were reduced with an average percentage of 14.6 % while the average reduction in bending moments at column bases was 48.4 %.

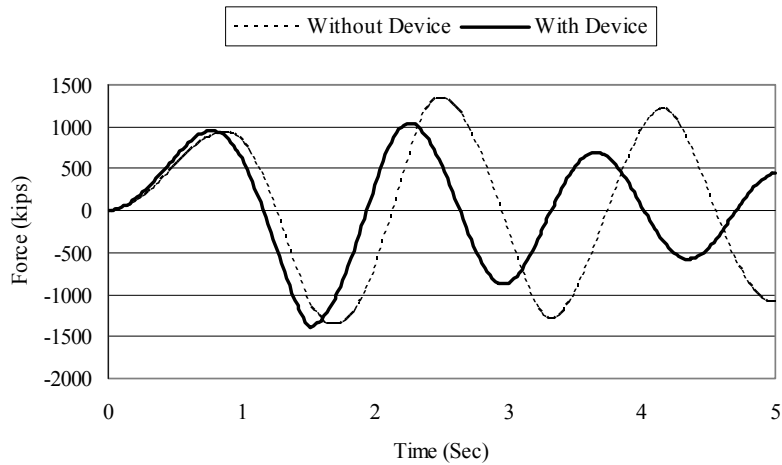
According to the results of the nine-story five-bay steel frame with one device per floor under different ground excitations, the devices enhanced the response of the frame in all cases. The use of the devices resulted in a significant reduction in floor displacements, total base shear, and overturning moments at the column bases. In most cases, the base shear was reduced under different types of ground excitations, which gives an important advantage for using the visco-plastic device instead of the conventional viscoelastic devices.



a) Top floor horizontal displacement.

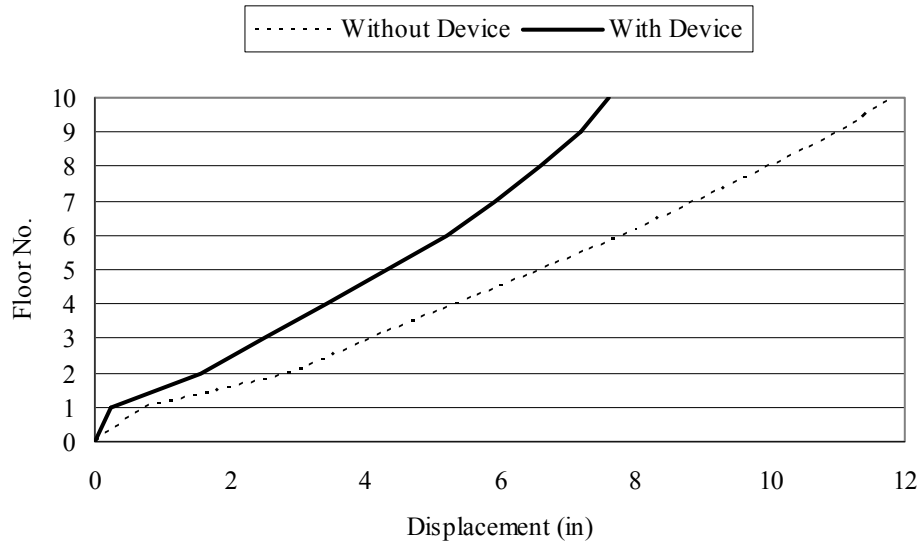


b) Fifth floor horizontal displacement.

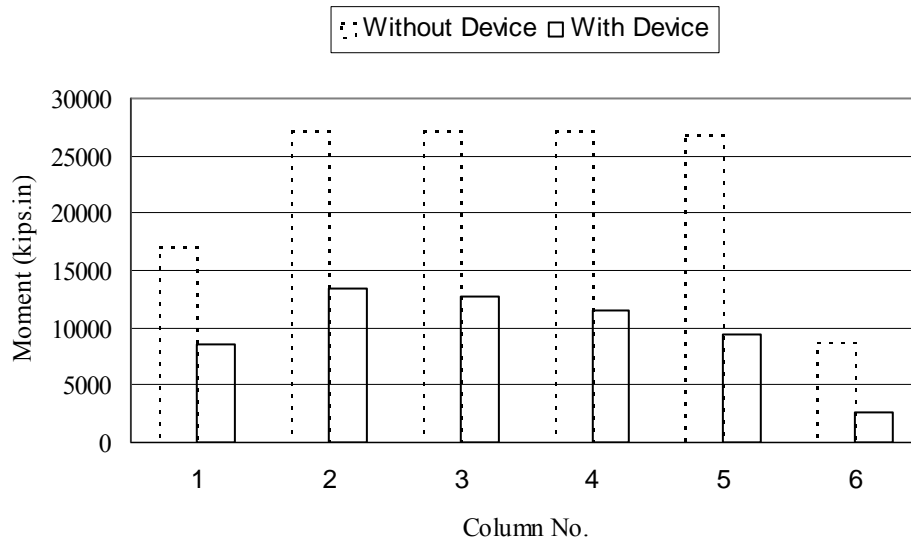


c) Total base shear.

Figure 8.3: Effect of the device on the response of the nine-story frame under harmonic excitation.

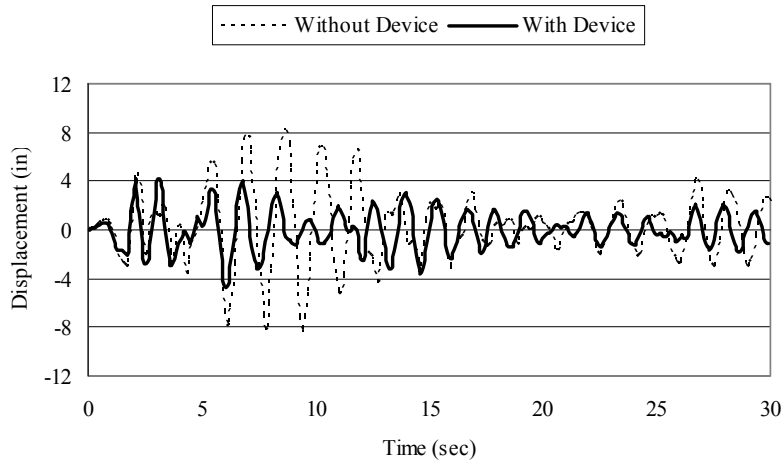


a) Story displacements at maximum top floor displacement.

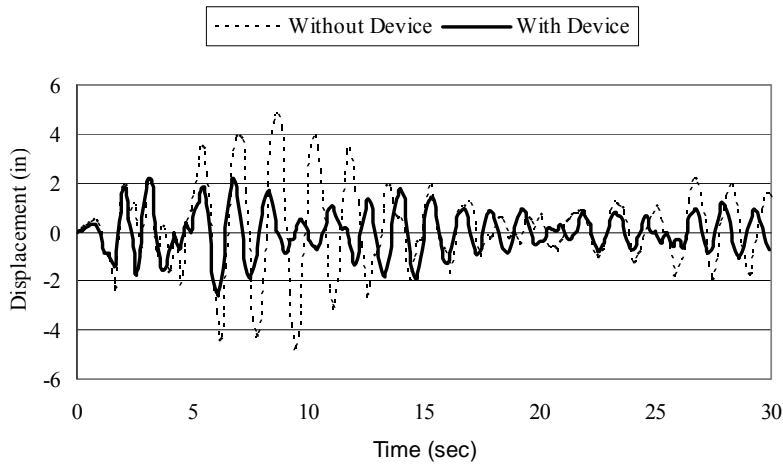


b) Bending moment on the column bases at maximum top floor displacement.

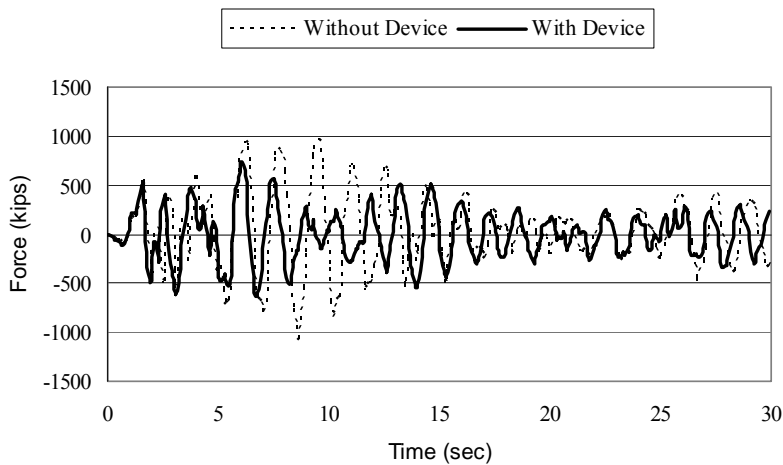
Figure 8.4: Effect of the device on the floor displacements and bending moments at column bases of the nine-story frame under harmonic excitation.



a) Top floor horizontal displacement.

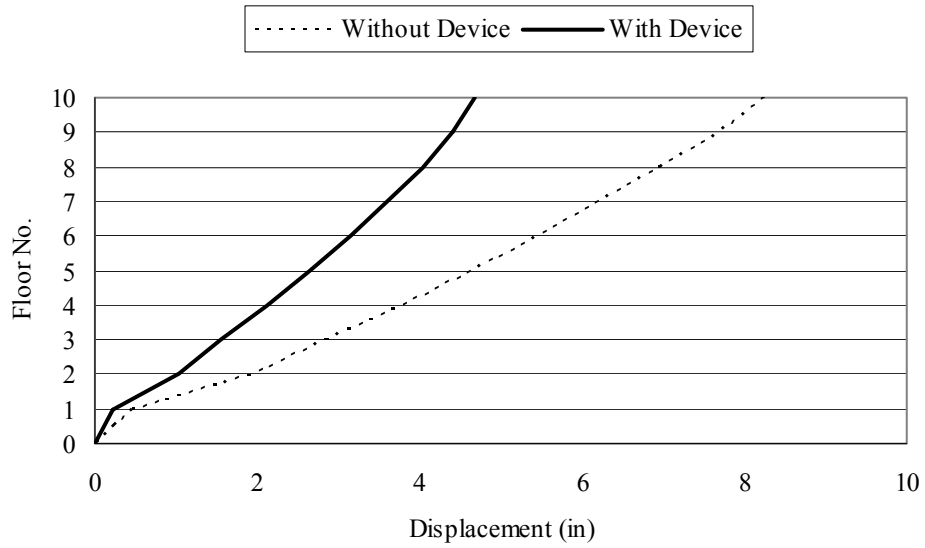


b) Fifth floor horizontal displacement.

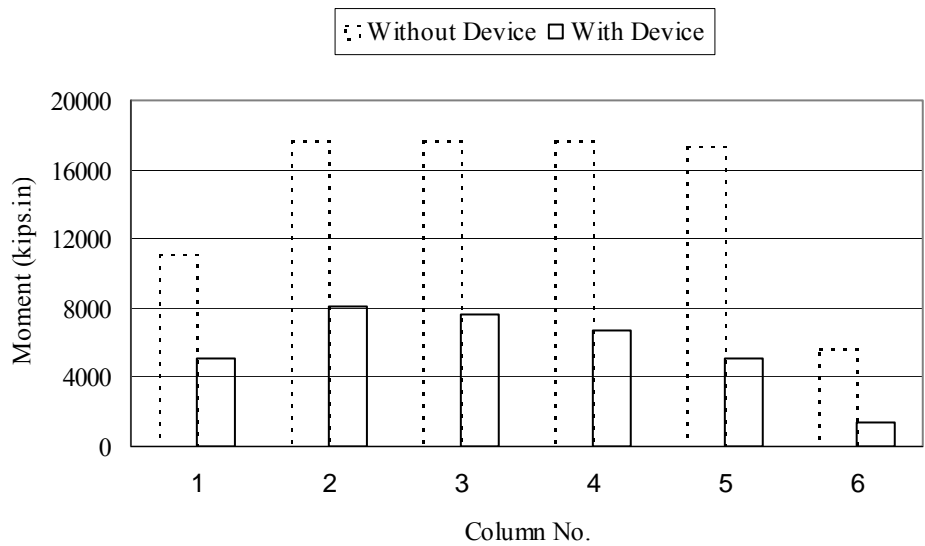


c) Total base shear.

Figure 8.5: Effect of the device on the response of the nine-story frame under El Centro earthquake.

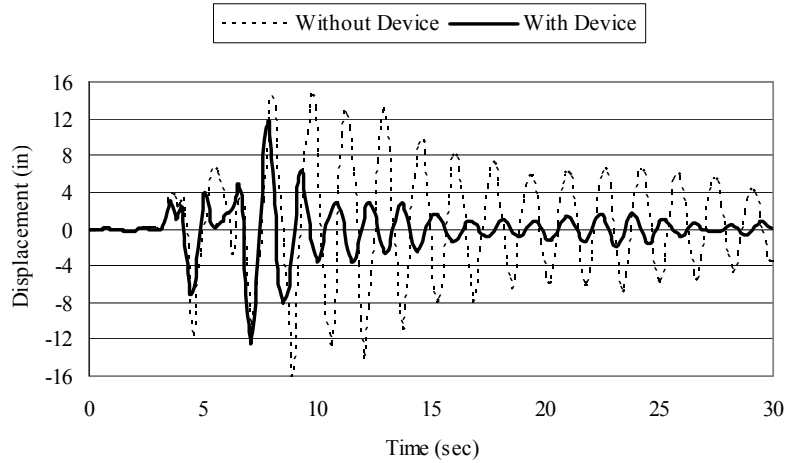


a) Story displacements at maximum top floor displacement.

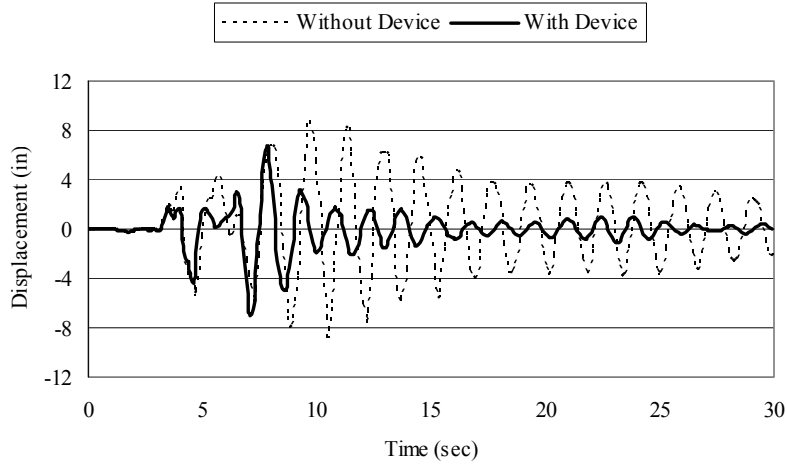


b) Bending moment on the column bases at maximum top floor displacement.

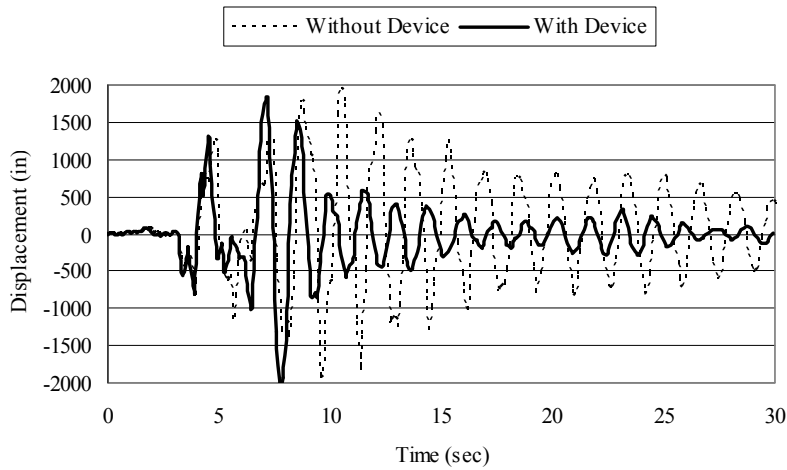
Figure 8.6 Effect of the device on the floor displacements and bending moments at column bases of the nine-story frame under El Centro earthquake.



a) Top floor horizontal displacement.

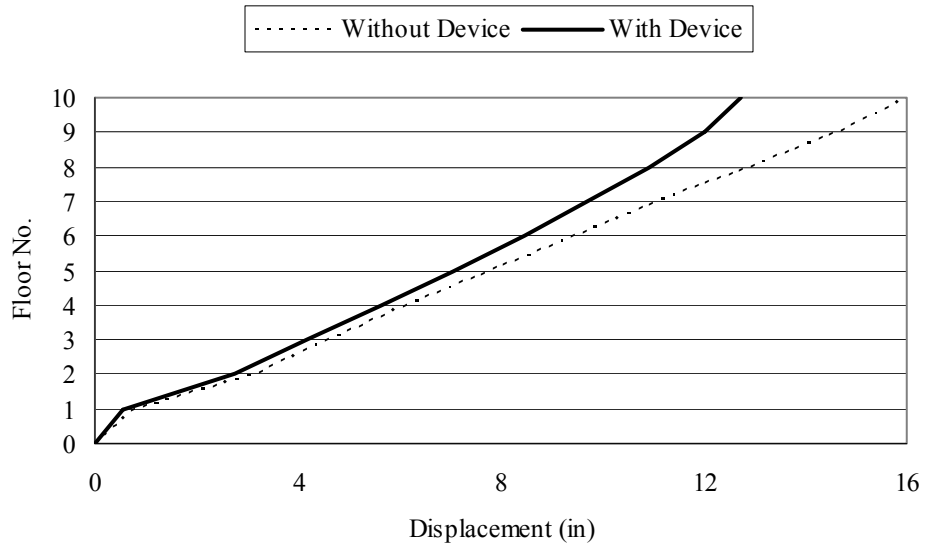


b) Fifth floor horizontal displacement.

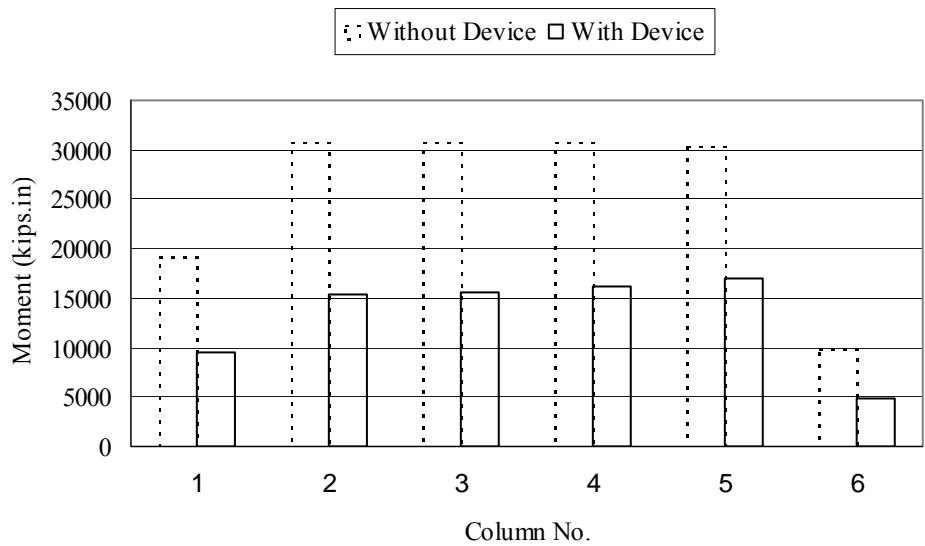


c) Total base shear.

Figure 8.7: Effect of the device on the response of the nine-story frame under Northridge earthquake.



a) Story displacements at maximum top floor displacement.



b) Bending moment on the column bases at maximum top floor displacement.

Figure 8.8: Effect of the device on the floor displacements and bending moments at column bases of the nine-story frame under Northridge earthquake.

8.2 Multi-Story Structure with Two Devices per Floor

The response of the nine-story steel frame was significantly improved by using one visco-plastic device per floor. There are many arrangements of these devices that can introduce more improvements on the response under different ground excitations. To check the possibility of improving the overall behavior of the nine-story steel frame, another arrangement is chosen. Two devices were attached to each floor of the steel frame as shown in Figure 8.9.

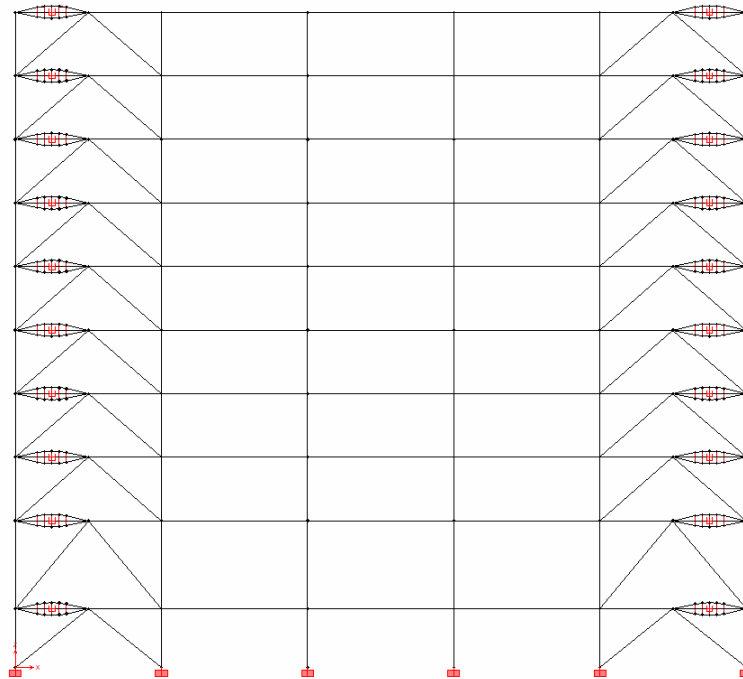


Figure 8.9: The analyzed nine-story frame with simplified model of devices. (Two devices per floor).

First, the steel frame with the new arrangement of the devices was analyzed under harmonic excitation. The results of this analysis were compared to the response of the steel frame without the devices. The comparison between the two cases is shown in Figure 8.10 and Figure 8.11. As a result of using this new arrangement, the response of the steel frame was greatly improved. The maximum top floor displacement was reduced from 12.0 in. to 5.6 in. with a significant reduction percentage of 53.7 %. The maximum fifth floor displacement was reduced from 6.8 in. to 4.4 in. with a reduction percentage of 35.8 %. The reduction in displacements of top and fifth floor was increased in the second

and third cycles. The base shear was reduced due to the use of the devices especially in the second and third cycles. The maximum base shear was reduced by 2.1 % during the first cycle. At the maximum top floor displacement, the story displacements were reduced by an average percentage of 55.0 %, which indicates a great improvement in the response of the steel frame under harmonic excitation. The bending moments at the column bases were significantly reduced with an average reduction percentage of 74.5 %, at the maximum top floor displacement.

The responses of the frame with two devices per floor and without the devices were compared under unscaled real records of El Centro earthquake. Figure 8.12 and Figure 8.13 show the results of this comparison. Due to the use of two devices per story, the maximum top floor displacement was reduced from 8.3 in. to 4.6 in. with a reduction percentage of 44.4 %. The maximum fifth floor displacement was reduced by 46.6 %. The maximum base shear was reduced from 1083.8 kips to 969.6 kips with a reduction percentage of 10.5 %. The bending moment at column bases and floor displacements were considerably reduced. At the maximum top floor displacement, the average reduction percentage in story displacements and bending moments at column bases were 46.9 and 67.7 %, respectively.

Finally, the nine-story steel frame with the new arrangement was analyzed under unscaled real records of Northridge earthquake and compared to the results of the steel frame without devices under the same earthquake. Due to the use of two devices per floor, the maximum top floor displacement was reduced from 16.2 in. to 9.9 in. with a reduction percentage of 39.1 %. The maximum fifth floor displacement was reduced from 8.9 in. to 5.5 in. with a reduction percentage of 37.6 %. Although the maximum base shear was slightly reduced from 1986.0 kips to 1966.9 kips with a reduction percentage of 1.0 %, the base shear was reduced significantly under the last 20 seconds of the earthquake. The new arrangement of the devices reduced effectively the story displacements. At maximum top floor displacement, the average reduction of the story displacements was 34.7 %. At maximum top floor displacement, the bending moment at

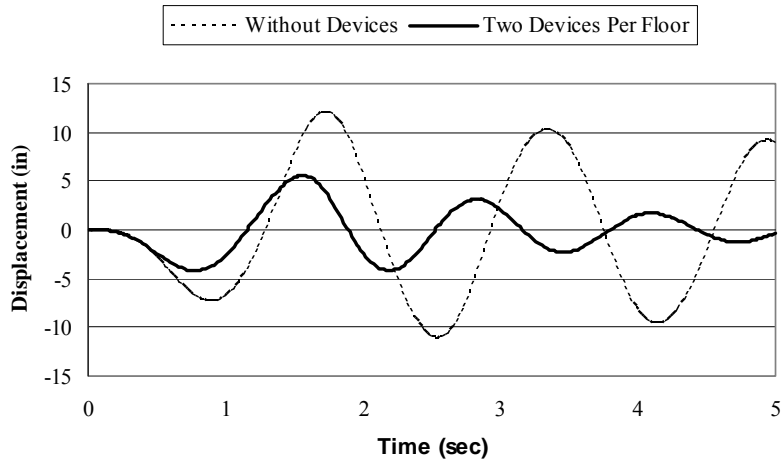
column bases were reduced in all columns with an average reduction percentage of 62.1 %. The results of this analysis are shown in Figures 8.14 and Figure 8.15.

According to the previous results, the new visco-plastic device improved significantly the structural response under different ground excitations. The use of the devices resulted in considerable reduction in floor displacements, base shears and bending moments at column bases. The base shear was reduced in most of the cases. The arrangement of the devices can be chosen to enhance the effectiveness of the devices on the structural response.

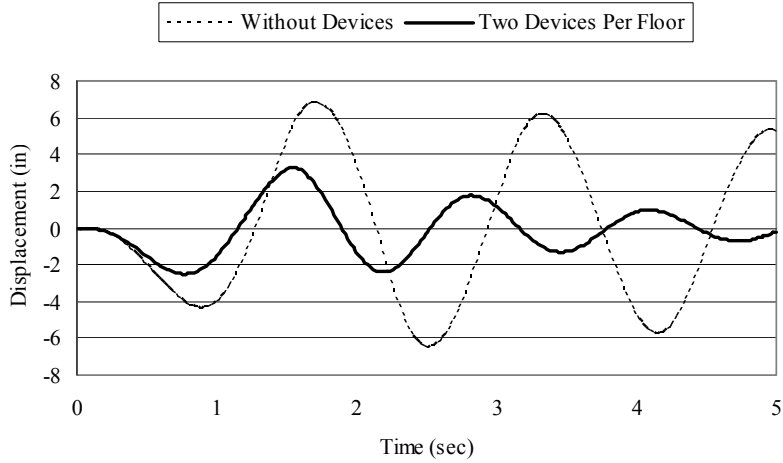
8.3 Summary

in order to investigate the effect of the visco-plastic device on the response of multi-story structures, the simplified model, M3, was attached to each floor of the nine-story five-bay steel frame. The frame with the simplified models was analyzed under harmonic excitation as well as the records of El Centro and Northridge earthquake excitations. The results of these analyses showed a significant improvement of the structural response under different ground excitations. The floor displacements and bending moment at column bases were considerably reduced. The base shear was reduced in most of the cases.

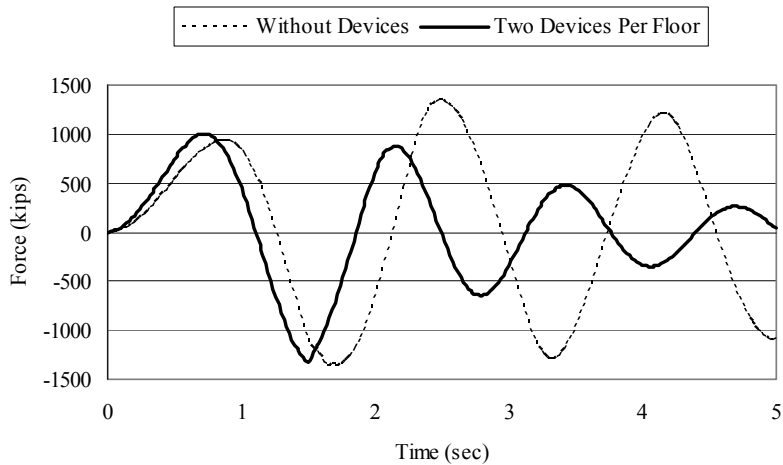
Another device arrangement was considered, which is placing two devices per floor. More improvement was noticed in the structural response under the different ground excitations.



a) Top floor horizontal displacement.

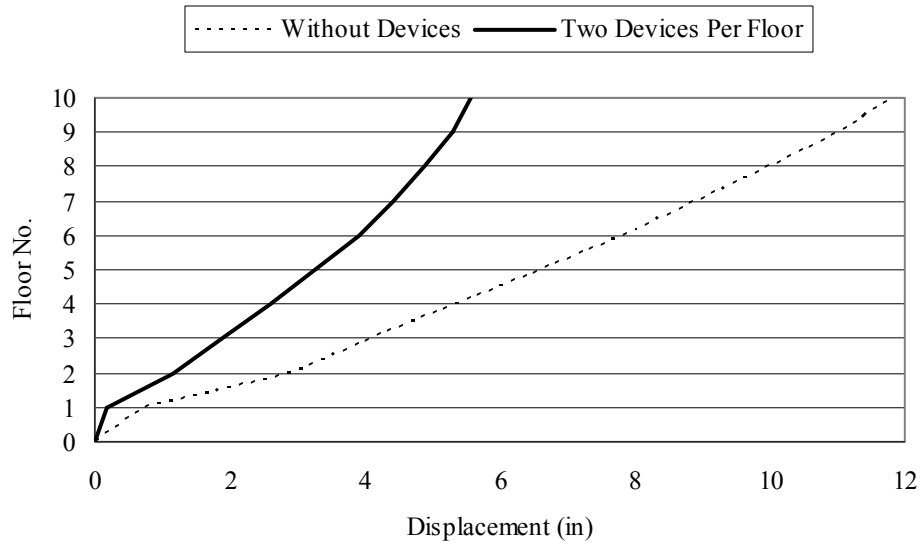


b) Fifth floor horizontal displacement.

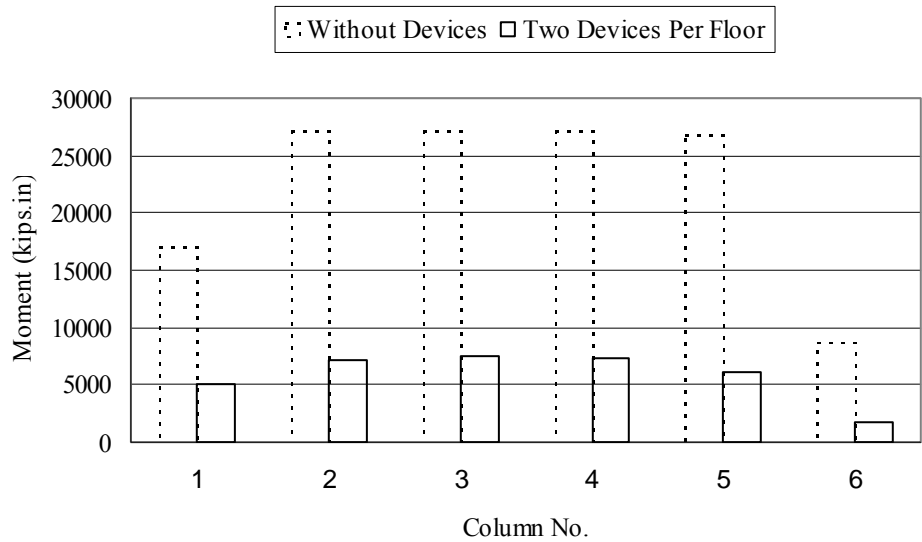


c) Total base shear.

Figure 8.10: Effect of using two devices per floor on the response of the nine-story frame under harmonic excitation.

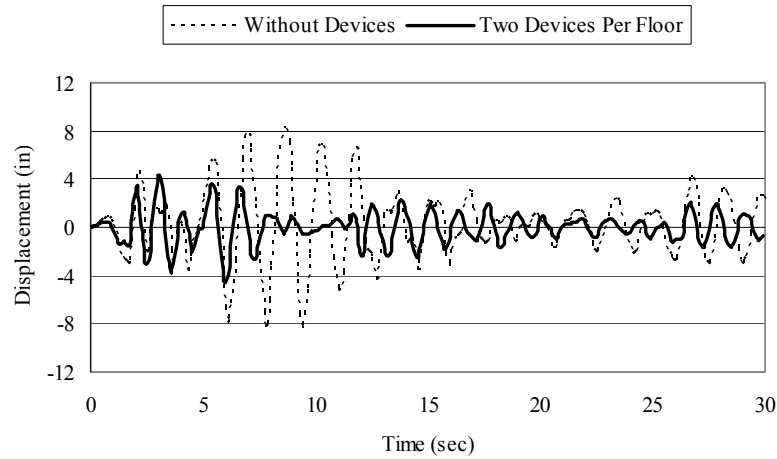


a) Story displacements at maximum top floor displacement.

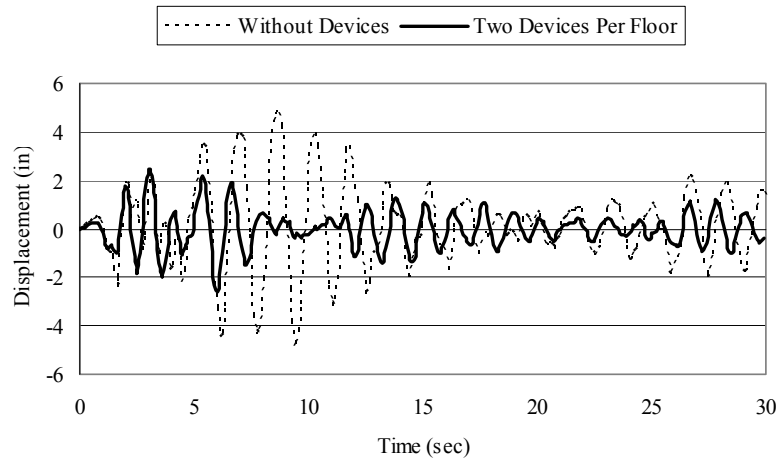


b) Bending moment on the column bases at maximum top floor displacement.

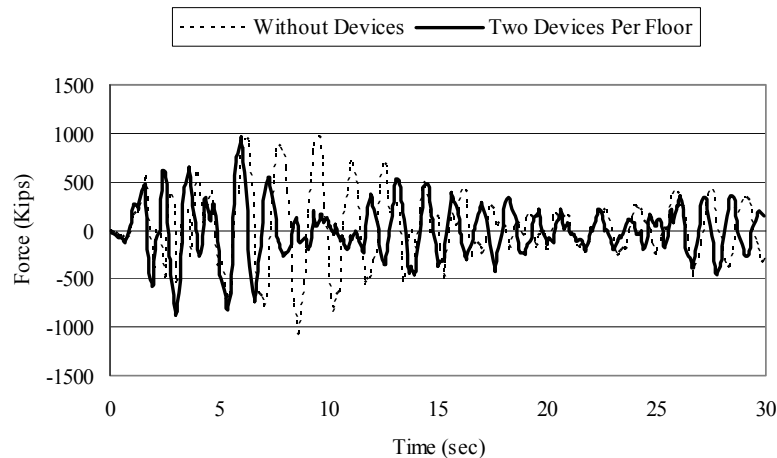
Figure 8.11: Effect of using two devices per floor on the floor displacements and bending moments at column bases of the nine-story frame under harmonic excitation.



a) Top floor horizontal displacement.

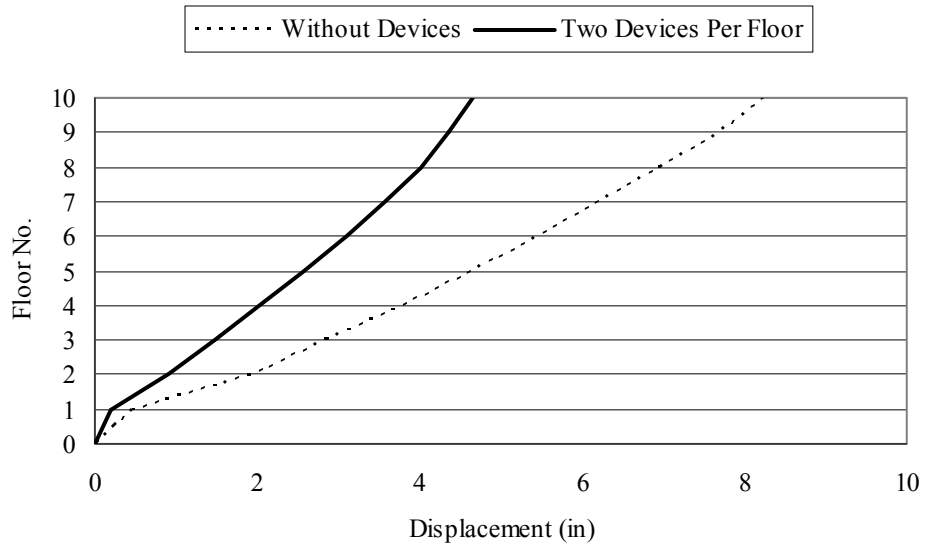


b) Fifth floor horizontal displacement.

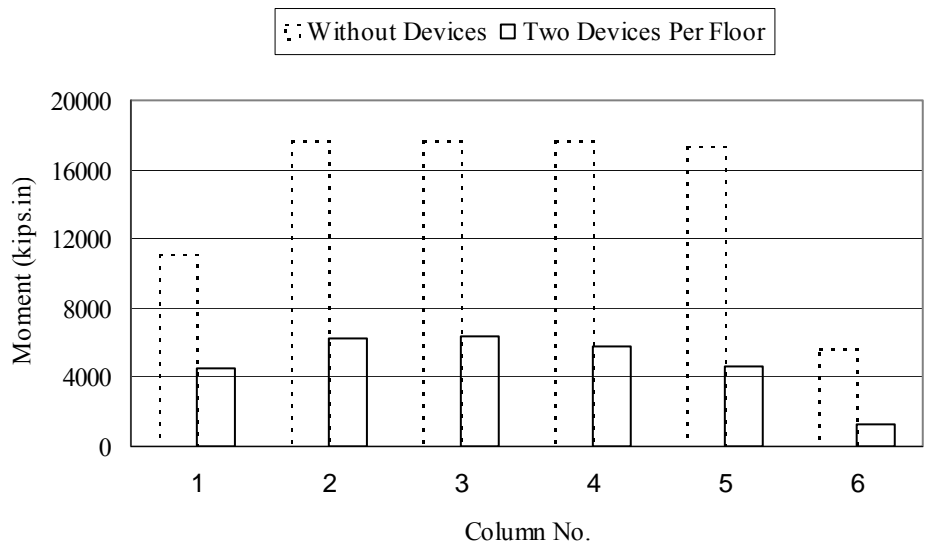


c) Total base shear.

Figure 8.12: Effect of using two devices per floor on the response of the nine-story frame under El Centro earthquake.

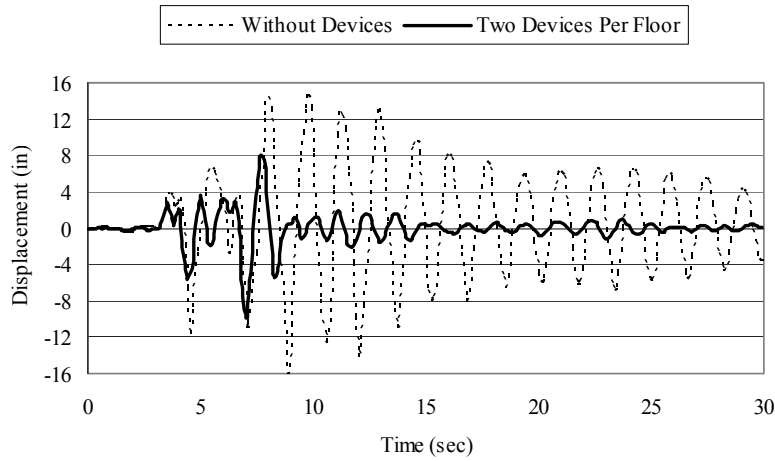


a) Story displacements at maximum top floor displacement.

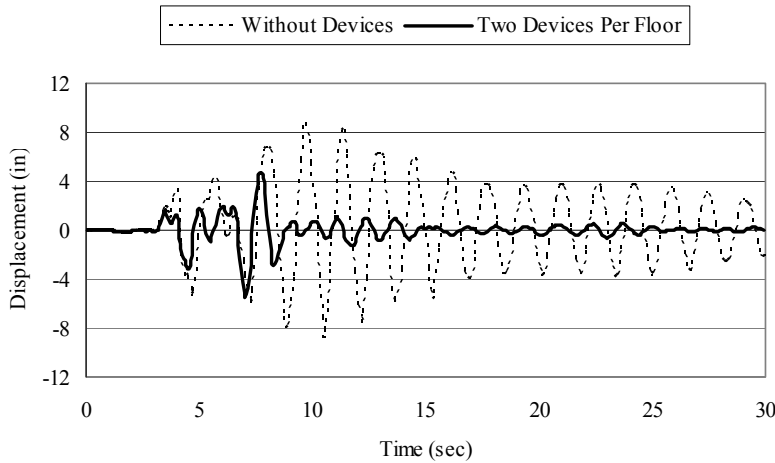


b) Bending moment on the column bases at maximum top floor displacement.

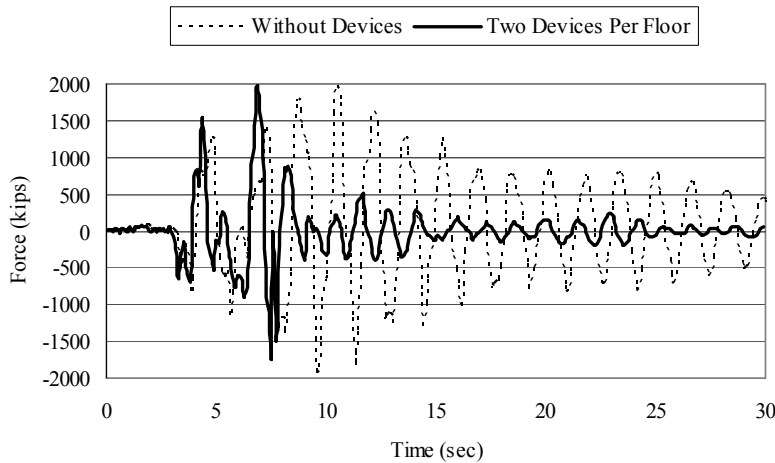
Figure 8.13: Effect of using two devices per floor on the floor displacements and bending moments at column bases of the nine-story frame under El Centro earthquake.



a) Top floor horizontal displacement.

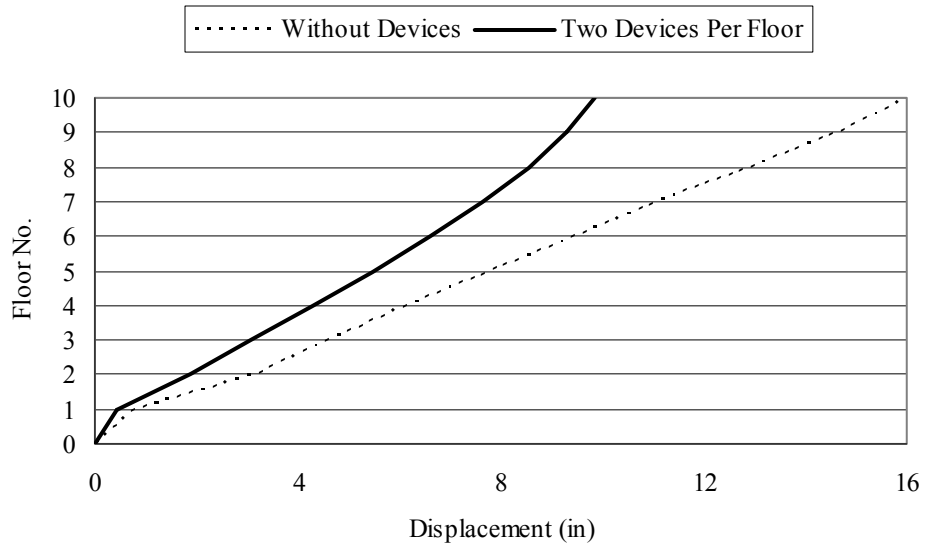


b) Fifth floor horizontal displacement.

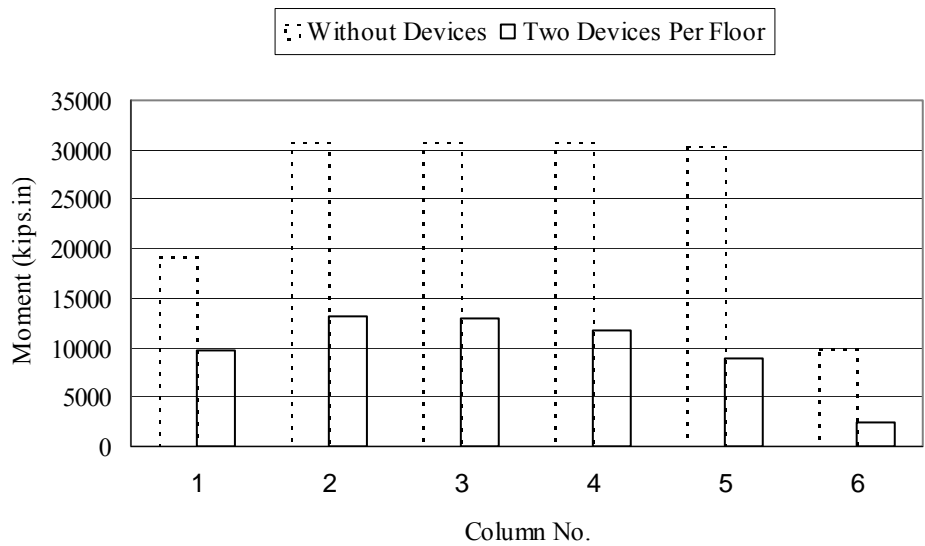


c) Total base shear.

Figure 8.14: Effect of using two devices per floor on the response of the nine-story frame under Northridge earthquake.



a) Story displacements at maximum top floor displacement.



b) Bending moment on the column bases at maximum top floor displacement.

Figure 8.15: Effect of using two devices per floor on the floor displacements and bending moments at column bases of the nine-story frame under Northridge earthquake.

Chapter 9: Summary and Conclusions

9.0 Summary

A new visco-plastic energy dissipation device is introduced to protect structures under seismic loads. The device is constructed from readily available materials that can be assembled in most structural steel fabrication plants. The device consists of a high-damping rubber block as a viscoelastic material sandwiched between two steel plates or shapes.

First, the device was modeled preliminarily using SAP2000. The rubber block was modeled as several discrete vertical dashpots and linear springs. The steel elements of the device were modeled using linear elastic beam elements during the preliminary analysis. Visco-plastic devices were attached to two structures, one-story single-bay and nine-story five-bay steel frames in order to check the effectiveness of the devices. Two different arrangements of the device, one device and a pair of devices per floor, were considered. The structures were analyzed under harmonic excitation as well as real records of El Centro and Northridge earthquake excitations. The response of the multi-story steel frame with traditional viscoelastic dampers was compared to the response of the same frame with the new devices. Large displacement and P- δ effects were considered.

A three-dimensional detailed finite element model for the visco-plastic device was developed using ABAQUS. The model considered the hyperelasticity and viscoelasticity of the rubber block. Experimental results of uniaxial tension-compression, biaxial tension and relaxation shear tests on high-damping rubber compounds were used. The rubber block was modeled using three-dimensional 20-node quadrilateral reduced-integration elements solid elements. The inelastic behavior of the steel elements was considered using the Von Mises yield criterion. The steel elements were modeled using 8-node quadrilateral reduced integration shell elements. Large-displacement analysis was conducted.

A parametric study was carried out on the device to investigate the effect of different parameters on the device behavior. Different types of loadings were considered in this study. The parameters considered are:

- Steel type (mild or high-strength steel)
- Device aspect ratio
- Breadth of rubber block
- Cross section of steel elements

According to the results of the parametric study, the following observations were obtained:

1. Devices with mild-steel elements dissipate more energy through yielding. However, steel yielding occurs under relatively small deformations. Moreover, devices with mild-steel experienced excessive yielding when exposed to moderate deformations, which reduces the device strength and its ability to undergo large deformations.
2. As the device aspect ratio increases, the device stiffness is reduced. Accordingly, larger deformations are developed in the viscoelastic material as well as the steel elements, which results in increasing the total energy dissipation through the device. On the other hand, devices with lower aspect ratios provide higher stiffness. Although higher device stiffness may lead to smaller structural deformations but on the other hand, excessive added stiffness may act as a “seismic attractor,” increasing base shears and increasing response accelerations, which result in damage to contents and nonstructural components. Accordingly, high aspect ratio is recommended for the device.
3. The smaller the viscoelastic material breadth, the larger the strains obtained in the device and accordingly the higher the energy dissipation through the viscoelastic and steel materials. On the other hand, smaller viscoelastic material breadth results in excessive inelastic deformation in steel elements under relatively small deformations. Very large viscoelastic breadth leads to limiting the deformations developed in the device, which reduces the total energy dissipation significantly.

- Accordingly, reasonable viscoelastic material breadth is recommended to provide a balance between the stiffness and energy dissipation provided by the device.
4. Devices with small cross sections of steel elements experience large deformations, which increase the energy dissipation through viscoelastic material and steel elements. However, these devices do not have the ability to undergo large deformations without severe yielding. On the other hand, large cross sections of steel elements reduce the deformations developed in the device. Accordingly, the efficiency of the device is considerably reduced. Accordingly, reasonable cross sections are recommended for the device in order to develop a balance between stiffness and damping provided by the device.

After selecting the different device parameters based on the parametric study, the device was analyzed under harmonic loading with different amplitudes and loading frequencies. Under low-level of deformations, the device behaved like viscoelastic damper in the way that the energy was dissipated through the viscoelastic material only. For high-level of deformations, significant energy dissipation was obtained from the inelastic behavior of the steel elements. The device performed well under different loading frequencies..

Finally, in order to facilitate the use of the visco-plastic device, a new simplified model using SAP2000 was introduced. First, different simplified models were compared to the detailed finite element model in order to determine the accuracy of the simplified model. Satisfactory matching results were obtained from one of these models, in which the hyperelastic behavior of rubber was modeled using an elastic material, with a high Poisson ratio, filling the area sandwiched between the steel channels. The viscoelastic behavior of rubber was modeled using a single vertical dashpot. The steel elements were modeled using beam elements. Flexural plastic hinges were used to model the steel yielding. The nine-story five-bay steel frame with the devices, modeled using the simplified model, was analyzed under harmonic excitation as well as real records of El Centro and Northridge earthquake excitations.

9.1 Conclusions

According to the results of the aforementioned analyses, the following conclusions were obtained:

1. The visco-plastic device is very controllable since it has many design parameters that can be selected carefully in order to optimize its use to dissipate energy for different structures. These parameters include the aspect ratio of the device, h/l , the dimension of the viscoelastic material, the type and cross section of the steel elements, the type of the viscoelastic material used and the location of the device throughout the structures to which the dampers be attached.
2. A small axial deformation along the device axis can be geometrically amplified considerably to produce large strains in the viscoelastic material, which increases the energy dissipation.
3. Under low levels of vibration such as wind induced vibrations, the visco-plastic device dissipates energy through the amplified tensile and compression strains developed in the viscoelastic materials. However, for high levels of vibration, like strong earthquake excitations, a significant source of energy dissipation is encountered through the yielding of the steel elements in addition to the viscoelastic energy dissipation.
4. The visco-plastic device improved the response of different structures significantly under different ground excitations. Structures with visco-plastic devices had significantly lower peak displacements, lower base shear and lower bending moments at column bases than systems without the devices. Also, placement of viscoelastic material in the proposed configuration was more effective than placement in a traditional configuration (wherein the viscoelastic material is stressed in direct shear). Unlike traditional viscoelastic dampers, in most of the cases, structures with visco-plastic devices did not experience increase in the base shear, which is the main drawback of the existing viscoelastic dampers.

9.2 Future work

1. To select the viscoelastic material for the device properly, different high-damping rubber compounds should be compared regarding their ability of energy dissipation, different mechanical properties, such as modulus of elasticity, tensile strength, and elongation at break, and finally the cost. Specimens of such materials should be tested under uniaxial and biaxial tension-compression tests in addition to creep or relaxation shear tests.
2. Prior to finalizing the design of the visco-plastic device, different detailing requirements must be addressed. These are the design of the connections at the two ends of the device, the connection between the braces and the device, which controls the out-of-plane stability, the proper manner for bending the steel plates, and the determination of whether the viscoelastic material must be bonded to the steel, or whether the steel may be “bent around” the viscoelastic material, causing a precompression, and thereby eliminating the need for physical bonding. If it is determined that the filler must be bonded to the plates, additional tests will be performed to test the effectiveness of the bond.
3. Having selected the suitable viscoelastic material and the appropriate design of the device, visco-plastic devices can be constructed at approximate one-half scale and then tested using a uniaxial seismic shaking table to drive the device. The tests can be performed with pseudo-static and dynamic cyclic loading applied along the axis of the device. The imposing motion should be harmonic at frequencies ranging from zero to 5 HZ. The purpose of this testing is to check the device behavior in elastic and inelastic range and compare it with the results of the finite element model.
4. Full-scale visco-plastic devices can be constructed at the NEES Fast Hybrid Testing (FHT) at the University of Colorado at Boulder and then tested similar to the previous testing. After that a physical substructure can be combined with a finite element model substructure and tested dynamically. Such testing combines real-time physical experiment with on-line model-based simulation in order to evaluate the seismic performance of structural systems.

References

Amin, A. F. M. S., Alam, M.S and Okui, Y. (2002). "An improved hyperelasticity relation in modeling viscoelasticity response of natural and high damping rubbers in compression: experiments, parameter identification and numerical verification" *Mechanics of Materials*, Vol. 34, Issue 2, pp. 75-95.

ASTM D 3849, (1990). "Annual Book of ASTM Standards" Vol. 09.01.

Bergman, D. M. and Goel, S.C. (1987). "Evaluation of cyclic testing of steel-plate devices for added damping and stiffness" Report No. UMCE 87-10, The University of Michigan, Ann Arbor, MI.

Black, C. J., Makris, N., and Aiken, I. D. (2004). "Component testing, seismic evaluation and characterization of buckling-restrained braces" *Journal of Structural Engineering*, ASCE, Vol. 130, Issue 6, pp. 880-894.

Chang, K.C., Soong, T.T., Oh, S.T., and Lai, M.L. (1991). "Seismic response of 2/5 scale steel structure with added viscoelastic dampers" Technical report NCEER-91-0012, National Center of Earthquake Engineering Research, Buffalo, NY.

Chang, K.C., Soong, T.T., Oh, S.T., and Lai, M.L. (1995). "Seismic behavior of steel frame with added viscoelastic dampers" *Journal of Structural Engineering*, Vol. 121, No. 10, pp 1418-1426.

Charney, F. A. and McNamara, R. J. (2002). "Use of damped mode shapes in visualizing the efficiency of an auxiliary damped 39-story office building" Seventh U.S. National Conference on Earthquake Engineering (7NCEE), Boston, Massachusetts

Chin, E. J., Lee, K. T., Winterflood, J., Jacob, J., Blair, D. G. and Ju, L., (2004). "Techniques for reducing the resonant frequency of Euler spring vibration isolators" *Classical and Quantum Gravity*, Vol. 21, issue 5 pp S959-S963.

Computers and Structures Inc. (2002). "SAP 2000 Analysis Reference Manual".

Constantinou, M.C., Soong, T.T. and Dargush, G.F. (1998). "Passive energy dissipation systems for structural design and retrofit" Monograph Series, Multidisciplinary Center for Earthquake Engineering Research, A National Center of Excellence in Advanced Technology Applications.

Constantinou, M. C. and Symans, M.D. (1993) "Experimental study of seismic response of buildings with supplemental fluid dampers" Structural Design of Tall Buildings, Vol. 2, pp. 93-132.

Constantinou, M. C., Symans, M.D., Tsopeles, P. and Taylor, D. P. (1993). "Fluid viscous dampers in applications of seismic energy dissipation and seismic isolation" Proceedings of ATC 17-1 on Seismic Isolation, Energy Dissipation and Active Control, Vol. 2, pp. 581-591.

Constantinou, M.C., Tsopeles, P., and Hammel, W. (1997). "Testing and modeling of an improved damper configuration for stiff structural systems", Center for Industrial Effectiveness, State University of New York at Buffalo, N.Y.

Constantinou, M.C., Tsopeles, P., Hammel, W., and Sigaher A. N. (2001). "Toggle-brace-damper seismic energy dissipation systems" Journal of Structural Engineering, Vol. 127, No. 2, pp. 105-112.

Derham, C. J., Kelly, J. M. and Thomas, A. G. (1985). "Nonlinear natural rubber bearings for seismic isolation" Nuclear Engineering Design, Vol. 84, No. 3, pp. 417-428.

Donnet, J., Bansal, R.C and Wang, M. (1993). "Carbon Black" New York: Marcel Dekker, Inc.

Federal Emergency Management Agency (FEMA) (1997). "NEHRP guidelines for the seismic rehabilitation of buildings" FEMA-274, Washington, D.C.

Freakley, P.K. (1978). "Theory and practice of engineering with rubber" Applied Science Publisher, London.

Fu, Y and Kasai, K. (1998). "Comparative study of frames using viscoelastic and viscous dampers" *Journal of Structural Engineering*, Vol. 124, No. 5, pp 513-522.

Gupta A and Krawinkler H. (1999). "Seismic demands for performance evaluation of steel moment resisting frame structures." John A. Blume Earthquake Engineering Center Report No. 132, Department of Civil Engineering, Stanford University.

Guth, E. (1945). "Journal of Applied physics" Vol. 16.

Guth, E. and Gold, O. (1938). "Physics Review" Vol. 53.

Hibbitt, Karlsson, and Sorensen, Inc. (2002). "ABAQUS/standard user's manual", Pawtucket, RI.

Keel, C. J. and Mahmoodi, P. (1986). "Design of viscoelastic dampers for the Columbia Center Building" *Building Motion in Wind*. (Eds N. Isyumov and T. Tschanz) ASCE, New York, pp 83-106.

Kelly, J. M., Skinner, R. I. and Heine, A. J. (1972). "Mechanisms of Energy Absorption in Special Devices for Use in Earthquake Resistant Structures" *Bulletin of New Zealand Society, Earthquake Engineering*, Vol. 5, Issue 3, pp 63-88.

Kimura, K., Takeda, Y., Yoshioka, K., Furuya, N., and Takemoto, Y. (1976). "An experimental study on braces encased in steel tube and mortar" *Proceedings of the Annual Meeting of the Architectural Institute of Japan*, Japan.

Kraus, G. (1965). "Reinforcement of Elastomers" New York: John Wiley & Sons.

Lin, R. C., Liang, Z., Soong, T. T. and Zhang, R. H. (1991). "An experimental study of seismic structural response with added viscoelastic dampers." *Engineering Structures*, Vol. 13, Issue 1, pp 75-84.

Lin, Wen-Hsiung and Chopra, A.K. (2003). "Earthquake response of elastic single-degree-of-freedom systems with nonlinear viscoelastic dampers" *Journal of Engineering Mechanics*, Vol. 129, Issue 6, pp. 597-606.

References

- Mahmoodi, P. Robertson, L. E., Yontar, M., Moy, C. and Feld, L. (1987). "Performance of viscoelastic structural dampers in World Trade Center Towers" Dynamics of Structures, Structure Congress' 87 Orlando, FL.
- Mahmoodi, P. (1969). "Structural dampers" Technical paper, Vibration control system, Construction Market, Engineering Materials 3 M Industrial Specialties Division.
- Martinez-Romero, E. (1993). "Experiences on the use of supplemental energy dissipators on building structures" Earthquake Spectra, Vol. 9, Issue 3, pp.581-625.
- Martinez-Rodrigo, M. and Romero, M.L. (2003). "An optimum retrofit strategy for moment resisting frames with nonlinear viscous dampers for seismic applications" Engineering Structures, Vol. 25, pp. 913-925.
- McDonald, G. C. and Hess, W. M. (1983). "Improved particle size measurement on pigments for rubber" Journal of Rubber Chemistry and Technology, Vol. 56.
- Meinecke, E. M and Taftaf, M. I. (1988). "Effect of carbon black on the mechanical properties of elastomers" Journal of Rubber Chemistry and Technology, Vol. 61.
- Miyazaki, M. and Mitsusaka, Y. (1992). "Design of a building with 20% or greater damping" Tenth World Conf. Earthquake Engineering, Madrid, pp. 4143-4148.
- Mullins, L. (1948). "Journal of Rubber Chemistry and Technology" Vol. 21.
- Mullins, L. (1950). "Journal of Rubber Chemistry and Technology" Vol. 23.
- Munshi, J.A. (1997). "Effect of viscoelastic dampers on hysteretic response of reinforced concrete elements" Engineering Structures, Vol. 19, No. 11, pp. 921-935.
- Naeim, F. and Kelly, J. (1999). "Design of seismic isolated structures" John Wiley and Sons, Inc., New York, NY.
- Nashif A.D., Jones, D. I. G. and Henderson, J. P. (1985). "Vibration Damping". New York:John Wiley & Sons, Inc.

Newmark, N. M. and Hall, W. J. (1982). "Earthquake spectra and design" Earthquake Engineering Research Institute, Berkley, California, pp. 53-54.

Oesterle, M. G. (2003). "Use of Incremental Dynamic Analysis approach to assess the performance of moment-resisting-frames with fluid viscous dampers" M.SC thesis, Virginia Tech.

Powell, Graham H. (1973). "DRAIN-2D User's Guide" UCB/EERC-73/22: Earthquake Engineering Research Center, University of California, Berkeley.

Raos, P. (1992). "Computation of model parameters for application in finite element analysis" Kautsch. Gummi Kunstst, Vol. 45, Issue 11, pp 957-963.

Ravey, J. C., Permilat, S. and Horn, P. (1970). "European Polymer Journal" Vol. 6.

Samali, B. and Kwok, K.S.C. (1995). "Use of viscoelastic dampers in reducing wind- and earthquake-induced motion of building structures" Engineering Structures, Vol. 17, Issue 9, pp. 639-654.

Schwahn, K. J. and Delinic, K. (1988). "Verification of the reduction of structural vibrations by means of viscous dampers" Seismic Engineering, ASME, Pressure Vessel and Piping Conference, Pittsburgh, PA, Vol. 144, pp. 87-95.

Shiba, K., Mase, S., Yabe, Y., and Tamura, K. (1998). "Active/passive vibration control systems for tall buildings" Smart Materials and Structures, Vol. 7, pp. 588-598.

Shukla, A.K. and Datta, T.K. (1999). "Optimal use of viscoelastic dampers in building frames for seismic force" Journal of Structural Engineering, Vol. 125, Issue 4, pp. 401-409.

Sigaher A. N. and Constantinou, M. C. (2003). "Scissor-Jack-damper energy dissipation system" Earthquake Spectra, Vol. 19, Issue 1, pp. 133-158.

Singh, M.P. and Moreschi, L.M. (2001). "Optimal seismic response control with dampers" *Earthquake Engineering and Structural Dynamics*, Vol. 30, Issue 4, pp. 553-572.

Singh, M.P. and Moreschi, L.M. (2002). "Optimal placement of dampers for passive response control" *Earthquake Engineering and Structural Dynamics*, Vol. 31, Issue 4, pp. 955-976.

Skinner, R. I., Kelly, J. M. and Heine, A. J. (1975). "Hysteresis dampers for earthquake-resistant structures" *Earthquake Engineering and Structural Dynamics*, Vol. 3, pp. 287-296.

Soong, T. T. and Dargush, G. F. (1997). "Passive Energy Dissipation systems in Structural Engineering" New York: John Wiley & Sons, Inc.

Studebaker, M. L. (1957). "Journal of Rubber Chemistry and Technology" Vol. 30.

Tarics, A. G., Way, D. and Kelly, J. (1984). "The implementation of base isolation for the Foothill Communities Law and Justice Center" Technical Report No. RTA-84, San Francisco, CA.

Tsai, K. C., Chen, H. W., Hong, C. P. and Su, Y. F. (1993). "Design of steel triangular plate energy absorbers for seismic-resistant construction" *Earthquake Spectra*, Vol. 9, Issue 3, pp. 505-528.

Uriz, P. and Whittaker, A.S. (2001). "Retrofit of Pre-Northridge steel moment-resisting frames using fluid viscous dampers" *The Structural Design of Tall Buildings*, Vol. 10, pp. 371-390.

Wada, A., Saeki, E., Takeuch, T., and Watanabe, A. (1989). "Development of unbonded brace." Column Technical Publication No. 115, Nippon Steel, Japan.

Watanabe, A., Hitomoi, Y., Saeki, E., Wada, A., and Fujimoto, M. (1988). "Properties of braces encased in buckling-restraining concrete and steel tube." *Proceedings of the 9th*

World Conference on Earthquake Engineering, Vol. IV, Tokyo-Kyoto, Japan, pp. 719–724.

Watanabe, A., and Nakamura, H. (1992). “Study on the behavior of buildings using steel with low yield point.” Proceedings of the 10th World Conference on Earthquake Engineering, Balkema, Rotterdam, Netherlands, pp. 4465–4468.

Whittaker, A. S., Bertero, V.V., Thompson, C. L. and Alonso, L. J. (1991). “Seismic testing of steel plate energy dissipation devices” Earthquake Spectra, Vol. 7, Issue 4, pp. 563-604.

Winterflood, J., Barber, T. and Blair, D. G., (2002). “Using Euler buckling spring for vibration isolation” Classical and Quantum Gravity, Vol. 19, Issue 7, pp 1639-1645.

Xia, C, Hanson, R.D. and Wight, J.K. (1990). “A study of ADAS element parameters and their influence on earthquake response building structures” Report UMCE 90-12, The University of Michigan, Michigan.

Xu, Y.L. and Teng, J. (2002). “Optimum design of active/passive control devices for tall buildings under earthquake excitation” The Structural Design of Tall Buildings, Vol. 11, pp. 109-127.

Yoshida J., Abe, M. and Fujino, Y. (2004). “Constitutive model of high-damping rubber” Journal of Engineering Mechanics, Vol. 130, Issue 2, pp. 129-141.

Zhang, Ri-Hui and Soong, T.T. (1992). “Seismic design of viscoelastic dampers for structural applications” Journal of Structural Engineering, Vol. 118, Issue 5, pp. 1375-1392.

VITA

Yasser El-Husseini Ibrahim was born in Zagazig, Egypt in 1971. He received his Bachelor degree in Civil Engineering with Honors from Zagazig University in 1994 and was on top of his class, which had 170 students. Upon graduation, he served his duties in the Egyptian Army until 1996. Yasser joined then Zagazig University, where he started his Master's program in Structural Engineering and worked as an assistant lecturer in courses such as Structural Analysis, Theory of Structures, Soil Mechanics, and Foundation Design. He was awarded the Master's Degree with Honors in 2000. Yasser got a full assistantship from the Egyptian Government to pursue a PhD program in Civil Engineering in the United States. He came to Virginia Tech in 2001 where he started his PhD work with the Structures Division of the Civil and Environmental Engineering Department. After the PhD graduation, Yasser will be returning to Egypt to work as an Assistant Professor in Civil Engineering at Zagazig University.